USAAVLABS TECHNICAL REPORT 66-25

STATISTICAL THEORY OF TURBULENCE

By

Yutaka Shigemitsu

June 1966

U. S. ARMY AVIATION MATERIEL LABORATORIES
FORT EUSTIS, VIRGINIA

CONTRACT DA 44-177-AMC-892(T)
MISSISSIPPI STATE UNIVERSITY
STATE COLLEGE, MISSISSIPPI

DEPARTMENT OF THE ARMY
U. S. ARMY AVIATION MATERIEL LABORATORIES
FORT EUSTIS, VIRGINIA 23604

This report has been reviewed by the U. S. Army Aviation Materiel Laboratories and is considered to be technically sound. It is disseminated for the exchange of information and the stimulation of ideas.

Task 1P125901A14203
Contract DA 44-177-AMC-892(T)
USAAVLABS Technical Report 66-25
June 1966

STATISTICAL THEORY OF TURBULENCE

Aerophysics Research Report No. 64

by

Yutaka Shigemitsu

Prepared by

The Aerophysics Department
Mississippi State University
State College, Mississippi

for

U. S. ARMY AVIATION MATERIEL LABORATORIES
FORT EUSTIS, VIRGINIA

ABSTRACT

The purpose of this report is to discuss the system of a statistical theory of turbulence in general cases from isotropic turbulence to turbulent boundary layer. In the first three chapters, mathematical formulations are given to the Euler correlation or the Reynolds stress, according to a basic physical picture of vortex chaos motion in which many kinds of vortices are carried along the flow in agitating situations. When the formula is combined with the Reynolds equations, quantitative discussions are developed by dividing the cases into two fundamental groups of wake or jet flow in Chapters Four through Seven and of boundary layer or pipe flow in Chapters Eight and Nine.

BLANK PAGE

PREFACE

In a flow of air or water, turbulent flow is usally found behind a grid or single body, in a pipe, along a wall, or in flow ejected from a nozzle. If an appropriate solution for these complicated states of flow can be derived from the nonsteady Navier-Stokes equations, the study of turbulent flow can be included in the hydrodynamics of a viscous fluid like the theory of laminar boundary layers. As a matter of fact, one is obliged to discuss only statistical characteristics depending upon the Reynolds equations derived by taking time means of the Navier-Stokes equations, because it is extremely difficult to make a mathematical analysis of the latter equations by giving initial and boundary conditions. It is well known, however, that since the Reynolds equations are not mathematically conclusive, they cannot be regarded as necessary and sufficient theoretical grounds for the general phenomena of turbulent flow.

Previous studies of turbulent flow are generally divided into two groups. One is the experimental investigation of the physical characteristics, especially of the microstructure of turbulent flow, and the other is a theoretical anticipation of the statistical quantities of flow. The statistical theory of the isotropic turbulence for a turbulent wake behind a grid, the transfer theory for a turbulent shear flow, and other theories are included in the latter category. In this category of study, the problem is to make the Reynolds equations be conclusive for the referring turbulent phenomena by introducing appropriate mathematical expressions of some other assumptions on statistical properties of the turbulent flow. Irrespective of the successful aspects of existing theories in their own regions, they surely have no common foundation such as a general theory of turbulence. Viewed as a turbulent phenomenon, the difference of the turbulent wake behind a grid and a single body is not conspicuous; but the scope of each theory for these cases cannot extend to the others. Furthermore, modern experimental techniques have revealed many properties of turbulent flow which are beyond the scope of existing theories.

The intention of the author, after making some studies on fully-developed turbulent flows, is to propose a unified statistical theory for a general case of turbulent flow. According to this intention, it is initially important to affirm a physical picture of the structure of general turbulent states of flow and not to make a phenomenological idealization of a special case of flow such as isotropic turbulence or turbulent shear flow. When the fundamental physical picture is made concrete, these mathematical formulas must be derived which will permit the inclusion of the Reynolds equations. Through this method, it may be possible to clarify the meaning of the basic assumptions of the previous theories and to extend their scope to a nontheorized field of the statistical properties. In order to develop practical studies of engineering, it is necessary to start with an investigation of the basic foundations of a general theory of turbulence.

Although many of the author's works have already been published, the purpose of these papers has been to present the originality of the investigator. The form of an ordinary paper was found to be unsuitable for the purpose of presenting the primary aim of the author. Therefore, by making the interrelations clear in the original works and other existing theories, the discussions will be projected into a theoretical system in this report.

An attempt of this description is different from a display of only the original works of the author, and at the same time, it must not be a historically arranged review of the previously proposed studies. Like a theory of mathematics, systemization should be given to quantitative interpretations of the statistical properties of general phenomena of turbulent flow. In this report, the turbulent flow shall be first classified into groups depending upon the basic physical picture, and mathematical idealizations shall be presented for these groups. In proceeding with the descriptions, theoretical deductions from the idealized mathematical expression must clearly be distinguished from physical interpretations of the natural phenomena themselves. Thus, the words "turbulence" and "turbulent flow" shall be used here for the idealized image and the natural phenomena of turbulent flow, respectively; and the description is limited to show only the structure of a system of the general theory of turbulence. It is desirable to rely upon other excellent reference books and reviews in periodicals for the precise phenomenological discussions in individual cases.

Once the phenomena are idealized into mathematical formulations, quantitative results must be drived, at least in principle, through mathematical analyses. At present, however, not all the statistical quantities of turbulent flow can be evaluated because of an insufficiency of the study of the physical conditions and mathematical treatments. This is especially true for the case of the vortex motion. However, less difficult mathematical analyses shall be advanced according to the system of the theory, and their results shall be checked by experimental evidences. The description will attempt to clarify the meaning of basic assumptions of the previously proposed successful theories, to give quantitative interpretations to uncomplicated observed statistical properties which are unattainable by these previous theories, and to anticipate some useful results for engineering problems.

In Chapters One through Three, basic formulations are made on statistical quantities of turbulence in a general case after relating the principal features of the turbulent flow. In Chapters Four through Nine, the basic formulations are developed to give quantitative discussions of two essentially different kinds: turbulent wake or jet with a decaying feature along the flow, and turbulent flow along a wall with a nondecaying feature.

CONTENTS

	Page
ABSTRACT	iii
PREFACE	v
LIST OF ILLUSTRATIONS	ix
LIST OF SYMBOLS	xvii
CHAPTER ONE. INTRODUCTION	1
1. EXISTENCE OF TURBULENT FLOW	1
2. HISTORICAL NOTES OF THE STUDY OF TURBULENT FLOW	2
3. DEVELOPMENT OF STATISTICAL STUDIES IN PHYSICS	4
4. THE SIGNIFICANCE OF THE STATISTICAL THEORY OF TURBULENCE	7
CHAPTER TWO. FUNDAMENTAL CHARACTER OF VORTEX CHAOS MOTION	11
5. FORMATION OF VORTEX CHAOS MOTION	11
6. TURBULENT FLOW OF A DECAYING CHARACTER	12
7. VISCOUS SUBLAYER NEAR THE WALL	14
8. TURBULENT FLOW OF NONDECAYING CHARACTER	15
CHAPTER THREE. STATISTICAL DESCRIPTION OF VORTEX CHAOS MOTION	18
9. THE REYNOLDS EQUATIONS	18
10. COEFFICIENTS OF THE EULER CORRELATION	21
11. PROBABILITY-DENSITY FUNCTION IN VORTEX CHAOS MOTION	22
12. TRANSFORMATION OF TIME MEANS INTO AREA MEANS	26
13. VORTEX CHAOS MOTION IN THE IDEAL STATE	30
14. CHARACTER OF A VORTEX MOTION	37
15. EXTENSION OF THE ERGODIC HYPOTHESIS	40
16. VORTEX CHAOS MOTION IN STATISTICAL EQUILIBRIUM	43
CHAPTER FOUR. SIMILARITY THEORY OF THE ISOTROPIC TURBULENCE	47
17. CONDITIONS OF HOMOGENEOUS AND ISOTROPIC TURBULENCE	47
18. CHARACTERISTICS OF THE CORRELATION FUNCTIONS	49
19. REPRESENTATION BY THE SPECTRUM FUNCTIONS	54
20. CONCEPTION OF SIMILARITY PRESERVATION	59
21. SIMILARITY PRESERVATION IN THE INITIAL PERIOD	64
CHAPTER FIVE. SIMILARITY THEORY IN THE INITIAL PERIOD	67
22. IDEALIZATION OF THE INITIAL PERIOD	67
23. INTENSITY AND SCALE OF THE SHEAR TURBULENCE	70
24. CONSERVATION OF MOMENTUM	73
25. PROPORTIONAL CHARACTER OF THE COMPONENTS OF TURBULENT INTENSITY	77

		Page
26.	FREE BOUNDARY OF THE SHEAR TURBULENCE	81
27.	DISTORTION OF THE HOMOGENEOUS AND ISOTROPIC TURBULENCE	85
28.	PROFILE OF TURBULENT INTENSITY	87
29.	LIMIT OF THE INITIAL PERIOD	88
CHAPTER SIX.	TRANSFER THEORY IN THE INITIAL PERIOD	90
30.	TRANSFER OF MOMENTUM IN THE SHEAR TURBULENCE	90
31.	TRANSFER OF VORTICITY	93
32.	REPRESENTATION OF TURBULENT SCALE	95
33.	TRANSFER HYPOTHESES IN THE INITIAL PERIOD	97
34.	TURBULENT WAKE	100
35.	TURBULENT JET	103
CHAPTER SEVEN.	NONSIMILARITY IN THE DECAYING TURBULENCE	107
36.	TRANSITION PROBABILITY IN THE CASCADE PROCESS	107
37.	POISSON PROCESS FOR THE CASCADE PHENOMENA	109
38.	NONSTATIONAL EXPRESSION FOR THE CORRELATION TENSOR	111
39.	PRODUCTION CONDITION OF A VORTEX MOTION	114
40.	DECAYING LAW	117
41.	DOUBLE CORRELATIONS IN THE ISOTROPIC TURBULENCE	118
42.	TRIPLE CORRELATION IN THE ISOTROPIC TURBULENCE	121
43.	LOCALLY ISOTROPIC TURBULENCE	123
44.	KOLMOGOROFF'S THEORY	124
45.	SPECTRUM FUNCTION IN THE ISOTROPIC TURBULENCE	127
CHAPTER EIGHT.	SIMILARITY CONCEPTION IN THE NONDECAYING TURBULENCE	131
46.	CHARACTER OF NONLOCAL EXPRESSION	131
47.	SIMILARITY CHARACTER OF THE CORRELATION TENSOR	133
48.	TURBULENT FLOW OF A SIMILARITY PRESERVATION	136
49.	PROPORTIONAL CHARACTER IN TURBULENT INTENSITY	136
50.	FREE-BOUNDARY PHENOMENA	140
CHAPTER NINE.	TRANSFER THEORY OF THE NONDECAYING TURBULENCE	141
51.	DISTRIBUTION OF THE MIXING LENGTH	141
52.	EQUATION OF MOTION FOR THE FLOW OF SIMILARITIES PRESERVATION	143
53.	SINGULARITY CHARACTER NEAR THE WALL	146
54.	CHANNEL OR PIPE FLOW	148
55.	TURBULENT BOUNDARY LAYER ALONG A FLAT PLATE	149
56.	SOLUTIONS OF SIMILARITIES FLOW OF TURBULENT BOUNDARY LAYER	151
57.	TURBULENT BOUNDARY LAYER WITH A SEPARATION	152
REFERENCES		224
DISTRIBUTION		231

ILLUSTRATIONS

Figure		Page
1	Observation of the Turbulent Flow of Water Behind a Two-Dimensional Lattice Moving With a Constant Velocity	154
2	Observation of the Turbulent Flow of Water in an Open Channel	155
3	Simultaneous Records of Velocity Fluctuations at Two Points in a Wind Tunnel Stream	156
4	Simultaneous Records of the u- and v-Components of Velocity Fluctuation at a Point on the Center Line Behind a Circular Cylinder	157
5	Photographs Showing the Change of the Probability Distribution of the u- and v-Fluctuation Behind a Circular Cylinder	158
6	The Distribution of the Intensity of the u-Fluctuation in the Turbulent Wake Behind an Airfoil	159
7	Probability Distribution of u-Fluctuation Around a Mean Velocity in a Wind Tunnel Stream	160
8	Photograph Showing the Probability Distribution of the u- and v-Fluctuation in a Wind Tunnel Stream	161
9	Photographs Showing the Formation of the Probability Distribution of the u- and v-Fluctuation in the Turbulent Wake Behind a Two-Dimensional Lattice	161
10	Laminar Boundary Layer Oscillation Along a Flat Plate	162
11	Development of Natural Laminar Oscillation in the Laminar Boundary Layer Along a Flat Plate in a Low-Turbulence Wind Tunnel	163
12	Observation of Natural Transition of Laminar Boundary Layer of Water Along a Flat Plate	164

Figure		Page
13	Measurement of the Mean and the Fluctuational Velocity at the Transition Region in the Laminar Boundary Layer Along a Flat Plate in a Wind Tunnel Stream ----------	165
14	Distributions of Mean Velocity (○) and the Intensity of the u-Fluctuation (●) in the Immediate Vicinity of a Flat Plate in a Turbulent Boundary Layer ----------	166
15	Distributions of the Intensities of the u-, v- and w-Fluctuation in Turbulent Boundary Layer Along a Curved Wall ----------	167
16	Observed Result of the Probability Distribution of the u-Fluctuation Around the Mean Velocity in a Turbulent Boundary Layer Along a Flat Plate ----------	168
17	Photograph Showing the Probability Distribution of the u- and v-Fluctuation in a Turbulent Boundary Layer ----------	168
18	Loci of the Intersections of the Nearest Vortex Filaments and the Perpendiculars to Them From A-Point ----------	169
19	The Variables r, θ, and ϕ Which Determine an Orientation of the V*-Vector ----------	169
20	D*-Domain in the x*y*z*-Space ----------	170
21	The V*- and V*'-Vectors, Respectively, at the A- and A'-Points Which Are due to the Nearest Vortex Motion to the A-Point ----------	170
22	Functional Forms of Turning Velocity $\overline{H} \propto (s)$ in (14.6) ----------	171
23	Conceptional Diagram Illustrating Transition Character of the P*-Function in a Vortex Chaos Motion ----------	172
24	Representation of Two Vectors $\overrightarrow{AA_1}$ and $\overrightarrow{A'A_1'}$, Respectively, at the A- and A'-Points in the Field of Flow ----------	173

Figure		Page
25	Fundamental Double and Triple Correlations	173
26	Definition of Microscale	174
27	Spectrum Distributions in a Uniform Turbulent Wake Behind a Grid	175
28	Correlation Distribution in a Uniform Turbulent Wake Behind a Grid	176
29	Functional Forms of the Similarity Correlation $f_\alpha(\xi)$ in (20.14)	176
30	Decay of u-Intensity in a Uniform Turbulent Wake Behind a Grid	177
31	Distributions of an Integral Scale in a Uniform Turbulent Wake Behind a Grid	177
32	Distribution of the Microscale λ in a Uniform Turbulent Wake Behind a Grid	178
33	Orientation of Vortex Filament Behind a Circular Cylinder	178
34	Distributions of u-, v- and w-Intensities Across the Turbulent Wake Behind a Circular Cylinder	179
35	Distribution of u-Intensity Across a Turbulent Wake Behind an Airfoil	180
36	Distribution of the g-Correlation in the Turbulent Wake Shown in Figure 35	180
37	Distribution of Turbulent Intensity and Scale Along the Turbulent Wake Shown in Figure 35	181
38	Representation of Velocity Profile Behind a Circular Cylinder	181
39	Distributions of Total Pressure Behind a Circular Cylinder	182
40	Illustration of Typical Decaying Shear Turbulence	183

Figure		Page
41	Distribution of u/w Across the Turbulent Wake Shown in Figure 34 ----------	183
42	Measurement of the Mean and the Fluctuational Velocity in the Turbulent Wake Behind a Circular Cylinder ----------	184
43	Illustration of the P*- and F-Functions at a Point in the Initial Period ----------	184
44	Distribution of the Intermittency Factor γ Across the Turbulent Wake Behind a Circular Cylinder ----------	185
45	Distribution of the Intermittency Factor γ Across a Turbulent Round Jet ----------	185
46	Distribution of the Nondimensional Dispersion σ Along the Flow ----------	186
47	Variation of the Nondimensional Dispersion σ Versus the Mean Velocity U_o in the Turbulent Wake Behind a Circular Cylinder ----------	186
48	Diagonal Sketch of a Nonuniform Shearless Turbulence ----------	187
49	Variation of v/u Versus the Contraction Ratio λ of (27.1) ----------	187
50	Calculated Curves of Relative Profiles of $C_u^2(\eta)$, C_v^2, and $C_{\overline{uv}}(\eta)$ of (25.2) Across an Idealized Symmetrical Shear Turbulence ----------	188
51	Distribution of Mean Velocity and u-Intensity Across a Half-Jet as Shown in Figure 40 (d) -----	188
52	Distribution of the Width of a Turbulent Wake Behind a Circular Cylinder ----------	189
53	Distribution of u-Intensity Along the Turbulent Wake in Figure 52 ----------	189
54	Representation of Velocities at Two Points Across a Shear Flow ----------	190

Figure		Page
55	Profiles of an Intermittency Factor γ and Velocity v Across a Decaying Turbulence	190
56	Distribution of Mean Velocity Across the Turbulent Wake Behind a Circular Cylinder	191
57	Diagonal Sketch of the Profiles of Different Values of ε Across the Wake Behind an Asymmetric Airfoil	191
58	Distribution of Mean Velocity Across a Turbulent Jet From a Two-Dimensional Slit	192
59	Distribution of Mean Velocity Across a Turbulent Jet From a Round Nozzle	192
60	Distribution of Mean Velocity Across a Half-Jet	193
61	General View of the Poisson Process of $\bar{P}^*$ of (37.3)	194
62	Variation of the Value of A_m Very Near the Production Instant of a Vortex Motion	194
63	Decay of u-Intensity Along Uniform Decaying Turbulence	195
64	Variation of the f-Correlation in Isotropic Turbulence	196
65	Variation of the g-Correlation in Isotropic Turbulence	196
66	Distribution of the g-Correlation in Isotropic Turbulence	197
67	Variation of the Triple Correlation h in Isotropic Turbulence	198
68	Growing of the h-Correlation Observed Along the Turbulent Wake Behind a Grid	198
69	Distribution of the f- and h-Correlations in Isotropic Turbulence Plotted Versus the Same Abscissa k/L_f	199
70	Observed Results of the One-Dimensional Spectrum F_1 of u-Fluctuation and the Shear-Correlation Spectrum $R_{uv} = (\overline{uv})_n/(u_n v_n)$	200

Figure		Page
71	Comparison of the 2/3-Power Law of (44.9) With the Curves of 1-f Shown in Figure 64 ----------	201
72	Local Characteristics of the Spectrum Function F(k) ----------	201
73	Observed Results of the One-Dimensional Spectrum in the Turbulent Wake Behind a Grid and the Curves of (45.4) and (45.5) ----------	202
74	Distribution of Function I for Two Points in Turbulent Boundary Layer Along a Flat Plate ----------	203
75	Distribution of u-Intensity Across Turbulent Boundary Layer Along a Flat Plate ----------	203
76	Distributions of Turbulent Shearing Stress Across a Circular Pipe ----------	204
77	Distributions of u-Intensity Across a Turbulent Boundary Layer With a Negative Constant Pressure Gradient Along the Flow ----------	205
78	Distribution of u-Intensity Across a Turbulent Boundary Layer With a Positive Constant Pressure Gradient Along the Flow ----------	206
79	Deviation From the Similar Profiles of u-Intensity in the Case of Turbulent Boundary Layer in Figure 78 ----------	207
80	Distributions of $u/\sqrt{u^2+v^2+w^2}$, $v/\sqrt{u^2+v^2+w^2}$, $\overline{uv}/(u^2+v^2+w^2)$ and u/w Across Nondecaying Turbulent Flows ----------	207
81	Distribution of the Function P* at Two Points A and A' Near η = 1 and 0, Respectively, in Turbulent Boundary Layer ----------	208
82	Distribution of the Intermittency Factor γ Across Turbulent Boundary Layer Along a Flat Plate ----------	208
83	Distribution of $\widetilde{P^*}\,\xi$, and the Location of ξ, for an A-Point ----------	209
84	Distribution of the Mixing Length in a Pipe Flow --	209

Figure		Page
85	Distribution of the Mixing Length in Turbulent Boundary Layer Along a Flat Plate	210
86	Distributions of Mean Velocity Across Turbulent Boundary Layer Expressed in $\bar{U}/U_\tau \sim \log(U_\tau y/\nu)$	211
87	Profile of Mean Velocity Across a Channel	212
88	Distributions of Turbulent Shearing Stress Across a Circular Pipe	212
89	Distributions of Mean Velocity of Turbulent Flow Across a Circular Pipe Expressed in $\bar{U}/U_\tau \sim \log(U_\tau y/\nu)$	213
90	Calculated Velocity Profiles Across the Turbulent Boundary Layer Without a Pressure Gradient	214
91	Distributions of Mean Velocity in the Expression of $(\bar{U}-U_o)/U_\tau \sim \eta$ in the Case of Turbulent Boundary Layer Along a Flat Plate	215
92	An Example of Computed Curves of f, $df/d\eta$ and $\int_0^\eta f\,d\eta$ Across a Similarities Boundary Layer of λ = -0.1 and c = 0.6	216
93	Computed Velocity Profiles of a Similarities Boundary Layer of λ = 1.5	217
94	Computed Velocity Profiles of a Similarities Boundary Layer of λ = -0.2	218
95	Computed Velocity Profiles of Similarities Boundary Layers Expressed in the Relative Form of $(\bar{U}-U_o)/(U_c-\bar{U}(0)) \sim \eta$	219
96	Computed Velocity Profiles Near the Critical Point of $\partial \bar{U}(0)/\partial y = 0$	220
97	Variations of the Momentum-(δ'_{**}) and Displacement-Thickness (δ'_{*}) Versus λ Evaluated From the Relative Profiles Shown in Figure 95	220

Figure		Page
98	Comparison of the Computed Profiles of λ = 0.5 and λ = 1.0 in Figure 95 With Experimental Data of the Mean Velocity of the Similarity Boundary Layer Shown in Figure 77 ----------	221
99	Comparison of the Computed Profiles of λ = 0.10 and λ = -0.05 in Figure 95 With Experimental Data of the Mean Velocity of the Similarity Boundary Layer Shown in Figure 78 ----------	222
100	Comparison of the Computed Relative Profiles of λ = -0.15 and λ = -0.20 in Figure 95 With Observed Mean Velocity of the Turbulent Boundary Layer With Positive Pressure Gradients ----------	223
101	Comparison of a Computed Profile of λ = -0.30 and c = 0.35 Near the Critical Condition $\partial \bar{U}/\partial y = 0$ With Observed Mean Velocity Near the Point of Turbulent Separation ----------	223

SYMBOLS

x, y, z	Cartesian coordinates in the field of flow
t	time
U, V, W	velocity components of the x, y, and z direction, respectively
P	static pressure
μ	coefficient of molecular viscosity
ν	coefficient of kinematic viscosity
u, v, w	fluctuating velocity components of the x, y, and z direction, respectively
A	a fixed point in the field of flow
V*	a turning velocity at the A-point owing to a vortex motion nearby in which curvature, elongation of the filament, and the effects of other vortices are neglected
r, θ, ϕ	independent variables to designate the location and orientation of the V* vector referring to the vortex center in the field of flow, which, at the same time, represent the coordinates of A*-point in the D*-domain
x*, y*, z*	Cartesian coordinates of an ideal space in which the variation of the V* vector for the time is represented
A*	a point in the x*y*z*-space whose position of the coordinates r, θ, ϕ corresponds to the situation of V* vector in the field of flow
D*	a domain in the x*y*z*-space in which the movement of the A*-point is included
Q*	volume of the D*-domain
t*	time interval in which the A*-point moves around from end to end on a boundary of the D*-domain
Δ t	excess time interval in which vortices are not in the nearest location to the A-point in the field of flow during the time interval t* of the A*-point

P^*	a probability density function to represent the movement of the A*-point in the D*-domain in the x*y*z*-space
$\widetilde{P^*}$	integrated value of P* in the D*-domain
ω	vorticity
Γ	circulation
N	number of the kind of vortex motions

Subscripts

α	type of vortex motion designated by the solutions of a two-dimensional viscous vortex
i	an i-th kind of vortices in the vortex chaos motion consisted of N kinds of vortices
o	origin of a reference position and time in the system of x, y, z, and t
$\overline{}$	time means $(=\lim_{t\to\infty} \frac{1}{t}\int_0^t dt)$
'	values referring to another point in the field of flow besides the A-point
x, y, z, yz, zx, xy	designation of the respective component

CHAPTER ONE. INTRODUCTION

1. EXISTENCE OF TURBULENT FLOW

In the state of fluid motion there are two types of flow: the so-called laminar flow and the turbulent flow. In the flow of air or water, the viscous force due to molecular motion is very small compared with the inertia force of the flow, and the Reynolds number easily attains the value of $10^5 \sim 10^7$. In this range of values of the Reynolds number, the flow usually becomes turbulent. As the Reynolds number decreases, the flow tends to be in a laminar state, and below the critical Reynolds number of the order of 10^2, the flow is always in the laminar state. As the Reynolds number increases with a large velocity, other phenomena such as the compressibility of air or the cavitation of water appear. Thus, the study of turbulent flow is considered to be important in the case of an ordinary Reynolds number.

In real fluid motion, an ideal stationary state does not exist, and a disturbance is incessantly transmitted to the flow. Even in laminar flow, the velocity fluctuations can be found by precise observations. Below the critical Reynolds number, however, the disturbances are all decreased by the strong viscous force of the fluid. Yet, in the case of an ordinary Reynolds number, some of them are increased. It is certain that this increasing disturbance plays a role in producing turbulent flow, although the detailed mechanism of the production of turbulent flow has not yet been clarified. By many observations, it can be seen that the turbulent state begins abruptly and is different from the laminar flow with a velocity fluctuation. In other phenomena such as compressibility of fluids, the effects appear gradually as the velocity increases. However, the turbulent state of flow cannot be connected to the laminar state. This is an important fact when considering the mechanism of turbulent flow.

For the instantaneous state of turbulent flow, it can be seen, as shown in Figures 1 and 2, that many parts of the fluid have a respectively independent motion. When one of these parts of fluid passes near a fixed point in the field of flow, this part gives to the velocity at this point the corresponding fluctuation of a certain frequency. It is an important feature that at a point in the field of flow the velocity fluctuations and these fluid parts have their respective definite mean values for time. They are the two independent basic quantities characterizing turbulent flow, i.e., the intensity and the scale. From many observations, it is known that the ratio of the intensity to mean velocity is about $0.1 \sim 0.001$. When the scale length - a measure of the turbulent scale - is compared with a standard length of the flow, the ratio is about $1 \sim 0.01$. The frequency of the velocity fluctuation which corresponds to the ratio of the scale length to the mean velocity is about $10 \sim 10^3$ per second.

Through precise observation, one finds that the velocity fluctuation is always a continuous function of location and time as shown in Figure 3.

In the molecular motion of a gas, the dimensions of molecules are neglected and their motion can be taken as that of a system of particles. However, the turbulent motion is different in this situation, yet theoretical or experimental evidence cannot be found that the Navier-Stokes equations do not hold in such a nonsteady motion of turbulent flow. At present, it is extremely difficult to solve these equations mathematically and to get the solution as a function of location and time under appropriate physical conditions accompanying the real state of complicated turbulent flow. Fortunately, the turbulent flow has definite mean values of intensity and scale. So, for all practical purposes, it is sufficient to know the mean values for time as functions of a location in the field of flow, even if an instantaneous state of flow cannot be found. Thus, the study of turbulent flow has been developed exclusively from this statistical point of view.

2. HISTORICAL NOTES OF THE STUDY OF TURBULENT FLOW

Since ancient days, people must have seen many turbulent states of flow in the current of a brook or in the rising smoke of a fire, but the beginning of the study of this problem is not so old. In the posthumous manuscripts of Leonardo da Vinci at the beginning of the sixteenth century, some sketches can be found of flow drawn clearly with a recognition of turbulent phenomena. Since the eighteenth century, papers of the study of turbulent flow have been proposed from the engineering point of view. In these papers the names of Hagen, Boussinesq and others can be found.

It was Osborne Reynolds who opened the way to the statistical study of turbulent flow. His early paper (reference 3) is concerned with the production of turbulent flow. By precisely observing many cases of flow of water in a tube, he found that a certain number, presently called the Reynolds number, attained a constant value when the laminar state broke into a turbulent state. He tried to explain the transition phenomenon as being dependent on the increase of energy of the fluctuating velocity contained in part of the fluid. The study of transition was developed into a survey of the stability of a given simple harmonic velocity fluctuation in flow where a linearized nonsteady Navier-Stokes equation was solved. This stability theory was proved first by Taylor (reference 4) to be appropriate in the case of flow between two circulating cylinders. The evaluated results by Tollmien (reference 5) and others in the case of a laminar boundary layer along a flat plate were also ascertained by experimental observation by Schubauer (reference 6) and others. However, the stability theory is concerned with only the laminar velocity fluctuation and does not treat the problem of the production of turbulent flow. On the other hand, Taylor (reference 7) proposed that the turbulent flow might be promoted by an instantaneous separation of the laminar boundary layer, and he then proceeded with a mathematical analysis. However, the mechanism of transition from laminar to turbulent flow is not yet completely clarified.

From the breakdown of laminar to the development of regular turbulent flow, some distance along the flow is necessary. As for the fully developed turbulent flow, Reynolds (reference 8) derived the equations of motion for the time means from the Navier-Stokes equations. In deriving the equations, he proved the existence of stress forces due to the nonlinear terms in the Navier-Stokes equations. Reynolds equations hold in every kind of flow having velocity fluctuations, if the velocity fluctuations have only definite mean values for time. As mentioned in Section 1, this condition holds in the actual state of turbulent flow. Thus, the Reynolds equations become basic necessary conditions in surveying mean values of velocity fluctuation of turbulent flow. The establishment of these equations is fundamentally the most important contribution in all the statistical studies of turbulent flow up to the present time. The Reynolds equations are not as critical as the Navier-Stokes equations, because the former treat only the value of time means. Moreover, because of the existence of the Reynolds stress due to the nonlinear terms in the latter equations, the Reynolds equations have become inconclusive. In other words, the Reynolds equations are not necessary and sufficient conditions to prescribe the statistical quantities of turbulent flow, and cannot be regarded as the unique theoretical base in the statistical study. In addition to the Reynolds equations, some other foundations are necessary to proceed with a statistical analysis of turbulent flow.

Since the Reynolds equations were established, the study of turbulent flow has been developed generally through two stages. In the first stage, mean-velocity distributions of so-called shear turbulent flow of wakes or jets were studied, especially from the practical point of view. Existence of the Reynolds shearing stress due to turbulent agitating motion means the transportation of momentum contained in a part of fluid across the mean direction of flow. Whatever physical supposition may be given to the mechanism of turbulent flow, this phenomenological character is always a fact. Thus, depending upon the transfer theory of gas in statistical dynamics, some attempts were made to clarify the meaning of the mixing length in the case of turbulent shear flow. As the scale length of turbulent flow, Taylor (reference 9) introduced the correlation for time of velocity fluctuation at a fixed point: the Lagrange correlation. Prandtl (reference 10) proposed a new concept of the mixing length which is adaptable to the turbulent shear flow of a continuous medium of fluid. With the introduction of Prandtl's mixing length, the momentum and vorticity transfer theories were developed respectively by Prandtl (reference 10) and Taylor (reference 11), and an improvement was made by Kármán (reference 12) to the concept of the mixing length. Their theoretical results on the mean-velocity distribution or the surface friction in shear turbulent flow were checked experimentally by the Pitot-tube technique, which was the unique experimental method of turbulent flow at that time. Recently, it has been prevalent to make an assumption on the distribution of the coefficient of Reynolds shearing stress instead of the mixing length. In a word, the feature of the transfer theory is to postulate a relation between the Reynolds shearing stress and the mean velocity by using the mixing length or the shearing-stress coefficient, and to make the Reynolds

equations conclusive for the mean-velocity distribution. Although definite interpretations are not given to the basic postulations, these phenomenological transfer theories are still making important contributions to engineering problems.

The second stage of the study of turbulent flow was opened by Taylor (reference 13). He introduced the concept of the correlation of velocity fluctuations at two points at the same time: the Euler correlation. He also defined the isotropic turbulence, in which components of mean values of velocity fluctuation at a point are assumed invariant even if the coordinate axes are rotated or reflected. Kármán and Howarth (reference 14) derived the fundamental equations of motion of this flow by using the Euler correlation. The tensor formula of the Euler correlation coefficients contains the expression of the Reynolds stress and is regarded as the general expression of the two fundamental quantities of the scale and intensity of turbulent flow. In isotropic turbulence, the Reynolds equations are reduced to a simple formula, and it becomes possible to survey the decay of turbulent intensity or the spreading of turbulent scale along the flow somewhat theoretically. These results could be checked experimentally by the hot-wire technique completed by Dryden (reference 15) at that time. Then the locally isotropic turbulence was defined by Kolmogoroff (reference 16), whose concept was to postulate the isotropic character defined by Taylor in only a small part of the fluid motion, even if it did not hold for the whole field of flow. The characteristic of local isotropy was confirmed experimentally in the high-frequency region of the velocity fluctuations in many cases of shear turbulent flow. Since then, studies have been developed into surveys of the spectrum function of velocity fluctuation of the isotropic or locally isotropic turbulence. In fundamental principle, however, the equations of motion in these cases do not differ from the Reynolds equations, and in order to solve the equation mathematically, some other physical hypotheses must be introduced. As one hypothesis, the concept of the similarity preservation has often been adapted, which postulates the invariance of some mean characteristics of velocity fluctuations along the direction of flow. Similarity preservation has also been widely assumed in the case of the transfer theory. Therefore, this hypothesis has been regarded as an important foundation of the study in addition to the Reynolds equations. It may be said that in the second stage the way was first opened to study the mechanism of the velocity fluctuation itself both theoretically and experimentally.

3. DEVELOPMENT OF STATISTICAL STUDIES IN PHYSICS

The object of all studies of turbulent flow is to determine mean values for time of velocity fluctuation as a function of location in the field of flow. According to this interpretation, they may be called statistical studies. Statistical studies, however, have been developed chiefly in the field of physics where they had been used for a considerable period prior to the beginning of the study of turbulent flow. It may be

worthwhile to review the general features of these statistical studies before relating our plan for developing the previous studies of turbulent flow.

Statistical study in physics, presently called statistical dynamics, began with the characteristics of gas. Statistical dynamics are based upon the following fundamental interpretation of a molecular chaos motion; namely, gas is considered to consist of many molecules, each of which is moving at random in space and colliding with others. When molecules are regarded as particles, the Newton dynamics of a system of particles becomes the necessary and sufficient principle for deriving quantitative results. From a mathematical point of view, however, it is extremely difficult to derive an exact solution related to an instantaneous state of the particles in their chaotic motion. It may be analogous to an attempt to solve the Navier-Stokes equations exactly in the case of a turbulent flow. As is well known, even the three-body problem that treats the motion of three particles under an arbitrary condition is not yet completely solved. Thus, it is sufficient to know only the mean states of the molecules for time. In fact, it has been observed that, under ordinary temperature and pressure of gas, the mean-molecular velocity and the mean-free path have the orders of 10^2 meters per second and 10^{-5} centimeters, respectively. The mean-free path is very small compared with a macroscopic standard length.

The mathematical formula for the equation of motion of a system of particles is not as complicated as the Navier-Stokes equations; therefore, the equation of dynamics can give some definite results, even if the time means are taken. At first, the Boyle-Charles law of a gas in the equilibrium state could be proved by attributing the temperature of gas in the macroscopic state to the kinetic energy of molecular chaos motion. As is well known, the Newton dynamics proves energy conservation, which cannot be altered even if the time means are taken. Thus, according to the dynamics, this equation can give definite interpretations to the first law of thermodynamics and to many other phenomenological laws. In a word, the intent of statistical dynamics at the first stage was to discuss the equation of dynamics by considering time means only.

At the next stage, a statistical quantity of the probability-distribution function of molecular velocities was introduced. Then, by considering the physical concept of a molecular chaos motion, the so-called Maxwell-Boltzmann law was proved by taking into account the distribution function. On the other hand, diffusion or heat-conduction phenomena were known for the case of a gas which was slightly deviated from the equilibrium state. Concerning such phenomena, the transfer theory was developed with the quantity of a mean-free path defined as a scale length of molecular chaos motion. This theory has given a theoretical interpretation to the postulation by which all the viscosity coefficients are made constant in the Navier-Stokes equations. But the Newton dynamics has given no direct contribution to the basis of the transfer theory, just as the Navier-Stokes equations have no direct connection to the transfer hypothesis introduced by Prandtl. It is characteristic at this stage that

the statistical quantities have been introduced first to denote the mean state of molecular chaos motion, just as in the stage when the statistical quantities of the mixing length or the Euler correlations were introduced to the study of turbulent flow.

An important feature of statistical dynamics may be found in the interpretation of the second law of thermodynamics. Certainly, such an irreversible feature as the increase of entropy is different from that of the Newton dynamics in which the mathematical process is always reversible. An important problem at that time was the interpretation of this irreversible phenomenon from the viewpoint of the Newton dynamics, as in the case of the first law of thermodynamics. Boltzmann attempted to answer this question by considering the entropy as a probability-distribution function, implying the grade of the randomness of molecular chaos motion. Through many discussions of his proposition, the theoretical meaning of regularity or irregularity has gradually been grasped.

In present statistical dynamics, mathematical formulations are made usually in the phase space, where the location and momentum of every molecule is designated on the coordinate axes. In this space, mean characteristics of molecular chaos motion are expressed in a probability-distribution function. According to the formulation in this space, the Hamilton-Jacobi equation of motion of a system of particles is transformed into the Liouville equation in an energy-constant domain. In order to make the expression of dynamics in the phase space convenient for mathematical analysis, the probability-density function is assumed to have a constant value in the energy-constant domain. It is too difficult to prove this assumption directly by the equation of dynamics, and it can be regarded as an expression of the physical concept of the irregularity of the state of molecular chaos motion. For example, let us consider the following situations of a system of many molecules in the crystal structure of metal. When the absolute temperature is zero, every molecule remains at rest in its respective position in the crystal structure, and each momentum is zero. In this case, the system of molecules is indicated by one point in the phase space. When the temperature is not zero, every molecule of the crystal structure makes an agitating motion around its original position of zero temperature, and the distribution function denoting these molecular motions takes the form of a continuous function in the phase space with its highest density at the point of zero temperature. It is easily supposed that, as the temperature rises, the agitating motion becomes strong, and the scope of a continuous distribution function becomes wider. At an extremely high temperature, a solid body changes into a gaseous state and every molecule moves around at random in space, freed from its original position in the crystal structure. In the gaseous state, it may be appropriate to assume that the probability density distributes with a constant value everywhere in an energy-constant domain in the phase space. This assumption is known as the Ergode hypothesis. According to this hypothesis, the time means of various characters of the molecular chaos motion can be transformed directly into the area means in

the phase space. Thus, it becomes easy to survey the characteristics of the time means of a molecular chaos motion depending upon the Newton dynamics. Namely, when the random phenomenon is expressed in mathematical form and introduced into the fundamental equation, a definite system of statistical dynamics is formed.

As reviewed above, in statistical dynamics the purely statistical hypotheses were at first intermingled with those of dynamics, and the theoretical foundations were not necessarily definite. In present statistical dynamics, two principles of the Newton dynamics and the Ergode hypothesis adapted to the physical image of a molecular chaos motion have developed fruitful quantitative discussions. Since the success of statistical dynamics, such a statistical method of study has also been applied to the phenomenon of a chaotic motion of electrons. Quantum statistical dynamics has been developed from the above-mentioned point of view. It is important that classic or quantum statistical dynamics has not merely been examining the Hamilton-Jacobi or the Schrödinger equation in time means, as did previous studies of turbulent flow. The essential feature of the present statistical theory in physics is that the concept of an irregularity belonging to the phenomenon is also expressed mathematically and is introduced into the basis of the theory.

4. THE SIGNIFICANCE OF THE STATISTICAL THEORY OF TURBULENCE

As mentioned in Section 2, the Reynolds equations are certainly basic, necessary conditions in the statistical studies of turbulent flow, although they are not mathematically conclusive. In all successful studies of turbulent flow since Reynolds' time, insufficient physical principles not implied in the Reynolds equations have been properly compensated for by some assumptions concerning the mean characteristics of the turbulent agitating motion. This fact should not be overlooked. For instance, the assumption of the distribution of the mixing length in the turbulent shear flow or of the similrity preservation of the Euler correlation functions in the isotropic turbulence seems to verify the essential point of the mechanism of turbulent flow.

In these assumptions, however, it is difficult to find any unification as a general theory of turbulence. As for the velocity fluctuations themselves, some theoretical studies were developed in the field of the isotropic turbulence. Due to the development of a hot-wire technique, fine structures of the velocity fluctuations of nonisotropic turbulent flows have been clarified, but these recognitions of the mechanism of nonisotropic turbulent flows are not yet expressed definitely in mathematical formulas. Also, it seems unreasonable to extend the theory of isotropic turbulence to the case of turbulent shear flow. In other words, the physical principles which the Reynolds equations have lacked are not yet established in the form of a statistical theory of turbulence in general cases.

The derivation of the Reynolds equation from the Navier-Stokes equations corresponds to early statistical dynamics in which only the Newton dynamics in time means played a predominant role. The Navier-Stokes equations consist of two parts: the Newton dynamics applied to the continuous medium of a fluid, and Hooke's Law, which postulates the linear relation between the stress and strain of the medium. Physical meaning of the equations is easily comprehended, but the mathematical expressions are very complicated Therefore, the Reynolds equations are not mathematically conclusive, unlike early statistical dynamics The source of confusion arose at the same time that the statistical study of turbulent flow was opened.

On the other hand, the Reynolds equations, even if they are not in the state called "turbulent flow", are widely adaptable to flows which have definite values of velocity fluctuations. At present, necessary and sufficient physical concepts of "turbulent flow" are not generally expressed in mathematical formulae. Therefore, to give a clear physical image to "turbulent flow", it becomes necessary to give appropriate mathematical expressions to the Reynolds stress which has made the Reynolds equations mathematically inconclusive. By doing so, it may be possible to lay unifiable, necessary and sufficient foundations for statistical study of "turbulent flow".

If only the time means are definite, can all kinds of flow having velocity fluctuations be called "turbulent flow"? Many researchers may give negative answers. If so, what is "turbulent flow" and why does the velocity fluctuate?

On this problem, the following supposition has been supported by many researchers since Reynolds' time; namely, in "turbulent flow" the velocity fluctuations are caused by many parts of the fluid which make their respective rotating motions and are carried by the mean flow in an irregular arrangement. The above situations may be understood by such an observation of flow as shown in Figure 1 or 2. This type of fluid flow has usually been called an "eddy current". If the above-mentioned physical image were not kept in mind, the concept of the scale of turbulence could not be introduced. Furthermore, it is doubtful whether the Euler correlation or even the isotropic turbulence could be defined in the study of turbulent flow. Thus, the concept of an "eddy current" can be taken as the physical background of all the previous studies of turbulent flow. However, it is also true that this physical image has not been formulated into a definite mathematical expression.

In order to grasp the concept of an "eddy current", one must further clarify the hydrodynamical meaning of an "eddy". By observing the actual turbulent flow, especially by taking photographs of an instantaneous state of flow as shown in Figure 1 or 2, one can regard an "eddy" as a vortex motion of fluid. Also, the "eddy current" may be interpreted as the flow in which many vortices are carried in their chaotic states. Such

a physical image of the structure encompasses all sorts of "turbulent flows": those from a nozzle, along a wall, in a pipe, and others. At the same time, the "eddy current" cannot be adapted to "nonturbulent flows" with the velocity fluctuations such as the laminar boundary layer flow and others with a Tollmien unstable wave.

In the physical image of an "eddy current", the concept of the chaotic state of the arrangement of vortices is important. Many researchers do not consider the flow of regularly arranged vortices, such as the Kármán vortex streets, as "turbulent flow". The term "eddy", however, has recently become indistinct, and sometimes it may mean a wave number of the spectrum of velocity fluctuation. Therefore, in order to make clear the above-mentioned physical image, another term, "vortex chaos motion", will be used.

It is not the intention in this report to discuss the study of turbulent flow according to the progress of statistical physics mentioned in the last section. However, the assumption of a vortex chaos motion will be used as a foundation for the statistical studies of turbulence. The concept of a vortex chaos motion consists of the two basic parts of an individual vortex motion and of their irregular arrangements. For the former, fluid motion around the vortex filament should be determined from the hydrodynamical equations of motion. At the same time, the latter concept of an irregularity may not have a direct connection with hydrodynamics. If attention is given only to the irregular arrangement, this concept must have the same meaning as it does in the case of classic or quantum statistical dynamics.

It may be the concept of the Ergode hypothesis that will give a mathematical expression to the characteristic of irregularity in the physical image of a vortex chaos motion. As a matter of course, the physical image of a vortex chaos motion is different from that of a molecular or electronic chaos motion, and it is not appropriate to adapt Boltzmann's hypothesis in the phase space to the case of a vortex chaos motion. On the other hand, it is certain that the previous statistical studies of turbulence have lacked a definite formulation of the concept of irregularity, similar to statistical dynamics before Boltzmann. It is proposed that the fundamental concept of the Ergode hypothesis is also introduced to the statistical study of turbulence. Thus, the physical image of a vortex chaos motion may give unifiable interpretations to the mean states of velocity fluctuations, depending on the two principles of the hydrodynamics of a vortex motion and of the statistical physics of their irregular arrangements.

If the Navier-Stokes equations were solved exactly in the case of a vortex chaos motion, the statistical principle could be avoided. Until such a mathematical treatment is completed, the essential meaning of the Ergode hypothesis is necessary as a theoretical principle. From the above-mentioned point of view, an attempt will be made to propose such a statistical theory of turbulence in general cases that may include the

previous successful theories as special cases and may give some quantitative results to other fields beyond the scope of the previous theories. The purpose of this work, then, is to present general descriptions of a statistical theory of turbulence.

CHAPTER TWO. FUNDAMENTAL CHARACTER OF VORTEX CHAOS MOTION

5. FORMATION OF VORTEX CHAOS MOTION

Real turbulent flow can be interpreted as vortex chaos motion; however, before expressing mathematically the vortex chaos motion, in this chapter, some important physical characteristics will be related which will classify vortex chaos motion into fundamental groups. Generally speaking, vortex chaos motion is formed when a solid body is put into the flow of a fluid. At least one vortex motion is produced just behind the body. At standard Reynolds number values, this vortex is carried away from the body and a new vortex is produced again at the same location. These vortices, being produced and separated one after another just behind the body, keep a regular arrangement at first and then gradually become irregular along the flow. The term "vortex chaos motion" refers to such an irregular arrangement of vortices and Figure 1 shows the transient condition of vortex chaos motion.

This transition phenomenon will be surveyed in detail for a typical case of a circular cylinder in uniform flow. Records of velocity fluctuations indicate generally regular wave forms just behind the cylinder, but at a distance from the cylinder they tend to become irregular. Some examples of these records are shown in Figures 4 and 5. When observations are made in water, it can be seen that, at first, vortices produced just behind a cylinder separate one after another and form a regular arrangement of Kármán vortex streets. Although these regular arrangements are retained, the Kármán vortex streets tend to be broken into an irregular chaotic state along the flow.

The physical mechanism of the formation of a vortex motion has not been clarified, not to mention the mathematical condition. Owing to many observations, however, the production of a vortex motion cannot be imagined in the case of a nonviscous flow, i.e., in the case where the momentum of the flow does not transfer across the flow. It is certain that the viscosity due to molecular or turbulent agitating motion plays an essential role in producing a vortex motion.

Moreover, concerning the transition phenomenon from a regular to an irregular arrangement of vortices, definite interpretations have not been given, depending upon the hydrodynamical equations of motion. If the following supposition is allowed, the transition may be made as follows: at first, the laminar boundary layer separates from a circular cylinder since it is unable to resist the adverse pressure gradient, and the separated laminar boundary layers are curled into two vortex motions at symmetrical positions just behind the cylinder. This unstable symmetrical arrangement of the two vortices is easily broken by disturbances contained in the main flow, and the vortices are diverted into the flow one after another. In these diverted vortices, molecular viscosity at first affects only the narrow region around each vortex center, so that the vortices are arranged

into the pattern of stable Kármán vortex streets. As the regions affected by viscosity expand along the flow, their actions on each other produce three-dimensional disturbances. Thus, since the Kármán vortex streets are proved to be neutrally stable in a nonviscous fluid, this flow pattern is easily broken and the arrangement of vortices changes gradually into an irregular one.

From the above interpretation, it may be concluded that in vortex chaos motion the viscosity of every vortex constantly affects other vortices near by. When two vortices with the same direction of circulation draw near, it is assumed that a new vortex is produced between them by taking some parts of their energy by viscosity, just as the primary vortex is produced by taking energy from the main flow by the viscosity in the boundary layer around a body. These new vortices may produce further small vortices in the same way, and a sort of cascade phenomenon can be presumed. Of course, there may be a chance that a primary and a new vortex will bring out a third one, and the cascade phenomenon in vortex chaos motion presents a very complicated situation. In the actual turbulent flow, the existence of newly created vortices, other than those of the primary vortices, has seldom been observed. It is more natural, however, to consider that the vortex chaos motion inevitably accompanies the cascade phenomenon, rather than to assume that the vortex chaos motion consists only of the primary vortices. In other words, in turbulent flow, chaotic motions of all these vortices produce velocity fluctuations everywhere in the field of flow.

6. TURBULENT FLOW OF A DECAYING CHARACTER

In turbulent flow, vortex chaos motion usually comprises many types of vortices depending upon the means of generation; however, the vortex chaos motion may be divided generally into two fundamental types. One is the wake flow behind a lattice or body or the jet from a mouth of a pipe, and the other is the boundary layer or pipe flow.

In the case of the turbulent wake or jet where the obstacle which produces the primary vortices is located at one position along the flow, the energy of the main flow is transmitted into vortices at only one place in the field. Although the cascade phenomenon is taken into account, small new vortices are produced from part of the energy of the ascending vortices. Therefore, the energy contained in the individual vortices decreases along the flow. The quantitative relation between the energy of vortex motion and the turbulent intensity at a point in the field of flow will be clarified later. However, in the case of the turbulent wake or jet, an important characteristic is that turbulent intensity decays inevitably along the flow. An example of the data in this case is shown in Figure 6.

In the case of the wake or jet, even if individual vortices and the conditions of their mixture depend on the pressure gradient along the flow and other factors, the origin of turbulent energy lies in the primary vortices and is transmitted to the small descending vortices along the flow.

Thus, the effect of the primary vortices may be succeeded by the descending ones along the flow, and this case will be called "decaying turbulent flow".

In decaying turbulent flow, consider a special case of flow behind a uniform lattice put across the main flow. Just behind the lattice, some regularity remains in the arrangement of the vortices produced from the rods of the lattice. As in the case of a circular cylinder, the mutual disturbance of these vortices becomes large along the flow. In this case, however, the breadth of the range of the whole chaos motion is far wider than the scale of the individual vortices in the flow, so that all the vortices become mixed completely with no observable regularity in the effect of their interaction. This fact may be comprehended by the observed results behind a two-dimensional lattice shown in Figure 1. It may be concluded, then, that in a turbulent field behind a lattice, the primary vortices and their descending vortices are all carried in their completely irregular state.

Thus, velocity fluctuation at a point downstream from a lattice is due to the independent and irregular causes of vortex motion. Furthermore, although many kinds of vortices pass near this point, their mean characteristics are definite. It is generally proved by the Gaussian central-limit theorem that when a fluctuating event occurs because of some causes of independent irregularity, but with definite mean characteristics, the probability distribution of this event obeys the Gaussian distribution function. The decaying turbulent flow behind a lattice is an example of this case. Examples of observed results on the probability distribution are shown in Figures 7, 8, and 9.

Situations of the velocity fluctuation behind a circular cylinder are considered in Section 5. In this case, even if the Kármán vortex streets tend to be irregular, it cannot be assumed that a vortex motion is affected uniformly from all directions by other vortices, as in the case of a lattice. A vortex carried on one side of the Kármán vortex streets is affected chiefly by the vortices of the other side, even though they are in a chaotic state. Therefore, it is difficult to mix into a completely irregular state just as in the case of flow behind a lattice. Such a situation is generally true in the case of the wake behind a body or of the jet from a pipe.

The descending small vortices produced through the cascade process may tend, even in the case of a wake or jet, to become completely irregular, being affected uniformly by the surrounding vortices because their dimensions are far smaller than the whole dimension of the vortex chaos motion, as are the primary vortices in the case of a lattice flow. Since some regularity remains in the primary vortices of high energy, the velocity fluctuation at a point in the field is due not entirely to independent causes for a particular time. Thus, unlike the case of a lattice flow, the central-limit theorem does not hold, and the probability distribution should differ somewhat from the Gaussian function.

From the above discussion, it may be concluded that when the breadth of a vortex chaos motion is far wider than the mean scale length of the individual vortices, the chaotic state of their arrangement becomes completely irregular; but when the whole breadth is comparable with the individual scale length, some regularity remains in their chaotic state. In the latter case, the regularity produces some nonzero values in $\overline{uv}$ and similar components of the velocity fluctuation at a point in the field which affects the turbulent shearing stress, giving distortion to the mean-velocity profile; the flow represents that which is called "turbulent shear flow". Thus, the decaying turbulent flow can be divided into two types, which shall be called "shear turbulent flow" of a wake behind a body or jet, and "shearless turbulent flow" behind a lattice.

7. VISCOUS SUBLAYER NEAR THE WALL

In the case of turbulent flow in a boundary layer or pipe, it is appropriate to regard the vortex chaos motion as consisting of many kinds of vortices rather than a single kind as in the case of the decaying turbulent flow. However, the circumstances of the production of vortices are entirely different from the decaying turbulent flow. When a fluid flows along a wall or a body, a laminar boundary layer is always formed from the forward stagnation point under an ordinary Reynolds number. Sometimes it separates from the body as it is. In many cases, however, the laminar boundary layer is broken into a turbulent state before the separation, and a turbulent boundary layer is still developed along the wall.

The mechanism of transition from a laminar to a turbulent boundary layer is not yet clearly comprehended. However, if the flow does not disturb the laminar boundary layer, the transition cannot be imagined before the boundary layer separates. From hot-wire observations, it is ascertained in the laminar boundary layer that the characteristic velocity fluctuation, which is known as the laminar oscillation, gradually grows along the flow. Figure 10 is an example of such an observation. Moreover, it is well known that when the main stream disturbances are small, the laminar oscillation has the same characteristics as the Tollmien-Schlichting unstable wave predicted by the linearized Orr-Sommerfeld equation of the unsteady laminar boundary layer. An example of observations in this case is shown in Figure 11.

This growing laminar oscillation, whether it is the Tollmien-Schlichting wave or not, seems to bring forth a vortex motion in the boundary layer. The interpretation of an instantaneous separation of the laminar boundary layer by the growing oscillation may be taken as one of the causes of a vortex motion. Although a definite verification on the instantaneous laminar separation is not available, it is observed that the laminar boundary layer, which does not separate as does the steady flow, abruptly brings forth a vortex motion. Figure 12 shows

such a situation of the outbreak of a vortex motion in a laminar boundary layer. When the laminar boundary layer oscillations are recorded at the region of transition, an intermittent high-frequency oscillation is usually perceived as shown in Figure 13. Its appearance also seems to indicate the outbreak of a vortex motion in the boundary layer.

When transition occurs, the laminar boundary layer loses the original meaning. However, when the vortices produced by transition do not separate from the body and a main flow still exists along the wall, it is generally supposed that due to the effect of molecular chaos motion that molecular viscosity exists in the immediate vicinity of the wall. In this case, just above the region of molecular viscosity, strong vortices produced by the transition are carried along, and they contribute great disturbances to this part. Thus, before growing into the normal state of a laminar boundary layer, the viscosity part is broken again and produces strong vortices. Such production of vortices will be repeated along the wall, and molecular viscosity is maintained as a very thin layer along the wall. Once transition has occurred in the laminar boundary layer, a kind of viscous layer, which cannot become an ordinary laminar boundary layer, remains, bringing out strong vortices successively along the wall. In Section 1, the existence of the stability limit is expressed by the Reynolds number of the order 10^2, where all the disturbances of the flow are decayed by the effect of viscosity. Within this extremely thin layer corresponding to this value of the Reynolds number of stability, the effect of molecular viscosity must be predominant. The above-mentioned condition is the previously proposed interpretation of the so-called laminar sublayer (reference 21). Although the state of flow in this layer is greatly influenced by the effect of viscosity, there are also large velocity fluctuations; and to avoid a misunderstanding, the term "viscous sublayer" will be used. Figure 14 shows an experimental result in the immediate vicinity of the wall in a turbulent boundary layer. Because of the rapid reduction of the fluctuations and mean velocity very near the wall and the decreasing of high-frequency fluctuations, the existence of the viscous sublayer may be ascertained.

Because the viscous sublayer is extremely thin, as shown in Figure 14, precise measurements are difficult and characteristics of this layer still remain unknown. However, the production of vortices from the wall can be clearly observed everywhere along the flow (reference 23). In the case of turbulent flow in a pipe, the observations are essentially the same as in the case of boundary layer flow. In other words, after the transition of the laminar boundary layer from the inlet of the pipe, the viscous sublayer is developed generating strong vortices along the inner wall. Such a condition may be understood by the observed result in Figure 2.

8. TURBULENT FLOW OF NONDECAYING CHARACTER

In the case of turbulent flow along a wall or in a pipe, discussions

in many cases are made concerning the region far downstream from the place of transition. In this region, all sorts of vortices produced upstream are carried in chaotic state. In the case of decaying turbulent flow, only the primary vortices are produced, receiving the energy of the main flow directly, and the descending vortices are produced from some of the energy of the ascending ones. The cascade phenomena, similar to that which might occur in a decaying turbulent flow, may also exist in the case of turbulent flow along a wall. Since the primary vortices of the same order of intensity are produced constantly along the wall, the effects of the descending vortices are far smaller than in the case of decaying turbulent flow. Vortices produced at a point are affected instantly by the primary vortices produced upstream from this point, and the velocity is influenced constantly by all primary vortices produced upstream. As the fluid goes down along the wall, the state of the turbulent flow is affected by the local characteristics of the newly produced primary vortices, and the upstream history of the flow is forgotten. This is an essentially different feature from the decaying turbulent flow in which the history of the primary vortices is succeeded by the descending vortices one after another. Thus, it is thought that the vortex chaos motion in the real turbulent flow should be divided at first into these two groups.

The kinetic energy of the primary vortices produced by the effect of the viscous sublayer may depend upon the pressure distribution along the flow, the roughness of the wall, and many other factors. However, since the primary vortices are produced along the wall, each with considerable energy, the intensity of the velocity fluctuation does not necessarily decay along the flow. This essential difference from the decaying turbulent flow can be easily detected by experimental observations. When the observed results shown in Figure 15 are compared with those in Figure 6, the difference between the two cases is clearly seen. This case will be called the "nondecaying turbulent flow".

All the vortices produced upstream from a fixed point in the nondecaying turbulent flow are carried nearby. With the exception of the low-energy descending vortices which were produced through the cascade process, the production of the primary vortices is entirely attributed to the effect of the viscous sublayer which exists only on the wall along the main flow, and the breadth of all the vortex chaos motion is not much wider than the width of the individual vortices. Therefore, it cannot be assumed that the effects of these vortices on a fixed point are completely random regardless of the direction of the field of flow. Similar to the decaying turbulent flow of a wake or jet, some regularity remains in the chaotic state, at least with the primary vortices having high energy. This characteristic may be observed in Figure 2. Because of some regularity in the arrangement of vortices, the nondecaying turbulent flow may be called shear turbulent flow. However, it must be realized that the nondecaying turbulent flow has a more essentially different mechanism from the decaying turbulent flow than the difference between

the shear and shearless turbulent flow in the case of the decaying turbulent flow.

As a matter of course, existence of some regularity produces nonzero values in the Reynolds shearing stress, causing further deviation of the mean-velocity profile. Namely, when the probability distributions of velocity are measured, they do not indicate the Gaussian distribution function as shown in Figures 16 and 17.

Thus, because of the above discussions on the fundamental mechanism of vortex chaos motion, the real turbulent flow may be systematized as follows:

A. Decaying turbulent flow
   1. Shearless turbulent flow
   2. Shear turbulent flow
B. Nondecaying (shear) turbulent flow

In the next chapter, fundamental mathematical expressions of the general vortex chaos motion will be given, and in the following chapters, quantitative discussions will proceed case by case according to these classifications of turbulent flow.

CHAPTER THREE. STATISTICAL DESCRIPTION OF VORTEX CHAOS MOTION

9. THE REYNOLDS EQUATIONS

For the case of a fluid with a constant density and temperature, the following equations of motion are given by Navier and Stokes (reference 25):

$$\rho\frac{\partial U}{\partial t} = \frac{\partial}{\partial x}(\sigma_x - \rho U^2) + \frac{\partial}{\partial y}(\tau_{xy} - \rho UV) + \frac{\partial}{\partial z}(\tau_{zx} - \rho UW),$$

$$\rho\frac{\partial V}{\partial t} = \frac{\partial}{\partial x}(\tau_{xy} - \rho UV) + \frac{\partial}{\partial y}(\sigma_y - \rho V^2) + \frac{\partial}{\partial z}(\tau_{yz} - \rho VW),$$

$$\rho\frac{\partial W}{\partial t} = \frac{\partial}{\partial x}(\tau_{zx} - \rho UW) + \frac{\partial}{\partial y}(\tau_{yz} - \rho VW) + \frac{\partial}{\partial z}(\sigma_z - \rho W^2),$$

$$\frac{\partial U}{\partial x} + \frac{\partial V}{\partial y} + \frac{\partial W}{\partial z} = 0,$$

$$\sigma_x = -p + 2\mu\frac{\partial U}{\partial x}, \qquad \sigma_y = -p + 2\mu\frac{\partial V}{\partial y}, \qquad \sigma_z = -p + 2\mu\frac{\partial W}{\partial z},$$

$$\tau_{yz} = \frac{\partial W}{\partial y} + \frac{\partial V}{\partial z}, \qquad \tau_{zx} = \frac{\partial U}{\partial z} + \frac{\partial W}{\partial x}, \qquad \tau_{xy} = \frac{\partial V}{\partial x} + \frac{\partial U}{\partial y}. \tag{9.1}$$

In equation (9.1) t is the time; x, y, and z are Cartesian coordinates in the field of flow; U, V, and W are velocity components of the x, y, and z direction, respectively; P is the static pressure, and μ is the coefficient of viscosity.

When the viscous terms multiplied by μ are neglected, the Navier-Stokes equations (9.1) become the Euler equations of a perfect fluid in which the Newton dynamics are applied to the continuous medium of a fluid by neglecting higher order terms in the Taylor expansions. As for the viscosity coefficient, μ, it is assumed by Hooke's law to be constant in the field of flow. Depending upon the statistical dynamics of gas, μ is expressed by the product of the mean velocity, the mean free path, and the density of the molecules. Therefore, at a position which is further from the wall than the length of a mean free path, the three quantities may be assumed to be constant, and Hooke's law can be adapted. It is fortunate for hydrodynamics, whose equations of motion are expressed in (9.1), that the mean free path of a gas at standard temperature has a length of the order of 10^{-5} centimeters and is far smaller than a macroscopic standard length in the field of flow.

In spite of many neglected terms in deriving the equations, one can

find no experimental evidence that the Navier-Stokes equations are inadequate to describe the real motion of a fluid. As mentioned in Chapter One, the chaotic motion in a turbulent flow has a macroscopic scale far larger than does the molecular chaos motion of gas. Even if it is mathematically difficult to prove, the Navier-Stokes equations are assumed to hold accurately in the actual state of turbulent flow.

When velocity fluctuations exist in the field of flow, velocity components at a point are written by dividing them into the mean and fluctuational parts,

$$U=\bar{U}+u, \qquad V=\bar{V}+v, \qquad W=\bar{W}+w, \tag{9.2}$$

where

$$\bar{U}=\lim_{t\to\infty}\left(\frac{1}{t}\int_{t'}^{t'+t} U\,dt\right), \quad \bar{V}=\lim_{t\to\infty}\left(\frac{1}{t}\int_{t'}^{t'+t} V\,dt\right), \quad \bar{W}=\lim_{t\to\infty}\left(\frac{1}{t}\int_{t'}^{t'+t} W\,dt\right). \tag{9.3}$$

In the above expressions, the limiting values of $\bar{U}$, $\bar{V}$, and $\bar{W}$ are assumed to be definite independently of the value of a starting time, t', of the integration. Hereafter, all the mathematical discussions will be based upon this assumption of the existence of definite mean values. For simplicity of description, t' is often replaced by 0, and sometimes mean values are denoted only by using the notation of a bar.

By expressions (9.2) and (9.3) it is easily proved that

$$\bar{u}=\bar{v}=\bar{w}=0, \tag{9.4}$$

and the mean values of their products,

$$\overline{u^2}=\lim_{t\to\infty}\left(\frac{1}{t}\int_0^t u^2\,dt\right), \quad \overline{v^2}=\lim_{t\to\infty}\left(\frac{1}{t}\int_0^t v^2\,dt\right), \quad \overline{w^2}=\lim_{t\to\infty}\left(\frac{1}{t}\int_0^t w^2\,dt\right),$$

$$\overline{vw}=\lim_{t\to\infty}\left(\frac{1}{t}\int_0^t vw\,dt\right), \quad \overline{wu}=\lim_{t\to\infty}\left(\frac{1}{t}\int_0^t wu\,dt\right), \quad \overline{uv}=\lim_{t\to\infty}\left(\frac{1}{t}\int_0^t uv\,dt\right), \tag{9.5}$$

do not necessarily vanish with definite values. For simplicity of expression, the root-mean-square values of $\sqrt{\overline{u^2}}$, $\sqrt{\overline{v^2}}$, and $\sqrt{\overline{w^2}}$ will be denoted by the Gothic letters $\mathfrak{u}$, $\mathfrak{v}$, and $\mathfrak{w}$.

When expressions (9.2) are substituted in the Navier-Stokes equations (9.1) and time means are taken, the equations can be written as

$$\rho\frac{d\bar{U}}{dt}=\frac{\partial}{\partial x}(\bar{\sigma}_x-\bar{U}^2)+\frac{\partial}{\partial y}(\bar{\tau}_{xy}-\bar{U}\bar{V})+\frac{\partial}{\partial z}(\bar{\tau}_{zx}-\bar{U}\bar{W}),$$

$$\rho\frac{d\bar{V}}{dt}=\frac{\partial}{\partial x}(\bar{\tau}_{xy}-\bar{U}\bar{V})+\frac{\partial}{\partial y}(\bar{\sigma}_y-\bar{V}^2)+\frac{\partial}{\partial z}(\bar{\tau}_{yz}-\bar{V}\bar{W}),$$

$$\rho\frac{d\bar{W}}{dt}=\frac{\partial}{\partial x}(\bar{\tau}_{zx}-\bar{U}\bar{W})+\frac{\partial}{\partial y}(\bar{\tau}_{yz}-\bar{V}\bar{W})+\frac{\partial}{\partial z}(\bar{\sigma}_z-\bar{W}^2),$$

$$\frac{\partial\bar{U}}{\partial x}+\frac{\partial\bar{V}}{\partial y}+\frac{\partial\bar{W}}{\partial z}=0,$$

$$\bar{\sigma}_x=-\bar{p}+2\mu\frac{\partial\bar{U}}{\partial x}-\rho\overline{u^2},\quad \bar{\sigma}_y=-\bar{p}+2\mu\frac{\partial\bar{V}}{\partial y}-\rho\overline{v^2},\quad \bar{\sigma}_z=-\bar{p}+2\mu\frac{\partial\bar{W}}{\partial z}-\rho\overline{w^2},$$

$$\bar{\tau}_{yz}=\mu\left(\frac{\partial\bar{W}}{\partial y}+\frac{\partial\bar{V}}{\partial z}\right)-\rho\overline{vw},\quad \bar{\tau}_{zx}=\mu\left(\frac{\partial\bar{V}}{\partial z}+\frac{\partial\bar{W}}{\partial x}\right)-\rho\overline{wu},$$

$$\bar{\tau}_{xy}=\mu\left(\frac{\partial\bar{V}}{\partial x}+\frac{\partial\bar{U}}{\partial y}\right)-\rho\overline{uv}\ .$$

(9.6)

In equation (9.6) $d\bar{U}/dt$ indicates that the mean velocity $\bar{U}$ may gradually change for a far longer scale of time than the time interval t in expressions (9.3). If the components of the tensor expression

$$\begin{pmatrix} -\overline{u^2}, & -\overline{uv}, & -\overline{uw} \\ -\overline{vu}, & -\overline{v^2}, & -\overline{vw} \\ -\overline{wu}, & -\overline{wv}, & -\overline{w^2} \end{pmatrix} \tag{9.7}$$

are added to the respective components of viscous stress in equations (9.1), equations (9.6) have the same mathematical expressions as (9.1). Equations (9.6) and expression (9.7) are known as the Reynolds equations and the Reynolds stress, respectively (reference 26).

The assumption of the existence of mean values which has been the foundation of expression (9.3) or (9.4) can be adapted widely to the real state of turbulent flow. Thus, the statistical study in which only the mean values are discussed has an important meaning in the study of turbulent flow. The Reynolds equations derived from the Navier-Stokes equations based upon the assumption of existence of mean values can be regarded as necessary conditions to determine mean values for the time of fluctuating motion of turbulent flow. In addition to the turbulent flow, however, there are many cases of unsteady flows in which the assumption of the existence of mean values can be adapted; for example, flow patterns of the

Kármán vortex streets behind a body and of the Tollmien-Schlichting oscillations in a laminar boundary layer. Therefore, the Reynolds equations cannot be regarded as the necessary and sufficient conditions to prescribe the mean state of turbulent flow. It is significant that the Reynolds stress, newly derived from the nonlinear terms when time means are taken, makes the Reynolds equations mathematically inconclusive. As mentioned in Chapter One, the cause of confusion arose when the statistical study of turbulent flow was opened.

10. COEFFICIENTS OF THE EULER CORRELATION

The value of the Reynolds stress in expression (9.7) depends largely upon the amplitude of velocity fluctuation and is regarded as a statistical quantity of the intensity of turbulent flow. The Reynolds equations are necessary conditions relating the turbulent intensity and mean velocity. As mentioned in Chapter One, there is another fundamental quantity of turbulent scale. Since formulas (9.6) and (9.7) are not concerned with this quantity, another statistical expression of turbulent scale must be established.

Letting u, v, and w and u', v', and w' be components of velocity fluctuations at two points A and A', respectively, and having coordinates x, y, and z and x', y', and z' in the field of flow, one can define the following tensor expression of the correlation coefficients:

$$\begin{pmatrix} \overline{uu'}, & \overline{uv'}, & \overline{uw'} \\ \overline{vu'}, & \overline{vv'}, & \overline{vw} \\ \overline{wu'}, & \overline{wv'}, & \overline{ww'} \end{pmatrix} = K. \qquad (10.1)$$

If the A'-point coincides with the A-point, every numerator of the component of (10.1) becomes every component of (9.7) of the Reynolds stress. In the turbulent state of flow, velocity fluctuation is generally a continuous function of the time and location. Even if the A'-point is slightly apart from the A-point, the patterns of velocity fluctuation are similar (cf. Figure 3), and the component of (10.1) does not necessarily vanish. However, when the A'-point is at a greater distance from the A-point, there will be no interrelation between the two velocity fluctuations, and all the components of (10.1) become zero. When the components of (10.1) are regarded as functions of the distance between the two points, the value of (10.1) may be regarded as a statistical quantity signifying the scale of fluctuating motion of turbulent flow. Expression (10.1) is introduced by Taylor (reference 13) as an extended formula of (9.7) of the Reynolds stress and is known as the Euler correlation.

According to the mathematical definition of the correlation

coefficient, (10.1) is a double correlation. If necessary, the triple correlation at two points and the i-th correlation at N points can be defined. Viewed mathematically, they are related to point probability which can be defined, based upon the assumption of the existence of mean values mentioned in the last section. Physically they signify details of the characteristics of the turbulent scale.

The tensor formula of the Euler correlation coefficients (10.1) is a general statistical expression of the two fundamental quantities of intensity and scale of fluctuating motion of fluid. However, the expression (10.1) holds not only for turbulent flow but for many other unsteady flows with definite mean values. The definition of (10.1) cannot be said to compensate for the Reynolds equations, which are the necessary conditions in the study of turbulent flow.

11. PROBABILITY-DENSITY FUNCTION IN VORTEX CHAOS MOTION

There are many kinds of unsteady flow to which the formulas in Sections 9 and 10 can be adapted. In order to establish a conclusive statistical theory of turbulent flow, however, it is necessary to distinguish the physical image of turbulent flow from the general case of unsteady flows. Then, depending upon this image, the components of the Euler correlation (10.1) or the Reynolds stress (9.7) must be expressed as functions of the location in the field of flow. Thus, combined with these formulas, the Reynolds equations (9.6) may give necessary and sufficient theoretical foundations for a general statistical description of turbulent flow.

The interpretation of a vortex chaos motion mentioned in the previous chapters will be taken as the mechanism of turbulent flow. In any case of turbulent flow, whether the decaying or the nondecaying turbulent flow, it is certain that many kinds of vortices are carried by the mean flow in an irregular motion, and that these vortices bring forth velocity fluctuations at every point in the field of flow.

In the above-mentioned physical image, a vortex motion means the state of the turning movement of part of a fluid around a linear part called the vortex filament. The characteristics of an individual vortex motion, the states of the vortex filament and the distribution of the turning velocity around the filament, may be observed. However, the vortex motion is a phenomenon of fluid motion and has no definite boundary as a rigid body.

In the turbulent state of flow, these vortices are carried in a chaotic state with constant interactions along the flow. Lengths, directions, curvatures, and relative locations of vortex filaments change while they are being carried away. For the situation of turning velocity, there are many kinds of intensity and scale. In this section, as the first step in deducing a statistical description of this physical image, a

probability-density function concerned chiefly with the flow of vortex filaments will be introduced.

Let a fixed point in the field of flow be called the A-point for convenience of explanation. In Cartesian coordinates x, y, and z in the field of flow, the x-axis is taken parallel to the direction of the mean flow through the A-point. With an increasing time t beginning at a fixed time t', the above-mentioned vortex chaos motion will be imagined near the A-point.

At the beginning time t', if perpendiculars are drawn from the A-point to vortex filaments nearby, definite intersections are determined in the field of flow. Among many vortex filaments, the nearest filament that has the shortest distance between the A-point and the intersection can be pointed out.

With an increasing time t, the nearest vortex filament at the beginning time t' moves near the A-point, varying the inclination, curvature and other characteristics. The perpendicular drawn from the A-point at the time t' moves, and the intersection forms a continuous curve in the xyz-space. After the nearest vortex filament at t' is carried away from the A-point, another filament comes into the nearest proximity of the A-point. An alternation of the nearest filament is repeated successively with an increasing time t. Thus, for an extended time t, the intersections of perpendiculars from the A-point to the nearest vortex filaments trace many kinds of three-dimensional curves in the xyz-space (cf. Figure 18).

Another characteristic of a vortex motion is the distribution of turning velocity. At the beginning time t', one perpendicular plane to the nearest vortex filament can include the A-point. The curvature, the elongation of the filament, and the effects of other vortices near the intersection of the nearest filament will be neglected. Then, the turning velocity of this two-dimensional vortex in the perpendicular plane is distributed around the intersection. Therefore, at the A-point a turning velocity of this vortex in the perpendicular plane is determined. This turning velocity is denoted by the following vector with the magnitude V*,

$$\boldsymbol{V}^{*}. \qquad (11.1)$$

The x'-, y'-, and z'-axes from the A-point will be taken, respectively, parallel to the x-, y-, and z-axes. The angles between $\boldsymbol{V}^{*}$ and the z'-axis, between the orthogonal projection of $\boldsymbol{V}^{*}$ to the x'y'-plane and the x'-axis are denoted, respectively, by ϕ and θ ; and the distance from the A-point to the nearest vortex filament is r (cf. Figure 19). Then, regardless of the type of vortex chaos motion, the quantities r, θ, and ϕ are determined uniquely at the beginning time t'. With an increasing time t, they are expressed as functions of t:

$$r(t), \quad \theta(t), \quad \phi(t). \tag{11.2}$$

Although the variables of (11.2) are continuous functions of t as long as the reference vortex remains at the nearest distance from the A-point, they vary discontinuously for long periods corresponding to the loci of the nearest intersections as shown in Figure 18.

Now, another set of Cartesian coordinates x*, y* and z* will be taken apart from the field of flow, and the variables of (11.2) will be considered as the movement of one point in the x*y*z*-space. Such an A*-point will be taken whose coordinates may be decided uniquely by the variables of (11.2) and whose motion in the x*y*z*-space may uniformly correspond to the motion of (11.2) in the r, θ, ϕ-space, as the polar coordinates shown in Figure 20. Then, the A*-point moves about in the x*y*z*-space discontinuously for long periods corresponding to the movements of the intersections in the xyz-space shown in Figure 18.

In a vortex chaos motion where many vortices are carried irregularly one after another, the value of r for the distance between the A-point and the nearest vortex filament is incapable of attaining an infinite value. The movement of the A*-point is also limited in a domain of a finite distance from the origin. Such a domain D* of finite area around the origin that contains all the loci of the A*-point in the time interval between t' and t'+t will be taken as shown in Figure 20.

For the movement of intersections of the perpendiculars from the A-point to the nearest vortex filaments in the field of flow, the parts before and after the time intervals when the filaments are in the nearest relation to the A-point (cf. Figure 18) will be considered. If such excess parts of the loci of the intersection in the field of flow are taken so that the A*-point may always move from end to end on one boundary of the D*-domain, then the movement of the A*-point in the D*-domain has some excessively repeated parts of time interval in the actual state of flow. When the total sum of the excess time in the actual time interval between t' and t' + t is denoted by Δ t, the movement of the A*-point is shown by a group of loci which are drawn in the time interval t*,

$$t^* = t + \Delta t. \tag{11.3}$$

In the D*-domain, a part domain having an infinitesimal volume dQ* around a fixed point (r, θ, ϕ) is taken. By letting the total sum of the infinitesimal time intervals when the A*-point passes through this part domain be denoted by

$$dt^*(r, \theta, \phi), \tag{11.4}$$

the following limiting value,

$$P^*(r,\theta,\phi)\,dQ^* = \lim_{t\to\infty}\{dt^*(r,\theta,\phi)/t^*\}, \tag{11.5}$$

can be determined. Of course, as in the case of the Reynolds equations, the limiting value in (11.5) is assumed to be determined definitely independent of the beginning time t'. For brevity, t' shall be replaced by 0 hereafter.

P* defined by (11.5) can be regarded as a function of r, θ, and ϕ in the D*-domain. It has the dimension of an inverse of volume, and the relation

$$\iiint_{D^*} P^*(r,\theta,\phi)\,dQ^* = 1 \tag{11.6}$$

holds. Clearly, P* (r, θ, ϕ) is a probability-density function by which the frequency of the existence of the A*-point is expressed in the D*-domain.

In the case of an ideal two-dimensional vortex chaos motion with all the vortex filaments parallel to the z-axis, motions of the nearest vortex centers from the A-point on the xy-plane can be expressed by the movements of the A*-point in the x*y*-plane which is taken in the same manner as in the three-dimensional case. When a two-dimensional D*-domain is taken to include all the loci of the A*-point and an infinitesimal part domain is fixed around the r, θ-point, then the quantities Δt, dQ* and dt* can be defined in the same manner, so that dQ* is an infinitesimal area in this case. Thus, the following two-dimensional probability-density function can be defined as

$$P^*(r,\theta)\,dQ^* = \lim_{t\to\infty}\{dt^*(r,\theta)/dt^*\}, \tag{11.5'}$$

with the relation

$$\iint_{D^*} P^*(r,\theta)\,dQ^* = 1. \tag{11.6'}$$

In actual turbulent flow, the vortex filaments and the turning velocity are in very complicated situations. If the concept of a vortex chaos motion is adapted, however, the P*-function of (11.5) can be defined. In the course of defining the function P*, the vector **V*** is taken as a characteristic only of the nearest vortex, and the effects of other vortices are not considered. It is another problem whether the actual instantaneous velocity fluctuation at the A-point may be equal to **V***. At this stage of the introduction of the P*-function, there is no need to distinguish between large and small or strong and weak vortices. The P*-

function can be defined only if many vortices with their respective filaments and turning velocities pass one after another near the A-point. The introduction of the P*-function is made only because it may play a convenient role in proceeding hereafter to the mathematical formulations of the statistical characters of a vortex chaos motion. In the study of a gas, quantitative discussions are made in the phase space, which is defined by the generalized location and momentum of molecules. The D*-domain may correspond to the phase space in statistical dynamics.

12. TRANSFORMATION OF TIME MEANS INTO AREA MEANS

In this section, transformation of the time means of the Reynolds stress (9.5) or the Euler correlation (10.1) into the area means in the D*-domain will be attempted by using the P*-function introduced in the last section. As an example, the u^2-component,

$$\overline{u^2} = \lim_{t\to\infty}\left(\frac{1}{t}\int_0^t u^2\,dt\right), \tag{12.1}$$

of the Reynolds stress is taken. The D*-domain is defined so that the nearest vortices pass near the A-point without interruption in a time interval $0\sim t$, although many excessively repeated time intervals may be included in $0\sim t^*$. Now a function $u_1^2(t)$ is introduced in $0\sim t^*$ that is equal to $u^2(t)$ in $0\sim t$ and is equal in Δt to the mean value of $u^2(t)$ during the time interval $0\sim t$:

$$u_1^2(t) = \begin{cases} u^2(t) & \text{in} \quad 0\sim t, \\ \dfrac{1}{t}\displaystyle\int_0^t u^2(t)\,dt & \text{in} \quad \Delta t. \end{cases} \tag{12.2}$$

Then the relation

$$\frac{1}{t^*}\int_0^{t^*} u_1^2(t)\,dt = \frac{1}{t}\int_0^t u^2(t)\,dt \tag{12.3}$$

can be easily proved. When the time progress in $0\sim t$ in the integration of (12.1) is indicated by the movement of the A*-point in the D*-domain, (12.1) is written as

$$\overline{u^2} = \lim_{t\to\infty}\left\{\frac{1}{t^*}\int_0^{t^*} u_1^2(r(t),\theta(t),\phi(t),t)\,dt\right\}. \tag{12.4}$$

In the expression (12.4), the variables r(t), θ(t), and ϕ(t) indicate the movement of the A*-point in the D*-domain, and the existence of the last variable t means that at different times u_1^2 does not necessarily take the same value even at the same location in the D*-domain.

In the integration of (12.4) in the time interval $0 \sim t^*$, when $\bar{u}^2(r, \theta, \phi)$ is taken as the contribution to $\bar{u}^2$ in the infinitesimal time interval $dt^*(r, \theta, \phi)$ of (11.4), it can be expressed as

$$\bar{u}^2(r,\theta,\phi) = \lim_{t\to\infty}\left\{\frac{1}{t^*}\int_{dt^*(r,\theta,\phi)} u_1^2(r,\theta,\phi,t)\,dt\right\}. \tag{12.5}$$

In expression (12.5), $u_1(r, \theta, \phi, t)$ is written as

$$u_1(r,\theta,\phi,t) = \bar{u}_1(r,\theta,\phi,dt^*(r,\theta,\phi)) + u_1'(r,\theta,\phi,t), \tag{12.6}$$

divided into the mean and fluctuational parts in the time interval $dt^*(r, \theta, \phi)$. The mean-square value of the fluctuational part is written as

$$\bar{u}_1'^2(r,\theta,\phi,dt^*(r,\theta,\phi)) = \frac{1}{dt^*(r,\theta,\phi)}\int_{dt^*(r,\theta,\phi)} u_1'^2(r,\theta,\phi,t)\,dt. \tag{12.7}$$

Then, $\bar{u}^2(r, \theta, \phi)$ in (12.5) is transformed as follows:

$$\bar{u}^2(r,\theta,\phi) = \lim_{t\to\infty}\left[\frac{1}{t^*}\int_{dt^*(r,\theta,\phi)}\left\{\bar{u}_1(r,\theta,\phi,dt^*(r,\theta,\phi)) + u_1'(r,\theta,\phi,t)\right\}^2 dt\right]$$

$$= \lim_{t\to\infty}\left[\frac{dt^*(r,\theta,\phi)}{t^*}\left\{\bar{u}_1^2(r,\theta,\phi,dt^*(r,\theta,\phi)) + \bar{u}_1'^2(r,\theta,\phi,dt^*(r,\theta,\phi,dt(r,\theta,\phi))\right\}\right]$$

$$= \left\{\lim_{t\to\infty}\frac{dt^*(r,\theta,\phi)}{t^*}\right\}\left\{\lim_{t\to\infty}\bar{u}_1^2(r,\theta,\phi,dt(r,\theta,\phi)) + \lim_{t\to\infty}\bar{u}_1'^2(r,\theta,\phi,dt^*(r,\theta,\phi))\right\}.$$

In the above transformations, all the limiting values are assumed to have definite values. The first term, $\lim_{t\to\infty}(dt^*(r, \theta, \phi)/t^*)$, is expressed by the P*-function in (11.5). When the limiting values in the bracket are denoted, respectively, by $\bar{u}_1^2(r, \theta, \phi)$ and $u_1'^2(r, \theta, \phi)$, one gets the following expression:

$$\bar{u}^2(r,\theta,\phi) = P^*(r,\theta,\phi)\left\{\bar{u}_1^2(r,\theta,\phi) + \bar{u}_1'^2(r,\theta,\phi)\right\}dQ^*. \tag{12.8}$$

Expression (12.8) is derived by collecting the parts in the

integration (12.4) which pass through a fixed infinitesimal part domain around the r, θ, ϕ-point at different times. It is clear by the definition of (12.2) that the function $u_1^2(t)$ of (12.4) is integrable in $0 \sim t^*$, and the order of integration $\int_0^{t^*} dt$ can be altered. Therefore, $\overline{u}^2$ of (12.4) can b expressed by the following integration in the whole area of the D*-domain:

$$\overline{u}^2 = \iiint_{D^*} P^*(r,\theta,\phi) \left\{ \overline{u}_i^2(r,\theta,\phi) + \overline{u}_i'^2(r,\theta,\phi) \right\} dQ^* \tag{12.9}$$

As for other components of the Reynolds stress, if such functions $v_1^2(t)$, $uv_1(t)$ and others are taken into account as defined by (12.2), they can be transformed, respectively, into the area integral in a D*-domain like (12.9). In an ideal two-dimensional vortex chaos motion, the same transformation can be made by taking the P*-function of (11.5'). Thus, turbulent intensity at the A-point fixed in the field of flow can be expressed by the following area integrals in the D*-domain:

$$\begin{aligned}
\overline{u}^2 &= \iiint_{D^*} P^*(r,\theta,\phi) \left\{ \overline{u}_i^2(r,\theta,\phi) + \overline{u}_i'^2(r,\theta,\phi) \right\} dQ^*, \\
\overline{v}^2 &= \iiint_{D^*} P^*(r,\theta,\phi) \left\{ \overline{v}_i^2(r,\theta,\phi) + \overline{v}_i'^2(r,\theta,\phi) \right\} dQ^*, \\
\overline{w}^2 &= \iiint_{D^*} P^*(r,\theta,\phi) \left\{ \overline{w}_i^2(r,\theta,\phi) + \overline{w}_i'^2(r,\theta,\phi) \right\} dQ^*, \\
\overline{vw} &= \iiint_{D^*} P^*(r,\theta,\phi) \left\{ \overline{vw}_i(r,\theta,\phi) + \overline{vw}_i'(r,\theta,\phi) \right\} dQ^*, \\
\overline{wu} &= \iiint_{D^*} P^*(r,\theta,\phi) \left\{ \overline{wu}_i(r,\theta,\phi) + \overline{wu}_i'(r,\theta,\phi) \right\} dQ^*, \\
\overline{uv} &= \iiint_{D^*} P^*(r,\theta,\phi) \left\{ \overline{uv}_i(r,\theta,\phi) + \overline{uv}_i'^2(r,\theta,\phi) \right\} dQ^*
\end{aligned} \tag{12.10}$$

and

$$\begin{aligned}
\overline{u}^2 &= \iint_{D^*} P^*(r,\theta) \left\{ \overline{u}_i^2(r,\theta) + \overline{u}_i'^2(r,\theta) \right\} dQ^*, \\
\overline{v}^2 &= \iint_{D^*} P^*(r,\theta) \left\{ \overline{v}_i^2(r,\theta) + \overline{v}_i'^2(r,\theta) \right\} dQ^*, \\
\overline{uv} &= \iint_{D^*} P^*(r,\theta) \left\{ \overline{uv}_i(r,\theta) + \overline{uv}_i'(r,\theta) \right\} dQ^*.
\end{aligned} \tag{12.10'}$$

The above transformation can also be made on the Euler correlation (10.1). For instance, uu'-correlation at the fixed A- and A'-points is defined by

$$\overline{uu'} = \lim_{t \to \infty} \frac{1}{t} \int_0^t uu' dt. \tag{12.11}$$

In the same manner as explained in Section 11, the P*-function in the

D*-domain can be defined concerning the A-point. As in the case of the definition of V* in (11.1), at the A'-point a turning velocity vector V'* due to the same vortex as that taken at the A-point will be assumed. Also, the effects of curvature, elongation and the effects of other vortices near the intersection of the perpendicular from the A-point (cf. Figure 21) shall be neglected. Then, corresponding to a position (r, θ, ϕ) of the A*-point in the D*-domain, the position (r', θ', ϕ') of the A'*-point is uniquely determined in the x*y*z*-space. It can be proved that when such a function,

$$uu_1'(t) = \begin{cases} uu'(t) & \text{in } 0 \sim t, \\ \frac{1}{t}\int_0^t uu'(t)dt & \text{in } \Delta t, \end{cases} \tag{12.12}$$

is introduced in the time interval $0 \sim t^*$, expression (12.11) is transformed into the area integral of the A*-point in the D*-domain.

Thus, the double correlations of (10.1) take the following three- or two-dimensional expressions with a parameter r', θ', ϕ' determined by r, θ, ϕ, and the vector $\overrightarrow{AA'}$:

$$\overline{uu'} = \iiint_{D^*} P^*(r,\theta,\phi)\{\overline{uu_1'}(r,\theta,\phi;r',\theta',\phi') + \overline{uu_1''}(r,\theta,\phi;r',\theta',\phi')\}dQ^*,$$

$$\overline{uv'} = \iiint_{D^*} P^*(r,\theta,\phi)\{\overline{uv_1'}(r,\theta,\phi;r',\theta',\phi') + \overline{uv_1''}(r,\theta,\phi;r',\theta',\phi')\}dQ^*,$$

$$\overline{uw'} = \iiint_{D^*} P^*(r,\theta,\phi)\{\overline{uw_1'}(r,\theta,\phi;r',\theta',\phi') + \overline{uw_1''}(r,\theta,\phi;r',\theta',\phi'\}dQ^*,$$

$$\overline{vu'} = \iiint_{D^*} P^*(r,\theta,\phi)\{\overline{vu_1'}(r,\theta,\phi;r',\theta',\phi') + \overline{vu_1''}(r,\theta,\phi;r',\theta',\phi'\}dQ^*,$$

$$\overline{vv'} = \iiint_{D^*} P^*(r,\theta,\phi)\{\overline{vv_1'}(r,\theta,\phi;r',\theta',\phi') + \overline{vv_1''}(r,\theta,\phi;r',\theta',\phi')\}dQ^*,$$

$$\overline{vw'} = \iiint_{D^*} P^*(r,\theta,\phi)\{\overline{vw_1'}(r,\theta,\phi;r',\theta',\phi') + \overline{vw_1''}(r,\theta,\phi;r',\theta',\phi')\}dQ^*,$$

$$\overline{wu'} = \iiint_{D^*} P^*(r,\theta,\phi)\{\overline{wu_1'}(r,\theta,\phi;r',\theta',\phi') + \overline{wu_1''}(r,\theta,\phi;r',\theta',\phi')\}dQ^*,$$

$$\overline{w'v'} = \iiint_{D^*} P^*(r,\theta,\phi)\{\overline{w'v_1'}(r,\theta,\phi;r',\theta',\phi') + \overline{w'v_1''}(r,\theta,\phi;r',\theta',\phi')\}dQ^*,$$

$$\overline{w'w'} = \iiint_{D^*} P^*(r,\theta,\phi)\{\overline{w'w_1'}(r,\theta,\phi;r',\theta',\phi') + \overline{w'w_1''}(r,\theta,\phi;r',\theta',\phi')\}dQ^*, \quad (12.13)$$

and

$$\overline{u'u'} = \iint_{D^*} P^*(r,\theta)\{\overline{u'u_1'}(r,\theta;r',\theta') + \overline{u'u_1''}(r,\theta;r',\theta')\}dQ^*,$$

$$\overline{u'v'} = \iint_{D^*} P^*(r,\theta)\{\overline{u'v_1'}(r,\theta;r',\theta') + \overline{u'v_1''}(r,\theta;r',\theta')\}dQ^*,$$

$$\overline{v'u'} = \iint_{D^*} P^*(r,\theta)\{\overline{v'u_1'}(r,\theta;r',\theta') + \overline{v'u_1''}(r,\theta;r',\theta')\}dQ^*,$$

$$\overline{v'v'} = \iint_{D^*} P^*(r,\theta)\{\overline{v'v_1'}(r,\theta;r',\theta') + \overline{v'v_1''}(r,\theta;r',\theta')\}dQ^*. \quad (12.14)$$

13. VORTEX CHAOS MOTION IN THE IDEAL STATE

The transformation from (12.1) to (12.9) is purely mathematical. It holds regardless of the shape of the D*-domain only if all the time interval $0 \sim t$ in the real flow is included in $0 \sim t^*$. As far as this transformation is concerned, any physical interpretation can be given to the functions of P* and $(\overline{u_1^2} + \overline{u_1'^2})$. In this section, an approximate formula of (12.9) will be proposed by inquiring into the physical meanings of the terms $(\overline{u_1^2} + \overline{u_1'^2})$ in the real states of a vortex chaos motion.

If the perpendicular plane is taken from the A-point to the nearest vortex filament and if the effects of other vortices are neglected, the turning velocity is distributed on this plane. This vector is distributed from the center of intersection of the filament to infinity, since in fluid mechanics a single vortex motion should have no boundary in the field of flow. Thus, the intensity and scale of a vortex motion can be determined relatively by the form of the distribution of the turning velocity in the perpendicular plane. The turning velocity **V*** at the A-point denoted by (11.1) has been introduced by neglecting all effects of the interactions of many vortices. In the real state of vortex chaos motion, however, the turning movement of a fluid around the filament has a respective finite range, and the effect of a vortex motion does not reach an infinitely long distance.

When the moving A*-point coincides with a fixed point (r, θ, ϕ) in the D*-domain, the nearest vortex filament has a constant relative location to the A-point in the field of flow. In this case, the direction of the **V***-vector at the A-point is constant regardless of the time t, but the

magnitude is assumed to vary generally with time. When $\bar{V}^*$ is the limiting value at $t \to \infty$ of the mean value of the magnitude of $\mathbf{V}^*$ in an infinitesimal time interval $dt^*(r, \theta, \phi)$, the magnitude $\bar{V}^*$ of the vector,

$$\bar{V}^*, \tag{13.1}$$

is determined uniquely at the (r, θ, ϕ)-point.

The vector $\bar{\mathbf{V}}^*$ indicates the mean state of the turning velocities which have a constant relative location of (r, θ, ϕ) of vortex filaments with respect to the A-point in the field of flow (cf. Figure 19). It is easily understood by the definition of r, θ, ϕ in Figure 19 that x-, y- and z-components of the mean-turning velocity in the field of flow are expressed by

$$\begin{aligned}
\bar{V}_x^* &= \bar{V}^* \cos\theta \sin\phi, \\
\bar{V}_y^* &= \bar{V}^* \sin\theta \sin\phi, \\
\bar{V}_z^* &= \bar{V}^* \cos\phi.
\end{aligned} \tag{13.2}$$

Now, in the formula (12.10) of every component of turbulent intensity, the functions of $(u_1^2 + u'^2)$ and others will be written by introducing the components of $(13.2)^1$ as follows:

$$\begin{aligned}
\bar{u}_1^2(r,\theta,\phi) + \bar{u}_1'^2(r,\theta,\phi) &= \{\bar{V}^{*2}(r,\theta,\phi) + \bar{V}_{xx}^*(r,\theta,\phi)\} \cos^2\theta \sin^2\phi, \\
\bar{v}_1^2(r,\theta,\phi) + \bar{v}_1'^2(r,\theta,\phi) &= \{\bar{V}^{*2}(r,\theta,\phi) + \bar{V}_{yy}^*(r,\theta,\phi)\} \sin^2\theta \sin^2\phi, \\
\bar{w}_1^2(r,\theta,\phi) + \bar{w}_1^2(r,\theta,\phi) &= \{\bar{V}^{*2}(r,\theta,\phi) + \bar{V}_{zz}^*(r,\theta,\phi)\} \cos^2\phi, \\
\bar{v}\bar{w}_1(r,\theta,\phi) + \bar{v}\bar{w}_1'(r,\theta,\phi) &= \{\bar{V}^{*2}(r,\theta,\phi) + \bar{V}_{yz}^*(r,\theta,\phi)\} \sin\theta \sin\phi \cos\phi, \\
\bar{w}\bar{u}_1(r,\theta,\phi) + \bar{w}\bar{u}_1'(r,\theta,\phi) &= \{\bar{V}^{*2}(r,\theta,\phi) + \bar{V}_{zx}^*(r,\theta,\phi)\} \cos\theta \sin\phi \cos\phi, \\
\bar{u}\bar{v}_1(r,\theta,\phi) + \bar{u}\bar{v}_1'(r,\theta,\phi) &= \{\bar{V}^{*2}(r,\theta,\phi) + \bar{V}_{xy}^*(r,\theta,\phi)\} \sin\theta \cos\theta \sin^2\phi.
\end{aligned} \tag{13.3}$$

Then (12.10) becomes

$$\overline{u^2} = \iiint_{D^*} P^*(r,\theta,\phi)\{\overline{V^{*2}}(r,\theta,\phi) + \overline{V^*_{xx}}(r,\theta,\phi)\}\cos^2\theta\sin^2\phi\, dQ^*,$$

$$\overline{v^2} = \iiint_{D^*} P^*(r,\theta,\phi)\{\overline{V^{*2}}(r,\theta,\phi) + \overline{V^*_{yy}}(r,\theta,\phi)\}\sin^2\theta\sin^2\phi\, dQ^*,$$

$$\overline{w^2} = \iiint_{D^*} P^*(r,\theta,\phi)\{\overline{V^{*2}}(r,\theta,\phi) + \overline{V^*_{zz}}(r,\theta,\phi)\}\cos^2\phi\, dQ^*,$$

$$\overline{vw} = \iiint_{D^*} P^*(r,\theta,\phi)\{\overline{V^{*2}}(r,\theta,\phi) + \overline{V^*_{yz}}(r,\theta,\phi)\}\sin\theta\sin\phi\cos\phi\, dQ^*,$$

$$\overline{wu} = \iiint_{D^*} P^*(r,\theta,\phi)\{\overline{V^{*2}}(r,\theta,\phi) + \overline{V^*_{zx}}(r,\theta,\phi)\}\cos\theta\sin\phi\cos\phi\, dQ^*,$$

$$\overline{uv} = \iiint_{D^*} P^*(r,\theta,\phi)\{\overline{V^{*2}}(r,\theta,\phi) + \overline{V^*_{xy}}(r,\theta,\phi)\}\sin\theta\cos\theta\sin^2\phi\, dQ^*. \qquad (13.4)$$

The two-dimensional formula (12.10') becomes

$$\overline{u^2} = \iint_{D^*} P^*(r,\theta)\{\overline{V^{*2}}(r,\theta) + \overline{V^*_{xx}}(r,\theta)\}\cos^2\theta\, dQ^*,$$

$$\overline{v^2} = \iint_{D^*} P^*(r,\theta)\{\overline{V^{*2}}(r,\theta) + \overline{V^*_{yy}}(r,\theta)\}\sin^2\theta\, dQ^*,$$

$$\overline{uv} = \iint_{D^*} P^*(r,\theta)\{\overline{V^{*2}}(r,\theta) + \overline{V^*_{xy}}(r,\theta)\}\sin\theta\cos\theta\, dQ^*. \qquad (13.4')$$

The expressions of turbulent intensity in (13.4) or (13.4') are obtained in order to connect every component of the intensity with the value of $\overline{V^*}(r, \theta, \phi)$ in the D*-domain. It is characteristic that all the independently defined components of u^2, v^2 and others are expressed with the P*- and $\overline{V^*}$-functions. Since the parts that cannot be expressed by the two functions are contained in $\overline{V^*_{xx}}$ and others, the formula (13.4) or (13.4') is a mathematical transformation from the original definition (9.5), without any neglect because of physical supposition.

The physical meaning of the terms $\overline{V^*_{xx}}$ and others will be interpreted in terms of a vortex chaos motion. At first, a simplified case in which only the same kinds of vortices are produced at one point upstream will be taken. In this case, when such a field of flow is taken which is completely filled with identical vortex motions having the same distribution of turning velocity within a finite range around every straight vortex filament, then the D*-domain can be determined definitely without any repeated time Δt. In such an idealized case, $\overline{V^*}$ means the turning velocity of every vortex motion, and $\overline{V^*_{xx}}$ and others become zero. By the relation (13.2), the formula (13.4) without $\overline{V^*_{xx}}$ and others holds exactly in this case.

In the real state of a vortex chaos motion, a similar image of situations cannot be adapted. Even in the simple case of a decaying

turbulent flow in which only the primary vortices produced just behind an obstacle body are taken into account with the cascade phenomena neglected, every turning velocity cannot be assumed to have an identical distribution around the filament. At a place far from the filaments, effects of their interactions may be conspicuous, and the situations in the middle of two filaments may be especially complicated. Of course, there is no boundary between two vortex motions. Moreover, the elongation or curvature of filaments is neglected in the definition of V^* of (11.1). Thus, in the expression (13.3), some nonzero values must remain in V^*_{xx} and others, corresponding to an arbitrarily elected D*-domain. By the above discussions, V^*_{xx} and others may be regarded as the fluctuational terms caused by the interactions of many vortices or three-dimensional characteristics, while V^* is the mean term of turning velocities.

The transformation from (9.5) to (13.4) is independent of the shape of the D*-domain only if the time interval $0 \sim t$ is included in $0 \sim t^*$. However, what values the fluctuational terms may take depends largely upon the shape of the D*-domain. A D*-domain will be taken so that the repeated time intervals Δt may be as small as possible. Then the fluctuational terms will be far smaller than the term $\bar{V}^{*2}$ caused by their original turning velocities.

In a vortex chaos motion that consists of one kind of vortex, if the fluctuational terms V^*_{xx} and others are neglected, expressions (13.4) and (13.4') become

$$\begin{aligned}
\bar{u}^2 &= \iiint_{D^*} P^*(r,\theta,\phi)\bar{V}^{*2}(r,\theta,\phi)\cos^2\theta\sin^2\phi\, dQ^*,\\
\bar{v}^2 &= \iiint_{D^*} P^*(r,\theta,\phi)\,\bar{V}^{*2}(r,\theta,\phi)\sin^2\theta\sin^2\phi\, dQ^*,\\
\bar{w}^2 &= \iiint_{D^*} P^*(r,\theta,\phi)\,\bar{V}^{*2}(r,\theta,\phi)\cos^2\phi\, dQ^*,\\
\overline{vw} &= \iiint_{D^*} P^*(r,\theta,\phi)\,\bar{V}^{*2}(r,\theta,\phi)\sin\theta\sin\phi\cos\phi\, dQ^*,\\
\overline{wu} &= \iiint_{D^*} P^*(r,\theta,\phi)\,\bar{V}^{*2}(r,\theta,\phi)\cos\theta\sin\phi\cos\phi\, dQ^*,\\
\overline{uv} &= \iiint_{D^*} P^*(r,\theta,\phi)\,\bar{V}^{*2}(r,\theta,\phi)\sin\theta\cos\theta\sin^2\phi\, dQ^*,
\end{aligned} \tag{13.5}$$

and

$$\begin{aligned}
\bar{u}^2 &= \iint_{D^*} P^*(r,\theta)\,\bar{V}^{*2}(r,\theta)\cos^2\theta\, dQ^*,\\
\bar{v}^2 &= \iint_{D^*} P^*(r,\theta)\,\bar{V}^{*2}(r,\theta)\sin^2\theta\, dQ^*,\\
\overline{uv} &= \iint_{D^*} P^*(r,\theta)\,\bar{V}^{*2}(r,\theta)\sin\theta\cos\theta\, dQ^*.
\end{aligned} \tag{13.5'}$$

Expression (13.5) or (13.5') is no more than a mathematical transformation from (9.5) but is an approximate expression of the relation, founded on the supposition that the intensity of turbulent flow is caused by only the mean characteristics of vortex chaos motion. Such a simplified state as written by (13.5) shall be called an ideal state of vortex chaos motion, while (13.4) is the description of the real state of the motion.

In the statistical dynamics, the concept of an ideal gas is introduced in which only the collision motion of every molecule is taken into account by neglecting the effects of their rotations and interactions. Quantitative discussions are made chiefly on this idealized state. The concept of an ideal state of vortex chaos motion may correspond to that of an ideal gas.

In consideration of the nondecaying turbulent flow along a wall, many kinds of primary vortices produced everywhere upstream must be treated. In the study of the cascade phenomena of the decaying turbulent flow, the situation is the same. In such a case, it is desirable to define the P^*- and V^*-functions, respectively, for the same kind of vortices. When different N kinds of vortices pass near the A-point, the P^*_i- and V^*_i-functions can be defined in the same manner as in (11.5) and (13.1)^i in the D^*_i-domain for an i-th kind of vortices.

When

$$\widetilde{P}^*_i = \iiint_{D^*_i} P^*_i \, dQ^*_i \tag{13.6}$$

is written, $\widetilde{P}^*_i$ means a nondimensional ratio by which the i-th vortices are mixed in all kinds of vortices, and the condition (11.6) is expressed by

$$\sum_{i=1}^{N} \widetilde{P}^*_i = 1. \tag{13.7}$$

When the transformation from (12.1) to (13.4) is applied to every kind of vortex, the real expression of turbulent intensity in this case is given by

$$\overline{u}^2 = \sum_{i=1}^{N} \left[\iiint_{D^*_i} P^*_i(r,\theta,\phi) \left\{ \overline{V}^{*2}_i(r,\theta,\phi) + \overline{V}^*_{xxi}(r,\theta,\phi) \right\} \cos^2\theta \sin^2\phi \, dQ^*_i \right],$$

$$\overline{v}^2 = \sum_{i=1}^{N} \left[\iiint_{D^*_i} P^*_i(r,\theta,\phi) \left\{ \overline{V}^{*2}_i(r,\theta,\phi) + \overline{V}^*_{yyi}(r,\theta,\phi) \right\} \sin^2\theta \sin^2\phi \, dQ^*_i \right],$$

$$\overline{w}^2 = \sum_{i=1}^{N} \left[\iiint_{D^*_i} P^*_i(r,\theta,\phi) \left\{ \overline{V}^{*2}_i(r,\theta,\phi) + \overline{V}^*_{zzi}(r,\theta,\phi) \right\} \cos^2\phi \, dQ^*_i \right],$$

$$\overline{vw} = \sum_{i=1}^{N} \left[\iiint_{D_i^*} P_i^*(r,\theta,\phi) \left\{ \bar{V}_i^{*2}(r,\theta,\phi) + \bar{V}_{yzi}^*(r,\theta,\phi) \right\} \sin\theta \sin\phi \cos\phi \, dQ_i^* \right],$$

$$\overline{wu} = \sum_{i=1}^{N} \left[\iiint_{D_i^*} P_i^*(r,\theta,\phi) \left\{ \bar{V}_i^{*2}(r,\theta,\phi) + \bar{V}_{zxi}^*(r,\theta,\phi) \right\} \cos\theta \sin\phi \cos\phi \, dQ_i^* \right],$$

$$\overline{uv} = \sum_{i=1}^{N} \left[\iiint_{D_i^*} P_i^*(r,\theta,\phi) \left\{ \bar{V}_i^{*2}(r,\theta,\phi) + \bar{V}_{xyi}^*(r,\theta,\phi) \right\} \sin\theta \cos\theta \sin^2\phi \, dQ_i^* \right].$$

(13.8)

When every D_i^*-domain is elected in the same manner as in (13.5), the ideal expression is obtained as follows:

$$\bar{u}^2 = \sum_{i=1}^{N} \iiint_{D_i^*} P_i^*(r,\theta,\phi) \, \bar{V}_i^{*2}(r,\theta,\phi) \cos^2\theta \sin^2\phi \, dQ_i^*,$$

$$\bar{v}^2 = \sum_{i=1}^{N} \iiint_{D_i^*} P_i^*(r,\theta,\phi) \, \bar{V}_i^{*2}(r,\theta,\phi) \sin^2\theta \sin^2\phi \, dQ_i^*,$$

$$\bar{w}^2 = \sum_{i=1}^{N} \iiint_{D_i^*} P_i^*(r,\theta,\phi) \, \bar{V}_i^{*2}(r,\theta,\phi) \cos^2\phi \, dQ_i^*,$$

$$\overline{vw} = \sum_{i=1}^{N} \iiint_{D_i^*} P_i^*(r,\theta,\phi) \, \bar{V}_i^{*2}(r,\theta,\phi) \sin\theta \sin\phi \cos\phi \, dQ_i^*,$$

$$\overline{wu} = \sum_{i=1}^{N} \iiint_{D_i^*} P_i^*(r,\theta,\phi) \, \bar{V}_i^{*2}(r,\theta,\phi) \cos\theta \sin\phi \cos\phi \, dQ_i^*,$$

$$\overline{uv} = \sum_{i=1}^{N} \iiint_{D_i^*} P_i^*(r,\theta,\phi) \, \bar{V}_i^{*2}(r,\theta,\phi) \sin\theta \cos\theta \sin^2\phi \, dQ_i^*.$$

(13.9)

The Euler correlation at the A- and A'-points of x, y, z and x', y', z' has been transformed into the area integrals of (12.13). When the following relation

$$\overline{uu}'(r,\theta,\phi;r',\theta',\phi') + \overline{uu}''(r,\theta,\phi;r',\theta',\phi')$$
$$= \left\{ \bar{V}^*(r,\theta,\phi) \bar{V}^*(r',\theta',\phi') + \bar{V}_{xx'}^*(r,\theta,\phi;r',\theta',\phi') \right\} \cos\theta \sin\phi \cos\theta' \sin\phi'$$

(13.10)

is given, the real expression in the case consisting of one kind of vortex is written as

$$\overline{uu'} = \iiint_{D^*} P^*(r,\theta,\phi)\left\{\bar{V}^*(r,\theta,\phi)\,\bar{V}^*(r',\theta',\phi') + \bar{V}^*_{xx'}(r,\theta,\phi;r',\theta',\phi')\right\}\cos\theta\sin\phi\cos\theta'\sin\phi'\,dQ^*, \tag{13.11}$$

and in the case of several kinds of vortices, it is

$$\overline{uu'} = \sum_{i=1}^{N}\left[\iiint_{D_i^*} P_i^*(r,\theta,\phi)\left\{\bar{V}_i^*(r,\theta,\phi)\,\bar{V}_i^*(r',\theta',\phi') + \bar{V}^*_{xx'_i}(r,\theta,\phi;r',\theta',\phi')\right\}\cos\theta\sin\phi\cos\theta'\sin\phi'\,dQ_i^*\right]. \tag{13.12}$$

In the ideal state, the following general expressions are derived by neglecting the fluctuational terms in every D_i^*-domain, defined in the same manner as in (13.5):

$$\overline{uu'} = \sum_{i=1}^{N}\iiint_{D_i^*} P_i^*(r,\theta,\phi)\,\bar{V}_i^*(r,\theta,\phi)\,\bar{V}_i^*(r',\theta',\phi')\cos\theta\sin\phi\cos\theta'\sin\phi'\,dQ_i^*,$$

$$\overline{uv'} = \sum_{i=1}^{N}\iiint_{D_i^*} P_i^*(r,\theta,\phi)\,\bar{V}_i^*(r,\theta,\phi)\,\bar{V}_i^*(r',\theta',\phi')\cos\theta\sin\phi\sin\theta'\sin\phi'\,dQ_i^*,$$

$$\overline{uw'} = \sum_{i=1}^{N}\iiint_{D_i^*} P_i^*(r,\theta,\phi)\,\bar{V}_i^*(r,\theta,\phi)\,\bar{V}_i^*(r',\theta',\phi')\cos\theta\sin\phi\cos\phi'\,dQ_i^*,$$

$$\overline{vu'} = \sum_{i=1}^{N}\iiint_{D_i^*} P_i^*(r,\theta,\phi)\,\bar{V}_i^*(r,\theta,\phi)\,\bar{V}_i^*(r',\theta',\phi')\sin\theta\sin\phi\cos\theta'\sin\phi'\,dQ_i^*,$$

$$\overline{vv'} = \sum_{i=1}^{N}\iiint_{D_i^*} P_i^*(r,\theta,\phi)\,\bar{V}_i^*(r,\theta,\phi)\,\bar{V}_i^*(r',\theta',\phi')\sin\theta\sin\phi\sin\theta'\sin\phi'\,dQ_i^*,$$

$$\overline{vw'} = \sum_{i=1}^{N}\iiint_{D_i^*} P_i^*(r,\theta,\phi)\,\bar{V}_i^*(r,\theta,\phi)\,\bar{V}_i^*(r',\theta',\phi')\sin\theta\sin\phi\cos\phi'\,dQ_i^*,$$

$$\overline{wu'} = \sum_{i=1}^{N}\iiint_{D_i^*} P_i^*(r,\theta,\phi)\,\bar{V}_i^*(r,\theta,\phi)\,\bar{V}_i^*(r',\theta',\phi')\cos\phi\cos\theta'\sin\phi'\,dQ_i^*,$$

$$\overline{wv'} = \sum_{i=1}^{N} \iiint_{D_i^*} P_i^*(r,\theta,\phi)\, \bar{V}_i^*(r,\theta,\phi)\, \bar{V}_i^*(r',\theta',\phi') \cos\phi \sin\theta' \sin\phi' \, dQ_i^*,$$

$$\overline{ww'} = \sum_{i=1}^{N} \iiint_{D_i^*} P_i^*(r,\theta,\phi)\, \bar{V}_i^*(r,\theta,\phi)\, \bar{V}_i^*(r',\theta',\phi') \cos\phi \cos\phi' \, dQ_i^* . \qquad (13.13)$$

In an idealized two-dimensional case, they are reduced to

$$\overline{uu'} = \sum_{i=1}^{N} \iint_{D_i^*} P_i^*(r,\theta)\, \bar{V}_i^*(r,\theta)\, \bar{V}_i^*(r',\theta') \cos\theta \cos\theta' \, dQ_i^* ,$$

$$\overline{uv'} = \sum_{i=1}^{N} \iint_{D_i^*} P_i^*(r,\theta)\, \bar{V}_i^*(r,\theta)\, \bar{V}_i^*(r',\theta') \cos\theta \sin\theta' \, dQ_i^* ,$$

$$\overline{vu'} = \sum_{i=1}^{N} \iint_{D_i^*} P_i^*(r,\theta)\, \bar{V}_i^*(r,\theta)\, \bar{V}_i^*(r',\theta') \sin\theta \cos\theta' \, dQ_i^* ,$$

$$\overline{vv'} = \sum_{i=1}^{N} \iint_{D_i^*} P_i^*(r,\theta)\, \bar{V}_i^*(r,\theta)\, \bar{V}_i^*(r',\theta') \sin\theta \sin\theta' \, dQ_i^* . \qquad (13.13')$$

14. CHARACTER OF A VORTEX MOTION

In the previous sections from 11 to 13, mathematical formulations are given to the Reynolds stress in order to make it convenient to introduce physical assumptions of the vortex chaos motion. These formulations are, so to speak, statistical kinematics of a vortex chaos motion. Now discussions will be continued on the physical grounds by which P^*, $\bar{V}^*$, and other functions shall be determined in the D^*-domain.

The real expressions in (13.8) or (13.12) contain the fluctuational terms of V^*_{xxi} and others in addition to the P^*- and $\bar{V}^*$-functions. It is too difficult, however, to presume characteristics of these fluctuational terms caused by interactions of many vortex motions. The presumption may be almost impossible unless unsteady solutions of the Navier-Stokes equations are obtained for a complicated vortex chaos motion. Approximate expressions of an ideal state have the characteristic that quantitative discussions can be developed depending upon only the two functions of P^* and $\bar{V}^*$ whose physical meanings are not too difficult to be defined. Particularly, the $\bar{V}^*$-function concerns the mean state of the turning velocities of many vortex motions with the elongation and curvature of filaments neglected, and the functional form can be studied in the field of hydrodynamics. In this section, some theoretical results already obtained in hydrodynamics on the state of one vortex motion in a fluid (reference 27) will be related.

In the ordinary case where the Reynolds equations (9.6) can be adapted, it is not necessary to consider the effect of compressibility of a fluid; however, the effect of molecular viscosity is important. If the Euler equations of a perfect fluid are the foundation, they will prove the preservation of a constant kinetic energy and of a constant scale in a vortex motion. This is obviously inconsistent with the real vortex chaos motion (cf. Figure 1). Even in the case of one vortex motion, it is difficult in viscous hydrodynamics to decide exactly the situation of the production and the development of the vortex filament and the distribution of the turning velocity. However, when a vortex has a straight filament without elongation or constriction, the turning velocity retains a two-dimensional character in the perpendicular plane with the condition of symmetry around the intersection. Thus, mathematical analysis based upon the Navier-Stokes equations is easily made.

The problem of a two-dimensional viscous vortex motion surveys the diffusion of vorticity which is initially concentrated at one point in a fluid. When ω and r are, respectively, the vorticity of the fluid and a distance from the center, and when the time t is taken since the beginning time 0, then the two-dimensional unsteady Navier-Stokes equations with the condition of round symmetry are reduced to

$$\frac{\partial^2\omega}{\partial r^2} + \frac{1}{r}\frac{\partial\omega}{\partial r} = \frac{1}{\gamma}\frac{\partial\omega}{\partial t}\,, \tag{14.1}$$

by eliminating the pressure terms. Letting

$$s = r^2/(4\gamma t) \tag{14.2}$$

and integrating (14.1) by separating the variable in the form $\omega\ (r,t) = \omega_1(t)\omega_2(s)$, the solution

$$\omega = C_\alpha\left\{1 + \sum_{i=1}^{\infty}\frac{(1-\alpha)(2-\alpha)\cdots(i-\alpha)}{i!}\frac{s^i}{i!}\right\}t^{-\alpha}\,,$$

$$(\alpha \geqq 1), \tag{14.3}$$

is derived with two constants of $C\alpha$ and α. By the definition of ω, the distribution of the turning velocity V* is written as

$$V^* = \frac{2}{r}\int r\omega\, dr\,, \tag{14.4}$$

Thus, under the boundary conditions

$$V^* = 0 \quad \text{at} \quad r = 0$$
$$V^* \to 0 \quad \text{at} \quad r \to \infty , \tag{14.5}$$

the V*-function is expressed in the form

$$V^* = F_\alpha(s)\, G_\alpha(t),$$
$$F_\alpha = \left\{ 1 + \sum_{i=1}^{\infty} \frac{(2-\alpha)(3-\alpha)\cdots(i+1-\alpha)}{(i+1)!} \frac{s^i}{i!} \right\} \sqrt{s}\, e^{-s}, \quad (\alpha > 1),$$
$$F_1 = (1 - e^{-s})/\sqrt{s}, \quad (\alpha = 1),$$
$$G_\alpha = 2 C_\alpha \sqrt{\gamma}\, t^{\frac{1}{2}-\alpha}, \quad (\alpha \geqq 1). \tag{14.6}$$

Expression (14.6) is the solution of V*, and the functional forms of F_α are shown in Figure 22 for several values of α. In the above solution only the boundary conditions are taken into account, and the index α, together with the constant C_α, must be determined depending on the initial condition at t = 0. As in the production of a vortex motion, the physical mechanism has not been clarified at present. Moreover, the above analysis concerns only the diffusion of vorticity concentrated primarily at one point. Therefore, this analysis is not necessarily appropriate in a discussion of the production mechanism of a vortex motion, and the determination of the values of α and C_α must be made by comparing theoretical results with experimental works.

In the case of $\alpha = 1$, some investigations have been made on the problem of production. When $\Gamma_{r,t}$ is the circulation around a circle of radius r, it is written by definition as

$$\Gamma_{r,t} = 4\pi C_1 \gamma (1 - e^{-s}). \tag{14.7}$$

Expression (14.7) does not contain t explicitly, and at the limits of $t \to 0$ and $r \to \infty$, $\Gamma_{\infty,0} = 4\pi C_1 \gamma$. Namely, when a circulation Γ is given at t = 0, C_1 is determined as

$$C_1 = \Gamma/(4\pi\gamma), \tag{14.8}$$

and the limiting value of V_1^* is reduced to

$$V_1^* = \frac{\Gamma}{\pi}\frac{1}{r} \qquad \text{at} \qquad r \to \infty . \tag{14.9}$$

It is well known that (14.9) indicates the state of a vortex motion of a perfect fluid; therefore, it is understood that the vortex motion of $\alpha = 1$ tends always to take the form of a perfect fluid at $r \longrightarrow \infty$.

When E_α is the kinetic energy of a vortex motion contained in the range $0 \sim s_0$, it is evaluated as

$$E_\alpha = \{8\pi C_\alpha^2 \gamma^2 \int_0^{s_0} F_\alpha^2(s)\,ds\}\, t^{2(1-\alpha)} . \tag{14.10}$$

In the case of $\alpha = 1$, it is reduced to

$$E_1 = 8\pi C_1^2 \gamma^2 \int_0^{s_0} F_1^2(s)\,ds , \tag{14.11}$$

which means the invariability of energy independent of t. For other cases it decreases with t as seen in (14.10). It may be interpreted that the amount of diffused energy from the center is generally less than that of the energy dissipated by molecular viscosity.

The above results are principal features which have been clarified in the case of a two-dimensional viscous vortex motion. In chaotic states of vortices, effects of elongation and curvature of a vortex filament cannot be neglected, nor can the interactions of many other vortices, and the formula (14.6) does not hold exactly for the V*-function. Founded on the above solutions, however, general characteristics of V* may be presumed to some extent. At least, compared with the solution of a vortex motion of a perfect fluid (14.9), it is appropriate to state for the real state of a vortex chaos motion that all the kinds of vortices of α have their respective similar distribution of F_α expanding at the rate of $\sqrt{t}$, as seen by (14.2), and have also the respective decaying term G_α of (14.6).

15. EXTENSION OF THE ERGODIC HYPOTHESIS

Vortex chaos motion means that many vortices are carried by the mean flow in an irregular agitating motion. In the case of a decaying turbulent flow behind a circular cylinder or of a nondecaying turbulent flow along a wall, transition phenomena from the production of vortices to their chaotic states are explained circumstantially in Chapter Two. In a word, regularly arranged vortices always tend to become irregular, probably because of the effects of viscosity, interaction, and other factors of many vortices. It is too difficult, however, to trace accurately the transition phenomena

based upon the Navier-Stokes equations. At any rate, the existence of such transition phenomena is true, although the above interpretations are merely suppositions founded on experimental observations. In this section there is no intention of further inquiry into the physical meanings of the transition phenomena. Attempts will be made only to give a mathematical expression in the form of the P*-function to the physical concept of a regular or an irregular state of vortex motions.

To make the essentials of the meaning easily understandable, an ideal case of the two-dimensional vortex chaos motion behind a circular cylinder will be taken first. If a pair of vortices just behind the cylinder keeps a stationary state, not being carried away into the flow as in the case of a very low Reynolds number, the relative location of the vortex center to the A-point is invariant and independent of the time. The magnitude and direction of the turning velocity **V*** at the A-point defined by (11.1) are invariant, and the variables r and θ in (11.2) are constant for the time. Therefore, the A*-point having the coordinates determined by r and θ does not move in the x*y*-space. If a D*-domain is taken with a finite area around the A*-point, the P*-function defined by (11.5') takes the value of infinity of the second order at the A*-point, and in another area in the D*-domain, it becomes zero.

If the vortices separated from a cylinder keep a regular flow pattern of the theoretical Kármán vortex streets, the V*-function at the A-point has a cyclic character for every vortex motion in the street, because every vortex which has the same distribution form of the turning velocity passes near the A-point in the same way. Therefore, in the D*-domain the A*-point repeats the same motion along one locus determined by r(t), θ (t) of (11.2), and the P*-function takes the value of infinity of the first order on this locus and vanishes in another area. When the vortices on the opposite side of the Kármán streets are taken into account, two loci must be considered in the D*-domain.

When the arrangement of vortices in the Kármán streets are disturbed as they are carried downstream, V* has somewhat different characteristics for each vortex, and the A*-point does not necessarily repeat the same motion in the D*-domain, because there is a uniform relation as mentioned in Section 11 between the motion of the A*-point and the variables r, θ of (11.2). Thus, the P*-function may show a continuous function which has the highest density on the locus in the case of the Kármán vortex streets and has some breadth of the distributions on both sides. It is easily assumed that the more irregular the Kármán vortex streets become, the more widely the P*-function distributes in the D*-domain.

In general, the following correspondence can be pointed out between the physical concept of regularity or irregularity of the arrangement of vortices and the mathematical form of the P*-function. In the case of a stationary vortex motion just behind a cylinder, which is the most regular arrangement, the P*-function takes the form of Dirac's delta function of the second order in the D*-domain, and in the regular flow pattern of

the Kármán vortex streets, it takes Dirac's delta function of the first order. As the Kármán vortex streets lose regularity in the arrangement, P* takes the form of a continuous function which has its peak at the position of the delta function of the first order. As the regularity decreases and the irregularity increases in the flow pattern of vortices, the range of a continuous P*-function becomes wider in the D*-domain with a low peak. At the limit of the most irregular state of a vortex chaos motion, the P*-function is assumed to be constant in all the D*-domain corresponding to random values of r and θ. It may be concluded that as the physical concept of irregularity of a vortex chaos motion increases, the P*-function changes the mathematical form from a singular type of the delta function to the simplest functional form of a constant. Figure 23 shows a conceptional diagram of the above explanations.

Transition phenomena from the production of vortices to their chaotic states of turbulent flow are widely observed in many cases of turbulent wake behind a lattice, turbulent flow in a pipe, turbulent jet, turbulent boundary layer along a wall and others. If detailed observations are made, some different characteristics may be found case by case. It can be said, however, that in all cases the P*-function in a three-dimensional D*-domain tends to take a more simple form, as a regular flow pattern of vortices develops into an irregular chaotic state. Furthermore, it is not easy to assume that an irregular chaotic motion of vortices reduces again into a regular pattern. Namely, the P*-function, characteristically, always tends to take a simpler functional form going downstream, and the process is not reversible. Thus, in all the turbulent flow of a vortex chaos motion, the following characteristic of every P^*_i-function of (13.6) can be obtained:

$$P_i^* = \text{simple continuous function of } r, \theta, \phi. \tag{15.1}$$

In general statistical studies of chaotic phenomena, other than the vortex chaos motion, the characteristic of irregularity or complexity has been usually expressed in a probability-density function of the phenomena. In a chaotic phenomenon which takes many kinds of situations for the time, such a probability-density function may be introduced which will indicate every kind of situation, like the P*-function in the D*-domain. If all the causes which make the phenomenon take on different characteristics are independent of each other, without any specially distinguishing causes, this phenomenon usually shows the character of "irregularity" or "complexity". In this case, the probability-density function shows the characteristic of uniformity. On the other hand, if all the causes are identical, the phenomenon takes the "regular" state independently of the time attributed to this cause, and the probability-density function takes a singular form of the delta function. Even in the phenomenon of an irregularity, if the causes are representative ones, the phenomenon shows the characteristics of some regularity, and the probability-density function takes the form of a nonuniform but nonsingular continuous function. Namely, if an appropriate probability-density function is defined, existence of the

above correspondence between the physical concept of irregularity and its functional form can always be pointed out. This may be an essentially important fact when statistical characteristics of chaotic phenomena in many cases are studied.

In the case of a gas, it is well known that as the absolute temperature rises from zero, a system of molecules changes the state generally from a solid to a gas. If this transition phenomenon is considered in the phase space, it can be found that the probability-density function changes from the delta function to a simple continuous function and, still further, to the simplest functional form of a constant. Detailed explanations are given in Section 3.

In the state of a gas, the probability-density function which indicates the situation of molecular chaos motion distributes uniformly in an energy-constant domain in the phase space. In statistical dynamics, this characteristic is called the Ergodic hypothesis and is taken as a foundation of the theory. Furthermore, the irreversible process in which the regularity tends inevitably to become irregular is serious according to the Entropy-increase principle. In other words, the Ergodic hypothesis in statistical dynamics is a specia' case of the above-mentioned general characteristics between the concept of irregularity and the probability-density function, which is adapted only to the case of the most irregular chaotic states of molecules. It is thought that the physical principle of the Ergodic hypothesis can be introduced to other chaotic phenomena as well as to the molecular chaos motion. Also, according to the degree of irregularity, it is appropriate to assume that the probability-density function takes the form of a simple continuous function other than a constant. The expression (15.1) is that which is extended from the physical principle of the Ergodic hypothesis in statistical dynamics and is applied to the case of a vortex chaos motion as a generalized expression.

16. VORTEX CHAOS MOTION IN STATISTICAL EQUILIBRIUM

The regularity characteristic of a vortex chaos motion always tends to become irregular. In the final state where the P*-function is assumed to distribute uniformly in the D*-domain, this chaotic state of vortices is unable to become more irregular and also does not revert to a more regular state. In the chaotic motion of N kinds of vortices, a following nondimensional probability-density function for an i-th kind of vortices will be taken,

$$P_{ii}^{*} = P_{i}^{*} Q_{i}^{*} / \widetilde{P}_{i}^{*}, \tag{16.1}$$

where P_{i}^{*} is given by (13.6) and Q_{i}^{*} is the volume of the D_{i}^{*}-domain. If the P_{ii}^{*}-function has the condition

$$P_{1i}^{*} = 1, \qquad (16.2)$$

it can be said that the i-th vortex chaos motion is in the completely irregular state (cf. Figure 23-D).

As mentioned in Chapter Two, the real vortex chaos motion usually consists of many kinds of vortices with different conditions of productions. If the idealization of (16.2) is adapted to every kind of vortex, such a chaotic motion of all the vortices is taken as a completely irregular vortex chaos motion. Furthermore, as seen from the physical concept of a vortex chaos motion, (16.2) holds not only at one point but in a finite range of the field of flow. The range of an idealized, completely irregular vortex chaos motion with the condition (16.2) for all the values of i will be called shearless turbulence. The shearless turbulent flow behind a lattice explained in Section 5 is appropriately idealized by the shearless turbulence. In the chaotic motion of N kinds of vortices, if at least one kind of i-th vortex does not have the condition of complete irregularity (16.2), this vortex chaos motion as a whole shall be called shear turbulence. In the decaying shear turbulent flow behind a circular cylinder mentioned in Section 6, the primary vortices produced just behind the body are considered not to be adapted by (16.2), because scales of these vortices are not small compared with the breadth of the turbulent wake. The turbulent wake is an example of shear turbulence.

Many cases of incomplete irregularity are seen in the real vortex chaos motions of turbulent flow. Exactly speaking, these vortex chaos motions usually tend to become more irregular downstream, and the P*-function cannot retain a constant functional form. However, the change in the statistical states of a vortex chaos motion along the flow is not as rapid as in the case of a molecular chaos motion. Therefore, in the statistical study of turbulent flow, such an idealization is preferable such that the condition

$$P_{1i}^{*} = \text{stationary continuous function in } D_{i}^{*} \qquad (16.3)$$

holds along a finite range of flow. An idealized state in which the functional form of P* is invariant regardless of the time and location in the field of flow is said to be in statistical equilibrium. Expression (16.3) or (16.2) is the condition of statistical equilibrium. Statistical studies of the real vortex chaos motions in the following chapters will be made on this idealization of statistical equilibrium.

In molecular chaos motion, the mean-free path of the molecules is far smaller than the macroscopic length as mentioned in Section 1, and statistical dynamics of gases chiefly treat the completely irregular state corresponding to (16.2). When a molecular chaos motion is not in the completely irregular state, it usually shows a strong tendency to change

into this state, and the assumption of a statistical equilibrium of incomplete irregularity is inappropriate. It is important that the problem is studied as a transition phenomenon into the completely irregular state. The statistical interpretations of the Entropy-increase principle in statistical dynamics were made from this point of view.

In vortex chaos motion, every vortex has a macroscopic scale and different situations. When every vortex scale is far smaller than the breadth of vortex chaos motion and the interactions of many surrounding vortices have no directional effect, the idealization of the complete irregularity (16.2) is adaptable. When the vortex scales are comparable with the breadth of the chaos motion, some directional effects remain in the interaction of vortices, and it is difficult for all vortices to come into the complete irregular state (16.2). The idealization of an equilibrium state not in the completely irregular state (16.3) is more appropriate in this case.

Since the technique of a hot-wire observation was completed (reference 15), the opinion has been widely supported that unsteady flow with a regular velocity fluctuation is not a turbulent flow, but it is turbulent if the fluctuation is irregular (cf. Figure 4). This consideration has provided the basic physical background for many researchers to participate in the study of turbulent flow. However, this is not expressed in the Reynolds equations (9.6) or in the Euler correlations (10.1), and few attempts have been made to introduce this concept definitely into the basis of statistical theories of turbulent flow. As a mathematical foundation of the analysis, one must depend solely upon the Reynolds equations, which in themselves are not mathematically conclusive.

In Section 12, the Euler correlation of time means has been transformed into the area means in the D*-domain by introducing the P*-function. The purpose of this transformation has been to make it easy to introduce the basic hypothesis of general statistical physics into the study of turbulent flow. The assumption (15.1) is that in which the physical meaning of the Ergodic hypothesis in statistical dynamics is extended and applied to the vortex chaos motion of turbulent flow. The conditions (16.3) or (16.2) denote the special state of a statistical equilibrium which corresponds to the stationary state in hydrodynamics. This statement is made only to avoid the difficulties of the foregoing statistical analysis.

In the field of hydrodynamics, if the Navier-Stokes equations were solved under the given initial and boundary conditions of the complicated flow of a vortex chaos motion, the state of every vortex motion could be determined as a function of x, y, z, and t in the field of flow. Then, the P*-function in the D*-domain can be derived from the definition (11.5). As for the $\overline{V}^*$-function, the functional form can be determined more accurately than the presumption of the solution of a single vortex motion, and the fluctuational terms $\overline{V}^*_{xx}$ and others can also be derived from exact solutions. At present, however, it is almost impossible in mathematical

treatments to get such a nonsteady solution under the complicated conditions of a vortex chaos motion. In the transition phenomena from the production of vortices to their chaotic motions, only a few cases of the formation of a pair of vortices just behind a circular cylinder and of the stability of the Kármán vortex streets have been proved based upon the equations of motion in hydrodynamics. Discussions founded on the P*-function in this chapter have essential meaning in the introduction of the basic statistical hypothesis made independently of hydrodynamics, to avoid the difficulties in obtaining nonsteady solution of hydrodynamics.

In statistical dynamics, some attempts have been made to prove the Ergodic hypothesis mathematically based upon Newtonian dynamics. One would like to expect that the assumptions of the P*-function could be derived directly from the Navier-Stokes equations in the near future. At that time, this statistical theory of turbulence may be included as a principle in hydrodynamics.

CHAPTER FOUR. SIMILARITY THEORY OF THE ISOTROPIC TURBULENCE

17. CONDITIONS OF HOMOGENEOUS AND ISOTROPIC TURBULENCE

Now the case of the shearless turbulence of decaying turbulence (reference 18) shall be considered. The shearless turbulence is defined as a vortex chaos motion in which the condition of complete irregularity (16.2) is adapted to all the N kinds of vortices. In the shearless turbulence, consider a special case that has a constant mean velocity in the field of flow. Then, the vortex chaos motion has the conditions

$$P_{1i}^{*} = 1, \qquad i = 1, 2, \cdots N,$$
$$\bar{U} = \bar{U}_0 \ (\text{constant}). \tag{17.1}$$

This kind of vortex chaos motion can be taken as the simplest case from both statistical and hydrodynamical points of view. This idealized vortex chaos motion is applicable to the turbulent flow behind a grid put in a uniform flow of a wind or water tunnel. The flow pattern shown in Figure 1 may be regarded as a two-dimensional example of this case.

The condition $P_{1i}^{*} = 1$ means that all the vortices are in the completely irregular state everywhere in the field of flow. Moreover, the condition indicates that the mean flow gives no effect of the mean pressure to the vortex motions in it. Thus, in addition to the growing effects of vortices caused by the molecular viscosity, the mean and fluctuational terms $\bar{V}_i^{*}$, $\bar{V}_{xxi}^{*}$ and other similar terms in the expressions of the real state (13.8) are independent of the locations in the field of flow. Namely, besides the variation along the x-direction, mean states of the velocity fluctuation are uniform in the field of flow. This is the same as the state of flow usually called homogeneous turbulence (reference 28).

In order to retain the state of a shearless turbulence, breadth of the vortex chaos motion must be far wider than the scale of individual vortices in it, as mentioned in Section 16. In other cases besides a uniform flow, effects of the pressure gradient of the mean flow cannot be neglected on the individual vortices, and it is also difficult to give a uniform effect in the whole field of flow. In addition to the case of a uniform flow, a homogeneous turbulence is not found which holds in the wide region of a real state of flow. In the case of shear turbulence, the shearing stress caused by an incompletely irregular arrangement of vortices gives a distortion to the mean-velocity profile even if the undisturbed flow upstream is uniform, and the condition of homogeneous turbulence cannot be adapted. This is the same for the nondecaying turbulent flow along a wall.

In the case of the completely irregular vortex chaos motion in a uniform flow, characteristics of the individual vortices in the time means

are constant, regardless of direction in the field of flow. Namely, the distribution of the mean turning velocity of the vortices is symmetrical around the filament, and the inclination of the filament is also completely irregular in a three-dimensional space. Therefore, when the variables γ, θ, ϕ of (11.2) which represent the orientations of turning velocities near the A-point are taken to be the polar coordinates of the A*-point in the x*y*z*-space, then the A*-point moves about in the completely irregular state near the origin, and in the distribution of the probability-density function P*, no directional effects remain. Thus, when a spherical D*-domain is taken around the origin of the x*y*z*-space, we can suppose that the mean and fluctuational turning velocities $\overline{V}_i^*$, $\overline{V}_{xxi}^*$, and other like terms have no directional effect. Therefore, the following conditions result:

$$\overline{V}_i^{*2}(r),$$

$$\overline{V}_{xxi}^* = \overline{V}_{yyi}^* = \cdots = \overline{V}_{xyi}^* = \cdots, \qquad (= \overline{V}_i^{*\prime}),$$

$$i = 1, 2, \cdots N. \tag{17.2}$$

In spherical coordinates, an infinitesimal volume dQ* is expressed as $r^2 \sin\phi \, dr\, d\theta\, d\phi$. Thus, in the case of a vortex chaos motion, expressions of the real state of flow in (13.8) are written as the following summations of integrals in every spherical D_i^*- domain,

$$\overline{u^2} = \sum_{i=1}^{N} \left[\{ (\tilde{P}_i^*/Q_i^*) \int_0^{R_i^*} \int_0^{2\pi} \int_0^{\pi} (\overline{V}_i^{*2}(r) + \overline{V}_i^{*\prime}(r)) \} \cos^2\theta \sin^2\phi \, r^2 \sin\phi \, dr\, d\theta\, d\phi \right],$$

$$\overline{v^2} = \sum_{i=1}^{N} \left[\{ (\tilde{P}_i^*/Q_i^*) \int_0^{R_i^*} \int_0^{2\pi} \int_0^{\pi} (\overline{V}_i^{*2}(r) + \overline{V}_i^{*\prime}(r)) \} \sin^2\theta \sin^2\phi \, r^2 \sin\phi \, dr\, d\theta\, d\phi \right],$$

$$\overline{w^2} = \sum_{i=1}^{N} \left[\{ (\tilde{P}_i^*/Q_i^*) \int_0^{R_i^*} \int_0^{2\pi} \int_0^{\pi} (\overline{V}_i^{*2}(r) + \overline{V}_i^{*\prime}(r)) \} \cos^2\phi \, r^2 \sin\phi \, dr\, d\theta\, d\phi \right],$$

$$\overline{vw} = \sum_{i=1}^{N} \left[\{ (\tilde{P}_i^*/Q_i^*) \int_0^{R_i^*} \int_0^{2\pi} \int_0^{\pi} (\overline{V}_i^{*2}(r) + \overline{V}_i^{*\prime}(r)) \} \sin\theta \sin\phi \cos\phi \, r^2 \sin\phi \, dr\, d\theta\, d\phi \right],$$

$$\overline{wu} = \sum_{i=1}^{N} \left[\{ (\tilde{P}_i^*/Q_i^*) \int_0^{R_i^*} \int_0^{2\pi} \int_0^{\pi} (\overline{V}_i^{*2}(r) + \overline{V}_i^{*\prime}(r)) \} \cos\theta \sin\phi \cos\phi \, r^2 \sin\phi \, dr\, d\theta\, d\phi \right],$$

$$\overline{uv} = \sum_{i=1}^{N} \left[\{ (\tilde{P}_i^*/Q_i^*) \int_0^{R_i^*} \int_0^{2\pi} \int_0^{\pi} (\overline{V}_i^{*2}(r) + \overline{V}_i^{*\prime}(r)) \} \cos\theta \sin\theta \sin^2\phi \, r^2 \sin\phi \, dr\, d\theta\, d\phi \right], \tag{17.3}$$

where Q_i^* and R_i^* are the volume and the radius, respectively, of the D_i^*-domain. For the mean value of $\overline{u^2 v}$ and other like terms, expressions similar to (17.3) can be derived. These expressions, including (17.3), easily lead to the following results:

$$\overline{u^2} = \overline{v^2} = \overline{w^2} \qquad (= u^2),$$

$$\overline{vw} = \overline{wu} = \overline{uv} = 0,$$

$$\overline{v^2 w} = \overline{w^2 u} = \cdots = 0, \qquad (17.4)$$

$$\cdots$$

The above derivation is made for conditions of the real state of flow, and the characteristics of (17.4) are no more than those of the isotropic turbulent flow defined by G. I. Taylor (reference 13). Namely, conditions (17.1) and (17.2) of a spherical symmetry in the D*-domain have proved the condition of the isotropic turbulent flow. Thus, it can be concluded that the statistically and hydrodynamically simplest vortex chaos motion is the homogeneous and isotropic turbulence.

In Taylor's definition of isotropic turbulence, an irregularity of the velocity fluctuation is not implied explicitly. In the real expression (13.8), his definition corresponds to the assumption of $P^*_{1i}(r)$, $\overline{V_i^{*2}}(r), \cdots$ instead of $P^*_{1i} = 1$, $\overline{V_i^{*2}}(r), \cdots$. Although his definition has a wide field of application, it is doubtful whether such an isotropic turbulent flow really exists having the condition $P^*_{1i}(r)$ instead of $P^*_{1i} = 1$.

Probably, the definition of isotropic turbulence may have been introduced according to the physical image of such a vortex chaos motion as shown in Figure 1. But, in order to develop theoretical studies based on this definition, another condition of $\overline{U} = \overline{U}_0$ (constant) must be assumed. In our statistical theory of turbulence, it shall be assumed that the statistical and hydrodynamical uniformities $P^*_{1i} = 1$ and $\overline{U} = \overline{U}_0$ bring forth the conditions of the homogeneous and isotropic turbulence.

18. CHARACTERISTICS OF THE CORRELATION FUNCTIONS

In the homogeneous and isotropic turbulence, components of the mean and fluctuational velocities have simple properties as expressed in (17.1) and (17.4). Owing to their properties, the Reynolds equations and the Euler correlations in Sections 9 and 10 become simple expressions.

Components of the Euler correlation of velocity fluctuations at two points A and A' of coordinates x, y, z and x', y', z', respectively, are generally expressed in the tensor formula K of (10.1). In the case of the homogeneous and isotropic turbulence, intensities of the velocity fluctuation are constant across the mean flow. As mentioned previously, the Euler correlation has a nonzero value in a region having a length approximately equal to the mean scale of the individual vortices. Over such a small distance along the flow, variation of the intensity is negligible, and all the denominators in the formula K can be written as u^2.

The numerators in K have the general formulas of (13.13). Because

of the completely irregular vortex chaos motion in a uniform flow, they can be expressed by the summations of integrals in spherical D*-domains of the A*-point as in the formula (17.3) of the intensity. As mentioned in Section 12, when the fixed A- and A'-filaments are transmitted into the x*y*z*-space, local curvatures of vortex filaments are neglected as shown in Figure 21, and for the same kind of i-th vortices the coordinates (r', θ', ϕ') of the A'*-point in the D*-domain are determined uniquely, depending upon the position of (r, θ, ϕ) of the A*-point. Thus, in this case of flow, the Euler correlation (10.1) can be expressed as follows by taking a spherical D*-domain of the A*-point:

$$\overline{uu'}=\sum_{i=1}^{N}\left[\{(\tilde{P}_i^*/Q_i^*)\int_0^{R_i^*}\int_0^{2\pi}\int_0^{\pi}\{\bar{V}_i^*(r)\bar{V}_i^*(r')+\bar{V}_{xx_i}^{*'}(r,r')\}\cos\theta\sin\phi\cos\theta'\sin\phi' r'^2\sin\phi\,dr\,d\theta\,d\phi\right],$$

$$\overline{uv'}=\sum_{i=1}^{N}\left[\{(\tilde{P}_i^*/Q_i^*)\int_0^{R_i^*}\int_0^{2\pi}\int_0^{\pi}\{\bar{V}_i^*(r)\bar{V}_i^*(r')+\bar{V}_{xy_i}^{*'}(r,r')\}\cos\theta\sin\phi\sin\theta'\sin\phi' r'^2\sin\phi\,dr\,d\theta\,d\phi\right],$$

$$\overline{uw'}=\sum_{i=1}^{N}\left[\{(\tilde{P}_i^*/Q_i^*)\int_0^{R_i^*}\int_0^{2\pi}\int_0^{\pi}\{\bar{V}_i^*(r)\bar{V}_i^*(r')+\bar{V}_{xz_i}^{*'}(r,r')\}\cos\theta\sin\phi\cos\phi' r'^2\sin\phi\,dr\,d\theta\,d\phi\right],$$

$$\overline{vu'}=\sum_{i=1}^{N}\left[\{(\tilde{P}_i^*/Q_i^*)\int_0^{R_i^*}\int_0^{2\pi}\int_0^{\pi}\{\bar{V}_i^*(r)\bar{V}_i^*(r')+\bar{V}_{yx_i}^{*'}(r,r')\}\sin\theta\sin\phi\cos\theta'\sin\phi' r'^2\sin\phi\,dr\,d\theta\,d\phi\right],$$

$$\overline{vv'}=\sum_{i=1}^{N}\left[\{(\tilde{P}_i^*/Q_i^*)\int_0^{R_i^*}\int_0^{2\pi}\int_0^{\pi}\{\bar{V}_i^*(r)\bar{V}_i^*(r')+\bar{V}_{yy_i}^{*'}(r,r')\}\sin\theta\sin\phi\sin\theta'\sin\phi' r'^2\sin\phi\,dr\,d\theta\,d\phi\right],$$

$$\overline{vw'}=\sum_{i=1}^{N}\left[\{(\tilde{P}_i^*/Q_i^*)\int_0^{R_i^*}\int_0^{2\pi}\int_0^{\pi}\{\bar{V}_i^*(r)\bar{V}_i^*(r')+\bar{V}_{yz_i}^{*'}(r,r')\}\sin\theta\sin\phi\cos\phi' r'^2\sin\phi\,dr\,d\theta\,d\phi\right],$$

$$\overline{wu'}=\sum_{i=1}^{N}\left[\{(\tilde{P}_i^*/Q_i^*)\int_0^{R_i^*}\int_0^{2\pi}\int_0^{\pi}\{\bar{V}_i^*(r)\bar{V}_i^*(r')+\bar{V}_{zx_i}^{*'}(r,r')\}\cos\phi\cos\theta'\sin\phi' r'^2\sin\phi\,dr\,d\theta\,d\phi\right],$$

$$\overline{wv'}=\sum_{i=1}^{N}\left[\{(\tilde{P}_i^*/Q_i^*)\int_0^{R_i^*}\int_0^{2\pi}\int_0^{\pi}\{\bar{V}_i^*(r)\bar{V}_i^*(r')+\bar{V}_{zy_i}^{*'}(r,r')\}\cos\phi\sin\theta'\sin\phi' r'^2\sin\phi\,dr\,d\theta\,d\phi\right],$$

$$\overline{ww'}=\sum_{i=1}^{N}\left[\{(\tilde{P}_i^*/Q_i^*)\int_0^{R_i^*}\int_0^{2\pi}\int_0^{\pi}\{\bar{V}_i^*(r)\bar{V}_i^*(r')+\bar{V}_{zz_i}^{*'}(r,r')\}\cos\phi\cos\phi' r'^2\sin\phi\,dr\,d\theta\,d\phi\right].$$

(18.1)

In the expressions of (18.1), variables r', θ', ϕ' are dependent upon

r, θ, ϕ of the A*-point. However, because of the complete irregularity of relative locations of the vector $\overrightarrow{AA'}$ and the vortex filaments, corresponding to one location of $\overrightarrow{A^*A'^*}$ in the x*y*z*-space the reversed orientations reflected to every y*z*-, z*x*, x*y*-plane always exist. If A- and A'-points are on a line parallel to the x-axis, many components of correlation become zero by cancelling the symmetrical positions in the spherical D*-domain, except the following two components:

$$(\overline{uu'})/u^2 = f,$$

$$(\overline{vv'})/u^2 = (\overline{ww'})/u^2 = g. \tag{18.2}$$

The discussion may be easily understood by taking a two-dimensional case of the vortex chaos motion. In the case of arbitrarily located A- and A'-points in the field of flow, the vanishing of the remaining components besides f and g is also proved by the feature of a spherical symmetry in the D*-domain, where f and g are taken as the correlation coefficients of the components respectively parallel and perpendicular to the direction of $\overrightarrow{AA'}$.

When A- and A'-points are taken at some locations in the field of flow with a distance r, a correlation of the velocity fluctuations to their arbitrary directions can be proved as follows, expressed only in f and g (reference 14). Namely, in Figure 24, let the vectors $\overrightarrow{AA_1}$ and $\overrightarrow{A'A_1'}$, represent instantaneous velocity fluctuation at the two points A and A', and let the x'-, y'-, and z'-axes from the A-point be taken parallel to the x-, y-, and z-axes, respectively. Further, let the three components of velocity fluctuations at the A- and A'-points parallel to $\overrightarrow{AA'}$, perpendicular to $\overrightarrow{AA'}$ and contained in the A_1AA'-plane, and parallel to $\overrightarrow{BA_1'}$, be u, v, w and u', v', w', respectively, where B is an intersection of the perpendicular from A_1'-point to the $A'AA_1'$-plane. The angles α, β, and γ are taken as shown in Figure 24. Then, the relations $u = u'\cos\alpha + v'\sin\alpha$ and $v = (u'\cos\beta + v'\sin\beta)\sin\gamma + w'\cos\gamma$ are proved, and this relation follows:

$$(\overline{uv'})/u^2 = (f\cos\alpha\cos\beta + g\sin\alpha\sin\beta)\sin\gamma. \tag{18.3}$$

Thus, the tensor formula K of the correlations (10.1) can be generally expressed as

$$K = \frac{f-g}{k_r^2}\begin{pmatrix} k_x k_x & k_x k_y & k_x k_z \\ k_y k_x & k_y k_y & k_y k_z \\ k_z k_x & k_z k_y & k_z k_z \end{pmatrix} + g\begin{pmatrix} 1 & 0 & 0 \\ 0 & 1 & 0 \\ 0 & 0 & 1 \end{pmatrix},$$

$$k_x = x' - x, \qquad k_y = y' - y, \qquad k_z = z' - z,$$

$$k_r^2 = k_x^2 + k_y^2 + k_z^2.$$

(18.4)

Furthermore, the fundamental correlations f and g are proved to be related to each other (reference 14). Namely, when the time means are taken of the continuity equations at the A'-point multiplied by u, v and w, respectively, at the A-point, they are combined into the following formula:

$$g = f + \frac{k_r}{2}\frac{\partial f}{\partial k_r}.$$

(18.5)

In the triple correlations of $\overline{u^2 v'}$ and other similar terms at two points with a distance k_r, only the three components h, k, and q shown in Figure 25 remain with other components vanished by the feature of spherical symmetry in the D*-domain. As in the case of the double correlations, the following interrelations,

$$k = -2h \quad \text{and} \quad g = h - \frac{k_r}{2}\frac{\partial h}{\partial k_r},$$

(18.6)

can be derived from the continuity equations. For the higher order correlations, some reduction of the expressions may be made in the same manner.

As a matter of course, functional forms of the Euler correlation signify the property of the scale of turbulence. Fundamental characteristics of the scale may be manifested by the functional form of the double correlations. It is seen by integration formulas in (18.1) that at a short distance of k_r, the value of f depends for the most part on the small-scale vortices, while at a long distance it depends on large vortices. The triple and higher order correlations can be regarded as describing in more detail the character of the scale of turbulence.

From the spherical symmetry of the D*-domain, it is seen that the fundamental double correlation f or g has a symmetrical form for positive and negative values of k_r. When a scale length such as

$$L_f = \int_0^\infty f \, dk_r \tag{18.7}$$

is introduced, L_f chiefly concerns the large-scale primary vortices produced just behind the grid. Let another scale length λ_f be defined by

$$\frac{1}{\lambda_f^2} = \lim_{k_r \to 0} \left(\frac{1-f}{k_r^2} \right) = -\frac{1}{2} f''(0), \tag{18.8}$$

under the assumption that f can be expanded into the Taylor series at the origin. As shown in Figure 26, λ_f is equal to the half of the segment on the k_r-axis cut by the parabola touching the top of the f-curve. Thus, λ_f designates the property of f near the origin and chiefly concerns the small-scale descending vortices produced by the cascade process. L_f and λ_f, called the integral- and micro-scales, respectively, can be regarded as the two general standards of the scale of turbulence (reference 13).

It can be proved further that the quantities f, h, and u are not independent, but are interrelated. Namely, when the three equations of the Navier-Stokes equations at the A-point are multiplied respectively by u', v', and w' at the A'-point, and the time means are taken, they become

$$\frac{\partial (u^2 f)}{\partial t} = 2\nu u^2 \left(\frac{\partial}{\partial k_r} + \frac{4}{k_r} \right) \left(\frac{\partial f}{\partial k_r} - \frac{h}{\nu} u \right). \tag{18.9}$$

It is easily seen that f and h in formula (18.9) come from the viscous and inertia terms, respectively, of the Navier-Stokes equations. The formula

(18.9) is the foundation for discussion of statistical quantities of the isotropic turbulence, known as Kármán-Howarth's propagation formula of the Euler correlations (reference 14).

When the limiting value at $k_r \to 0$ is taken in (18.9), it becomes

$$\frac{du}{dt} = -10\nu \frac{u^2}{\lambda_f^2} ,$$

$$\frac{1}{\lambda_f^2} = \frac{1}{5} \lim_{k_r \to 0} \left\{ \frac{u}{\nu} \left(\frac{\partial h}{\partial k_r} + \frac{4}{k_r} h \right) - \left(\frac{\partial^2 f}{\partial k_r^2} + \frac{4}{k_r} \frac{\partial f}{\partial k_r} \right) \right.$$

(18.10)

If the Taylor expansion is possible at $k_r = 0$, λ^{-2} takes the same form as (18.8). Formula (18.10) is called the decaying formula, which denotes an interrelation of the turbulent intensity u and the microscale λ_f (reference 13).

19. REPRESENTATION BY THE SPECTRUM FUNCTIONS

Characteristics of the Euler correlation mentioned in the last section may also be represented by the spectrum functions. For instance, when the u-component of velocity fluctuation is taken at an A-point, this is an irregularly oscillating function for the time, which contains many kinds of frequency as shown in Figure 3. The intensity $u^2 = \lim_{t \to \infty} (1/t) \int^t u^2(t)\, dt$ will be divided into many infinitesimal regions contributed by the same value of a frequency n. When the wave number is taken as $k_1 = (2\pi n)/\bar{U}_0$ and the contribution to u^2 by the region between k_1 and $k_1 + dk_1$ is $u^2 F_1(k_1) dk_1$, then $F_1(k_1)$ is generally called the spectrum function, and the total intensity is expressed as

$$u^2 = u^2 \int_0^\infty F_1(k_1)\, dk_1 .$$

(19.1)

When the Fourier transformation of an instantaneous velocity function u(t) is written as $\phi_u(k_u)$ with $k_u = 2\pi n$, this relation is obtained:

$$\phi_u(k_u) = \frac{1}{\sqrt{2}} \int_{-\infty}^{\infty} u(t)\, e^{-k_u t}\, dt ,$$

and

and

$$u(t) = \frac{1}{\sqrt{2\pi}} \int_{-\infty}^{\infty} \phi_u(k_u) e^{-ik_u t} dk_u. \tag{19.2}$$

Furthermore, if the Lagrange correlation of velocity fluctuations at one point for different times t and $t-k_t$ is denoted by

$$R_{uu}(k_t) = \overline{u(t)\, u(t-k_t)} / u^2, \tag{19.3}$$

the following relations,

$$g(n) = 4 \int_0^{\infty} R_{uu}(k_t) \cos 2\pi n k_t \, dk_t$$

and

$$R_{uu}(k_t) = \int_0^{\infty} g(n) \cos 2\pi n k_t \, dn, \tag{19.4}$$

can be derived by taking formula (19.1) into account (reference 29).

In the vortex chaos motion of turbulent flow, an instantaneous state of the chaotic motion incessantly changes with time and position. However, in homogeneous and isotropic turbulence, scales of vortices are far smaller than the breadth of the flow, and the mean flow gives no effect to the individual vortices by the pressure gradient and other forces. Thus, it can be considered that in a narrow region along the flow of the same order of the mean scale as that of the vortices, the vortex chaos motion retains approximately constant situations of motion. Namely, in the region of nonzero value of the Euler correlation, the function u(t) at a point is assumed to be transported in the same form by a constant mean velocity $\overline{U}_0$. This assumption, known as Taylor's hypothesis, was introduced at the same time as the definition of isotropic turbulence (reference 13). In accordance with this hypothesis, we have put a constant denominator in the tensor expression K of (10.1).

Based on this hypothesis, it is easily seen that the Lagrange correlation $R_{uu}(k_t)$ in (19.4) is the same as the Euler correlation $f(k_r)$ at two points with the distance $k_r = \overline{U}_0 k_t$. Then, the formulas in (19.4) can be written as

$$f(k_T) = \int_0^\infty F_1(k_1) \cos k_1 k_T \, dk_T$$

and

$$F_1(k_1) = \frac{2}{\pi} \int_0^\infty f(k_T) \cos k_1 k_T \, dk_T \tag{19.5}$$

by using the function $F_1(k_1)$ of (19.1). The function f and F_1 are quantities which can be measured by experiment. Figures 27 and 28 show examples of the observed results on the relations of (19.5), where Taylor's hypothesis seems to be supported in the case of a uniform turbulent wake behind a grid.

The above discussions on the spectrum function have been made by taking only the wave number k_1 to the x-direction. Strictly speaking, however, the Fourier analysis of a velocity fluctuation should be done with three components of the wave number k_1, k_2, and k_3 respective to the x-, y-, z-direction (reference 30). The three-dimensional expression of the u-component of velocity fluctuation which corresponds to (19.2) is written as

$$u(t) = \frac{1}{(2\pi)^{3/2}} \iiint_{-\infty}^{\infty} \Xi_u(k_1, k_2, k_3) \, e^{i(k_1 x + k_2 y + k_3 z)} \, dk_1 dk_2 dk_3 . \tag{19.6}$$

The intensity u^2 is expressed in the integration of (19.6) in a large volume Q. This representation is the same as that for the v- and w-fluctuations. Thus, when a function such as F_3 is introduced,

$$u^2 F_3(k) = \frac{4\pi k^2}{3Q} \left\{ |\Xi_u|^2 + |\Xi_v|^2 + |\Xi_w|^2 \right\} k^2 \, dk,$$

$$k = \sqrt{k_1^2 + k_2^2 + k_3^2}, \tag{19.7}$$

and the following integration,

$$u^2 = u^2 \int_0^\infty F_3(k) \, dk, \tag{19.8}$$

is obtained for the expression of u^2.

Although the formula (19.8) is similar to (19.1), F_3 is clearly a different expression of a combination of the three components of wave number. Usually, F_1 and F_3 are distinguished as the one- and three-dimensional spectrums. It is proved by their definition that they are not independent but are related to each other by the following expressions:

$$F_1(k_1) = \frac{3}{2}\int_{k_1}^{\infty} F_3(k)\,\frac{k^2-k_1^2}{k^3}\,dk,$$

$$F_3(k_1) = \frac{k_1^3}{3}\frac{d}{dk_1}\left(\frac{1}{k_1}\,\frac{dF_1}{dk_1}\right). \tag{19.9}$$

As seen in (19.5), the Euler function f can be related to the spectrum function F_1 or F_3. Corresponding to the propagation formula (18.9) of the Euler correlation, a similar expression of the spectrum functions must exist. Namely, when equation (18.9) is multiplied by $(2/\pi)\cos kk_r$ and is integrated by k_r in $0\sim\infty$, it leads to

$$\frac{\partial}{\partial t}\left(u^2\frac{2}{\pi}\int_0^{\infty} f\cos kk_r\,dk_r\right) + \frac{4}{\pi}u^3\int_0^{\infty}\left(\frac{\partial h}{\partial r}+\frac{4}{r}h\right)\cos kk_r\,dk_r$$

$$= \frac{4\nu}{\pi}u^2\int_0^{\infty}\left(\frac{\partial^2 f}{\partial r^2}+\frac{4}{r}\frac{\partial f}{\partial r}\right)\cos kk_r\,dk_r.$$

If

$$H(k) = \frac{2}{\pi}\int_0^{\infty} h(k_r)\sin kk_r\,dk_r \tag{19.10}$$

and the one-dimensional spectrum F_1 of (19.5) is taken, the above expression becomes

$$\frac{\partial(u^2F_1)}{\partial t} + 2u^3\left\{Hk + 4\int_k^{\infty} H\,dk\right\} = -2\nu u^2\left\{F_1k^2 + 4\int_k^{\infty} F_1\,k\,dk\right\}. \tag{19.11}$$

When the differentiation process denoted by the second expression in (19.9) is carried out in the expression (19.11), the following formula of the three-dimensional spectrum F_3 is obtained.

$$\frac{\partial(u^2F_3)}{\partial t} + 2u^3W_3 = -2\nu u^2F_3k^2, \tag{19.12}$$

where

$$W_3 = kH - k^2\frac{dH}{dk} + \frac{k^3}{3}\frac{d^2H}{dk^2}\ . \tag{19.13}$$

This formula of the propagation of the spectrum function is often expressed simply as

$$\frac{\partial E}{\partial t} + W = -2\nu k^2E,$$

$$E = u^2F_3, \quad \text{and} \quad W = 2u^3W_3\ . \tag{19.12'}$$

As is easily seen by the definitions, the terms E and W are related respectively to the double and triple correlation functions which are derived from the viscous and inertia terms in the Navier-Stokes equations, respectively.

It is mentioned in Section 17 that basic quantities of the intensity and scale of the isotropic turbulence are represented by the components u and f or h, respectively. The three-dimensional spectrum functions F_3 and W_3 which correspond to f and h, do not have different components according to the x-, y- and z-direction in the field of flow. The isotropic turbulence is that in which these fundamental quantities vary only along the x-direction of the flow. In this sense, the isotropic turbulence is essentially a one-dimensional flow.

Discussions in Sections 17, 18, and 19 concern the kinematical characteristics of the isotropic turbulence. The work which we shall have to do hereafter is to evaluate the behaviors of these fundamental functions along the flow in accordance with the real states of the isotropic turbulent flow. Viewed from a theoretical principle, the kinematical formulas (18.9), (18.10), or (19.12) are no more than transformations from the Reynolds equations in the case of the homogeneous

and isotropic turbulence of the completely irregular vortex chaos motion in a uniform flow. Namely, these formulas are not those which have compensated for the insufficiency of some physical principles in the Reynolds equations. For instance, in the decaying formula (18.10), two independent variables u and λ_f are involved. The propagation formula (18.9) of the Euler correlation has the three variables u, f, and h. The situations are the same for the spectrum-propagation formula (19.12) having u, F_3, and W_3. Even if the propagation of the triple correlation is formulated similarly to (18.9), the formula may further contain the fourth correlation and shall never become a mathematically conclusive system. Of course, this is the same as for the spectrum propagation. Namely, the basic obstacle in the study of turbulent flow, that the Reynolds equations are not conclusive because of the inertia terms of the Navier-Stokes equations, has not yet been overcome, even in the simplest case of the homogeneous and isotropic turbulence.

20. CONCEPTION OF SIMILARITY PRESERVATION

Fundamental formulas (18.9), (18.10), and (19.12) of the isotropic turbulence have far simpler mathematical expressions than those of the Reynolds equations. On account of the simple expressions, these formulas are available, combined with other physical assumptions, to investigate the characteristics of statistical quantities of the isotropic turbulence. Similarity preservation has been introduced as one of the physical assumptions in the previous studies of isotropic turbulence. This section will consider the basic conception of the similarity preservation, based upon the physical interpretations of a vortex chaos motion.

It is mentioned that the definition of the isotropic turbulence is deduced from the completely irregular chaotic states of many kinds of vortices in a uniform mean flow, and the discussions in Sections 17, 18, and 19 hold for these chaotic motions of all the vortices of N kinds. Now, such an idealized isotropic turbulence shall be considered as consisting of one kind of vortex produced at a fixed location x=0, and shall take the approximation of an ideal state mentioned in Section 13. Then, the representations of the intensity (17.3) and correlation (18.1) are written by the following integrations in a single spherical D*-domain with a radius R*.

$$u^2 = \frac{1}{Q^*} \iiint_{D^*} \bar{V}^{*2}(r) \cos^2\theta \sin^2\phi \, dQ^*,$$

$$\overline{uu'} = \frac{1}{Q^*} \iiint_{D^*} \bar{V}^*(r) \bar{V}^*(r') \cos\theta \sin\phi \cos\theta' \sin\phi' \, dQ^*,$$

$$Q^* = \frac{4}{3} R^{*3}. \tag{20.1}$$

Since the elongation and curvature of a vortex filament have been neglected in the definition of the V*-function of (11.1), the ideal state of the isotropic turbulence refers to the three-dimensional and completely irregular state of vortices which keep two-dimensional characteristics in a uniform flow. Thus, the solution (14.6) of the viscous vortex motion can be taken as a functional form of $\overline{V}^*(r)$ in (20.1). By the solution (14.6) the extension of a vortex motion is seen to be proportional to $\sqrt{t}$, and the radius R* is appropriately chosen as

$$R^* = \sqrt{4\gamma s_0}\ \sqrt{t}, \tag{20.2}$$

where s_0 is a constant independent of t in (14.2). From the solution (14.6), the function $\overline{V}^*(r)$ in (20.1) can be written with a suffix α which denotes the condition of production.

$$\overline{V}^* = F_\alpha(s) G_\alpha(t),$$

$$s = \frac{r^2}{4\gamma t}. \tag{20.3}$$

In (20.3), F_α is a function of s in the interval $0 \sim s_0$ in the D*-domain. G_α is a function of the time t since the production of vortices, and is not dependent upon the coordinates in the D*-domain.

Thus, the turbulent intensity in (20.1) is written as

$$u^2 = \{\iiint_{D^*} F_\alpha^2(s) \cos^2\theta \sin^2\phi \, dQ^*\}\{G_\alpha^2(t)/Q^*\}, \tag{20.4}$$

where the first term is a definite integral in the spherical D*-domain with a radius R* of (20.2) and does not involve t explicitly.

For the correlation f at A- and A'-points of a distance k_x to the x-direction, the numerator $\overline{uu'}$ of (20.1) is written as

$$\overline{uu'} = \left\{ \iiint_{D^*} F_q(s) F_q(s') \cos\theta \sin\phi \cos\theta' \sin\phi' \, dQ^* \right\} \left\{ G_q^2(t) / Q^* \right\} . \tag{20.5}$$

In the above expression, s, θ, ϕ and s', θ', ϕ' are the coordinates of the A*- and A'*-points in the D*-domain, and the latter are decided uniquely with the former as interpreted in Section 12. In the case of isotropic turbulence, when the same spherical D*-domain as in (20.4) is taken and a parameter such as

$$s_x = \frac{k_x^2}{4\gamma t} \tag{20.6}$$

is used instead of k_x, then the first term in (20.5) is regarded as a function of s, θ, ϕ, s_x in the expanding D*-domain along the flow as denoted by (20.2). Thus, the correlation function f is written as

$$f = \frac{\iiint_{D^*} F_q(s) F_q(s') \cos\theta \sin\phi \cos\theta' \sin\phi' \, dQ^*}{\iiint_{D^*} F_q^2(s) \cos^2\theta \sin^2\phi \, dQ^*} , \tag{20.7}$$

and is considered to be a function only of s_x independently of t.

This independency characteristic also holds in the triple correlation. For instance, the correlation h is reduced to

$$h = \frac{\iiint_{D^*} F_q^2(s) F_q(s') \sin^2\theta \sin^2\phi \cos\theta' \sin\phi' \, dQ^*}{\iiint_{D^*} F_q^3(s) \cos^3\theta \sin^3\phi \, dQ^*} \tag{20.8}$$

in the same manner as f of (20.7). Furthermore, in this case and on account of the spherical symmetry, the integrand multiplied by $\cos\theta' \sin\phi'$ is cancelled at symmetrical positions in the spherical D*-domain, as is easily seen in the two-dimensional vortex chaos motion, and the value of h vanishes. This is the same for k and q, and

$$h = k = g = 0 \tag{20.9}$$

is obtained. The above results in (20.7) and (20.9) are no more than

those which Kármán and Howarth have introduced as the assumptions of similarity preservation in isotropic turbulence (reference 14).

It is suggested by the above discussions that in expressions (13.9) and (13.13) of the ideal state of N=1 vortices when two fundamental functions P* and V* have respective similarity characteristics independent of t in the D*-domain, the Euler correlations preserve their similar functional forms along the flow. Namely, according to the physical interpretation of a vortex chaos motion, it is found that the similarity preservation in turbulent flow consists of two kinds of similarities: a hydrodynamical similarity of the V*-function which is proved by the solution of the Navier-Stokes equations, and a statistical similarity of the P*-function given a priori as a statistical hypothesis. Kármán-Howarth's similarity assumption for isotropic turbulence belongs to the case where the P*- and V*-functions, respectively, have similarity conditions in their simplest forms.

By integrating (20.4), the following expression results:

$$u^2 = C_{u^2}\, t^{1-2\alpha}, \qquad (\alpha \geqq 1),$$

$$C_{u^2} = \{(2C_\alpha^2 \gamma)/S_o^{3/2}\} \int_o^{S_o} F_\alpha^2(s)\sqrt{s}\, ds. \tag{20.10}$$

In the exponential formula (20.10), C_{u^2} is obviously independent of the time t since the production of the vortices, and t is related to the mean speed U_o with

$$\bar{U}_o = \frac{x}{t}\ . \tag{20.11}$$

Namely, (20.10) suggests that the intensity u should be plotted versus t instead of x. If plotted versus x, experimental data may be scattered with different mean speed U_o.

As for the correlation function, the propagation formula (18.9) takes the form of an ordinary differential equation owing to the features of (20.7), (20.9), and (20.10). When the nondimensional length,

$$\xi = 2\sqrt{s_x} = k_x/\sqrt{\gamma t},$$

(20.12)

is taken and f is regarded as a function of ξ, (18.9) becomes

$$f''(\xi)+(\frac{4}{5}+\frac{\xi}{4})f'(\xi) + \frac{2\alpha-1}{2} f(\xi) = 0,$$

(20.13)

where ' denotes d/d ξ. The equation (20.13) is the same form as that derived by Kármán-Howarth, and the solution is proved to be expressed as a hypergeometric function as follows (reference 14):

$$f_\alpha(\xi) = 2^{\frac{15}{2}} \xi^{-\frac{5}{2}} \exp\left\{\frac{-\xi^2}{16}\right\} M_{2\alpha-\frac{9}{4},\frac{3}{4}}\left(\frac{\xi^2}{8}\right),$$

$$M_{k,m}(z) = z^{\frac{1}{2}+m} e^{-\frac{z}{2}}\left\{1+\sum_{i=1}^{\infty} \frac{(m-k+\frac{1}{2})(m-k+\frac{3}{2})\cdots(m-k+\frac{2i-1}{2})}{i!\,(2m+1)(2m+2)\cdots(2m+i)} z^i\right\}.$$

(20.14)

Figure 29 shows the functional forms of (20.14).

The integral- and microscale of (18.7) and (18.8) are expressed as

$$L_f^2 = C_{L_f^2}\gamma t, \qquad C_{L_f^2} = \left\{\int_0^\infty f_\alpha(\xi)\,d\xi\right\}^2,$$

$$\lambda_f^2 = C_{\lambda_f^2}\gamma t, \qquad C_{\lambda_f^2} = 10/(2\alpha-1).$$

(20.15)

Even if the microscale λ_f is not equal to the integral-scale L_f, the meaning of a finite value of λ_f may be understood by the physical picture of a chaotic motion of one kind of vortex in which the production of infinitesimal small vortices by the cascade process is neglected.

21. SIMILARITY PRESERVATION IN THE INITIAL PERIOD

In the expressions of the similarity law, the selection of the value of α concerns the condition of production of a vortex motion in the real flow, and the selection cannot be made from a purely theoretical point of view. Investigations must be made in the light of experimental works. At first, the theoretical results of (20.10) to (20.15) shall be checked by comparison with experimental results.

In a uniform flow behind a grid, it is easy to use the hot-wire technique to measure velocity fluctuations to determine the turbulent intensity. Except for the transition region just behind the grid, many previous experimental results indicate that for a fairly long distance behind the grid, an empirical formula such as

$$u^2 \propto \frac{1}{t} \tag{21.1}$$

can be adapted, and that further downstream the decaying process is more rapid. The formula (21.1) is usually expressed as $u^{-2} \propto t$, and is called the linear-decay law. Figure 30 shows an example of measurements.

In the real states of turbulent flow behind a grid, effects of the cascade phenomena and three-dimensional characteristics of vortices cannot be neglected, and the idealizations mentioned in the last section do not hold exactly. However, in a region along the flow where the primary vortices which are produced directly from the grid are predominant, the above-mentioned idealizations may have significance.

When the empirical formula (21.1) is compared with the theoretical result (20.10), it may be correct to take

$$\alpha = 1. \tag{21.2}$$

As explained in Section 14, the solution of $\alpha = 1$ in (14.6) applies far from the vortex center to the vortex motion of a perfect fluid. This fact favors regarding the primary vortices produced by the energy of the potential flow outside the boundary layer as those of the solution of $\alpha = 1$. Theoretical results (20.15) of the turbulent scales hold independently of the suffix α. However, they are also supported by many observations as shown in Figures 31 and 32.

When the theoretical curves of the correlation function f in Figure 29 are compared with an experimental measurement in Figure 27, it turns out that the solution of $\alpha = 1$ in (20.14) is difficult to adapt to the real

state of the isotropic turbulent flow. Departure from the axis of the f-curve at a large value of k_r may be attributed to the approximative description of the ideal state in which the value of uu' is expressed with a connection of a single kind of $\alpha = 1$ vortex, even at a large value of k_r.

Near the origin $k_r = 0$, however, the theoretical curve of $\alpha = 1$ does not have a sharp peak, as indicated by experimental observations. This is also recognized in other cases of $\alpha > 1$, and the real state of the correlation seems to have a different nature near the origin from all the similar solutions. Moreover, it is proved experimentally that the triple correlation coefficients do not vanish although the numerical values are small, at most no larger than 0.03 (reference 31). Probably, the discrepancy of the correlation functions near the origin may be caused by the production of small vortices through the cascade process. Namely, the newly produced small vortices give a direct effect to the functional form near the origin $k_r = 0$, even if the total scale length L_f and the intensity u^2 are slightly affected by them. Existence of a nonzero value of the triple correlation is also difficult to comprehend without considering a cascade phenomena. Considering the propagation formula (18.9) of the correlation functions, the effect of a nonzero value of h may be integrated along the flow to alter the functional form of f near $k_r = 0$, although the value of h, itself, is small. The above-mentioned considerations of the correlations must be the same for the spectrum functions, which are the Fourier transformations of the correlation functions.

From the above-mentioned interpretations, it may be understood that in isotropic turbulence, when the primary vortices are made to correspond to those of $\alpha = 1$, and ideal expressions of the completely irregular state of two-dimensional vortex motions are taken, at least the two fundamental quantities of the total intensity and the scale length are considered to be supported by observed results. This idealized picture of a vortex chaos motion is easily adapted to cases other than that of the completely irregular state in a uniform flow. Thus, let the ideal expressions of such a vortex chaos motion be generally called the law in the initial period, and especially when the P^*- and V^*-functions have their similarity conditions, they shall be called the similarity law in the initial period.

Since the definition of the isotropic turbulence was introduced and the propagation formula of the correlation or the spectrum was established, a study was first made to solve these fundamental formulas by assuming the similarity preservation. Then, from the results of many experimental studies on the distribution of the turbulent intensity, the relation (21.1) was ascertained, and the region where (21.1) can be supported experimentally is called the initial period by Batchelor-Townsend (reference 28). The initial-period similarity-law mentioned in Sections 20 and 21 is that used to derive the Kármán-Howarth similarity assumption from the physical interpretation of a vortex chaos motion and has given physical meaning to the conception of the initial period as detected by experimental observations.

It is certain, however, that the similarity assumption has not derived a satisfactory result for the correlation or the spectrum function. In this chapter, discussions are made only on similarity preservation. The fundamental meaning of similarity preservation must be grasped before proceeding to the study of nonsimilarity. If the similarity preservation is derived, not as an assumption, from some fundamental hypotheses, from these hypotheses some suggestion will be obtained to guide us in our search for the characteristics of nonsimilarity.

On the other hand, it seems that in other cases of turbulent shear flow, the approximative expression of the similarity law has a more important significance. From the standpoint of a vortex chaos motion, it is possible to extend the simplest hydrodynamical and statistical similarity conditions directly to the case of the decaying turbulence. Thus, the following two chapters will discuss problems of the extended initial-period law, and the nonsimilarity problems will be studied later from a wider viewpoint of the decaying turbulence.

CHAPTER FIVE. SIMILARITY THEORY IN THE INITIAL PERIOD

22. IDEALIZATION OF THE INITIAL PERIOD

As mentioned in Section 21, the essential meaning of the law in the initial period exists in taking an expression of the ideal state of the chaotic state of the $\alpha = 1$ vortices in their statistical equilibrium. In the case of an isotropic turbulence, both the P*- and V*-functions have their respective similarity characteristics owing to the completely irregular chaotic states in a uniform flow, which have proven the similarity preservation of the flow. Further, by applying a two-dimensional solution to the V*-function, simple expressions of the distributions of the intensity and scale along the flow have been obtained. In general cases of the decaying turbulence, however, the initial-period law does not necessarily derive the similarity character, and expressions for the intensity and scale become somewhat complicated.

A nonisotropic, shearless turbulence will first be considered. This case of flow is still a completely irregular motion of N kinds of vortices, but the mean-velocity distribution is not uniform. Because of the complete irregularity, the vortex chaos motion does not bring about any shearing stress, and the effect of normal pressure caused by the chaotic motion is small. Thus, when the potential function of the mean flow is denoted by $\bar{\Phi}$, the condition of the flow is written as

$$P_{1i}^{*} = 1, \qquad i = 1, 2, \ldots N,$$

$$\bar{U} = \frac{\partial \bar{\Phi}}{\partial x}, \qquad \bar{V} = \frac{\partial \bar{\Phi}}{\partial y}, \qquad \bar{W} = \frac{\partial \bar{\Phi}}{\partial z}, \tag{22.1}$$

corresponding to (17.1) in the isotropic turbulence.

In the case of the completely irregular vortex chaos motion, effects of the potential function $\bar{\Phi}$ to the vortex motions are only to the directions of the x-, y-, z-axes, and, as assumed in a two-dimensional vortex chaos motion, the V*- and V*'-functions are regarded as symmetrical to the axes in the D*-domain. Thus, in the real expression (13.8), the terms of vw, wu, uv vanish. Namely, the potential function of $\bar{\Phi}$ (x, y, z) means the flow without a shearing stress. But, unlike the result (17.4) of the isotropic turbulence, components of the intensity u, v, w generally have different values in respect to each other.

In a wind tunnel, the air stream from a rectifying grid is led to the test section through a contracting section. Vortices produced from

the grid may be mixed into a completely irregular state, but they must be affected by the pressure gradient of the mean flow in a contracting section. By experimental measurement, the values of u, v, w are generally different, although correlation components $\overline{uv}$ and other like terms vanish. This case of a contracting stream corresponds to an example of the non-isotropic shearless turbulence.

Only the primary vortices of $\alpha = 1$ shall be taken into account in the shearless turbulence. Even if three-dimensional effects of elongation of the vortex filaments are neglected as in the case of the similarity law in isotropic turbulence, the $\overline{V}^*$-function is affected by the pressure gradient caused by $\overline{\Sigma}(x, y, z)$ unlike the case of a uniform flow. According to a given field of $\overline{\Sigma}(x, y, z)$, however, it is difficult to derive an exact formula of the $\overline{V}^*$-function from the hydrodynamical equations of motion, and as the first approximative expression,

$$\overline{V}^*(s, \theta, \phi; x, y, z)\,(2c\sqrt{\gamma}\,t^{-\frac{1}{2}}),$$

$$s = \frac{r^2}{4\gamma t},$$

(22.2)

will be taken as an extended expression of (14.6) in isotropic turbulence. Hereafter, the suffix 1 denoting the $\alpha = 1$ vortices shall be neglected for brevity.

The condition $P_1^{*\prime}=1$ in (22.1) has statistical similarity independent of the coordinates x, y, z. On the other hand, the $\overline{V}^*$-function in (22.2) does not necessarily have hydrodynamical similarity. Therefore, the description of an ideal state based upon (22.1) and (22.2) does not generally derive the result of similarity preservation, although their description is based upon the same theoretical foundation as the Kármán-Howarth similarity hypothesis in isotropic turbulence.

The turbulent wake behind a circular cylinder in a uniform flow will be considered as a simple example of the decaying shear turbulence. In the case of the turbulent wake behind a grid, production of vortices from a rod of the grid is not affected by situations downstream and is not influenced by other vortices produced by other rods. Namely, the condition of production of vortices may be the same, both in the cases behind a circular cylinder and in a grid consisting of the same kind of cylinders. It is natural to assume that the primary vortices in the decaying turbulence all belong to those of $\alpha = 1$.

When the co-ordinate axes are fixed as shown in Figure 33, the mean-velocity distribution keeps a two-dimensional character in the xy-plane. The primary vortices are first separated alternatively from both sides of

the cylinder with the vortex filaments parallel to the z-axis, and then the Kármán vortex streets can be observed on the xy-plane. As far as the theoretical Kármán vortex streets are observed, probably the vortex filaments keep nearly parallel to the z-axis. However, as the vortex streets break into an irregular state, the filaments probably begin to take on a three-dimensional fluctuation around the z-direction. In chaotic states of vortices far from the cylinder, three-dimensional effects of the filaments cannot be neglected. Thus, the idealization of an initial-period law in this case could be the chaotic motion of the $\alpha = 1$ vortices which keep two-dimensional features themselves, with only the direction of filaments fluctuating around the z-direction.

The vortices of $\alpha = 1$ become irregular as they go downstream. But, as interpreted in Section 6, it is difficult for them to become completely irregular because of the directional effects in the interaction of vortices produced from the cylinder. And, even at a position of x, the functional form of P*, indicating the statistical situation of the running of vortices, varies with the y-direction. But, the $\overline{V}$*-function expressing mean states of the vortices produced at one position upstream is unaltered in the y- or z-direction and is not affected by the pressure gradient of the mean flow.

The chaotic motion of the $\alpha = 1$ vortices in this case may be reasonably assumed to be in a statistical equilibrium, but not in a wide region along the flow. Thus, as an extension of the case of the isotropic turbulence, the initial-period law in this case is expressed by

$$P^* = P_1^*(s, \theta, \phi; \eta) / \Omega^*,$$

$$\overline{V}^* = F(s, \theta, \phi)(2C\sqrt{\nu}\, t^{-\frac{1}{2}}),$$

$$s = \frac{r^2}{4\nu t}, \qquad \eta = \frac{y}{\sqrt{4\nu t}}. \tag{22.3}$$

Namely, even if the mean-velocity distribution is two-dimensional in the xy-plane, a finite value of the z-component of turbulent intensity exists, and the initial-period law gives a similarity preservation in this case.

In the decaying turbulence, there are many kinds of shear and shearless turbulence. According to the particular cases, the P*- and $\overline{V}$*-functions may take different expressions. For instance, in the case of a round jet, an elongation of the vortex ring cannot be neglected even in the initial period. In the case of a two-dimensional wake in a nonuniform mean flow, a distortion of the $\overline{V}$*-function in (22.3) caused by the pressure gradient must be evaluated. However, if the statistical similarity expressed in the P*-function is assumed for the chaotic motion of the

primary vortices of $\alpha = 1$, an idealized expression of the vortex chaos motion can be obtained. It is proved in Sections 21 and 22 that in the case of isotropic turbulence this idealization supports the Kármán-Howarth similarity assumption. In this chapter some investigations on the extended formulas of the initial-period law of the decaying turbulence shall be made (references 18 and 37).

23. INTENSITY AND SCALE OF THE SHEAR TURBULENCE

As a typical case of the decaying shear turbulence, a turbulent wake behind a circular cylinder will be taken and the distributions of the turbulent intensity and scale under the condition of the initial-period similarity-law shall be surveyed. Expressions for the intensities of the $\alpha = 1$ vortices can be written as follows, with formula (22.3) substituted into (13.5):

$$\overline{u^2} = C_{u^2}(\eta)\,t^{-1}, \qquad \overline{v^2} = C_{v^2}(\eta)\,t^{-1}, \qquad \overline{w^2} = C_{w^2}(\eta)\,t^{-1},$$

$$\overline{vw} = C_{\overline{vw}}(\eta)\,t^{-1}, \quad \overline{wu} = C_{\overline{wu}}(\eta)\,t^{-1}, \quad \overline{uv} = C_{\overline{uv}}(\eta)\,t^{-1}, \quad \eta = y/\sqrt{4\nu t},$$

$$C_{u^2}(\eta) = \frac{4c^2\gamma}{Q^*}\iiint_{D^*} P_1^*(s,\theta,\phi;\eta)F^2(s,\theta,\phi)\cos^2\theta\sin^2\phi\,dQ^*,$$

$$C_{v^2}(\eta) = \frac{4c^2\gamma}{Q^*}\iiint_{D^*} P_1^*(s,\theta,\phi;\eta)F^2(s,\theta,\phi)\sin^2\theta\sin^2\phi\,dQ^*,$$

$$C_{w^2}(\eta) = \frac{4c^2\gamma}{Q^*}\iiint_{D^*} P_1^*(s,\theta,\phi;\eta)F^2(s,\theta,\phi)\cos^2\phi\,dQ^*,$$

$$C_{\overline{vw}}(\eta) = \frac{4c^2\gamma}{Q^*}\iiint_{D^*} P_1^*(s,\theta,\phi;\eta)F^2(s,\theta,\phi)\sin\theta\sin\phi\cos\phi\,dQ^*,$$

$$C_{\overline{wu}}(\eta) = \frac{4c^2\gamma}{Q^*}\iiint_{D^*} P_1^*(s,\theta,\phi;\eta)F^2(s,\theta,\phi)\cos\theta\sin\phi\cos\phi\,dQ^*,$$

$$C_{\overline{uv}}(\eta) = \frac{4c^2\gamma}{Q^*}\iiint_{D^*} P_1^*(s,\theta,\phi;\eta)F^2(s,\theta,\phi)\cos\theta\sin\theta\sin^2\phi\,dQ^*. \tag{23.1}$$

The coordinates of the field of flow are taken as shown in Figure 33. In (23.1), t is the time since the outbreak of the $\alpha = 1$ vortices and is obviously connected with the mean velocity by the relation

$$t = \int_0^x \bar{U}^{-1} dx. \tag{23.2}$$

For the Euler correlation, discussions in the case of an isotropic turbulence can be extended. For instance, when $g = \overline{uu'}/$, $(\overline{uu'})$ is taken as a correlation coefficient at two points A and A' with a distance k_y to the y-direction, the ideal expression for g similar to expression (20.7) is written as follows:

$$g = \frac{\iint_{D^*} P_1^*(s,\theta,\phi;\eta) F(s,\theta,\phi) F(s',\theta',\phi') \cos\theta \sin\phi \cos\theta' \sin\phi' dQ^*}{\left\{\iint_{D^*} P_1^*(s,\theta,\phi;\eta) F^2(s,\theta,\phi) \cos^2\theta \sin^2\phi dQ^*\right\}^{\frac{1}{2}} \left\{\iint_{D^{*'}} P_1^{*'}(s',\theta',\phi';\eta') F^2(s',\theta',\phi') \cos^2\theta' \sin^2\phi' dQ^{*'}\right\}^{\frac{1}{2}}}. \tag{23.3}$$

In the numerator s, θ, ϕ and s', θ', ϕ' are the respective co-ordinates of the A*- and A*'-points in the D*-domain; in the denominator P^* and F'^2 are the functions defined in the D*'-domain for the A'-point, and 1 are the respective ordinates of the A- and A'-points in the field. In this field of shear turbulence, a vortex motion, although not disturbed by others, may still be distorted by the shearing stress of the mean flow, and the turning velocity $\mathbf{V}^*$ of (11.1) may not be in circular symmetry. As mentioned in Section 12, however, s', θ', and ϕ' are determined uniquely in the D*-domain according to the coordinates s, θ, ϕ, and a distance k_y. Thus, when a parameter

$$s_y = \frac{k_y^2}{4\nu t} \tag{23.4}$$

is introduced, (23.3) is seen to be a function of s_y only as in (20.7) for isotropic turbulence. Namely, the similarity preservation expressed in (20.7) still holds in this case of shear turbulence.

When the scale lengths of L_g and λ_g are defined as (18.7) and (18.8), their distribution in the x-direction is written as

$$L_g^2 = C_{L_g^2} \nu t,$$

$$\lambda_g^2 = C\lambda_g^2 \nu t, \tag{23.5}$$

as (20.15). Other components of correlation function and their scale lengths can also be defined as (23.3) and (23.5).

In nonisotropic decaying turbulence, the field of flow is not homogeneous, and the condition of spherical symmetry as in isotropic turbulence does not hold. These results complicate the situation. Namely, even in the simple case of a two-dimensional wake, there are different components of the intensity and functional forms of the correlation, which cannot be reduced to the two elements u and f only, as in the case of isotropic turbulence. It is also difficult to prove the vanishing of the triple correlations under the idealized expression of the initial-period similarity-law. Thus, we cannot expect such a simple propagation formula of the correlation function as (18.9), and it becomes difficult to extend phenomenological discussions based on the propagation formula into general cases of the decaying turbulence. In the case of isotropic turbulence, when the approximation of the initial-period similarity is taken, the correlation functions can easily be derived from the propagation formula without evaluating the integration of (20.7). In other cases, however, (23.3) will have to be evaluated directly for the purpose of determining the functional forms.

The above-mentioned results of the initial-period similarity-law can be ascertained by experimental measurements. Observed results on the distribution of C_{u^2} and other terms in the y-direction in (23.1) are shown in Figure 34. In the case of isotropic turbulence, these coefficients of the intensity are reduced to a constant, and the similarity preservation must be examined by observing the form of f or another correlation function. In shear turbulence, however, this characteristic can also be seen in the profile of C_{u^2} and others. As another example of measurements, observed results of C_{u^2} and the g-correlation behind an airfoil are shown in Figures 35 and 36. Downstream from the airfoil, similarity is seen to be preserved in the g-function, although it has an asymmetrical form in the y-direction.

For the distribution of turbulent intensity along the flow, (23.1) proves that when the data at locations of the same value of η are plotted, a linear-decay law $u^2 \sim t^{-1}$ must be obtained as in isotropic turbulence. Far downstream from the obstacle body, the mean velocity $\bar{U}$ is taken to be approximately constant along these locations, and an essential character of the linear-decay law in this case can be checked experimentally by taking $t \sim x$. As seen from (23.1) and (23.5), the scale length defined by the correlation g or the profile of the coefficient C_{u^2} in the y-direction increase along the flow proportionally to $t^{\frac{1}{2}}$. Figure 37 indicates the characteristics of the linear-decay law of the initial period in the case of turbulent wake behind an airfoil.

24. CONSERVATION OF MOMENTUM

In this section variation of the mean velocity along the x-direction of the decaying shear turbulence shall be investigated. At first, a simple case of the two-dimensional wake in a uniform flow shall be examined. As a matter of course, it is the Reynolds equations that connect turbulent intensity with the mean velocity. As seen in Figure 6, the region in the y-direction of the turbulent wake is far smaller than that in the x-direction, and the shearing stress is represented by $\partial \overline{uv}/\partial y$, with the effect of molecular viscosity neglected. Then, as in the laminar boundary layer, the Reynolds equations (9.6) are reduced to

$$\bar{U}\frac{\partial \bar{U}}{\partial x} + \bar{V}\frac{\partial \bar{U}}{\partial y} = -\frac{\partial \overline{uv}}{\partial y} , \tag{24.1}$$

where the velocity components are taken as shown in Figure 38. Apart from the body, U_1 and V_1 become far smaller than U, unlike the case of boundary-layer flow. When they are neglected, (24.1) is approximated by

$$\bar{U}_o\frac{\partial \bar{U}_1}{\partial x} = -\frac{\partial \overline{uv}}{\partial y} . \tag{24.2}$$

On the other hand, the relations from (23.1) and (23.2) are

$$\overline{uv} = C_{\overline{uv}}(\eta)\, t^{-1},$$

$$\eta = \frac{y}{\sqrt{4\nu t}} , \qquad t = \frac{x}{\bar{U}_o} . \tag{24.3}$$

Therefore, (24.2) is integrated into the form

$$\bar{U}_1 = C_{\bar{U}_1}(\eta)\, t^{-\frac{1}{2}},$$

$$C_{\bar{U}_1}(\eta) = -\frac{dC_{\overline{uv}}(\eta)}{d\eta}\Big/\sqrt{\nu} . \tag{24.4}$$

Figure 39 shows an observed result of this relation.

In a two-dimensional wake in a uniform flow, momentum loss M of the mean flow across a section is written as

$$M = \rho \int_{-\infty}^{\infty} \bar{U}(\bar{U}_0 - \bar{U}) dy . \tag{24.5}$$

Since $\bar{U}_1$ is taken to be small, (24.5) is approximated by

$$M = \rho \bar{U}_0 \int_{-\infty}^{\infty} \bar{U}_1 dy . \tag{24.6}$$

Thus, by using (24.4), it can be proved that the relation

$$M = \text{constant} \tag{24.7}$$

holds independently of t.

From a phenomenological standpoint, momentum loss in a section across a wake must be balanced with the resistance of the body affected by the main flow. Namely, by evaluating (24.6) with an observed $\bar{U}_1$-distribution, an approximative value of the resistance can be obtained. The relation (24.7) means that (24.6) gives a constant value of the resistance at any section along the wake where it is evaluated.

According to the physical picture of the structure of turbulent flow, the primary vortices formed by the effect of the boundary layer around the body are successively thrown away and carried along, accompanied by a cascade phenomenon. Thus, the kinetic energy of a uniform flow is first transformed into that of the primary vortices and is further transmitted into the descending small vortices where it is partly dissipated into heat. If the momentum loss of the mean velocity may be proved to vary along the flow, the effects of these vortices on velocity fluctuation are exactly evaluated, because the Reynolds equations strictly connect the mean flow to the turbulent intensity. In Section 14, a vortex motion of $\alpha = 1$ is shown to conserve a constant kinetic energy in itself. It seems that this characteristic causes the initial-period law, which was derived considering only the primary vortices to give the result (24.7).

In order to measure the resistance of a body, the Pitot-traverse method is often used, whereby resistance of a body is found by measuring the profile of $\bar{U}_1$ by a Pitot tube and evaluating the integration (24.6). It is seen from many experiments that an exact value of resistance is obtained regardless of the location of the Pitot-traverse if the location

is somewhat apart from the body. This fact may be regarded as experimental support of the idealization of the initial period.

The above discussion is concerned with a simple case of a two-dimensional wake in a uniform flow, where the feature $U_1 \ll U$ makes it easy to develop the initial-period similarity-law of isotropic turbulence into a definite expression. In other cases of decaying turbulence, however, it becomes difficult to obtain definite expressions, because the simple condition of a uniform mean flow or neglection of the elongation of the vortex filaments cannot generally be adapted. In many cases, U_1 cannot be neglected versus U, and the relation between x and t is also intricate. Therefore, it is difficult to derive a definite result from the initial-period law. However, from the common viewpoint of the ideal state of the chaotic motion of the $\alpha = 1$ vortices, the characteristic of conservation of momentum may be widely adapted to the general decaying turbulence in its initial period.

When the main flow of a decaying shear turbulence is uniform without a pressure gradient, the profiles of turbulent intensity across the flow may be assumed to preserve their similar form along the flow, as indicated by (22.3) in the case of a two-dimensional wake. By letting $f_{\overline{uv}}$ and L_r, respectively, be the distribution of $\overline{uv}$ across the flow and the scale length to this direction, an expression

$$\overline{uv} = f_{\overline{uv}}(\zeta_r)\bar{x}^{m}, \qquad \zeta_r = \frac{r}{L_r},$$
$$L_r = x^{-n}, \tag{24.8}$$

is obtained, where m and n are unknown exponents and r is a distance across the flow. When (24.8) is substituted into the Reynolds equations and the condition of momentum conservation is used, the exponents m and n can be determined together with the distribution of mean velocity along the flow. In the two-dimensional wake, for instance, when (24.8) is substituted into (24.2) with r = y, then m=1, n=½ from condition (24.7) is obtained. As x is proportional to t in this case, the relations (24.3) and (24.4) can be proven inversely.

In the turbulent wake behind an axisymmetric body, the expressions of the Reynolds equations and of the momentum conservation are written as

$$\bar{U}_0 \frac{\partial \bar{U}_1}{\partial x} = \frac{1}{r}\frac{\partial}{\partial r}(r\overline{uv}),$$
$$2\pi\rho\bar{U}_0\int_{-\infty}^{\infty}\bar{U}_1 r\,dr = \text{constant}, \tag{24.9}$$

with $\bar{U}_o$ and $\bar{U}_1$ taken as shown in Figure 38. Combining with (24.8),

$$\overline{uv} = f_{\overline{uv}}(\zeta_r)\, x^{-m},$$

$$\bar{U}_1 = f_{\bar{U}_1}(\zeta_r)\, x^{-\frac{1}{2}m}$$

$$m = \frac{4}{3}, \qquad n = \frac{1}{3},$$

(24.10)

is obtained. For a two-dimensional jet in a still fluid, the expressions

$$\bar{U}\frac{\partial \bar{U}}{\partial x} + \bar{V}\frac{\partial \bar{U}}{\partial y} = -\frac{\partial \overline{uv}}{\partial y},$$

$$2\rho\int_{-\infty}^{\infty} \bar{U}^2\, dy = \text{constant},$$

(24.11)

are used to derive the following relations:

$$\overline{uv} = f_{\overline{uv}}(\zeta_r)\, x^{-m}$$

$$\bar{U} = f_{\bar{U}}(\zeta_r) x^{-\frac{1}{2}m}, \qquad \bar{V} = f_{\bar{V}}(\zeta_r)\, x^{-\frac{1}{2}m}$$

$$m = 1, \qquad n = 1.$$

(24.12)

In an axisymmetric jet, the relations

$$\bar{U}\frac{\partial \bar{U}}{\partial x} + \bar{V}\frac{\partial \bar{U}}{\partial y} = -\frac{1}{r}\frac{\partial}{\partial r}(r\overline{uv}),$$

$$2\pi\rho\int_{0}^{\infty} \bar{U}^2 r\, dr = \text{constant},$$

(24.13)

lead to

$$\overline{uv} = f_{\overline{uv}}(\zeta_r)\, x^{-m},$$

$$\bar{U} = f_{\bar{U}}(\zeta_r)\, x^{-\frac{1}{2}m}, \quad \bar{V} = f_{\bar{V}}(\zeta_r)\, x^{-\frac{1}{2}m},$$

$$m = 2, \qquad n = 1.$$

(24.14)

In the case of a half jet, the character of flow is essentially the same as (24.12). However, if the decaying of the term $\overline{uv}$ is neglected near x = 0,

$$m = 0, \qquad n = 1$$

(24.15)

is arrived at from the conditions

$$\bar{U}\frac{\partial \bar{U}}{\partial x} + \bar{V}\frac{\partial \bar{U}}{\partial y} = \frac{\partial \overline{uv}}{\partial y},$$

$$\bar{U} = \text{constant}.$$

(24.16)

Figure 40 shows the above-mentioned results graphically.

In general cases of decaying turbulence, it is difficult to derive exactly the distributions of turbulent intensity and scale from the expressions of P*- and V*-functions of the initial-period law. The condition of momentum conservation, which is proved by the initial-period similarity-law to hold approximately in the case of a two-dimensional wake, is important in determining the distribution of the velocity in the x-direction. Results from (24.10) to (24.15) will be taken as the foundations of the studies for practical purposes.

25. PROPORTIONAL CHARACTER OF THE COMPONENTS OF TURBULENT INTENSITY

In the previous sections, distributions of turbulent intensity and scale along the x-direction have been studied. Then, under the condition of the initial period, discussions will be made on the characteristics of turbulence in a direction across the flow.

In the case of isotropic turbulence, the components of turbulent intensity are proved to be equal to each other because of the completely irregular chaotic motion of circular vortices in a uniform flow. Of course, this is not adapted to general cases of decaying turbulence. However, because of the significance of a vortex chaos motion, components of turbulent intensity cannot be independent at all, although decaying turbulence is not in a completely irregular state. Even in a turbulent shear flow, one large component of the turbulent intensity is usually accompanied by other components which are not small. Owing to experimental

observations, it is hardly supposed that turbulent flow has only one extremely intensive component.

In the case of a two-dimensional wake in a uniform flow, components of the turbulent intensity are expressed in (23.1) by the initial-period similarity-law. In (23.1) vortex motions are taken to be two-dimensional in themselves as previously interpreted. If all the directions of vortex filaments are assumed to be parallel to the z-axis, (23.1) becomes a purely two-dimensional expression of the functions $P(s,\theta;\eta)$ and $F(s,\theta)$. Now, in an idealization of the initial-period in a two-dimensional wake, we shall use the supposition that the vortices fluctuate their direction of filaments around the z-axis with equal probability, regardless of the location in the field of flow (cf. Figure 33). Thus, the initial-period similarity-law is represented by two-dimensional expressions with a correction term of the inclination ϕ_1 to the z-axis.

As seen in Figure 33, the z-component of turbulent intensity comes from the values of the x-component and the inclination ϕ_1. When the probability distribution around the z-direction is denoted by $P^*_z(\phi_1)$, at least the relation

$$P_z^*(\phi_1) = P_z^*(-\phi) \tag{25.1}$$

holds from the characteristic of an equal probability. Thus, the expressions $C_{u^2}(\eta)$ and other terms in (23.1) are written as

$$C_{u^2}(\eta) = \left\{4C^2\gamma \int_0^{2\pi}\int_0^{s_0(\theta)} P_1^*(s,\theta;\eta)F^2(s,\theta)\cos^2\theta\, d\theta ds \int_{-\frac{\pi}{2}}^{\frac{\pi}{2}} \cos^2\phi_1 P_z^*(\phi_1)d\phi_1\right\} \Big/ \int_0^{2\pi} s_0(\theta)d\theta,$$

$$C_{v^2}(\eta) = \left\{4C^2\gamma \int_0^{2\pi}\int_0^{s_0(\theta)} P_1^*(s,\theta;\eta)F^2(s,\theta)\sin^2\theta\, d\theta ds\right\} \Big/ \int_0^{2\pi} s_0(\theta)d\theta,$$

$$C_{w^2}(\eta) = \left\{4C^2\gamma \int_0^{2\pi}\int_0^{s_0(\theta)} P_1^*(s,\theta;\eta)F^2(s,\theta)\cos^2\theta\, d\theta ds \int_{-\frac{\pi}{2}}^{\frac{\pi}{2}} \sin^2\phi_1 P_z^*(\phi_1)d\phi_1\right\} \Big/ \int_0^{2\pi} s_0(\theta)d\theta,$$

$$C_{\overline{vw}}(\eta) = \left\{4C^2\gamma \int_0^{2\pi}\int_0^{s_0(\theta)} P_1^*(s,\theta;\eta)F^2(s,\theta)\sin\theta\cos\theta\, d\theta ds \int_{-\frac{\pi}{2}}^{\frac{\pi}{2}} \sin\phi_1 P_z^*(\phi_1)d\phi_1\right\} \Big/ \int_0^{2\pi} s_0(\theta)d\theta,$$

$$C_{\overline{wu}}(\eta) = \left\{4C^2\gamma \int_0^{2\pi}\int_0^{s_0(\theta)} P_1^*(s,\theta;\eta)F^2(s,\theta)\cos^2\theta\, d\theta ds \int_{-\frac{\pi}{2}}^{\frac{\pi}{2}} \sin\phi_1\cos\phi_1 P_z^*(\phi_1)d\phi_1\right\} \Big/ \int_0^{2\pi} s_0(\theta)d\theta,$$

$$C_{\overline{uv}}(\eta) = \left\{4C^2\gamma \int_0^{2\pi}\int_0^{s_0(\theta)} P_1^*(s,\theta;\eta)F^2(s,\theta)\sin\theta\cos\theta\, d\theta ds \int_{-\frac{\pi}{2}}^{\frac{\pi}{2}} \cos\phi_1 P_z^*(\phi_1)d\phi_1\right\} \Big/ \int_0^{2\pi} s_0(\theta)d\theta, \tag{25.2}$$

where $s_o(\theta)$ denotes the boundary of the D*-domain. On account of condition (25.1), $C_{\overline{vw}}$ and $C_{\overline{wu}}$ are easily proved to vanish, and the mean-velocity distribution remains two-dimensional although a finite intensity of the z-component exists.

Now, in (24.2), we write

$$a_1 = 4C^2\gamma \Big/ \int_0^{2\pi} s_o(\theta)\,d\theta,$$

$$a_2 = \int_{-\frac{\pi}{2}}^{\frac{\pi}{2}} \cos^2\phi_1\, P_z^*(\phi_1)\,d\phi_1,$$

$$a_3 = \int_{-\frac{\pi}{2}}^{\frac{\pi}{2}} \cos\phi_1\, P_z^*(\phi_1)\,d\phi_1, \tag{25.3}$$

and

$$\cos\theta = \varepsilon(\theta), \qquad 1 \geqq \varepsilon^2(\theta) \geqq 0. \tag{25.4}$$

Then, $C_{u^2}(\eta)$ in (25.2) can be transformed as follows:

$$C_{u^2}(\eta) = a_1 a_2 \int_0^{2\pi} \left\{ \int_0^{s_o(\theta)} P_1^*(s,\theta;\eta) F^2(s,\theta)\,ds \right\} \varepsilon^2(\theta)\,d\theta = a_1 a_2 \int_0^{2\pi} F_1'(\theta;\eta)\varepsilon^2(\theta)\,d\theta,$$

$$\left(F_1'(\theta;\eta) = \int_0^{s_o(\theta)} P_1^*(s,\theta;\eta) F^2(s,\theta)\,ds \right) = a_1 a_2 \varepsilon_1^2(\eta) \int_0^{2\pi} F_1'(\theta;\eta)\,d\theta,$$

$$\left(\varepsilon_1^2(\eta) = \int_0^{2\pi} F_1'(\theta;\eta)\varepsilon^2(\theta)\,d\theta \Big/ \int_0^{2\pi} F_1'(\theta;\eta)\,d\theta \right) = a_1 a_2 F_2'(\eta)\varepsilon_1^2(\eta),$$

$$\left(F_2'(\eta) = \int_0^{2\pi} F_1'(\theta;\eta)\,d\theta \right).$$

Namely,

$$C_{u^2}(\eta) = a_1 a_2 F_2'(\eta)\varepsilon_1^2(\eta),$$

$$C_{v^2}(\eta) = a_1 F_2'(\eta)(1-\varepsilon_1^2(\eta)),$$

$$C_{\omega^2}(\eta) = a_1(1-a_2^2)F_2'(\eta)\varepsilon_1^2(\eta),$$

$$C_{\overline{uv}}(\eta) = a_1 a_3 F_2'(\eta)\varepsilon_2^2(\eta),$$

$$\left(\varepsilon_2^2 = \int_0^{2\pi} F_2' \sin\theta\cos\theta\, d\theta \Big/ \int_0^{2\pi} F_2' d\theta\right),$$

(25.5)

and

$$u/\sqrt{u^2+v^2+w^2} = a_2\varepsilon_1^2(\eta),$$

$$v/\sqrt{u^2+v^2+w^2} = 1-\varepsilon_1^2(\eta),$$

$$w/\sqrt{u^2+v^2+w^2} = (1-a^2)\varepsilon_1^2(\eta),$$

$$\overline{uv}/(u^2+v^2+w^2) = a_3\varepsilon_2^2(\eta).$$

(25.6)

are obtained. In the integration, $\varepsilon_1^2(\eta) = \int_0^{2\pi} F_1'(\theta;\eta)\,\varepsilon^2(\theta)\,d\theta \Big/ \int_0^{2\pi} F_1'(\theta;\eta)\,d\theta$, ε_1^2 takes some value in 0∼1 at a position of η, since $\varepsilon^2(\theta) = \cos^2\theta$ varies in 0∼1, and

$$1 > \varepsilon_1^2 > 0, \qquad 1 > \varepsilon_2^2 > 0.$$

(25.7)

Namely, by the definite integral in the interval 0∼2π of θ, ε_1^2 or ε_2^2 approaches a finite value between 0 and 1. Thus, even in the shear turbulence, it may be comprehended that every component of turbulent intensity has a tendency to take the same order of magnitude.

The above-mentioned proportional characteristic of the components of turbulent intensity comes from the integrations by the trigonometric functions contained in the fundamental expression (23.1) of the initial period. This characteristic holds in every kind of vortex chaos motion. The above derivation is also adapted to the case of a two-dimensional jet. In the case of an axisymmetric wake or jet the same kind of discussions lead to

the result

$$u/\sqrt{u^2+v^2+w^2} = a_2\mathcal{E}_1^2(\eta),$$
$$v/\sqrt{u^2+v^2+w^2} = \sqrt{1-\mathcal{E}_1^2(\eta)},$$
$$\overline{uv}/(u^2+v^2+w^2) = a_3\mathcal{E}_2^2(\eta),$$
$$v = w. \qquad (25.8)$$

The above-mentioned formulations are made under the idealization of the initial period. As seen in (13.8), however, the real-state expressions contain similar integration formulas through trigonometric functions and the proportional characters may be expected. The character of (25.6) in the observed results in Figure 34 has already been found. In Figure 41, the distribution of u/w of this case is shown.

26. FREE BOUNDARY OF THE SHEAR TURBULENCE

In order to determine $F_2'(\eta)$, $\mathcal{E}_1^2(\eta)$, and other functions concerning the profiles of turbulent intensity as indicated by (25.5), the functional forms of $P_1^*(s, \theta; \eta)$ and $F^2(s,\theta)$ in the D*-domain must first be found. With reference to the P*-function of an incompletely irregular state, free-boundary phenomena of the shear turbulence will be investigated in this section.

If a boundary is imagined in the field of flow having on one side the completely irregular vortex chaos motion and on the other side no vortex motion, the velocity fluctuation must show the completely turbulent state on the former side and the laminar state on the latter. Also, in a regular arrangement of vortices such as the Kármán vortex streets, the velocity fluctuation at a point must decrease its intensity while retaining the same regular wave form as the point moves across the path of the centers of vortices.

In the case of decaying shear turbulence, the region of vortex chaos motion is not very wide across the mean flow. The strong vortices of α = 1 are not in the completely irregular state, and the value of P* distributes in the D*-domain with a high and low density as shown in Figure 23(C). When a fixed A-point is taken at a position not near the center part of the vortex chaos motion, the high density part may not lie at the center of the D*-domain, namely the vortex centers. Therefore, velocity fluctuations in the range of $0 \sim t$ are due, for the most part, to the small values of the V*-function far from the center in the D*-domain. However, because of a finite breadth of the distribution of the P*-function in the D*-domain, velocity fluctuations are sometimes caused by large values of V*

near the center. As the A-point moves far from the center part of th vortex chaos motion, parts of the velocity fluctuation of large values must be decreased.

In order to proceed with a statistical treatment, introduction of the P* function is made by taking only the mean values of the velocity fluctuations consisting of large and small values. As the A-point moves across the flow, the functional form of P* gradually changes in the D*-domain. Thus, the values of $C\,\overline{u^2}\,(\eta)$ and other terms decrease continuously in the y- or z-direction. This is also true for the mean-velocity profile $C_{\overline{U}}(\eta)$, as shown in Figures 34 and 39. However, if velocity fluctuation is observed with the time, this means that an irregular mixing of the parts of large and small values is taking place. When the A-point moves far away, the parts of large velocity fluctuations decrease. Namely, on account of the characteristic of an incomplete irregularity of the P*-function, the existence of some region in the field of flow where large and small velocity fluctuations are mixed intermittently is assumed. Therefore, without a statistical meaning, the boundary of shear turbulence cannot be defined.

Figure 42 shows the velocity fluctuations in a turbulent wake behind a circular cylinder. The figures represent a kind of discontinuous phenomena such as that of the transition situation from the laminar to turbulent boundary layer shown in Figure 13. These phenomena have been widely observed in other turbulent shear flows of wakes, jets, and boundary layers. They are known as the intermittency phenomena at the free boundary and are regarded as important characteristics of the turbulent shear flow.

For convenience, let the part of the velocity fluctuation that is less than critical be laminar and the larger part be turbulent. If the summation of time intervals of the laminar parts in the range $0 \sim t$ is denoted by t_ℓ, a limiting value

$$\gamma = \lim_{t\to\infty}\left(1 - \frac{t_\ell}{t}\right) \tag{26.1}$$

can be defined that has been introduced by Townsend (reference 40) as an intermittency factor representing the ratio of the combined laminar and turbulent parts. It is assumed from the incompletely irregular P*-function that the value of γ distributes with the value $0 \sim 1$ in a fairly wide region in the field of flow not near the center of the vortex chaos motion.

Then, in the case of a two-dimensional turbulent wake, quantitative discussions that are based on the initial-period similarity-law shall be made. An A-point is taken in the xy-plane in Figure 33, and this point is moved in the y-direction. By virtue of the expressions (25.2) of the initial period, statistical features of the movement of the intersections

of the xy-plane and the vortex filaments can be expressed in the function of $P^*(s, \theta; \eta)$ in a two-dimensional D*-domain, regardless of their inclination to the z-axis. This is also the same for the function F. When the two functions are written as

$$P_1^*(\xi^*, \eta^*; \eta), \qquad F(\xi^*, \eta^*),$$

$$\xi^* = \frac{x^*}{\sqrt{4\nu t}}, \qquad \eta^* = \frac{y^*}{\sqrt{4\nu t}} \tag{26.2}$$

in the two-dimensional D*-domain of the x*y*-plane, the one-dimensional distributions along the y*-axis of the probability density and of the mean turning velocity become

$$P^*(0, \eta^*; \eta), \qquad F(0, \eta^*). \tag{26.3}$$

In the field of flow of the xy-plane, let us consider the situations when a vortex with the shortest distance from the A-point passes the parallel line AA' from the A-point in the y-direction. The mean turning velocity of the $\alpha = 1$ vortices has the same profile for every vortex on the AA'-line as shown in Figure 22. At a finite distance from the vortex center on the AA'-line, a critical point η^* shall be taken as shown in Figure 43 (A). Inside this point, the flow may be regarded as being turbulent with a large velocity fluctuation, but outside this point the flow is considered laminar, with a small fluctuation.

Let us consider the situations in the $\xi^*\eta^*$-plane of the D*-domain. Since the variable θ of the turning-velocity function is constant on the AA'-line, the functional form of $F(0, \eta^*)$ on the η^*-axis in the D*-domain is the same as that on the AA'-line in the field of flow. Therefore, the critical point on the AA'-line can be transmitted to the η_c^*-point on the η^*-axis with the same distance from the origin. On the other hand, distribution of the P*-function is given by $P_1^*(0, \eta^*; \eta)$ in (26.3), as shown in Figure 43(B). Then, from the definition of the P*-function the relation

$$\lim_{t\to\infty} \frac{t_e}{t} = \int_{\eta_c^*}^{\infty} P_1^*(0, \eta^*; \eta)\, d\eta^* \Big/ \int_{-\infty}^{\infty} P_1^*(0, \eta^*; \eta)\, d\eta^* \tag{26.4}$$

is deduced by neglecting the effect of the laminar part in the $-\eta^*$-direction.

As the P*-function in (26.3) is concerned with the $\alpha = 1$ vortices produced at one position in the field of flow, the functional form is relatively constant regardless of the value η of the A-point on the AA'-line, with only varying distribution position of the probability density with an increasing value of η. Therefore, when P* is expressed in a func ion of η *' measured from the point of the highest probability as shown in Figure 43(C),

$$\int_{\eta_c^*}^{\infty} P_1^*(0,\eta^*;\eta)\,d\eta^* = \int_{\eta_c^{*\prime}-\eta}^{\infty} P_1^*(\eta^{*\prime})\,d\eta^{*\prime}$$

is obtained, where $\eta_c^{*\prime}$ is the distance between the points of η_c^* and the highest density of $P_1^*(0,\eta^*;0)$ on the η^*-axis. Thus, the intermittency factor $\gamma(\eta)$ is expressed in the simple integration formula,

$$1-\gamma(\eta) = c_1 + c_2 \int_{-\eta}^{\infty} P_1^*(\eta^{*\prime})\,d\eta^{*\prime}, \qquad (26.5)$$

where the constants c_1 and c_2 are determined by the location of the critical point η_c^* and the condition $\lim_{y\to\infty} \gamma \longrightarrow 0$, respectively.

The functional form of P* in the shear turbulence must be given a priori as a hypothetical foundation of the statistical theory. The assumption P*=constant of the complete irregularity in the shearless turbulence has a common feature of the Ergodic hypothesis for the vortex chaos motion and for many other phenomena. On the other hand, no general discussions on the expression of an incomplete irregularity in statistical physics is obtained, and in the statistical theory of turbulence a mathematical expression must be given according to the real states of the vortex chaos motion. In the idealization of the initial-period law, we have assumed the statistical equilibrium of the P*-function. It is further assumed that P* is a function of η * only as shown in Figure 23(C), and it may be appropriate as the first approximative description to assume the Gaussian distribution of η*. Namely, taking H as the dispersion and c as a constant,

$$P_1^* = c\, e^{-\frac{\eta^{*2}}{\sigma^2}}, \qquad \sigma = \frac{H}{\sqrt{4\gamma t}}, \qquad (26.6)$$

is arrived at where σ is regarded as the nondimensional dispersion.

The intermittency factor γ is connected to the P*-function by a simple mathematical expression and, at the same time, is directly observed. By (26.5) and (26.6), the following relation of the intermittency factor

$$\gamma = C_1 + C_2 \int_{\eta}^{\infty} e^{-\frac{\eta^{*\prime 2}}{\sigma^2}} d\eta^{*\prime}$$

(26.7)

is obtained.

Although the above derivation applies to the case of a two-dimensional wake, the assumption of the Gaussian distribution of the P*-function may be generally adapted to other cases of shear turbulence. In the case of a round jet as shown in Figure 40(C), the above derivation still holds in the plane containing the center axis, and formula (26.7) can be checked experimentally. Figures 44 and 45 show observed results of the distributions of γ in these cases. The observed results, as pointed out by Corrsin (reference 41), are well represented by the Gaussian-integral curve. The formula (26.7) is that which has given a quantitative interpretation to the empirical recognition of the intermittency factor, according to the idealized treatment of the initial-period similarity-law. Even if theoretical evaluations of the dispersion H are difficult, (26.6) gives a constant value to σ regardless of x. Figure 46 is an experimental verification of this result, and in Figure 47, σ does not seem to be dependent on the mean speed, U_o.

27. DISTORTION OF THE HOMOGENEOUS AND ISOTROPIC TURBULENCE

In order to derive quantitative results from the initial-period law, it is necessary to decide the functional form of V* as well as the function of P*. In the case of isotropic turbulence, the solution of a two-dimensional viscous vortex motion is taken as the fundamental form of V*, because of the spherical symmetry in the completely irregular vortex chaos motion. In other cases, the field of flow is not uniform and the deviation of the V*-function is widely observed from the simplest case of spherical symmetry. The problem of distortion of the isotropic turbulence in shearless turbulence shall be taken in this section as a simple case of the deviation.

As a matter of course, the essential characteristic of shearless turbulence is the condition P*=constant of the completely irregular vortex chaos motion. Therefore, in the flow of shearless turbulence, an intermittency phenomenon cannot be observed, due to P*≠constant of the incomplete irregularity. As detected in a wind tunnel stream when the mean velocity is made nonuniform, the turbulent flow deviates from the state of isotropic turbulence into that having different values of the components of turbulent intensity. This tendency may be attributed to the deviation of the V*-function from the symmetrical form, in spite of the complete irregular arrangement denoted by P*=constant.

Even with the idealization of the initial-period of the $\alpha = 1$ vortices, it is difficult in hydrodynamics to decide the functional form of $\overline{V}^*$ in accordance with an arbitrarily given pressure distribution of the mean flow. As a way to show the process of the statistical study on this problem, the following ideal case is surveyed.

Namely, such a nonuniform field of flow as shown in Figure 48 is taken and the two-dimensional, completely irregular vortex chaos motion along the center line of the x-axis is considered. In the uniform flow upstream, the vortex chaos motion shall present the situation of an idealized, two-dimensional, isotropic turbulence. When the mean velocity is accelerated, however, circular vortices may be deformed. When we write

$$\frac{\overline{U}(x)}{\overline{U}_o} = \lambda_o \ , \tag{27.1}$$

with $\overline{U}_o$ and $\overline{U}(x)$ at the uniform and contraction parts, respectively, effects of the pressure gradient of the mean flow may be represented by the parameter λ_o as the first approximation. With an undisturbed mean turning velocity of vortices $\overline{V}^* = F(s)(2C\sqrt{\nu}\, t^{-\frac{1}{2}})$ and the effect of deformation $F'(s, \theta; \lambda_o)$, the following expression for the $\overline{V}^*$-function at a point x is obtained:

$$\overline{V}^* = F(s)\,(2C\sqrt{\nu}\, t^{-\frac{1}{2}})F'(s, \theta; \lambda_o) \ . \tag{27.2}$$

It is now difficult to evaluate the functional form of $F'(s, \theta; \lambda_o)$ exactly by the Navier-Stokes equations for the viscous vortex motion. However, under the assumption of a perfect fluid, a square part of the fluid is transformed approximately into a rectangular form at the contracted part, and a circular vortex is deformed into an elliptic form. According to the continuity condition, the ratio of the axes of the rectangle, or of the ellipse, can be connected to the parameter λ_o of (27.1). For the perfect fluid, the turning velocity around an elliptic body can be evaluated. Thus, by estimating F' of the mean turning velocity of deformed vortices at x as above and integrating in the elliptic D*-domain, the following expressions (reference 37) are obtained:

$$u^2 = \frac{c^2}{2s_o}\,\frac{\lambda_o^2+1}{2\lambda_o^2}\int_o^{\frac{(\lambda_o^2+1)^2}{4\lambda_o^2}s_o} F^2(s)\,ds\; t^{-1},$$

$$v^2 = \frac{c^2}{2s_o}\,\frac{\lambda_o^2+1}{2}\int_o^{\frac{(\lambda_o^2+1)^2}{4\lambda_o^2}s_o} F^2(s)\,ds\; t^{-1},$$

$$\overline{uv} = 0. \qquad (27.3)$$

By putting a two-dimensional lattice upstream where the flow is parallel, a nonhomogeneous shearless turbulent flow such as that shown in Figure 48 can be roughly realized. An experimental check of relation (27.3) is shown in Figure 49. The deformation phenomena have been widely observed, and some theoretical studies proposed (reference 38). The course of analysis, however, is to evaluate the deformation effects of regularly placed vortices, and is difficult to prove the vanishing of the shearing stress even if the variation of turbulent intensities u and v can be evaluated (reference 43). The analysis treats the states of Figure 23(B) and does not touch an essential point of the statistical study. The course of the two-dimensional analysis leading to (27.3) contains many neglections in itself, and the conditions of the observed flow may include three-dimensional effects of the vortex chaos motion although the flow is behind a two-dimensional lattice. The quantitative criterion in Figure 49 does not have a very important meaning. However, it may turn out that the initial-period law can include the quantitative interpretation of the deformation of the isotropic turbulence without an essential contradiction to the real states of flow.

In large-scale wind tunnels, it has also been observed that various values of u, v and w in the contracting section behind a rectifying grid tend to be equal to each other again in the test section, probably caused by the small descending vortices produced by the cascade phenomena downstream. These phenomena are clearly beyond the scope of the initial-period law.

28. PROFILE OF TURBULENT INTENSITY

In this section profiles of the Reynolds-stress components across the mean flow will be evaluated by using the functional forms of P^* and $\bar{V}^*$ of the expressions in the initial period discussed in the last two sections. For the purpose of presenting only the process of analysis, take the following ideal case of the shear turbulence of a two-dimensional vortex chaos motion. In the case of a half-jet as shown in Figure 40(d), the $\alpha = 1$ vortices produced at the edge of the wall are carried away in their incompletely irregular state. Unlike other cases of shear turbulence, the vortices produced at the edge are not disturbed by another kind of the primary vortices produced at the opposite side. Thus, this case of flow can be compared to the simplest case of decaying shear turbulence.

As the mean-velocity profile is not uniform across the flow, the mean form of the vortices shall be oblique, unlike the distorted shearless turbulence. Because of a lack of precise studies on the individual vortex motions, it is now almost impossible in hydrodynamics to decide an exact

functional form of $\overline{V}^*$ for the viscous vortex motion in this case. If a tentative case of the numerical values is taken, such that the obliqued elliptic form of the mean vortices in the 45° direction is twice the ratio of the axes and the Gaussian distribution of P^* is three times that of the relative dispersion σ , then the distributions in the y-direction of u, v , and $\overline{uv}$ can be evaluated by formula (25.2) of the initial-period similarity-law (reference 37). The mean velocity profile can also be determined by solving the Reynolds equation (24.16).

Calculated results and experimental comparison are shown in Figures 50 and 51. Of course, they have no more significance than the supposition that the initial-period law also may derive appropriate results on the profiles of turbulent intensities across the mean flow, if the fundamental functions of P^* and $\overline{V}^*$ for the $\alpha = 1$ vortices are clarified by future investigations.

29. LIMIT OF THE INITIAL PERIOD

In all previous sections in this chapter, theoretical studies in the initial period are made of the distributions of turbulent intensity and the scale, both parallel and perpendicular to the mean flow. The initial-period law, however, is obviously an approximate description which is expected to hold at locations not far behind the body. In isotropic turbulence, an insufficiency of the description is detected, particularly in the correlation functions as mentioned in Section 21. In order to check this point for decaying shear turbulence, an experimental work has been performed on the turbulent wake behind a circular cylinder.

As seen in (22.2), the region in which the initial-period law is adaptable depends principally on the time t since the outbreak of the $\alpha = 1$ vortices. Thus, observations, as for downstream as possible, were made of the profiles of the mean and fluctuational velocities behind a small cylinder in a low-speed flow. Although velocity profiles were seen to preserve their similar form in the downstream flow, a gradual variation could be found. As shown in Figure 52, the similar form of the profiles becomes narrower at the bottom and wider at the top. The same tendency was also found in the profiles of u. Moreover, as the similar profiles of the mean and fluctuational velocities became broken, the decaying of u became faster than the relation $u \sim t^{-1}$. Figure 53 shows the observed results of the distribution of u along points with similar relative locations in the profiles.

In isotropic turbulence, the coefficients $C_{\overline{u}}$, C_{u^2}, and others are respectively constant in the y- or z-direction, and the character of similarity preservation should be investigated with respect to the form of the correlation function or the decay of turbulent intensity. It is mentioned in Section 21 that observed results of the correlation function cannot be supported by the theoretical curve of the initial period. If the correlation function can be evaluated definitely by the formula of the initial

period, such as (13.13) with N=1 in the shear turbulence, discrepancy between the evaluated and observed results may be determined earlier than the deviation from the similar profile of the mean- or fluctuational-velocity is detected. The similarity character is broken because of cascade phenomena. As mentioned in Section 5, production of new vortices can be assumed because of the disturbing effects of vortices in their chaotic state. Thus, in completely irregular vortex chaos motion of isotropic turbulence, a disturbance to one vortex that is affected by others is more critical than in shear turbulence. An experimental verification of the breakdown of a similar profile in a turbulent wake or jet can seldom be found. Therefore, it is concluded that the idealized expression of the initial-period law can be taken to be more useful in shear turbulence than in the case of shearless turbulence of an isotropic or contracting flow.

CHAPTER SIX, TRANSFER THEORY IN THE INITIAL PERIOD

30. TRANSFER OF MOMENTUM IN THE SHEAR TURBULENCE

An essential operation in the statistical theory of turbulence is to introduce expressions of the Reynolds stress as functions of location in the field of flow by means of appropriate statistical and hydrodynamical hypotheses in the P*- and V*-functions. With these expressions combined with the Reynolds equations, mean velocity can be determined. The purpose of the theory is to give a unifiable theoretical process of evaluating statistical quantities of mean and fluctuational velocities in general cases of turbulent flow. Idealization of the initial-period law is no more than a postulation by which the P*- and V*-functions may be easily determined. By taking the approximative description of the initial-period, some quantitative results mainly related to the velocity fluctuation were discussed in the last chapter.

However, a strict calculation of the distribution of the Reynolds stress in the field of flow is generally difficult. Although it does not seem difficult to grasp the functional form of the Gaussian distribution for the P*-function, there is little reliable foundation for the functional form of V*. Present investigations of the real states of an individual vortex motion are few. Therefore, it is difficult to proceed with a consistent study of the evaluation, especially of the mean velocity which depends on this theory. Generally speaking, as the study proceeds toward theoretical unification, the process used between foundation and evaluation of practical problems becomes lengthy. When viewed as an interesting engineering problem in fluid mechanics, analysis of the mean velocity is important in the case of a shear turbulent flow. Only if the real state of the mean velocity is anticipated can many practically important problems be solved, although there is no knowledge about the velocity fluctuations themselves. The character of the transfer theory proposed by Prandtl (reference 10) should be interpreted from this point of view. This theory has been used with many appropriate results in regard to the mean-velocity profiles, and has played an important role, up to date, as a practical theory of turbulent flow.

However, the transfer theory has a narrow scope of application. This theory holds only in the decaying or nondecaying shear turbulent flow and loses meaning in the case of shearless turbulence, as this is a particular theory adaptable to a narrow field of turbulent phenomena. On the other hand, the theory of isotropic turbulence was developed, as mentioned previously, by referring to the velocity fluctuations themselves in the simplest case of the shearless turbulence. However, it seems impossible to connect the basic hypotheses of the transfer theory with those of isotropic turbulence. In the study of transfer theory, few considerations are made of the basic hypotheses. It is thought that such a situation prevents the application of the transfer theory to a wide field of practical problems. Before questioning the meaning of the hypotheses based on the

standpoint of the statistical theory of turbulence, the foundations of the transfer theory shall first be summarized.

In statistical dynamics of gas, Maxwell's transfer theory applies to the molecular chaos motion slightly deviated from an equilibrium state (reference 44). This theory explains the inner structure of a viscous flow as follows. For brevity, consider a laminar viscous flow with constant temperature which consists of only one kind of molecule and which has a mean-velocity profile changing only in the y-direction as shown in Figure 54. According to the physical image of a molecular chaos motion, many molecules of a fluid are carried along by the mean flow at speed U and collide with each other in their agitating motions. The viscous shearing force τ_m is assumed to be equivalent to the amount of momentum of the flow that is transferred across the flow by the effect of molecular chaos motion.

When a molecule at y=h moves across the mean flow with a molecular velocity C_m and with momentum mU(h), it loses its momentum by colliding with another molecule at $y=h_1$. The increase of momentum of the molecule at $y=h_1$ is written as $mU(h)-mU(h_1)$, with m as the mass of a molecule. Complying with this assumption, $-\tau_m$ at $y=h_1$ is expressed as

$$-\tau_m = \rho \overline{C_m \{U(h)-U(h_1)\}}, \qquad \rho = Nm, \tag{30.1}$$

when the time mean is taken. Here, N is the number of molecules in a unit volume at $y=h_1$, and ρ is the density of fluid. When higher terms are neglected in the Taylor expansion of $U(h)-U(h_1)$, (30.1) becomes

$$-\tau_m = \rho \overline{C_m L} \frac{dU}{dy}, \qquad L = h-h_1. \tag{30.2}$$

When (30.2) is written as

$$\tau_m = \rho C_m' l_m' \frac{dU}{dy}, \tag{30.3}$$

with C_m' the root-mean-square value of C_m of the N molecules, l_m' can be taken as the mean free path; that is, the mean value of the distance between collisions of molecules. Namely, for the viscosity coefficient μ in the Navier-Stokes equations (9.1), the following relation

$$\tau_m = \mu \frac{dU}{dy}, \qquad \mu = \rho C'_m l'_m, \tag{30.4}$$

can be obtained.

As mentioned previously, l'_m has an order of the value 10^{-5} cm which is far smaller than a macroscopic standard length in the field of flow. Namely, in a macroscopic field of flow the molecular chaos motion can be regarded as homogeneous inside an extremely thin region of the thickness of about 10^{-5}cm from a body. C'_m and l'_m have respectively constant values which lead to a constant value of μ in the whole field of flow with this thin region neglected. Therefore, the formula (30.4) of the transfer theory of a molecular chaos motion cannot give a more useful contribution to the fluid mechanics of a viscous flow in which μ is phenomenologically assumed to be constant in the field of flow.

In turbulent flow in which a vortex motion in its chaotic state is considered to consist of many small parts of fluid, these small fluid parts are supposed to possess an agitating motion like that of molecular chaos motion. It may be said that the physical picture of a vortex chaos motion is proposed in order to seek the cause of this agitating motion of the fluid parts. Whatever physical interpretation is given to the structure of turbulent flow, existence of the phenomena of an agitating motion of the fluid parts is acknowledged. Thus, in turbulent shear flow, the mean momentum is assumed to transfer across the flow in the same manner as in molecular chaos motion. In this case, τ and ε are expressed as

$$\tau = \varepsilon \frac{d\bar{U}}{dy}, \qquad \varepsilon = \rho v l', \tag{30.5}$$

where v is the intensity of velocity fluctuation in the y-direction, and l' is a mean free path of the mean value of the distance in this direction of many fluid parts.

As a characteristic of vortex chaos motion, the scale length of the agitating motion has a macroscopic order. The values of v and l' are not constant in the field of flow, and ε cannot generally be regarded as a constant, unlike the case of a molecular chaos motion. But compared with the original expression

$$\tau = -\rho \overline{uv}, \tag{30.6}$$

(30.5) has a feature that is expressed in the two quantities v and l', which have respective definite physical meaning in the agitating motion of the fluid parts.

It is still difficult to consider the two quantities at the same time, and the following attempt expresses them as one quantity. Since (30.5) and (30.6) lead to

$$\frac{\overline{uv}}{v^2} = \frac{l'}{v}\left|\frac{d\bar{U}}{dy}\right| , \tag{30.7}$$

(30.5) may be expressed as

$$\tau = \rho l^2 \left|\frac{d\bar{U}}{dy}\right| \frac{d\bar{U}}{dy} , \tag{30.8}$$

when a length

$$l^2 = \frac{v l'}{\left|\frac{d\bar{U}}{dy}\right|} = \frac{\overline{uv}}{v^2} l'^2 \tag{30.9}$$

is introduced.

The quantity l given by (30.9) has a somewhat different meaning from l' of the mean distance of fluid parts. However, the expression (30.8) contains only the scale length l as an unknown quantity, and here the character of τ can be considered more easily than in (30.5). The above-mentioned procedure is an outline of the transfer theory of turbulence proposed by Prandtl (reference 10), where (30.9) is known as the formula of momentum transfer and l as Prandtl's mixing length.

Strictly speaking, the mixing length l depends on the two independent quantities. As proved in Section 25, however, the correlation coefficient $\overline{uv}/v^2$ in (30.9) has a tendency to be constant across the flow, unlike the intensity v in (30.5). Thus, the mixing length l of (30.9) can be regarded as approximately proportional to the mean free path l' .

If the distribution of ε of the product of v and l' can be presumed in some way, the deduction of (30.9) loses its meaning. If such a presumption is difficult, (30.8) has an important meaning with l taken to be proportional to the l' . This is a point of Prandtl's transfer theory of shear turbulent flow.

1. TRANSFER OF VORTICITY

According to the continuity characteristic of a fluid, a small part may certainly exist in which the fluid has almost a simultaneous motion. It is not unreasonable to compare this agitating motion to the molecular chaos motion. On the other hand, owing to the continuity of the fluid, it

is also certain that the turbulent agitating motion is not discontinuous, but is a continuous phenomenon with respect to the time and location in the field of flow. In an agitating motion of fluid parts, when one part moves out, another part of the fluid must enter into this position. Namely, fluid parts move about causing a constant interference with the surrounding fluid. It is difficult to suppose that the original momentum is exactly conserved until the moving part of fluid changes direction. The fundamental formula (30.5) of the momentum transfer theory is derived with the effect of this interference neglected.

In an example of two-dimensional shear flow shown in Figure 54, if a line part of fluid parallel to the x-direction makes an agitating motion as a whole in the y-direction with no value of vorticity, the formula of momentum transfer strictly holds. But in turbulent flow of a vortex chaos motion, such a situation cannot happen. Thus, in the physical image of an agitating motion of fluid parts, it may be vorticity rather than momentum that is transferred as it is. This is a basic conception of the vorticity transfer theory proposed by Taylor (reference 11).

In the Navier-Stokes equations, when the viscous terms are neglected they are transformed into

$$\frac{\partial U}{\partial t}+\frac{\partial}{\partial x}\left(\frac{U^2+V^2+W^2}{2}\right)-(V\Omega_z-W\Omega_y)=\frac{-1}{\rho}\frac{\partial P}{\partial x}\,,$$
$$\frac{\partial V}{\partial t}+\frac{\partial}{\partial y}\left(\frac{U^2+V^2+W^2}{2}\right)-(W\Omega_x-U\Omega_z)=\frac{-1}{\rho}\frac{\partial P}{\partial y}\,,$$
$$\frac{\partial W}{\partial t}+\frac{\partial}{\partial z}\left(\frac{U^2+V^2+W^2}{2}\right)-(U\Omega_y-V\Omega_x)=\frac{-1}{\rho}\frac{\partial P}{\partial z}\,, \qquad (31.1)$$

with the vorticity components in the x-, y- and z-direction, respectively, denoted by Ω_x, Ω_y, and Ω_z. When U, Ω_x, and other like terms are written respectively as $\bar{U}+u$, $\bar{\Omega}_x+\omega_x$, etc., and with the mean and fluctuational parts divided and time means taken in (31.1),

$$\bar{U}\frac{\partial\bar{U}}{\partial x}+\bar{V}\frac{\partial\bar{U}}{\partial y}+\bar{W}\frac{\partial\bar{U}}{\partial z}=\frac{-1}{\rho}\frac{\partial\bar{P}}{\partial x}-\frac{\partial}{\partial x}\left(\frac{\overline{u^2+v^2+w^2}}{2}\right)+\overline{v\omega_z}-\overline{w\omega_y}\,,$$
$$\bar{U}\frac{\partial\bar{V}}{\partial x}+\bar{V}\frac{\partial\bar{V}}{\partial y}+\bar{W}\frac{\partial\bar{V}}{\partial z}=\frac{-1}{\rho}\frac{\partial\bar{P}}{\partial y}-\frac{\partial}{\partial y}\left(\frac{\overline{u^2+v^2+w^2}}{2}\right)+\overline{w\omega_x}-\overline{u\omega_z}\,,$$
$$\bar{U}\frac{\partial\bar{W}}{\partial x}+\bar{V}\frac{\partial\bar{W}}{\partial y}+\bar{W}\frac{\partial\bar{W}}{\partial z}=\frac{-1}{\rho}\frac{\partial\bar{P}}{\partial z}-\frac{\partial}{\partial z}\left(\frac{\overline{u^2+v^2+w^2}}{2}\right)+\overline{u\omega_y}-\overline{v\omega_x} \qquad (31.2)$$

is obtained. When a two-dimensional flow is considered for brevity,

$$\bar{\Omega}_x = \bar{\Omega}_y = 0, \qquad \bar{\Omega}_z = -\frac{d\bar{U}}{dy} \tag{31.3}$$

is obtained and (31.2) is simplified to

$$\frac{d\bar{P}}{dx} = \rho \overline{v\omega_z} \tag{31.4}$$

with the variation of turbulent intensity in the x-direction neglected. As the Reynolds equations in this case are simplified to

$$\frac{d\bar{P}}{dx} = \frac{d\tau}{dy}, \tag{31.5}$$

the relation

$$\frac{d\tau}{dy} = \rho \overline{v\omega_z} \tag{31.6}$$

is obtained. According to the supposition of transfer of vorticity across the flow, the expression

$$-\overline{v\omega_z} = v l' \frac{d\bar{\Omega}_z}{dy} \tag{31.7}$$

is arrived at in the same manner as the deduction of (30.3) where v and l' are the same as in (30.5). When Prandtl's mixing length l of (30.9) is introduced, (31.7), (31.6), and (31.3) lead to

$$\frac{d\tau}{dy} = \rho l^2 \left|\frac{d\bar{U}}{dy}\right| \frac{d^2\bar{U}}{dy^2}. \tag{31.8}$$

This is the formula of the vorticity transfer theory proposed by Taylor (reference 11), which corresponds to (30.8) of the momentum transfer theory.

32. REPRESENTATION OF TURBULENT SCALE

Expressions of the transfer theory connect turbulent shearing stress with

the mean velocity, using an unknown quantity of the mixing length ℓ. The length ℓ is further interpreted to be approximately proportional to ℓ' of the mean free path of fluid parts. Thus, in the transfer theory, an essential problem is inquiry into general characteristics of the mean free path in the real states of turbulent flow. First, the previously proposed statistical representations (reference 9) of the quantity of turbulent scale whose definition holds in any case of shear or shearless turbulence will be reviewed.

When L_t is considered to be the distance moved by a fluid particle across the flow in a time interval $0 \sim t$, it is written as

$$L_t = \int_0^t v(t-k_t)\,dk_t , \tag{32.1}$$

and the correlation between L_t and v becomes

$$\begin{aligned} \overline{L_t v} &= \overline{v(t)\int_0^t v(t-k_t)\,dk_t} \\ &= \int_0^t \overline{v(t)\,v(t-k_t)}\,dk_t \\ &= v^2 \int_0^t R_{vv}(k_t)\,dk_t , \end{aligned}$$

$$R_{vv}(k_t) = \overline{v(t)v(t-k_t)} \,/\, v^2 . \tag{32.2}$$

(32.2) is one of the Lagrange correlations as denoted by expression (19.3). Since $\overline{L_t v}$ is written as

$$\overline{L_t v} = \overline{L_t \frac{dL_t}{dt}} = \frac{1}{2}\,\frac{d\overline{L_t^2}}{dt} , \tag{32.3}$$

$$\frac{1}{2}\,\frac{d\overline{L_t^2}}{dt} = v^2 \int_0^t R_{vv}(k_t)\,dk_t \tag{32.4}$$

is obtained. As in the case of the Euler correlation, when k_t is made large, $R_{vv}(k_t)$ tends rapidly to zero and $\overline{L_t^2}$ attains a constant value of

$$\overline{L_t^2} = 2v^2 t \int_0^\infty R_{vv}(k_t)\, dk_t .$$

(32.5)

Therefore, by (32.2) the coefficient of turbulent shearing stress (30.5) is expressed as

$$\varepsilon = \rho l' v = \lim_{t\to\infty} \overline{L_t v} = \rho v^2 \int_0^\infty R_{vv}(k_t)\, dk_t .$$

(32.6)

As mentioned previously, the conception of the transfer theory is based on the Lagrangian point of view of the movement of a fluid part. Thus, with the Lagrange correlation taken into account, the fundamental quantity can be directly represented.

As a quantity concerning the turbulent scale, the Euler correlation includes the expression of the Reynolds stress as a special case. The scale length L_f of (18.7) or λ_f of (18.8) is defined by the correlation whose definitions can be extended into general cases of nonisotropic turbulence. In the case of isotropic turbulence, the Lagrange and Euler correlations are connected by Taylor's hypothesis, as mentioned in Section 19. But, in shear turbulent flow, where the transfer theory can be applied, Taylor's hypothesis does not hold, and it becomes difficult to connect the mean free path l' to the general expression of the Euler correlation.

The interpretation of a vortex chaos motion introduced to clarify the cause of the turbulent agitating motion belongs to a Lagrangian interpretation of a physical image. The basic formulas with the D*-domain introduced in Chapter Three are attempts to deduce the Eulerian expressions of the Reynolds stress from this Lagrangian view of the phenomena. According to this physical picture, the mean free path l' at a point corresponds to the relative mean value of diameters across the flow of many vortices passing near this point. For example, when R_{yi} is taken to be a relative length in the y-direction of the i-th vortices in an idealized two-dimensional chaos motion consisting of N kinds of vortices, an expression

$$l' \sim \sum_{i=1}^{N} \tilde{P}_i^* R_{yi}$$

(32.7)

may be the most direct representation of the mean free path l', where $\tilde{P}_i^*$ given by (13.6) means the ratio by which the i-th vortices are mixed.

33. TRANSFER HYPOTHESES IN THE INITIAL PERIOD

In this section, foundations of the transfer theory shall be surveyed according to the idealization of the initial-period law mentioned in the last chapter. As a representative example of the decaying shear turbulence, a two-dimensional wake in a uniform flow shall be considered. In the initial period, the profile of the mean velocity or shearing stress can be expressed by the parameter $\eta = y/\sqrt{4\nu t}$. This representation supports the discussion in Section 30, where relative variations of the profiles along the x-direction are neglected.

In the expression (30.5) of the coefficient of shearing stress ε, l' of (32.7) is represented by R_y of the α =1 vortices in the initial period and is proportional by (22.3) to $t^{\frac{1}{2}}$,

$$l' \backsim t^{\frac{1}{2}}. \tag{33.1}$$

Thus, since

$$v \backsim t^{-\frac{1}{2}} \tag{33.2}$$

in (23.1), a relation

$$\varepsilon = \text{constant} \tag{33.3}$$

is obtained along the x-direction. When δ and $\bar{U}_1$ are taken, respectively, as the breadth of wake and the defected mean velocity as shown in Figure 33, they may be proved to be proportional, respectively, to $t^{\frac{1}{2}}$ and $t^{-\frac{1}{2}}$. Then

$$\varepsilon \backsim \delta \bar{U}_1 \tag{33.3'}$$

is obtained. Expression (33.3) or (33.3') is the same as the assumption proposed by Prandtl in the transfer theory (reference 45).

As for the profile of ε in the y-direction, l' in (30.5) is constant in this direction because of the α =1 vortices. Thus,

$$\varepsilon \backsim v(y). \tag{33.4}$$

In this case of the turbulent wake, expressions of velocity fluctuation are attributed essentially to the two-dimensional description as described in

Section 25, and by (25.2), (33.4) becomes

$$\varepsilon \backsim \iint_{D^*} P_1^*(s,\theta;\eta)\,\bar{V}^{*2}(s,\theta)\sin^2\theta\, d\Omega^*, \tag{33.5}$$

with the coefficient terms in (25.2) neglected. If we further assume that the value of ν is constant in a fully-developed turbulent state and that $V^* \sin\theta$ is independent in the D*-domain, the integration of (33.5) presents the profile of the intermittency factor γ of (26.5), and the formula

$$\varepsilon \backsim \gamma(\eta) \tag{33.6}$$

is obtained.

In the transfer theory, a simple expression of the basic assumption is preferable to the strict representation of the phenomena, as far as deriving useful results for practical problems is concerned. Thus, the expression (33.5) or (33.6) simplified as

$$\varepsilon = \begin{cases} \text{constant} & \delta^2 \geqq y^2 \\ 0 & \delta^2 < y^2 \end{cases} \tag{33.7}$$

shall be assumed as shown in Figure 55. The expressions (33.6) and (33.7) are the same as proposed by Townsend (reference 40). In view of expressions (33.3) and (33.7), ε is considered constant in the whole region of the turbulent wake. This is the simplest expression of the assumption. In the real state of a vortex chaos motion, ε of (33.5) must be taken for many kinds of vortices, and such a simple deduction as the above-mentioned one becomes difficult.

The mixing length l is represented by l' if $\overline{uv}/\nu^2$ is assumed to be constant. With this assumption, (33.1) leads to

$$\frac{l}{\delta} = \text{constant}. \tag{33.8}$$

Namely, the mixing length l increases in the x-direction proportionally to the breadth of flow and is constant in the y-direction in the wake. Expression (33.8) is also the assumption proposed by Prandtl (reference 45). As seen in Figure 41, however, it is a problem to assume a constant profile of $\overline{uv}/\nu^2$, and it is difficult to discriminate between (33.7) and (33.8) at this stage. At any rate, in the approximation of the initial period,

the above descriptions may hold in other cases of decaying shear turbulence.

34. TURBULENT WAKE

Formulas (33.7) and (33.8), which are derived from the initial-period similarity-law, are simple expressions of the fundamental assumption of the transfer theory. However, merits of the two should be discussed by comparing computed and experimental results. Analytical works on the mean-velocity profile in the initial period shall be presented in this section. In the case of a two-dimensional wake, the Reynolds equation is approximated by (24.2), and the time t in (23.2) is taken to be proportional to x. Therefore, the velocity profile is expressed as

$$\frac{\overline{U_1}}{\overline{U_0}} = f(\eta')\, x^{-\frac{1}{2}},$$

$$\eta' = \ast\, x^{-\frac{1}{2}}. \tag{34.1}$$

In the formula of the momentum transfer theory which contains the mixing length, the turbulent shearing stress is written by (30.9) and (33.8) as

$$\tau = \rho \ell^2 \overline{U_0}^2 f'(\eta')^2 x^{-2}$$

$$\ell = a_1 x^{\frac{1}{2}}. \tag{34.2}$$

By substituting (34.1) and (34.2) into (24.2), the Reynolds equation becomes

$$f(\eta_1') + \eta_1' f'(\eta_1') - 4 f'(\eta_1') f''(\eta_1') = 0,$$

$$\eta_1' = a_1^{-\frac{2}{3}} \eta', \tag{34.3}$$

where the prime of f denotes differentiation by η_1'. The boundary conditions are given by

$$f = 0, \quad f' = 0 \qquad \text{at} \qquad \eta_1' = a_1^{-\frac{2}{3}} x^{-\frac{1}{2}} \delta. \tag{34.4}$$

By solving (34.3) with (34.4), the expression

$$\frac{f}{f(0)} = (1-\eta_1^{\frac{3}{2}})^2,$$
$$\eta_1 = \frac{y}{\delta},$$

(34.5)

is obtained (reference 39).

According to vorticity transfer theory, (31.8) gives the expression of shearing stress. However, since the value of ℓ is independent of the y-direction, (31.8) takes essentially the same form as (30.9) of the momentum transfer. Namely, by putting

$$\ell = \sqrt{2}\, a_1 x^{\frac{1}{2}},$$

(34.6)

the same expression as (34.3) of the Reynolds equation and the solution of (34.5) is developed.

Using the shearing-stress coefficient ε, (24.2) and (33.7) lead to the equation

$$f(\eta_2) + \eta_2 f'(\eta_2) + 2f''(\eta_2) = 0,$$
$$\eta_2 = y\left(\frac{\varepsilon x}{U_0}\right)^{-\frac{1}{2}},$$

(34.7)

where the boundary conditions are taken as

$$f' = 0 \qquad \text{at} \qquad \eta_2 = 0,$$
$$f = 0 \qquad \text{at} \qquad \eta_2 = \delta\left(\frac{\varepsilon x}{U_0}\right)^{-\frac{1}{2}}.$$

(34.8)

Since the coefficient ε is constant in the flow, (34.7) is of the same form as the equation of a two-dimensional viscous wake, and the solution with $\delta \to \infty$ (reference 46) is

$$\frac{f}{f(0)} = e^{-\frac{\eta_2^2}{4}}.$$

(34.9)

In formula (33.6), an ordinary differential equation is derived when the profile of γ is given by (26.7) of the initial-period law. The solution may be proved to be

$$\frac{f}{f(0)} = \exp\left\{a\eta^2\left(1+\frac{\eta^4}{b}\right)\right\}, \tag{34.10}$$

with constants a and b (reference 42).

Figure 56 shows a comparison of the above evaluated results with experimental works in turbulent flow behind a circular cylinder, where (34.5) and (34.10) are shown by two curves in the figure. Although (34.9) and (34.10) are almost the same, the latter seems to give better results near the boundary (reference 42). This is reasonable because the assumption of (34.10) is undoubtedly a more accurate description of the flow, when compared with (34.9). At any rate, discrepancies of the evaluated results are small. As a practical method of evaluation, the essential purpose of the transfer theory, the simple expression of (33.7) seems to be appropriate. Namely, mathematical analysis in this case of the turbulent wake takes the same form as in laminar viscous flow. There are no grounds on which to state that the numerical value of ε is independent of the state of flow. By comparing the solution (34.9) with experimental results in Figure 56, $\varepsilon \doteqdot 0.047\ U_i(0)$ (reference 46) is obtained, and the order of ε/ρ becomes

$$\frac{\varepsilon}{\rho} \doteqdot 10^4 \frac{cm^2}{sec}, \tag{34.11}$$

a value far larger than that of the kinematic viscosity $\mu/\rho \doteqdot 10^{-1}\ cm^2/sec$ of the air. Signifying the difference of the scale of the molecular and vortex chaos motions, it is regarded as the reason to neglect molecular viscosity in the study of shear turbulent flow, as done in Section 24.

The numerical value of the mixing length ℓ can also be presumed by comparing evaluted and experimental results (references 40 and 48). Owing to measurements of the two-dimensional wake,

$$\ell \doteqdot 0.3\delta \tag{34.12}$$

is arrived at. Thus, although the coefficient of ratio may vary case by case, the mean free path ℓ' has the same order of magnitude as δ, because ℓ, seen by (30.9), compares with ℓ'. This fact signifies that the scale of vortex chaos motion which causes the turbulent agitating motion compares to the whole breadth of the shear turbulent flow, as mentioned before.

The essential point of the above-mentioned discussions of the typical case of a two-dimensional wake can hold in other cases of decaying shear turbulence (references 39 and 47, 39, 48 and 49.) In the region of the initial period, only outlines of the analyses shall be related. In the initial period of an axisymmetric turbulent wake, the velocity profile is written, by referring to (24.10), as

$$\frac{\overline{U_1}}{\overline{U_0}} = f(\eta')x^{-\frac{2}{3}}, \qquad \eta' = rx^{-\frac{1}{3}},$$

and the mixing length is expressed by (33.8) as

$$\ell \backsim x^{-\frac{1}{3}}.$$

Then the Reynolds equation (24.9) is integrated into (reference 50)

$$\frac{f}{f(0)} = (1-\eta^{\frac{3}{2}})^2,$$

$$\eta = \frac{y}{\delta}. \qquad (34.13)$$

Based upon the assumption (33.7) that ε = constant, the Reynolds equilibrium may also be integrated into a definite expression of the velocity profile (reference 38).

In many other cases of the turbulent wake, the above-mentioned treatment may still be applied; for instance, to an asymmetrical two-dimensional wake as shown in Figures 6, 35, 36 and 37. In the initial period, the two kinds of vortex chaos motions are assumed to preserve their respective similarity characteristics, with the effects of the descending vortices neglected. At a position behind the body, v and ℓ' may have different values on both sides of the wake. Thus, formula (33.7) or (33.8) holds for numerical values as shown in Figure 57, and the relatively similar profiles of (34.5) or (34.9) are derived with a different value of δ .

35. TURBULENT JET

When a turbulent flow blows into a still fluid from a two-dimensional slit, the Reynolds equations are given by (24.11). Referring to (24.12) of the initial-period similarity-law, the equation takes the form of an ordinary differential equation. Namely, with the assumption ε = constant of (33.7), (24.11) becomes

$$f^2 + f' \int_0^\eta f\,d\eta + f'' = 0,$$

$$f = \frac{\bar{u}(\eta)}{\bar{U}_o}\sqrt{\frac{d}{x}}, \qquad \eta = \frac{dy}{x}, \tag{35.1}$$

where $\bar{U}_o$ is the velocity in the slit and d is the breadth as shown in Figure 40. When (35.1) is solved with the boundary conditions,

$$f' = 0 \qquad \text{at} \qquad \eta = 0$$

$$f \to 0 \qquad \text{at} \qquad \eta \to \infty, \tag{35.2}$$

a solution

$$\frac{f}{f(0)} = \operatorname{sech}^2 \eta \tag{35.3}$$

is derived (reference 46).

According to the momentum transfer theory, with ℓ = constant from (33.8), the Reynolds equation (24.11) becomes

$$f^2 + f' \int_0^\eta f\,d\eta + (f'^2)' = 0, \tag{35.4}$$

which can be integrated (reference 51). Using the vorticity transfer theory with a constant mixing length, the same equation as that of the two-dimensional wake may be obtained. The solution is compared with experimental results in Figure 58. With the assumption ε = constant from (33.7) in the case of an axisymmetric jet, the equation of motion is written as

$$\eta f^2 + f' \int_0^\eta f\,d\eta + f' + \eta f'' = 0,$$

$$f = \frac{\bar{u}(\eta)}{\bar{U}_o}\frac{d}{x}, \qquad \eta = \frac{a_1 r}{x} \tag{35.5}$$

by (24.13) and (24.14) and the solution

$$\frac{f}{f(0)} = \left(1 + \frac{\eta^2}{a_2^2}\right)^{-2} \tag{35.6}$$

is derived (reference 49). When relation (33.8) of the mixing length is considered in the momentum-transfer theory, equation (24.13) becomes

$$\frac{d}{d\eta}\left(\frac{f\int_0^\eta f\,d\eta}{\eta}\right) - \frac{d}{d\eta}\left\{\frac{1}{\eta}\left(f' - \frac{f}{\eta}\right)^2\right\} = 0 \tag{35.7}$$

and can be integrated (reference 51). Figure 59 shows a comparison of the evaluated and observed results.

In the case of a half-jet, if the assumption ε = constant from (33.7) is used in (24.15) and (24.16), the equation

$$f'' + f'\int_0^\eta f\,d\eta = 0,$$

$$f = \frac{\bar{U}(\eta)}{\bar{U}_0}, \qquad \eta = \frac{a_1 y}{x} \tag{35.8}$$

is derived. The boundary conditions are given by

$$f = 1 \quad \text{at} \quad \eta \to \infty$$

$$f = 0 \quad \text{at} \quad \eta \to -\infty. \tag{35.9}$$

But (35.8) is not easily solved by (35.9). If

$$\int_0^\eta f\,d\eta \backsim \eta \tag{35.10}$$

is taken, (35.8) is integrated into the expression (reference 46):

$$f = 1 + \frac{2}{\sqrt{\pi}}\int_0^\eta e^{-\eta^2} d\eta. \tag{35.11}$$

Considering the relation l/δ = constant of (33.8), equation (24.15) becomes

$$\int_0^\eta f d\eta + f'' = 0, \tag{35.12}$$

which is easily solved (reference 51). Figure 60 shows the experimental comparison.

In this case of a half-jet, in Section 28 an attempt was made to derive a profile of the mean velocity, together with turbulent intensities, directly from the initial-period similarity-law. Compared with that attempt, the transfer theory can give a preferable result of the mean velocity profile, depending on the simple assumption and analysis. Thus, if the purpose of the study is confined to the evaluation of only the mean velocity of turbulent shear flow, the transfer theory shall still be important. On the other hand, the initial-period law based on the P^*- and $\overline{V}^*$-function mentioned in the last chapter has the purpose of giving a statistical interpretation, unificatively, to the general phenomena of turbulent flow. Therefore, as far as the mean velocity is concerned, the above P^* - V^* function approach shall have accomplished this role if the fundamental assumptions of the transfer theory of a practical purpose may be derived from this description of the initial-period law.

As a matter of course, the basic assumption (33.7) or (33.8) is adaptable to the approximative description of the initial period, and as mentioned in Section 29, deviation from the initial-period law in the decaying shear turbulence is not as conspicuous as it is in the turbulent flow behind a grid. This characteristic makes the simple formula of (33.7) or (33.8) especially useful in the analysis of the transfer theory. However, in order to evaluate the deviation of the mean velocity profile from that of the initial period, there must be a search for the effect of the descending vortices on the profile of $\mathcal{E}$ or $\mathcal{L}'$. In the following chapter, mathematical descriptions of cascade phenomena shall be attempted in the general cases of shear or shearless decaying turbulence.

CHAPTER SEVEN. NONSIMILARITY IN THE DECAYING TURBULENCE

36. TRANSITION PROBABILITY IN THE CASCADE PROCESS

Theoretical foundations of the discussions in the previous two chapters come from the idealized description of the initial period. As seen in Section 21, however, the similarity assumption does not yield a satisfactory result for the correlation or spectrum function, even in the case of isotropic turbulence. As mentioned in Section 18, the triple correlations come from the inertia terms of the Reynolds equations, and the theoretical result (20.9) means that an expression of the ideal state neglects the inertia terms in the Reynolds equations. In the previous studies of isotropic turbulence, interests were focused on the inertia terms, since the Kármán-Howarth equation had been precisely investigated. Namely, studies were made in many respects of the physical meaning of W_3 of (19.13) of the transformed function of a triple correlation, and mathematical treatments were made on the propagation formula (19.12) of the spectrum function. Consequently, some local characteristics of the spectrum function have been gradually clarified in narrow regions of the wave numbers. In our statistical theory, the work in the next stage is to search for the fluctuational terms V* and others, which correspond to the inertia terms of the Reynolds equations, in the real expressions of vortex chaos motion. In this chapter, depending upon the physical conception of a vortex chaos motion, a general discussion of deviation from the initial-period law from a wider viewpoint of the decaying turbulence shall be attempted.

According to the interpretation of a vortex chaos motion, the fluctuational terms V^*_{xx} and others have an essential interrelation with the production of small vortices by the cascade process mentioned in Section 6. As mentioned in Section 5, when the molecular viscosity around vortex centers in a regular pattern interfere with each other, the vortices tend to become irregular. At the same time, small descending vortices are easily formed by the interference of the original vortices. In the decaying turbulence, let the primary vortices of $\alpha = 1$ be called vortices of the first generation; the vortices produced by the interference of the first-generation vortices be those of the second generation; those produced by the first- and second-generation vortices be of the third generation, and so on. Generally speaking, a new vortex motion is produced from at least two kinds of vortices, and the vortices produced in the process of the cascade phenomena should be signified with a double suffix of the ascending vortices. For simplicity, however, a positive rational number m shall be used to express the number of generation as above. Even in the study of continuous phenomena of turbulent flow, if many kinds of vortices are taken into account, such a discontinuous rational number must be introduced. In order to proceed with a mathematical description of the cascade phenomena, a function of transition probability will be further introduced.

In the initial-period law, the time t is counted from the production instant of the $\alpha = 1$ vortices just behind a body. In the study of cascade

phenomena, the origin of time shall be shifted to the time when the $\alpha = 1$ vortices form an irregular state and the cascade phenomena begins. Namely, scales of the m=1 vortices have grown up already to some extent at t=0, and the descending vortices of $m \geqq 2$ are produced constantly with $t \geqq 0$. Of course, the ordinate x is connected definitely to t by the relation $t = \int_{x_0}^{x} \bar{U}^{-1} dx$ of (23.2).

Now, the vortices of an m-generation produced in a time interval $t_o \sim t_o + dt_o$ shall be denoted with a suffix

$$m(t_o) . \tag{36.1}$$

When the time t is taken so that $t > t_o$, a functional relation between t and x of the location in the field of flow is determined. A fixed A-point is taken at a position of x, and the $m(t_o)$-vortices passing nearby are considered. At this A-point, the probability-density function defined by (11.5) for these vortices is written as

$$P^{*'}_{m(t_o),t}(r,\theta,\phi)\,dt_o . \tag{36.2}$$

In (36.2) the function P*' is concerned with the m-vortices produced in a unit time interval at t_o, where r, θ, ϕ are the coordinates in the $D_{m(t_o),t}$ domain and the suffix t means that the state of irregularity of these vortices generally changes along the flow. The ratio by which the $m(t_o)$-vortices are mixed in the whole kinds of vortices passing near the A-point is expressed as

$$\tilde{P}^{*'}(m(t_o),t)\,dt = \iiint_{D^*_{m(t_o),t}} \{P^{*'}_{m(t_o),t}(r,\theta,\phi)\,dt_o\}\,dQ^{*}_{m(t_o),t} ,$$

(36.3)

as defined by (13.6). The nondimensional probability-density function for these vortices is given by (16.1) as follows:

$$P^{*}_{1}(r,\theta,\phi;\, m(t_o),t) = \frac{P^{*'}_{m(t_o),t}(r,\theta,\phi)\,Q^{*}_{m(t_o),t}}{\tilde{P}^{*'}(m(t_o),t)} .$$

(36.4)

The ratio by which the vortices of m-generation produced in $0 \sim t$ are mixed in the whole kinds at the A-point is written as

$$\tilde{P}^*(m,t) = \int_0^t \tilde{P}^{*\prime}(m(t_0),t)\,dt_0 \,. \tag{36.5}$$

For all the kinds of vortices, the relation

$$\sum_{m=1}^{\infty} \tilde{P}^*(m,t) = 1 \tag{36.6}$$

holds independently of t as formula (13.7).

According to the physical interpretation of the cascade phenomena, a vortex of some generation is produced from at least two vortices of the ascending generations. However, vortices of an ascending generation bring about vortices of some descending generation by the disturbances from other vortices of the same or different generations from these ascending ones. Let the probability with which $m(t_0)$-vortices produce some vortices of n-generation ($n>m$) in a time interval $t\sim t+dt$ be written as

$$p^*(m(t_0)\to n(t))\,dt. \tag{36.7}$$

Namely, we take a ratio between the number of the $m(t_0)$, t-vortices passing near the A-point in some time interval and that of the n(t)-vortices produced by the above vortices in the region $t\sim t+dt$ along the flow in the same time interval. The limiting value of the ratio is also taken by making the time interval infinite. The function p*dt of (36.7) is the limiting value of this. The form p* has the dimension of the inverse of time and corresponds to a kind of transition probability in statistical mathematics.

37. POISSON PROCESS FOR THE CASCADE PHENOMENA

In the statistical theory of turbulence, it is characteristic to express the degree of irregularity of a vortex chaos motion in the P*-function. The function P_1^* of (36.4) is a relative probability-density function in the D*-domain for the $m(t_0)$,t-vortices, in which the previously discussed statistical features of the shear or shearless turbulence can be adapted. In the study of cascade phenomena, the function $\tilde{P}^{*\prime}(m(t_0),t)dt_0$ denoting the mixture of different kinds of vortices must be taken into account. In this section this functional form shall be discussed by surveying the transition probability p* of (36.7) (reference 54).

The function p* of (36.7) has the independent variables m, t_0, n, t. In the real state of cascade phenomena it may have a complicated functional form, and it is difficult to imagine the functional expression even by means

of experimental observations. However, since t originates when cascade phenomena begin, p* cannot be assumed to vanish for all the m- and n-vortices at t = 0. p* must have a nonzero value, at least for the m=1 vortices. Thus, when the function p* is expanded into the Taylor series for the independent variables, at least the first term must remain as a nonzero constant.

As the first approximative expression for the p*-function, a constant value of p* that is independent of $m(t_0)$ and n(t) will be assumed by taking only the first term of the series. This assumption means that vortices of m generation are produced only from those of the previous m-1 generation at a constant rate that is independent of the generation and time. Namely, the expression

$$p^*((m-1)(t_0) \to m(t)) = p^* \quad (\text{constant}), \tag{37.1}$$

will be made to be the basic assumption of the study of the cascade process. If p* in (37.1) is made zero, the foregoing descriptions shall be reduced to the formula of the initial-period law. When a constant of p* is not zero, it is possible to evaluate the effect of cascade phenomena in the simplest way of a statistical analysis. It is easily supposed that as a generation m increases, such an idealization of the situations becomes more inaccurate for the real states of the cascade phenomena. The assumption (37.1) allows a survey of the deviation process from the initial-period law caused by the cascade phenomena of young generation vortices.

When a time interval $0 \sim t$ is divided into N equal small intervals, the ratio by which vortices of some generation produce the next ones in each interval is given by

$$p^* \frac{t}{N} .$$

Namely, it is supposed that in the first time interval of N=1, only the m=1 vortices exist, and in the following intervals of $N \geqq 2$ many kinds of vortices of $m \geqq 2$ are produced from those of their respective previous generations. In this case, the probability distribution of each generation is proved in statistical mathematics to be expressed in the binomial distribution

$$\frac{N!\left(p^* \frac{t}{N}\right)^{m-1}\left(1 - p^* \frac{t}{N}\right)^{N-m+1}}{(m-1)!\,(N-m+1)!} .$$

Because of the relation $\lim_{N\to\infty}(1-p^*\frac{t}{N})N = \exp(-p^*t)$, the limiting value at $N \to \infty$ of the binomial distribution may be proved to become the so-called Poisson distribution.

Thus, with the assumption (37.1) of the transition probability, the functional forms $\widetilde{P}^{*\prime}$ or $\widetilde{P}^{*}$ of (36.3) or (36.5) of the mixture of vortices can be stated as the following Poisson distributions:

$$\widetilde{P}^{*\prime}(m(t_o),t) = \frac{t_o^{*m-2}e^{-t^*}}{(m-2)!}dt_o^*, \quad (m=2,3,\ldots),$$

$$t_o^* = p^* t_o, \tag{37.2}$$

or

$$\widetilde{P}^{*}(m,t) = \frac{t^{*m-1}e^{-t^*}}{(m-1)!}, \quad (m=1,2,\ldots),$$

$$t^* = p^* t. \tag{37.3}$$

(37.2) and (37.3) are obviously connected by the integration formula of (36.5).

An important feature of (37.2) or (37.3) is that the variable t or t_o in (36.3) or (36.5) is replaced by t* or t_o^*. According to the discussions of the initial-period law in Section 20, the variable along the flow should be taken by t, not by the ordinate x itself, because by the latter variable the effect of the mean velocity $\overline{U}_o$ appears explicitly. For the same reason, when the cascade process is taken into account, t should be replaced by t*= p*t of a nondimensional time. Otherwise, there will be many kinds of relations depending on different values of p*, namely, on different intensities of the cascade process. At any rate, the combination of a parametric constant p* of (37.1) and of the time t into a new independent variable t* will make the subsequent statistical analysis somewhat easier. Figure 61 shows the distribution of (37.3).

38. NONSTATIONAL EXPRESSION FOR THE CORRELATION TENSOR

In the real state of flow, $m(t_o)$-vortices produced at a time t_o are simultaneously carried along and affected by other kinds of vortices, and these effects make it difficult to preserve a similarity characteristic for any large distance along the flow. Even with a simplified treatment of the Poisson process, the mixing situation of different kinds of vortices does not represent a similarity characteristic versus the variable t* as shown in Figure 61. Namely, the functional form of $P^{*\prime}$ of the $m(t_o)$-vortices at a time t varies generally with $t-t_o$ as denoted by (36.2). Also as in the case of expression (22.2), the function of the mean turning velocity $\overline{V}^*$ for

the $m(t_o)$-vortices at t may be generally written as

$$\bar{V}^*_{m(t_o),t} = F_{m(t_o)}(r,\theta,\phi;\, t-t_o)\,G_{m(t_o)}(t-t_o), \tag{38.1}$$

with a decaying term $G_m(t_o)(t-t_o)$

In the derivation of the Poisson distribution in the last section, there was no need to relate the functional form of $P^{*\prime}_{m(t_o),t}$ to the $D^*_{m(t_o),t}$ domain. It has been explained that the similarity preservation in the initial period comes from the two similarities of the P*- and $\bar{V}$*-functions. Corresponding to the idealization of the Poisson process of the mixture of different kinds of vortices, the two functions of $P^*_{m(t_o),t}$ and $\bar{V}^*_{m(t_o),t}$ shall be simplified by taking only their respective first terms of the Taylor expansions versus t_o-t. Namely, in the study of the cascade process, the two fundamental similarities shall also be assumed for every group of $m(t_o)$-vortices Even if the whole field of flow shows a shear turbulent state, the P*- and $\bar{V}$*-function for every kind of $m(t_o)$-vortices are assumed to preserve their respective similar functional forms along particular positions (x, y_o, z_o) in the field of flow. As for the nonsimilarity characteristic of the cascade phenomena, only Poisson distribution characteristics shall be considered Let the above-mentioned similarity for all $m(t_o)$-vortices be called local similarity.

At the position corresponding to a time t which has elapsed since the beginning of the cascade phenomena, the ideal expression of u-intensity is given by (13.9) as follows:

$$u^2 = \sum_{m=1}^{\infty}\Big[\int_0^t \Big\{\iiint_{D^*_{m(t_o),t}} P^{*\prime}_{m(t_o),t}\;\bar{V}^{*2}_{m(t_o),t}\cos^2\theta\sin^2\phi\, dQ^*_{m(t_o),t}\Big\}dt_o\Big].$$

(38.2)

When the Poisson distribution (37.2) or (37.3) is substituted into (38.2), it takes the form of

$$u^2 = u'^2_1 e^{-t^*} + \sum_{m=2}^{\infty}\int_0^{t^*} u'^2_{m(t_o^*),t^*}\,\frac{t_o^{*m-2}}{(m-2)!}e^{-t^*}\,dt_o^*,$$

$$u'^2_{m(t_o^*),t^*} = \iiint_{D^*_{m(t_o^*),t^*}} P^{*\prime}_{m(t_o^*),t^*}\,\bar{V}^{*2}_{m(t_o^*),t^*}\cos^2\theta\sin^2\phi\, dQ^*_{m(t_o^*),t^*}, \quad (m\geq 2),$$

$$u_1'^2 = \iiint_{D_1^*} P_{1,t^*}^{*\prime} \bar{V}_{1,t^*}^{*2} \cos^2\theta \sin^2\phi \, dQ_{1,t^*}^*,$$

(38.3)

with the nondimensional time introduced.

In the initial-period law, the expression of $\bar{V}^*$ for the m=1 vortices is based on the solution (14.6) for the two-dimensional viscous vortex motion. Furthermore, it has been observed that when the primary vortices of m=1 are elected as those of $\alpha = 1$, favorable agreement between theoretical and experimental results is obtained. In the study of cascade phenomena, it is assumed that the production condition is the same, independent of the production instant t as for the vortices of an identical kind or m-generation. The relation between a generation of vortices m and their kind α is written as

$$\alpha(m), \qquad \alpha(1) = 1.$$

(38.4)

In order to make the expression (38.3) more definite, elongation or contraction of vortex filaments is neglected, as discussed for the initial-period similarity-law of a two-dimensional turbulent wake. In this case the decaying term in (38.1) is written as

$$G_{m(t_o),t}(t-t_o) = 2C_{\alpha(m)}\sqrt{\gamma}\,(t-t_o)^{\frac{1}{2}-\alpha(m)}$$

(38.5)

from the solution (14.6). In (14.6) t is the elapsed time since the beginning of a vortex motion, and in (38.5) the term due to the period before the beginning of cascade phenomena is contained in the constant term $C_{\alpha(m)}$. The P*- and V*-functions of local similarity for $m(t_o)$-vortices can be expressed as

$$P_{m(t_o),t}^{*\prime} = P_{\alpha(m)}^{*\prime}\left(r/\sqrt{4\gamma(t-t_o)}, \theta, \phi\right),$$

$$\bar{V}_{m(t_o),t}^{*} = F_{\alpha(m)}'\left(r/\sqrt{4\gamma(t-t_o)}, \theta, \phi\right)(t-t_o)^{\frac{1}{2}-\alpha(m)},$$

$$F_{\alpha(m)}' = 2C_{\alpha(m)}\sqrt{\gamma}\,F_{\alpha(m)},$$

(38.6)

from formula (22.3) for the case of the initial-period similarity-law.

When (38.6) is substituted in (38.3), the intensity of the u-component is written as follows, with U the mean velocity:

$$\left(\frac{u}{U}\right)^2 = \frac{A_1}{t^*} e^{-t^*} + \sum_{m=2}^{\infty} \int_0^{t^*} \frac{A_{m(t_0^*),t^*}}{(t^*-t_0^*)^{2\alpha(m)-1}} \frac{t_0^{*m-2} e^{-t^*}}{(m-2)!} dt_0^*,$$

$$A_{m(t_0^*),t^*} = \bar{U}^{-2} \iiint_{D^*_{m(t_0^*),t^*}} P^{*\prime}_{\alpha(m)}(r/\sqrt{4\nu(t-t_0)}, \theta, \phi) F'_{\alpha(m)}(r/\sqrt{4\nu(t-t_0)}, \theta, \phi) \rho^{*2\alpha(m)-1} \cos^2\theta \sin^2\phi \, dQ^*_{m(t_0^*),t^*},$$

$$A_1 = \bar{U}^{-2} \iiint_{0^*_1} P_1^{*\prime}(r/\sqrt{4\nu t}, \theta, \phi) F_1'(r/\sqrt{4\nu t}, \theta, \phi) \rho^{*} \cos^2\theta \sin^2\phi \, dQ_1^*. \quad (38.7)$$

When the Euler correlation function of the u-fluctuation at two points of (x, y, z) and ($x+k_x$, y, z) is denoted by $f(k_x;t^*)$, the correlation functions for many groups of $m(t_o)$-vortices preserve their respective similar forms by the assumption of local similarity. Thus, when their respective nondimensional ordinates are denoted by $s_{m(t_o)}$, corresponding to the distance k_x, their correlation function is expressed as

$$f_{\alpha(m)}(s_{m(t_0^*)}) \quad (38.8)$$

independently of $t^*-t_o^*$. By substituting (38.8) into the Poisson distribution as in the case of (38.7), the following formula is obtained:

$$\left(\frac{u}{U}\right)^2 f(k_x;t^*) = \frac{f_1(s_1)}{t^*} e^{-t^*} + \sum_{m=2}^{\infty} \int_0^{t^*} \frac{f_{\alpha(m)}(s_{m(t_0^*)}) A_{m(t_0^*),t^*}}{(t^*-t_0^*)^{2\alpha(m)-1}} \frac{t_0^{*m-2} e^{-t^*}}{(m-2)!} dt_0^*. \quad (38.9)$$

Here, $A_{m(t_0^*),t^*}$ is given in (38.7). Of course, (38.9) can be reduced to (38.7) with $k_x=0$. Expressions for other components can be obtained in the same manner.

Along a direction perpendicular to the mean flow, the function $P^{*\prime}_{m(t_o),t}$ in (38.6) varies generally as in the initial-period law in shear turbulence. Only different parametric values of p* can be attributed to the Poisson process of the cascade phenomena. Thus, either (38.9) or (38.7) is regarded as an extended formula from that of the initial-period law to the cascade phenomena of the decaying turbulence.

39. PRODUCTION CONDITION OF A VORTEX MOTION

At present it is not clear which sort of vortices of α may be produced under what kinds of conditions in the real state of flow. The assumption of $\alpha=1$ for the primary vortices in the initial period has no theoretical ground, but this assumption is made to give the decaying law

$u^2 \sim t^{-1}$ of turbulent intensity, the momentum conservation of the mean-velocity profile, and other results preferable to the real state of the decaying turbulent flow.

According to the discussions in Section 14, the solution of a vortex motion can take any values of $\alpha \geqq 1$ under the boundary condition of zero value of turning velocity at the center and infinity, and there is no reliable ground to decide the function $\alpha(m)$ of (38.4). It is sure, however, that production conditions of $m \geqq 2$ vortices are not the same as in the case of m=1 vortices, because the m=1 vortices are produced with the energy of the nonviscous main flow supplied by means of the boundary layer around a body, while m 2 vortices are produced with the energy of the viscous vortex motion of the preceding generation. Therefore, although m is a positive rational number, $\alpha(m)$ may be taken to be proportional to m, not to be a constant term, as the first approximative expression. Thus, as the simplest assumption of the functional form of $\alpha(m)$ having the condition $\alpha(1)=1$,

$$\alpha = m \tag{39.1}$$

shall be taken.

If p* is made zero in (38.7), it becomes the form $(u/\bar{U})^2=(A_1/p^*)t^{-1}$ of the initial-period law. In the case of the isotropic turbulence, the solution (14.6) for two-dimensional viscous vortex motion of $\alpha=1$ can be taken as the function F_1' in A_1 of (38.7) together with the condition $P_1^{*\prime}=1$, and (38.7) is reduced to

$$\left(\frac{u}{\bar{U}}\right)^2 = \frac{A_1}{p^*}\, t^{-1},$$

$$\frac{A_1}{p^*} = \frac{2C_1^2}{\bar{U}^2}\, s_0^{\frac{3}{2}} \int_0^{s_0} F_1^{\prime 2}(s)\sqrt{s}\, ds,$$

$$s = \frac{r^2}{4\nu t}\,, \tag{39.2}$$

of the same form of (20.10) of $\alpha=1$, where the time t is taken from the production instant of the $\alpha=1$ vortices. In the initial-period law, the coefficient A_1/p^* can be regarded as a constant, since s_o is independent of t for $t>0$.

At t=0 in (39.2), the radius r also becomes zero and the coefficient A_1/p^* becomes indefinite. If A_1/p^* is definite, $(u/\bar{U})^2$ diverges. The solution (14.6) of the equation (14.1) with a boundary condition (14.5) represents only the diffusion of vorticity concentrated at first at one point in a fluid. (14.1) is an equation of diffusion, and the solution

(14.6) does not concern a problem of the production of a vortex motion. Namely, the decaying formula (38.2) in the initial period has a singularity character at t=0. But, the period in which the α=1 vortices come into a chaotic state can be excluded from the discussions. This holds in other cases of the decaying turbulence, and there is no need to question the singularity character in relation to the initial period law.

In the cascade phenomena, new vortices are produced incessantly along the flow, and the consideration of the production cannot be avoided from the analysis. In the real state of flow behind a circular cylinder, a vortex motion is first formed by taking some energy from the main flow and then is carried along the flow separated from the body. Probably a vortex motion may begin to obey the growing condition (14.1) of vorticity diffusion after it has attained a finite region of vorticity in some period of the production. In the production period, there is no equation governing the states of flow. Speaking of the growing condition of a vortex motion, the constant term $A_{m(t_o^*),t^*}$ in (38.7) derived from the equation (14.1) seems to vanish at $t^*=t_o^*$, decreasing its value in the production period as shown in Figure 62, and prevents the divergency of the value of u/U. It is more important to consider the magnitude of an initial constant C_α contained in A_m than to discuss a relative functional form of A_m near $t^*=t_o^*$. In the case of m=1, C_1 can be related to the circulation Γ at t=0. In the case of $m \geqq 2$, the constant C_α may be proportional, at least approximately, to the energy of the preceding vortex motions.

It is not of much value, however, to continue the present indistinct presumption of the difficult problem of the production of a vortex motion. In this section, for the purpose of giving an example of estimation of the nonstationary formulas (38.9) or (38.7), a following provisional assumption will be made. Namely, A_m is assumed constant for simplicity, and to prevent the divergency at $t^*=t_o^*$ of the term $(t^*-t_o^*)^{1-2m}$ in (38.9), it is replaced by $(1+t^*-t_o^*)^{1-2m}$. Further, to determine constant values of C_m, turbulent intensities u_1, u_2, ... due to the vortices of m=1, 2, ... are made

$$\left(\frac{u_1}{U}\right)^2 = A t^{*-1} e^{-t^*},$$

$$\left(\frac{u_2}{U}\right)^2 = \int_0^{t^*} \left\{C\left(\frac{u_1}{U}\right)^2 / e^{-t^*}\right\} (1+t^*-t_o^*)^{-3} e^{-t^*} dt_o^*,$$

$$\left(\frac{u_3}{U}\right)^2 = \int_0^{t^*} \left\{C\left(\frac{u_2}{U}\right)^2 / (t^* e^{-t^*})\right\} (1+t^*-t_o^*)^{-5} t^* e^{-t^*} dt_o^*, \qquad (39.3)$$

where A means a rate of energy supplied from the main flow, and C corresponds to that of $m \geqq 2$ vortices supplied from the preceding generations.

On the other hand, the α =1 vortices are proved to conserve their energy in their expanding regions, and their decaying indicates the linear relation $u^{-2} \backsim t$. Thus, in an imaginary case of the cascade process consisting of the same kind of α =1 vortices, the decaying shall indicate $u^{-2} \backsim t$. By this estimation, the value of C is found to be 1.5, and such a relation of the coefficients in (38.9),

$$\frac{A_{m(t_o^*),t^*}}{A} = 1.5^{m-1} \frac{(t^* - t_o^*)^{2m-1}}{(1+t^*-t_o^*)^{2m-1} t^{*m-1}} , \qquad (39.4)$$

is obtained. Of course, this is a temporary expression until exact conditions of the production of vortex motion in the real state of flow are clarified.

40. DECAYING LAW

In the decaying formula (38.7) of the turbulent intensity due to the cascade process, $(u/U)^2$ is expressed in a function of t* with a constant term A multiplied, if the presumptions (39.1) and (39.4) are introduced. Calculated result of the relation $(u/U)^{-2} A \sim t^*$ is shown in Figure 63. As in the case of the initial-period law, this decaying curve is adaptable to the general decaying turbulence of the wake flow behind a grid or a cylindrical body, for instance.

In Figure 63 the result of an imaginary case of $\alpha(m)=1$ is also given, which indicates a nearly linear relation in about $t^*=0 \sim 1.7$. It is, of course, due to the rough presumption (39.4) of the production condition that the curve does not completely coincide with a straight line. On the other hand, if another imaginary case of $\alpha(m \geqq 2)=\infty$ with $\alpha(1)=1$ is taken, all energy of $m \geqq 2$ vortices are instantly dissipated into heat, and (38.7) indicates the decaying characteristic $(u/\bar{U})^{-2} \backsim t^* e^{t^*}$ of only the m=1 vortices. Decaying curve of the case $\alpha(m)=m$ ought to lie between those mentioned above. Although it is not easy to survey analytical features of the expression (38.7), the decaying seems to become increasingly rapid with an increasing nondimensional time t*, as shown in the figure. Probably this feature should be attributed to the Poisson process in (38.7), rather than the presumption in (39.4); and for the decaying process of the cascade phenomena, it may be inappropriate to assume the simple power expression $u^{-2} \backsim t^n$, which is characteristic of the similarity laws.

It is widely observed in turbulent wake behind a grid that the turbulent intensity u^2 decreases, at first proportionally to x or t, and then more rapidly downstream. In order to check the above-mentioned decaying law, experimental data were chosen in which departures from the linear-decay law are clearly observed. Since it is difficult to evaluate

experimentally the values of an initial constant A and a transition probability p*, it is necessary to compare them with the theoretical curve by multiplying adjustable constants to both sides of the relation $(u/U)^{-2} \sim t$ of the experimental data. The theoretical curve is adaptable also to the case of a shear turbulent flow of two-dimensional wake in a uniform flow. The experimental data behind a circular cylinder in Figure 53 are shown in Figure 63.

Even in the region of the linear-decay law of the isotropic turbulence, the intensity decreases along the flow increasingly proportionate to x^{-1}, and it becomes extremely difficult to carry on a measurement unless far downstream. Nevertheless, according to Figure 63, experimental data attain at most about 1.6 of the nondimensional time t*. Situations of the mixing of vortices in this region of the Poisson process can be seen in Figure 61. Thus, it can be assumed that even with precise experimental observations, only the beginning part of the cascade process can be attained. This may be the basis by which a simple idealization of the Poisson process, although with a rough presumption (39.1) or (39.4), can cover the previously proposed experimental data with fair accuracy.

41. DOUBLE CORRELATIONS IN THE ISOTROPIC TURBULENCE

Correlation function of the u-fluctuations at two points with a distance k_x along the flow is expressed in (38.9). It is first necessary to know the functional forms of $f_{\alpha(m)}$ of the local similarity. In the case of isotropic turbulence, the functional forms of $f_{\alpha(m)}$ are given by the Kármán-Howarth's solution (20.14). Namely, when the relation $\alpha(m) = m$ is taken and t is replaced with t^* and $t^* = t^*_0$, in the case of $m=1$ and $m \geqq 2$, respectively, then the correlation function f_m of m-generation is given by

$$f_m(\xi_m) = (2m-1)^{\frac{5}{4}} \xi_m^{-\frac{5}{2}} \exp\{-\xi_m^2/(4m-2)\} M\{(2m-\tfrac{9}{4}), \tfrac{3}{4}(\xi_m^2/(4m-2))\},$$

$$\xi_1 = \left(\sqrt{\tfrac{5}{4}}\sqrt{\tfrac{r^*}{10}}\,k\right)/\sqrt{\gamma t^*}, \qquad (=\xi),$$

$$\xi_m = \sqrt{\frac{(2m-1)\,t^*}{t^* - t_0^*}}\,\xi, \qquad (m \geqq 2), \tag{41.1}$$

where $M\{(2m-\frac{9}{4}), \frac{3}{4}(\xi_m^2/(4m-2))\}$ represents the hypergeometric function $M_{k,m(z)}$ in (20.14). Substituting the solution (41.1) into the Poisson process (38.9), the expression f can be obtained as a function of ξ and t*.

In the formula (38.9), $f(\xi, t^*)$ always has the characters of

$f(0,t^*)=1$, $f(\xi,t^*)<1$, and $f(\xi,0)=f_1(\xi)$. For the locally similar f_m-function, Figure 29 of the solution indicates the relation $f_m(\sqrt{(2m-1)t^*/(t^*-t_o^*)}\,\xi) < f_1(\xi)$, and in (38.9), $f(\xi,t^*) < f_1(\xi)$ is obtained. Since $df_m/d\xi_m$ tends to the order of 0^1 at $\xi_m \to 0$, $\partial f(0,t^*)/\partial \xi = 0$ is easily proved. As $\partial^2 f_m(0)/\partial \xi_m^2 = -1$ in (41.1), the relations (39.1), (39.4) and (38.9) lead to the expression,

$$\frac{1}{A}\left(\frac{u}{U}\right)\frac{\partial^2 f(0,t^*)}{\partial \xi^2} = \frac{-e^{-t^*}}{t^*}\left\{1+\sum_{m=2}^{\infty}\frac{1.5^{m-1}(2m-1)}{(m-2)!}\int_0^{t^*}\frac{t^*(1-\frac{t^{*\prime}}{t^*})^{m-2}}{t^{*\prime}(1+t^{*\prime})^{2m-1}}\,dt^{*\prime}\right\},$$

$$t^{*\prime} = t^* - t_o^*. \tag{41.2}$$

Since the term $(1-t^{*\prime}/t^*)^{m-2}/(1+t^{*\prime})^{2m-1}$ in (41.2) becomes 1 at $t^{*\prime}=0$, the integration by $dt^{*\prime}$ diverges with the order of log 0. Namely, the function $f(\xi, t^*)$ has the following features:

$$f(0,t^*) = 1,$$

$$f(\xi,0) = f_1(\xi),$$

$$f(\xi,t^*) < f_1(\xi) < 1,$$

$$\frac{\partial f(0,t^*)}{\partial \xi} = 0,$$

$$\frac{\partial^2 f(0,t^*)}{\partial \xi^2} = -\infty. \tag{41.3}$$

In the case of similarity laws, the correlation function of (20.14) can be expanded into a power series at the origin, and the microscale λ_f defined by (18.8) is proved to have some nonzero value. The meaning of this may be comprehended by the physical background of the similarity law of the chaotic motion of one kind of vortex having finite extents. When the cascade phenomena are considered.

$$\lambda_f = 0 \tag{41.4}$$

is arrived at by (41.3). This is understood by the physical interpretation of the cascade process by which $m \geqq 2$ vortices are produced along the flow from zero extent as denoted in (39.4). If the real states of

mechanism are clarified in the production of a vortex motion and, instead of (39.4), precise formulations are made of the growing period of vortices after the production period, the result $\lambda_f \neq 0$ will be obtained instead of (41.4).

The functional form of f can be calculated by (38.9), (39.1), (39.4) and (41.1). The evaluated curves of f versus ξ are shown in Figure 64, according to several parametric values of t*. The correlation of g defined by (18.2) is evaluated in the same manner as the local similar solutions g_m of Kármán-Howarth, as shown in Figure 65. Since the relation of (18.5) to the locally similar f_m and g_m is known, f and g of the cascade process may also be proved to be connected with the same formula (18.5) of the continuity condition.

It is now difficult to survey the character of $\partial f/\partial t^*$ by mathematical analysis. In Figure 64 or 65, however, a rapid convergence near t*=0 is seen in f_1 or g_1 of the initial period to the characteristic form of the cascade process, with a sharp peak at the origin. This tendency was anticipated by the characteristic $\partial^2 f(0,t^*)/\partial \xi^2 = -\infty$ of (41.3). In the decaying law of the cascade process, Figure 63 suggests a gradual departure from the linear-decay law of the initial period. The correlation function f or g of the cascade process has a contrasting characteristic in this point. Locally similar f_m or g_m cannot be evaluated now in general cases of decaying turbulence. However, if an extended Kármán-Howarth's solution is obtained in other cases than in isotropic turbulence, the above-mentioned characteristic of the rapid convergence to the form of the cascade process may be proved.

In uniform turbulent flows behind a grid, measurements are made of the g-correlation for the sake of experimental convenience, for the most part. For experimental comparison, three curves of g at t*=0.4, 1.0, and 1.6 in Figure 65 are drawn versus k_y/L_g in Figure 66, where L_g is the integral scale similar to that defined by (18.7). Since it is difficult, on the other hand, to evaluate an exact value of L_g by experimental measurements, experimental data are plotted in Figure 66 with a suitable constant multiplied to the abscissa value. In this figure, observed results of the characteristic sharp peaks of the correlation functions are almost covered by the theoretical curves of the cascade process. However, because of a rapid convergence to the cascade form shown in Figure 65, variations in relative forms of the theoretical curves are small, and it is difficult to check the time-dependent characteristics of the g curves by experimental results in Figure 66. In some cases of the data, the decayings of $(u/U)^2$ are shown in Figure 63 at the same time. Referring to Figures 63 and 66, we know that the decaying of intensity and the form of correlation of the isotropic turbulent flow are generally supported by the theoretical curves in the region t*=0~1.6 of the Poisson process.

In uniform turbulent flows behind a grid, the g correlation is observed to take usually a negative value at a large distance from the

origin; however, all the curves in Figure 65 indicate positive value. As a matter of course, in the real vortex chaos motion, effects of a single vortex motion are retained in a finite region from the center. In reference to the initial-period similarity-law, this discrepancy at a large distance is caused by the approximative description of the ideal state as mentioned in Section 21, in which the value of $\overline{uu'}$ or $\overline{vv'}$ is expressed with a connection of a single kind of the $\alpha = 1$ vortices up to an infinite distance from the center. Figure 66 proves that even by the Poisson process which evaluates the production of new small vortices, the discrepancy at a large distance has not been improved.

42 TRIPLE CORRELATION IN THE ISOTROPIC TURBULENCE

In the case of isotropic turbulence, it is the Kármán-Howarth's propagation formula (18.9) that interrelates the correlation functions at two points. As mentioned previously, this is a mathematical transformation from the Reynolds equations containing three independent variables of f, h, and u. According to the similarity laws, the triple correlation h is proved to vanish. It is also known that the triple correlation h is derived from the inertia terms in the Navier-Stokes equations. Thus, in the case of cascade process in which u and f, respectively, have nonsimilarity characteristics as mentioned in the previous sections, h may be proved also to have a finite nonzero value.

When u and f, evaluated by the Poisson process, are substituted into the propagation formula (18.9), it can be regarded as a differential equation for $h(\xi, t^*)$. Namely, with the continuity equation utilized, (18.9) is transformed into

$$\frac{-\partial\left(\left(\frac{u}{U}\right)^2 f\right)}{\partial t^*} + \frac{\left(\frac{u}{U}\right)^2}{4\xi t^*}\frac{\partial(f+2g)}{\partial \xi} = \frac{1}{\sqrt{2}}\left(\frac{u}{U}\right)^3 \frac{1}{\sqrt{t^*}}\left(\frac{dh'}{d\xi} + \frac{4}{\xi}h'\right),$$

$$h = \frac{\sqrt{\rho^* \nu}}{U} h'(\xi, t^*). \tag{42.1}$$

Since f, g, and u/U are given as functions of ξ and t*, (42.1) can be regarded as an ordinary linear differential equation of the first order for h' with a parametric value of t*. The solution, under the boundary condition h=0 at $\xi = 0$, is easily derived as

$$h(\xi, t^*) = \sqrt{\frac{2}{A}}\frac{\sqrt{\rho^* \nu}}{U}\frac{\int_0^{\xi} H(\xi, t^*)\xi^4 d\xi}{\xi^4},$$

$$H(\xi,t^*)=\left\{-It^*\frac{\partial\left(\frac{f}{I}\right)}{\partial t^*}+\frac{1}{4\xi}\frac{\partial(f+2g)}{\partial\xi}\right\}\Big/\sqrt{\frac{I}{t^*}}\ ,\quad I=A\left(\frac{u}{\bar{U}}\right)^{-2}$$

(42.2)

By (42.2), the proportional relation

$$h \propto \sqrt{p^*}$$

(42.3)

is seen. An important result is that the Poisson process in the physical picture of cascade phenomena has given a quantitative interpretation to the character of nonlinear terms in the Navier-Stokes equations.

Seen from the curve of $(u/\bar{U})^{-2}$ in Figure 63, the value of λ in the decaying formula (18.10) seems to have no singularity characteristic. Probably the singularity of f''(0) may have been cancelled by that of h'(0) in the expression of λ^{-2} in (18.10). Anyhow, it must not be overlooked that the definition of λ by (18.8) holds only when the correlation functions have no singularity at $k_r=0$.

Introducing the calculated results of f, g, and $(u/\bar{U})^{-2}$ into (42.2), the functional form of h can be obtained. Near the origin $\xi=0$, reliable results of computation cannot be expected because of the above-mentioned singularity characteristic of h. General characteristics of the evaluated results of h can be seen in Figure 67, although the derivation may have insufficient accuracy because of the numerical differentiation of f or g in (42.2). The nonzero value of the curve of h at $t^*=0$ means that even at the beginning time of $t^*=0$, the vortex chaos motion is not identical with the state of the initial period, although the cascade process has begun at this instant. Then, the curve of h increases gradually with $t^*>0$, whose tendency is similar to the decaying curve which gradually deviates from the linear-decay law, unlike the case of the double correlations.

Generally, it is not easy to make a measurement of the triple correlation by means of a hot-wire anemometer, and there are not many experimental data, even in the simple flow of isotropic turbulence. Further, it is difficult to check the variation of h versus t^* by determining the value of t^* experimentally. Due to an example of measurement shown in Figure 68, it is ascertained that the functional form of h increases gradually along the flow. Fortunately, the previous measurements were made on both h and f at the same time. In the same manner as in Figure 66, experimental results of f are compared with the calculated curves at $t^*=0.4$, 1.0 and 1.6, and using the same abscissa, comparisons of h are made. Figure 69 shows the results. For the double correlation f, there is good agreement, as in the case of g. For the triple correlation h,

some shift is found in the theoretical and experimental results, although their relative forms are almost the same. As seen by (42.2), h corresponds to the differentiated expression of f or g, and small disagreements in f may have been magnified in the triple correlation h. At any rate, their disagreements are caused by analysis of the simplest idealization of the Poisson process of the cascade phenomena, with an indefinite initial condition of a vortex motion.

43. LOCALLY ISOTROPIC TURBULENCE

In the case of isotropic turbulence, there is an interrelation formula, (19.5) or (19.9), between the correlation and the spectrum functions, depending upon Taylor's hypothesis. By this transformation, nonstationary characteristics of f or h derived by the Poisson process shall be presented in the one- or three-dimensional spectrum function. If a complete analysis can be obtained of either the correlation or the spectrum function, discussion of the other function is unnecessary. As mentioned in the computed results of f or h in the previous sections, accuracy is not sufficient, especially in the region far from the origin $\xi = 0$. When these nonsimilar correlation functions are transformed into the spectrum functions by means of (19.5) or (19.9), this local inaccuracy gives unfavorable effects to the spectrum function in the whole region of the wave number. Thus, for the spectrum function at present, study of another aspect based on somewhat phenomenological analyses may be necessary.

From the physical picture of the cascade phenomena in the decaying turbulence, large-scale vortices, beginning from the primary vortices of $\alpha = 1$, incessantly produce the following small-scale vortices along the flow. Viewed from the standpoint of spectrum analysis, it can be assumed that the region of low-frequency wave numbers produces high-frequency regions. As seen from the initial-period similarity-law of isotropic turbulence, an irregular vortex chaos motion produces a continuous spectrum function from high to low wave numbers, even if they consist of one kind of vortex. However, as seen by (19.4), the spectrum function of a chaotic motion of large-scale vortices occupies chiefly a low-frequency region rather than the small-scale vortices. Therefore, the physical picture of the cascade phenomena of a vortex chaos motion leads to, at least qualitatively, the interpretation of the cascade process in wave numbers of spectrum. On the other hand, it is not difficult to separate experimentally velocity fluctuations into the components of frequency, and it becomes easy to check theoretical results of the spectrum analyses by direct measurements.

Now, let us consider the difference of the shear and shearless turbulence in the decaying turbulence. When the scales of vortices are far smaller than the breadth of turbulent flow, according to the interpretation of a vortex chaos motion, mutual disturbances of vortices lose a directional effect, and their chaotic motion attains a completely

irregular state. On the other hand, when the scales of vortices are compared with the breadth of flow, directional effects remain in their disturbances, and the chaotic motion does not attain a completely irregular state. The scale and energy of vortices produced on the cascade phenomena are far smaller and weaker than the previous vortices. Also these small vortices are easily disturbed by other vortices, and they come easily into the completely irregular state. Even if the large-scale vortices $\alpha = 1$ of the initial period are in an incompletely irregular state, newly produced vortices easily tend to have the condition of complete irregularity. In a small area near the production place of small vortices, effects of the mean pressure gradient or of mean velocity profile of the field of flow are small. However, small vortices are produced everywhere along the flow. Thus, small vortices produced by the cascade process have a tendency to attain the state of isotropic turbulence, regardless of their position in the field of flow.

From spectrum analysis, the high-frequency region of the velocity fluctuation tends to be in the isotropic state even if the lower-frequency region is in a shear-turbulence state, as shown by experimental evidence in Figure 70. Of course, this fact holds when the primary vortices have the condition of the isotropic turbulence. Thus, it is significant to generally assume the isotropy to the high-frequency fluctuations, regardless of the states of the low frequencies which have almost all the fluctuational energy. This assumption is the conception of the locally isotropic turbulence proposed by Kolmogoroff (reference 16).

44. KOLMOGOROFF'S THEORY

According to the conception of the locally isotropic turbulence, Kolmogoroff proposed the following basic assumptions and proceeded with mathematical formulations (references 16, 62, and 63). Namely, velocity fluctuations, which have far smaller scale length than the integration scale L_f of (18.8) or which have far shorter frequency than the time interval L_f/u, are all fulfilled with the conditions of isotropic turbulence and of a statistical equilibrium. A large-scale region of the components of velocity fluctuation having a comparative value of L_f or L_f/u need not be assumed.

Only the part of velocity fluctuations of the local isotropy shall be considered. At first, the following tensor expression B of the correlations of the differences of velocity-fluctuation components is taken at two points of A and A' with a short distance k_r:

$$B = \begin{pmatrix} \overline{(u-u')(u-u')} & \overline{(u-u')(v-v')} & \overline{(u-u')(w-w')} \\ \overline{(v-v')(u-u')} & \overline{(v-v')(v-v')} & \overline{(v-v')(w-w')} \\ \overline{(w-w')(u-u')} & \overline{(w-w')(v-v')} & \overline{(w-w')(w-w')} \end{pmatrix}. \quad (44.1)$$

When B_{dd} and B_{nn} are taken as the correlations of differences of velocity-fluctuation components, parallel and perpendicular to the AA'-direction, respectively, the relation

$$B = \frac{B_{dd}-B_{nn}}{k_r^2} \begin{pmatrix} k_x k_x & k_x k_y & k_x k_z \\ k_y k_x & k_y k_y & k_y k_z \\ k_z k_x & k_z k_y & k_z k_z \end{pmatrix} + B_{nn} \begin{pmatrix} 1 & 0 & 0 \\ 0 & 1 & 0 \\ 0 & 0 & 1 \end{pmatrix} \quad (44.2)$$

can be obtained in the same manner as the formula (18.4), and the continuity equation leads to

$$B_{nn} = B_{dd} + \frac{1}{2} k_r \frac{dB_{dd}}{dk_r}, \quad (44.3)$$

as in (18.5). When f, g, h, and others are taken as the double and triple correlations as shown in Figure 25, the following formulas owing to the local isotropy can be easily obtained:

$$\begin{aligned} B_{dd} &= 2u^2(1-f), \\ B_{nn} &= 2u^2(1-g), \\ B_{ddd} &= -12u^3 h, \\ &\cdots \end{aligned} \quad (44.4)$$

The Kármán-Howarth's propagation formula (18.9), which holds in the locally isotropic turbulence, can be transformed into

$$\frac{du^2}{dt} = \left(\frac{d}{dk_r} + \frac{4}{k_r}\right)\left(\frac{1}{6}B_{ddd} - \nu \frac{dB_{dd}}{dk_r}\right), \quad (44.5)$$

with substitution of (44.4). Due to the basic assumption of stationary state, B_{dd} or B_{ddd} becomes a function of only k_r and (44.5) takes the expression of an ordinary differential equation with an independent

variable k_r. With the boundary condition of $B_{ddd} = 0$ at $k_r=0$, (44.5) can be integrated into

$$\frac{1}{6} B_{ddd} = \nu \frac{dB_{dd}}{dk_r} + \frac{1}{5} \frac{du^2}{dt} k_r . \tag{44.6}$$

The above-mentioned equations reflect the kinematical characteristics of the locally isotropic turbulence.

From the previously mentioned supposition of the cascade phenomena of a vortex chaos motion with the relation $\alpha(m)=m$ of (39.1), one may arrive at an interpretation that the fluctuating energies are incessantly transferred from low-frequency region to high-frequency region, with some of them being dissipated into heat. Now, when the transferred fluctuating energy from the lower-frequency region is denoted by ε per unit mass of fluid and in a unit time interval, then ε is taken in the phenomenological study as a principal quantity characterizing the cascade process of the wave numbers, just as was the transition probability p* in the physical picture of the cascade process of a vortex chaos motion. On the other hand, the kinematic viscosity ν represents the dissipation of energy by molecular viscosity, which in the previous physical picture corresponds to the suffix α (=m) of the kind of vortex motion. Thus, in general, situations of the cascade process may be decided by the two basic quantities of ε and ν, which is the first hypothesis of the theory of locally isotropic turbulence proposed by Kolmogoroff. Namely, this hypothesis is transformed from the previously mentioned interpretation of the cascade phenomena of vortex chaos motion into the simplest quantitative expression in the cascade process of the wave number.

When l_k and v_k are taken, respectively, as a representative length and velocity expressed in the two quantities of ε and ν, they are expressed as:

$$l_k = \frac{\nu^{\frac{3}{4}}}{\varepsilon^{\frac{1}{4}}} ,$$

$$v_k = (\nu\varepsilon)^{\frac{1}{4}} . \tag{44.7}$$

Since B_{dd} or B_{ddd} is a function of k_r only, the expressions

$$B_{dd} = (\nu\varepsilon)^{\frac{1}{2}} \beta_{dd}\left(\frac{k_r}{l_k}\right) ,$$

$$B_{ddd} = (\nu\varepsilon)^{\frac{3}{4}} \beta_{ddd}\left(\frac{k_r}{l_k}\right) , \tag{44.8}$$

are obtained by easy dimensional analyses. In (44.8), β_{dd} or β_{ddd} is a definite nondimensional function of a nondimensional length k_r/l_k.

α = m of (39.1) is proposed as a basic assumption to derive quantitative results from the interpretation of the cascade phenomena of vortex chaos motion. Due to this assumption, dissipation of energy by molecular viscosity becomes more intensive as the generation m of the vortex motion increases, while the largest-scale vortices of m=1 have no effect of dissipation. Namely, in comparatively large vortices of young generations the effects of viscosity are small. Thus, from the standpoint of the cascade process of the wave numbers, statistical characters at A- and A'-points depend chiefly upon ε rather than ν when the distance k_r is larger than l_k. In an approximative meaning, the statistical characters in these circumstances may be assumed to be decided by ε only, reflecting Kolmogoroff's second hypothesis of the locally isotropic turbulence.

According to Kolmogoroff's second hypothesis, B_{dd} or B_{ddd} in (44.8) must not contain the term ν. If n is made 2/3 in the expression of $B_{dd}=(\nu\varepsilon)^{\frac{1}{2}}(k_r/l_k)^n$, the exponent of $(\nu\varepsilon)$ vanishes in (44.7). Thus, with a constant coefficient C_{dd} or C_{ddd}, the following expressions are obtained:

$$B_{dd} = C_{dd}(\varepsilon k_r)^{\frac{2}{3}},$$

$$B_{ddd} = C_{ddd}(\varepsilon k_r).$$

(44.9)

From (44.9) and (44.4), the expression $f=1-\frac{C}{2U^2}(\varepsilon\nu)^{\frac{2}{3}}$ is derived. Figure 71 indicates that in the solution of f in Figure 64, the region approximated by (44.9) is increased as small vortices are produced by the cascade phenomena.

45. SPECTRUM FUNCTION IN THE ISOTROPIC TURBULENCE

Characters of the locally isotropic turbulence discussed in the last section in the form of spectrum functions shall be expressed according to the analyses of Heisenberg (references 64 and 65). The propagation formula (19.12') is expressed as

$$-\frac{\partial}{\partial t}\int_0^k E\,dk = T(k) + 2\nu\int_0^k Ek^2\,dk,$$

$$T(k) = \int_0^k W(k)\,dk,$$

(45.1)

if every term is integrated by k. As mentioned in Section 19, the terms E and W are derived from the viscous and inertia terms, respectively, in the Navier-Stokes equations. Thus, by the supposition of the cascade process of wave numbers, the first term of (45.1) is regarded as the energy which is transferred from the region of frequencies lower than k to that of the higher frequencies, and the second term is regarded as the energy being dissipated into heat by the effect of viscosity in the region of frequencies higher than k.

In order to derive quantitative results from the interpretation of the cascade process of wave numbers, the energy transfer from lower to higher frequencies implied in the first term shall be compared to a dissipation phenomenon by a virtual viscosity. When the energy transfer is denoted by

$$T(k) = 2\nu_H(k) \int_0^k E(k) k^2 dk, \tag{45.2}$$

as in the second term of (45.1), $\nu_H(k)$ is similar to one kind of kinematic viscosity varying with k. Then the problem becomes one of determining the functional form of $\nu_H(k)$. Since $\nu_H(k)$ concerns the whole region of frequencies higher than k, it is appropriate to assume the integration formula $\int_k^\infty f'(k')\,dk'$ to $\nu_H(k)$. When f' is assumed to be a function of E(k) and k, such an expression can be derived by dimensional analyses,

$$\nu_H(k) = c \int_k^\infty \sqrt{E(k)/k^3}\, dk, \tag{45.3}$$

with a numerical constant c, because ν_H, f', E, and k have their dimensions respectively of $cm^2\ sec^{-1}$, $cm^3\ sec^{-1}$, $cm^3\ sec^{-2}$, and cm^{-1}.

When the region of large values of k is taken, the left-side term of (45.1) expressing a decrease of total energy can be interpreted as the rate of transferring energy ε. Thus, irrespective of k, (45.1) must be a constant, and the expression

$$E(k) = \left(\frac{\varepsilon c}{2\nu k}\right)^2 k^{-7} \tag{45.4}$$

is derived from (45.1), (45.2), and (45.3). When the viscous term is neglected in a region of smaller values of k, the form

$$E(k) = \left(\frac{8\varepsilon}{9c}\right)^{\frac{2}{3}} k^{-\frac{5}{3}} \tag{45.5}$$

is obtained. These formulas of (45.4) and (45.5) are expected to hold in the region of wave numbers of higher frequencies.

In the region of low frequencies, other considerations are necessary. Owing to the interpretation of the cascade phenomena of vortex chaos motion, the vortices of $\alpha = 1$ are predominant in the region of low frequencies. In the cascade process of wave numbers, one must give considerable thought to the energy of velocity fluctuations, rather than to the energy transfer $\mathcal{E}$ or the dissipation γ. Heisenberg proposed some evaluations according to such an interpretation. Taking D_H as a momentum presented by a standard length and velocity, he combined D_H, t, and k into a nondimensional quantity $k\sqrt{D_H t}$. Then, the nondimensional expressions of the two terms $t^{\frac{1}{2}} D_H^{-3/2} E(k)$ and $t^2 D_H^{-1} T(k)$ in (45.1) must be functions of only $k\sqrt{D_H t}$, and (45.1) takes the form of an ordinary differential equation with a parameter D_H/γ. The first term of the expansion of the solution becomes

$$E(k) \backsim D_H^2 k. \tag{45.6}$$

Namely, in a region of low frequencies of isotropic turbulence, the character of (45.6) is related to the spectrum function.

The above-mentioned results (45.4), (45.5), and (45.6) concern local characteristics of the spectrum function of the isotropic or the locally isotropic turbulence. The regions where these formulas are adapted are called the viscous (C), inertial (B), and the lowest-frequency subranges (A), respectively, according to the meanings of their derivations. Figure 72 shows a conceptional diagram of the regions. Figure 73 shows observed results of the one-dimensional spectrum $F_1(k_1)$, in which the formulas of (45.4) and (45.5) are used; and local states of the real spectrum function are seen to be represented by these formulas. However, due to the phenomenological studies of the cascade process of wave-numbers, determination of the spectrum function cannot be derived in the whole region of the wave numbers. To derive a correct spectrum or correlation function in the isotropic or the locally isotropic turbulence, more precise mathematical formulations must be given to the physical considerations of the cascade phenomena of vortex chaos motion.

An introduction of the Poisson process in this chapter is made in order to survey the cascade phenomena, particularly near the region of breakdown of the initial-period law. Expressions (45.4) and (45.5) of the results of phenomenological studies of the locally isotropic turbulence can also be adapted in this region. The beginning of the cascade process from the initial period is regarded to be particularly important, because in the real state of decaying turbulent flows, turbulent energy decreases rapidly far downstream, and it becomes difficult to make an experimental measurement there. From only an ideal viewpoint, however, discussions are possible on the ultimate stage of the decaying turbulence far downstream.

In the vortex chaos motion of large values of the generation $m = \infty$, the effect of viscosity becomes intensive, and the inertia force is neglected in the ultimate stage of the cascade process. When the inertia term in the propagation formulas (18.9) or (19.12') is neglected, definite analyses become possible. Namely, (19.12') without W is integrated into

$$E(k,t) = E(k,t') \exp\{-2\nu k^2 (t-t')\}, \tag{45.7}$$

which is further simplified into

$$E(k,t) = \frac{J}{3\pi} k^4 \exp\{-2\nu k^2 (t-t')\},$$

$$J = u^2 \int_0^\infty f k_r^4 \, dk_r, \tag{45.8}$$

taking only the first term of the expansion of E(k, t'). The total intensity $u^2 = \frac{2}{3}\int_0^\infty E dk$ becomes

$$u^2 = \frac{J}{4\nu\sqrt{2\pi}} \{\nu(t-t')\}^{-\frac{5}{2}}. \tag{45.9}$$

If the fourth moment of the correlation J is assumed to be independent of t, (45.9) expresses a simple formula of the decay of turbulent intensity, the analyses proposed by Batchelor in the final period of decay (reference 55).

CHAPTER EIGHT. SIMILARITY CONCEPTION IN THE NONDECAYING TURBULENCE

46. CHARACTER OF NONLOCAL EXPRESSION

The following interpretations are related in Sections 7 and 8 for the structure of the nondecaying turbulent flow along a wall. In the immediate vicinity of a wall, the effect of molecular viscosity is conspicuous, and a thin layer of the viscous sublayer exists with the critical Reynolds number of the lower limit of stability. Outside the sublayer, the stability condition is broken and strong vortices are incessantly produced along the wall. These primary vortices may bring about descending, small, weak vortices by the cascade process, and it becomes necessary to imagine an extraordinarily complicated chaotic motion of all these vortices, unlike the case of decaying turbulence.

To give mathematical expressions to turbulent intensity and scale based upon this physical picture, the descending vortices are first neglected because of their small effects as compared to the strong primary vortices that are produced continuously along the wall above the viscous sublayer. Namely, in the analysis of nondecaying turbulence, the expression of the ideal state shall be taken. Thus, the problem is the extension of the initial-period law of the decaying turbulence into the case of nondecaying turbulence.

When an A-point is fixed in a nondecaying turbulent flow, many kinds of strong vortices produced everywhere upstream run away near the A-point, even if only the primary vortices are taken into account. Thus, for the intensity of turbulence, an ideal-state expression of (13.9),

$$u^2 = \sum_{i=1}^{N} \iiint_{D_i^*} P_i^*(r,\theta,\phi)\,\bar{V}_i^{*2}(r,\theta,\phi)\cos^2\theta\sin^2\phi\,dQ_i^*, \qquad (46.1)$$

is deduced by taking the function of P_i^* of (13.6). Suffix i denotes the position of production, and the operation $\sum_{i=1}^{N}$ is made upstream from the A-point.

It is too difficult to derive the functional forms of P_i^* and $\bar{V}_i^*$ in the D_i^*-domain by making strict analyses of the hydrodynamical equations of motion. As mentioned in Section 8, however, at least some strong vortices may be in an incompletely irregular state with large scales comparative with the breadth of the flow. In (46.1), it is difficult to assume that $\rho\overline{uv}$ vanishes, even if there are many small vortices in the completely irregular state. Namely, in the case of a nondecaying turbulence, description of the ideal states of the primary vortices can be compared to that of the cascade process of decaying turbulence.

When the x-axis is taken parallel to the flow on the wall of zx-plane and the thickness of viscous sublayer is neglected, suffix i is designated

by the x-ordinate. If the coordinates of the A-point are x, y, z and the nondimensional ordinate of x is ξ, then the position of production discriminated by i should be expressed in a differential value $\xi' d\xi'$. If the position of the beginning of turbulence is denoted by ξ_0, $\xi_0 \leqq \xi' \leqq \xi$ is obtained, and $\sum_{i=1}^{N}$ in (46.1) shall be replaced by the integration $\int_{\xi_0}^{\xi} d\xi'$.

It is difficult to derive the different kinds of vortex motions produced from the wall by the effect of a viscous sublayer, from the primary vortices of $\alpha = 1$ in the case of the decaying turbulence, because the decaying turbulence is the case where the vortices produced by the separation of boundary layer are carried apart from the body, and the nondecaying turbulence is the case where these vortices are still carried along the wall of a body. In the expression of the ideal state of (46.1), each V*-function is written with a decaying term separated as in (22.2) of the initial-period law of the decaying turbulence. Thus, (46.1) becomes

$$u^2 = \int_{\xi_0}^{\xi} \left\{ \iiint_{D^*_{\xi'}} P^*_{\xi'}(r,\theta,\phi) F^2_{\xi'}(r,\theta,\phi) G^2(t_{\xi'}) \cos^2\theta \sin^2\phi \, dQ^* \right\} d\xi',$$

$$G(t_{\xi'}) = 2C\sqrt{\nu}\, t_{\xi'}^{-\frac{1}{2}}, \qquad (46.2)$$

where $t_{\xi'}$ is a time interval in which the vortices produced at a location of ξ' come to the A-point.

Expression (46.2) is an extended expression of the initial-period law. However, selection of the initial constant C according to a position ξ' is a difficult problem, even if the kind of vortex is designated by $\alpha = 1$. Unlike the cascade phenomena in the decaying turbulence, it may be inappropriate to assume that the vortices at $\xi', \xi'+d\xi'$ are produced by taking a part of the energy of the preceding ones at $\xi'-d\xi', \xi'$. They must be produced independently along the flow and have their values of C of the same order. It is also difficult to elect only one kind of conspicuous vortex in (46.2) as the primary vortices in the cascade process. The effect of the integration $\int_{\xi_0}^{\xi} d\xi'$ is generally caused by many kinds of vortices produced in a fairly wide region upstream, and the effect of vortices produced far upstream may be decreased with the decaying term $G(t_{\xi'})$.

In the decaying turbulence, statistical character at an A-point in the field is dependent on the initial condition of the primary vortices and on the position of the A-point. In the nondecaying turbulence, even if an approximative description of the ideal state is taken, turbulent intensity at an A-point is not decided alone by the local value x, y, z of this point, but is also dependent upon the integral effect upstream. This nonlocal description is a principally important character of the nondecaying turbulence and means also that along the wall, turbulent flow comes to

forget its history. This characteristic should be extended to the mean-velocity profile through the Reynolds equations. Because of this nonlocal character, previous empirical attempts were not necessarily successful in characterizing the mean-velocity profile of turbulent boundary layer in an arbitrary pressure gradient by means of a local value at the section alone.

In the expression (46.2), every decaying term $G^2(t\,\xi')$ is proportional principally to $(\xi - \xi')^{-1}$ and is excluded from the integration $\iiint_{D^*\xi'} dQ^*_{\xi'}$ as in the case of the initial-period law. These terms are further integrated by $\int_{\xi_0}^{\xi} \alpha\, \xi'$ into a function depending upon the initial values of ξ_0 and ξ of the A-point. Of course, the distribution of turbulent intensity along the x-direction is not decided without an exact evaluation of (46.2). However, if ξ is taken far apart from ξ_0, vortices produced near ξ_0 have little effect at ξ owing to their rapidly decaying feature of the terms G^2. Therefore, although ξ is taken more remotely from ξ_0, the integrated value of $\int_{\xi_0}^{\xi} \alpha\xi'$ does not decrease rapidly, but preserves nearly a constant value. Experimental data shown in Figures 6 and 15 may speak of the above-mentioned interpretation.

47. SIMILARITY CHARACTER OF THE CORRELATION TENSOR

In the formula (46.2), functional forms of $P^*_{\xi'}$ and $F_{\xi'}$ in the $D^*_{\xi'}$-domain depend generally on the situations of flow upstream near the location of the A-point. As the upstream effects, one can take thickness of the laminar boundary layer from the stagnation point, location of the transition to turbulent flow, pressure distribution by the free-stream, roughness or curvature of the wall and others.

From the standpoint of the study of a fully-developed turbulence, it is sufficient to treat only the region far downstream from the transition. In the formulas of turbulent intensity such as (46.2), effects far upstream are decreased rapidly by the decaying term G, and the integration $\int_{\xi_0}^{\xi} \alpha\xi'$ is replaced approximately by $\int_{-\infty}^{\xi} \alpha\, \xi'$. For the turbulent scale, a vortex motion, generally, extends proportionally to $t^{\frac{1}{2}}$, namely, to $(\xi - \xi')^{\frac{1}{2}}$. Owing to the rapidly decaying intensity, however, the scale of vortices produced far upstream may lose their meaning in the chaotic motion of strong vortices of the nondecaying turbulent flow.

In the two-dimensional turbulent wake in a uniform flow of the decaying turbulence, the process by which the initial-period law is reduced into the formula of similarity preservation was interpreted. In the nondecaying turbulence, the character of similarity preservation along the flow shall be considered by taking a simple case of the turbulent boundary layer along a flat plate. In this case, the pressure distribution of the free-stream has no effect on the vortex chaos motion in the boundary layer, unlike the case of a turbulent wake in a uniform flow. A vertical section to the flow is taken at a fixed point x on the plate. In turbulent boundary layer, production of strong primary vortices is limited to the surface of the

plate, and the complicated vortex chaos motion passing through this section is confined in a finite region near the plate. Referring to this region, a scale length of the boundary-layer thickness is determined, usually denoted by

$$\delta(x) \tag{47.1}$$

as a function of x.

When the effects far upstream are neglected in (46.2), turbulent intensity at an A-point of the co-ordinates x, y is approximated by the expression,

$$u^2(x,y) = \int_{-\infty}^{\xi} I_{x,y}(\xi')\,d\xi',$$

$$I_{x,y}(\xi') = \left\{\iiint_{D^*_{\xi'}} P^*_{\xi'}(r,\theta,\phi)F^2_{\xi'}(r,\theta,\phi)\cos^2\theta\sin^2\phi\,dQ^*\right\}G^2(t_{\xi'}). \tag{47.2}$$

In (47.2), it is difficult to determine the functional form of $P^*_{\xi'}F^2_{\xi'}$ in the $D^*_{\xi'}$-domain. As shown in Figure 74, however, the function I tends to zero upstream owing to the decaying term G^2, and the integration of (47.2) shall be taken as an idealized expression, neglecting the effects far upstream.

Even at a given section of x, functional form of $I(\xi')$ depends upon the value of y. But, in a flat-plate boundary layer flow, pressure gradients of the free-stream and others have no effect on the function $I(\xi')$ in (47.2) upstream from the x-section. Thus, states of vortex chaos motions are determined only by the interaction of vortices outside the sublayer upstream. Further, in a fully developed turbulent boundary layer along a flat plate, the production condition of the primary vortices outside the sublayer cannot be assumed to vary along the flow. Therefore, even if another section is taken at x_1, it is difficult to find a different character in the two chaotic motions of vortices produced before the two points. For the scale of turbulence, vortices produced far upstream with vanishing intensities have little effect on the boundary-layer thickness δ. Thus, in a fully turbulent state, δ may also be dependent chiefly on the vortices produced in a finite region upstream from x.

In the x_1-section, such an A_1-point is taken that has the relation

$$\frac{y}{\delta} = \frac{y_1}{\delta_1} = \eta ,$$

(47.3)

where δ_1 is the thickness of the layer at x_1-point. Then, at the two points, functional forms of I become identical through the above-mentioned discussions. Thus, by (47.2), the following expressions can be obtained for the components of turbulent intensity:

$$\overline{u^2}(x,y) = \overline{u^2}(x_1,y_1) = C_{\overline{u^2}}(\eta)\, v_o^2 ,$$

$$\overline{v^2}(x,y) = \overline{v^2}(x_1,y_1) = C_{\overline{v^2}}(\eta)\, v_o^2 ,$$

$$\overline{w^2}(x,y) = \overline{w^2}(x_1,y_1) = C_{\overline{w^2}}(\eta)\, v_o^2 ,$$

$$\overline{vw}(x,y) = \overline{vw}(x_1,y_1) = C_{\overline{vw}}(\eta)\, v_o^2 ,$$

$$\overline{wu}(x,y) = \overline{wu}(x_1,y_1) = C_{\overline{wu}}(\eta)\, v_o^2 ,$$

$$\overline{uv}(x,y) = \overline{uv}(x_1,y_1) = C_{\overline{uv}}(\eta)\, v_o^2 ,$$

$$\frac{y}{\delta} = \frac{y_1}{\delta_1} = \eta .$$

(47.4)

In the above expressions, v_o^2 derived from F^2 is a representative fluctuating velocity decided by the velocity of the free-stream.

The intensity formula (47.4) corresponds to the initial-period similarity-law in a uniform decaying shear turbulence in which the primary vortices preserve the similarity with the decaying term. There is no need to assume local similarity along the flow for the vortices produced at a point ξ' in (47.4). Even in the simple case of a flat-plate boundary layer, it is difficult to assume a similarity character of disturbance by which vortices produced at ξ' are affected by the surrounding vortices along the flow, and probably the functional form of $P_{\xi'}^{*}F_{\xi'}^{2}$ in the $D_{\xi'}^{*}$-domain varies along the flow. It is characteristic that the similarity preservation in (47.4) has been obtained only by the distribution of I along the flow. This similarity is in contrast to that of the cascade process of the decaying turbulence, in which local similarities of all kinds of vortices are combined into a nonsimilarity character through the Poisson process. Figure 75 is an example of measurements of the profiles of u-intensity along a flat plate far downstream from the transition.

48. TURBULENT FLOW OF A SIMILARITY PRESERVATION

In addition to the flat-plate boundary layer flow, the case will be considered in which the expression (46.2) is reduced to a similarity formula, using a fully-developed pipe flow with a constant cross section. As is well known, the flow has no undisturbed free-stream, and has a constant pressure gradient along the flow, retaining an energy balance with the surface friction. The situations of flow upstream from two sections of x and x_1 are assumed to be the same as in the case of a flat-plate boundary layer when the effects near the inlet of pipe are neglected. Namely, it is difficult to imagine a different character along the flow in the vortices produced outside the sublayer, which probably leads to the conclusion of nondecaying similarity as expressed in (47.4).

It is too difficult to see the interrelation between the initial constant C of the primary vortices produced by the effect of viscous sublayer and the condition of the mean states of flow. However, because of the nature of viscous vortex motions, the constant value may depend principally on the Reynolds number of the mean flow. Figure 76 shows a similarity character of two cases of pipe flow having the same value of the Reynolds numbers.

As mentioned in the last section, similarity preservation in the case of a flat plate comes from an invariance of situations of vortex chaos motions before two arbitrary points along the flow. In the general case of a fully developed turbulent boundary layer along a smooth wall, the pressure gradient of the free-stream has an important effect on the vortex chaos motion in the layer. Thus, if the pressure gradient gives relatively the same effects upstream before two points of x and x_1, vortex chaos motions passing through these sections take on characteristics of the situation. Therefore, the turbulent intensities have relatively the same profile, with local values of the intensity $v_o(x)$.

It is difficult to ascertain the exact mathematical expression by which pressure force of the free-stream affects the vortex chaos motion in the layer. It is certain, however, that the effect is caused by the pressure force dP_o/dx itself, and as the first approximation it may be natural to specify the value of dP_o/dx. According to this supposition, a turbulent boundary layer with a constant dP_o/dx like the uniform pipe flow was made, and similarity character in the profiles of u-intensity along the flow (reference 68) was checked. Figures 77, 78, and 79 show the results. Although they cannot be taken as strict evidence of the similarity in this case of flow, these results may prove that the profiles of turbulent intensity are determined by the integral effects upstream, at least for the nonlocal character of the flow.

49. PROPORTIONAL CHARACTER IN TURBULENT INTENSITY

Discussions in the previous sections concern the distribution of

turbulent intensity along the flow. Now, under the idealization of an extended formula (46.2) of the initial-period law, characters of turbulence across the flow will be surveyed. In Section 25, it is interpreted through the initial-period law that every value of the components of turbulent intensity has a tendency to become equal to each other independently of their position. The discussion shall be applied to the case of a non-decaying turbulence.

A fully-developed turbulent boundary layer along a flat-plate will simplify the explanation. When the vortices produced at ξ'-point upstream are taken into account in the vortex chaos motion passing near a fixed A-point in the flow, discussions referring to the two-dimensional turbulent wake in Section 25 may be applied. Namely, in the orientation of filaments of the primary vortices produced from the wall, an intensive tendency can be assumed, to keep always parallel to the zx-plane of the wall because of the existence of wall. Owing to the random character of a vortex chaos motion, it is difficult to point out in the zx-plane a special orientation of the distribution of vortex filaments, and the discussions still hold for a group of vortices produced at a point of ξ' in a two-dimensional wake. When the coordinates of the A-point are denoted by ξ, η, the function $I_\eta(\xi')$ in (47.2) due to the ξ'-vortices is written as

$$I_\eta(\xi') = \Big[\Big\{4C_{\xi'}^2\nu \int_0^{2\pi}\int_0^{s_0(\theta)} P^*_{1\xi'}(s,\theta;\eta)\, F^2_{\xi'}(s,\theta)\cos^2\theta\, d\theta\, ds \int_{-\frac{\pi}{2}}^{\frac{\pi}{2}} \cos^2\phi_1 P^*_{2\xi'}(\phi_1)\, d\phi_1\Big\} \Big/ \int_0^{2\pi} s_0(\theta)\, d\theta\Big] G^2(t_{\xi'}),$$

$$P^*_{2\xi'}(\phi_1) = P^*_{2\xi'}(-\phi_1), \tag{49.1}$$

in reference to (25.1) and (25.2). For brevity of description suffix ξ is omitted in the function I.

When the reduction from (25.2) to (25.6) is applied to the ξ'-vortices, the same result as (25.8) is obtained for these vortices. Namely, (25.3), (25.4), and (25.5) lead to the expression

$$I_\eta(\xi') = a_{1\xi'} a_{2\xi'} F'_{2\xi'}(\eta)\, \mathcal{E}^2_{1\xi'}(\eta)\, G^2(t_{\xi'}),$$

$$a_{1\xi'} = 4C^2_{\xi'}\nu \Big/ \int_0^{2\pi} s_0(\theta)\, d\theta,$$

$$a_{2\xi'} = \int_{-\frac{\pi}{2}}^{\frac{\pi}{2}} \cos^2\phi_1 \, P^*_{2\xi'}(\phi_1)\, d\phi_1,$$

$$F'_{2\xi'}(\eta) = \int_0^{2\pi} F'_{1\xi'}(\theta;\eta)\, d\theta,$$

$$F'_{1\xi'}(\theta;\eta) = \int_0^{s_0(\theta)} P^*_{1\xi'}(s,\theta;\eta)\, F^2_{\xi'}(s,\theta)\, ds,$$

$$\mathcal{E}^2_{1\xi'}(\eta) = \int_0^{2\pi} F'_{1\xi'}(\theta;\eta)\, \mathcal{E}^2_{\xi'}(\theta)\, d\theta \Big/ \int_0^{2\pi} F'_{1\xi'}(\theta;\eta)\, d\theta,$$

$$\mathcal{E}^2_{\xi'}(0) = (\omega^2\theta)_{\xi'}.$$

(49.2)

If $u_{\xi'}$ is made to indicate the part of value u due to the ξ'-vortices, the same expression as (25.6),

$$u_{\xi'} \Big/ \sqrt{u^2_{\xi'} + v^2_{\xi'} + w^2_{\xi'}} = a_{2\xi'}\, \mathcal{E}^2_{1\xi'}(\eta),$$

(49.3)

is obtained. Therefore, when u'_{ξ} and l'_{ξ} are taken as the upper and lower limits, respectively, of $\mathcal{E}^2_{1\xi'}(\eta)$ in $\eta = 0 \sim 1$, the following relation is also proved by (25.7):

$$1 > u'_{\xi'} \geqq \mathcal{E}^2_{1\xi'}(\eta) \geqq l'_{\xi'} > 0.$$

(49.4)

Thus, $\mathcal{E}^2_{1\xi'}(\eta)$ becomes a constant value in $1 \sim 0$.

In a fully-developed boundary layer flow, u-intensity at the A-point is written as

$$u^2(\eta) = \int_{-\infty}^{\xi} I_\eta(\xi')\, d\xi',$$

(49.5)

by (47.2). Expression (49.2) can be transformed further into

$$u^2(\eta) = f_{u^2}(\eta)\, \mathcal{E}^2_1(\eta),$$

$$f_{u^2}(\eta) = \int_{-\infty}^{\xi} \{a_{1\xi'}\, a_{2\xi'}\, F'_{2\xi'}(\eta)\, G^2(t_{\xi'})\}\, d\xi',$$

$$\mathcal{E}_1^2(\eta) = \int_{-\infty}^{\xi} \{a_{1\xi'} a_{2\xi'} F'_{2\xi'}(\eta) \mathcal{E}_{1\xi'}^2(\eta) G^2(t_{\xi'})\} d\xi' \Big/ \int_{-\infty}^{\xi} \{a_{1\xi'} a_{2\xi'} F'_{2\xi'}(\eta) G^2(t_{\xi'})\} d\xi'. \tag{49.6}$$

Thus, the same formulas as in (25.6) can be obtained for the components of turbulent intensity,

$$\begin{aligned}
u/\sqrt{u^2+v^2+w^2} &= a_2 \mathcal{E}_1^2(\eta), \\
v/\sqrt{u^2+v^2+w^2} &= 1 - \mathcal{E}_1^2(\eta), \\
w/\sqrt{u^2+v^2+w^2} &= (1-a_2)\mathcal{E}_1^2(\eta), \\
\overline{uv}/(u^2+v^2+w^2) &= a_3 \mathcal{E}_2^2(\eta),
\end{aligned} \tag{49.7}$$

where a_1, a_2, and a_3 are constants determined by the integrations of $\int_{-\infty}^{\xi} d\xi'$ containing $a_{1\xi'}$, $a_{2\xi'}$ and $a_{3\xi'}$.

As in the case of a decaying turbulence, the relation (49.4) for the ξ'-vortices is proved by the integration of a function which is multiplied by $\cos^2\theta = 1 \sim 0$. Expression (49.7) is derived further by the integration of $\int_{-\infty}^{\xi} d\xi'$ multiplied by $\mathcal{E}_{1\xi'}^2$ of the relation (49.4). Therefore, for the same reason, the relation

$$1 > u'_{\xi'} > u' \geqq \mathcal{E}_1^2(\eta) \geqq l' > l'_{\xi'} > 0 \tag{49.8}$$

is obtained with u' and 1', respectively, the upper and lower limits of $\mathcal{E}_1^2(\eta)$. Namely, with repetitions of an integration containing trigonometric functions, the values of $\mathcal{E}_{\xi'}^2$, $\mathcal{E}_{1\xi'}^2$, and $\mathcal{E}_1^2$ gradually approach a constant value of $0 \sim 1$. It is significant that in the nondecaying turbulence, the value of $\mathcal{E}_1^2$ is supposed to have a character more independent of η than in the case of a decaying turbulence.

The above-mentioned concerns the simple case of a flat-plate boundary layer flow. The essential point of discussions, however, is the repetition of integrations for the vortex chaos motion, which holds, obviously, in other cases of nondecaying turbulence. In the case of a pipe flow, for instance, such a formula as (25.8) will be obtained in the same manner. Figure 80 shows examples of the measurements of the proportionality character. By comparison with Figure 41, the conspicuous convergence in the case of a nondecaying turbulence can be seen.

50. FREE-BOUNDARY PHENOMENA

To derive quantitative results from the extended formula (47.2) or (49.1) of the initial-period law, functional forms of every $P^*_{\xi'}$ and $F^2_{\xi'}$ must be known, and the integration $\int_{-\infty}^{\xi} d\xi'$ is evaluated as a function of η. In this section, some elementary characters of the P*-function will be discussed. When

$$\widetilde{P}^*_{\xi'} = \iiint_{D^*_{\xi'}} P^*_{\xi'}(r,\theta,\phi)\, dQ^*_{\xi'},$$

$$\int_{-\infty}^{\xi} \widetilde{P}^*_{\xi'}\, d\xi' = 1 \tag{50.1}$$

is written like (13.6), $\widetilde{P}^*$ as a function of η means the probability with which the ξ'-vortices are mixed in all the vortices passing through the A-point at (ξ, η).

The vortex chaos motion is considered to be passing through a section at ξ. Near $\eta = 1$, the value of $P^*_{\xi'}$ may be large far upstream from the ξ-section, and near $\eta = 0$ it may be large just before the section. This is concluded from the existence of a viscous sublayer which adheres to the wall. Large-scale vortices produced far upstream may be carried near the boundary of the layer, and small-scale vortices produced just upstream may be conspicuous near the wall. At two points of A and A' taken near $\eta = 1$ and 0, respectively, in the ξ-section, their P*-functions may present such forms as shown in Figure 81.

For every $P^*_{\xi'}$-function in the $D^*_{\xi'}$-domain, a functional form must be given *a priori*. As in the case of the decaying turbulence, it may be appropriate to take the first approximative expression as the Gaussian distribution, as (26.6). In Section 26, the intermittency factor γ of (26.1) is proved by the Gaussian expression of the P*-function to distribute with the Gaussian integral form as (26.7). This character can be applied to every intermittency factor γ of the ξ'-vortices. Therefore, if observations are made on the distribution of γ near the boundary of a turbulent boundary layer, the Gaussian-integral form caused by representative large-scale vortices must be detected. Examples of the measurements shown in Figure 82 may prove the above-mentioned suppositions.

CHAPTER NINE. TRANSFER THEORY OF THE NONDECAYING TURBULENCE

51. DISTRIBUTION OF THE MIXING LENGTH

The significance of the transfer theory viewed from the statistical theory of turbulence is related in Chapter Six. In the case of the nondecaying turbulence, it becomes difficult to derive quantitative results, even of the velocity fluctuations, from the formula of the extended initial-period law. Thus, in this case of flow, the transfer theory is taken to be especially important, and the scope of application must be extended by making the foundations clear, depending upon the discussions of vortex chaos motion.

Vortex chaos motion in the nondecaying turbulence presents the shear-turbulence state of an incompletely irregular character, and the background of the momentum-transfer theory mentioned in Section 30 still holds. Namely, when the mean-velocity profile in a section is distorted across the flow, the formula (30.5) of the turbulent shearing force and the coefficient are written as

$$\tau = \varepsilon \frac{d\bar{U}}{dy}, \qquad \varepsilon = \rho v l', \tag{51.1}$$

and when Prandtl's mixing length of (30.9),

$$l^2 = \frac{\overline{uv}}{v^2} l'^2, \tag{51.2}$$

is introduced, the formula (30.8)

$$\tau = \rho l^2 \left|\frac{d\bar{U}}{dy}\right| \frac{d\bar{U}}{dy} \tag{51.3}$$

is obtained.

Determination of ε or l across a nondecaying turbulent flow must be made depending upon the basic physical interpretation that the primary vortices are produced continuously along the wall. Namely, the value of ε or l at an A-point must be estimated for every group of vortices produced upstream. In the case of nondecaying turbulence, however, two quantities of v and l' of ε must be estimated for every ξ'-vortex, together with the mixing ratio $\widetilde{P^*}_{\xi'}$, whose evaluations are difficult. On the other hand, the correlation coefficient uv/v^2 in (51.2) which is

expressed in $a_3\,\varepsilon_2^2(\eta)/(1-\varepsilon_1^2(\eta))^2$ by (49.7), has a more intensive tendency to be independent of η than in the case of a decaying turbulence. Therefore, Prandtl's mixing length l in (51.2) is considered to represent the mean free path of fluid parts more accurately, and it is sufficient to consider only the length l'. In the case of decaying turbulence, discussions based on the coefficient ε can be made because of the simple physical picture of the initial-period law, and the evaluated results are somewhat better than those depending upon l. Thus, in the case of the nondecaying turbulence, the analysis due to Prandtl's mixing length seems to play the essential role of the transfer theory.

In nondecaying turbulence, many vortices produced everywhere along the wall are carried with their growing regions around the filaments being kept almost parallel to the wall. The mean free path l' of fluid parts at an A-point depends on the vertical length of the region of every vortex passing near this point. When $\overline{R}_y$ is taken as the mean value of the vertical lengths of vortices passing through the A-point, the value of l' or l is regarded to be proportional to $\overline{R}_y$, and the point of discussions is reduced to the distribution of $\overline{R}_y$ across the nondecaying turbulent flow.

Along the wall surface, the scales of vortices at their production instants are all regarded to be zero, and $\overline{R}_y = 0$ holds there. Namely, the condition

$$l = 0 \qquad \text{at} \qquad y = 0 \tag{51.4}$$

holds in all the cases of nondecaying turbulence. If the thickness of a nondecaying turbulence is denoted by δ and the mean velocity is two-dimensional for simplicity, then many small vortices must exist near the wall and many large ones must exist near the boundary. Taking into account the wall condition (51.4), the general expression of l is given by

$$\frac{l}{\delta} = c_1\eta + c_2\eta^2 + c_3\eta^3 + \cdots, \qquad \eta = \frac{y}{\delta}. \tag{51.5}$$

Near the wall, (51.5) may be approximated by

$$\frac{l}{\delta} = c_1\eta \qquad \text{near} \qquad \eta = 0, \tag{51.6}$$

which is the assumption proposed by Prandtl (reference 10) in the case of a nondecaying turbulent flow. Near the free boundary of the turbulent flow, large-scale vortices produced far upstream are predominant. If these large

vortices are represented by a representative single kind of vortex as mentioned on the intermittency factor γ in Section 50, the value of $\overline{R}_y$ for this flow is taken to be constant as (33.8) in the initial-period law. Namely, such an approximative expression,

$$l = \text{constant} \quad \text{near} \quad \eta = 1, \tag{51.7}$$

is arrived at which is the same as the assumption of the wake flow near the free boundary of turbulent boundary layer proposed by Coles (reference 70).

It is too difficutl to evaluate the coefficients c_1, c_2, ... of the series (51.5), and a general expression of l/δ in $\eta = 0 \sim 1$ shall be attempted. Let an A-point have the coordinates (ξ , η) in a nondecaying turbulent flow as shown in Figure 83, and let the production position be ξ_1 of the representative vortices whose vertical scale R_y is equal to the mean value of those of the vortices passing near the A-point. According to the physical interpretations of the vortex chaos motion, assume that $\xi - \xi_1$ is proportional to η . On the other hand, scale length of a vortex motion increases proportionally to the square root of the time interval since the production instant. And if the time interval since the production instant at ξ_1 is taken to be approximately proportional to the distance $\xi - \xi_1$ by a uniform mean-velocity profile, regardless of the position of η , R_y is proportional to $\xi - \xi_1$, namely to η . Therefore, the general character,

$$\frac{l}{\delta} = c_2 \sqrt{\eta} , \tag{51.8}$$

is obtained. Near η =0 the assumption of a uniform mean-velocity may be doubtful, and near η =1 the proportional assumption between η and $\xi - \xi_1$ may lose meaning. Thus, the formula (51.8) should be considered as the first approximative expression of l near the center of $\eta = 0 \sim 1$.

It is difficult to evaluate experimentally the value of l according to the definition of (51.2). However, when the turbulent shearing stress τ is measured directly or indirectly with the mean-velocity profile, the value of l can be obtained by the formula (51.3). Figures 84 and 85 show examples of measurements of l in nondecaying turbulent flows.

52. EQUATION OF MOTION FOR THE FLOW OF SIMILARITIES PRESERVATION

The Reynolds equations play a fundamental role in discussions of the mean velocity depending upon the transfer hypotheses. In turbulent shear flow, the effect of molecular viscosity can be neglected compared with that of the turbulent viscosity. A turbulent boundary layer is taken where the x- and y-axes are considered parallel and perpendicular, respec-

tively, to the flow, with the variation of mean velocity to the z-direction neglected. When $\bar{U}$, $\bar{V}$ and $\bar{P}_o$ are taken, respectively, as the x-, y-components of the mean velocity in the layer and the free-stream pressure outside, the Reynolds equations take the following form of Prandtl's equation:

$$\bar{U}\frac{\partial \bar{U}}{\partial x} + \bar{V}\frac{\partial \bar{U}}{\partial y} = \frac{-1}{\rho}\frac{dp_o}{dx} + \frac{\partial(-\overline{uv})}{\partial y},$$

$$\frac{\partial \bar{U}}{\partial x} + \frac{\partial \bar{V}}{\partial y} = 0. \tag{52.1}$$

The similarity character of the Reynolds stress of the nondecaying turbulence is discussed in Sections 47 and 48. In this section the similarity character in the mean-velocity distributions will be surveyed. When $\bar{U}_o$, v_o, δ, and L are the free-stream velocity outside the layer, a representative turbulent intensity in a section of the layer, the boundary layer thickness and a standard length to the x-direction, respectively, then the mean velocity and the shearing stress are generally expressed in the series

$$\frac{\bar{U}(x,y)}{U_o(x)} = f(\eta) + \xi f_1(\eta) + \xi^2 f_2(\eta) + \cdots,$$

$$\frac{-\overline{uv}(x,y)}{v_o^2(x)} = g(\eta) + \xi g_1(\eta) + \xi^2 g_2(\eta) + \cdots. \tag{52.2}$$

The similarity flow discussed in the last chapter corresponds to the case where g_1, g_2, ... are made zero in (52.2). In this case, if f_1, f_2, ... are also assumed to vanish, the Reynolds equation (52.1) becomes

$$(f'\int_0^\eta f'\eta d\eta - ff'\eta) + (f^2 - f'\int_0^\eta f d\eta - 1)\left[\frac{U_o'\delta}{U_o\delta'}\right] = g'\left[\frac{(v_o/U_o)^2}{\delta/L}\right], \tag{52.3}$$

with the Bernoulli equation $P_o + \frac{1}{2}\rho U_o^2 = \text{constant}$ utilized. Primes on f, g, and U_o, δ denote differentiations, respectively, by η and ξ. Since f and g are functions of only η, λ and c' of the expressions,

$$\frac{U_o'\delta}{U_o\delta'} = \lambda,$$

$$\frac{(v_o/U_o)^2}{\delta/L} = c', \tag{52.4}$$

shall be constant so that (52.3) may hold irrespectively of the ordinate x.

When the shearing stress at $\eta = 0$ is denoted by $\tau_w = -\rho\overline{uv}(0)$, λ is written as

$$\lambda = \left\{\frac{-\frac{dP_o}{dx}\delta}{\tau_w}\right\}[c'g(0)],$$

which represents the ratio of the two forces of the pressure and the shearing stress in a section of the layer. Therefore, λ can be taken as a parameter of the pressure gradient outside the layer. In the theory of laminar boundary layer, the pressure-gradient parameter,

$$\frac{-\frac{dP_o}{dx}\delta}{\rho\nu\frac{U_o}{\delta}},$$

is given by Pohlhausen. λ in (52.4) may be corresponded to Pohlhausen's parameter in the case of a turbulent boundary layer. On the other hand, ν_o, U_o, δ', and L in (52.4) are related directly to the x-Reynolds number of the flow or the surface roughness. Thus, c' may be taken as a Reynolds-number parameter.

In the case of a decaying turbulence, the initial-period similarity-law derives the similarities of both the Reynolds stress and the mean velocity as mentioned in Section 24. As mentioned in Section 47 for the case of a nondecaying turbulence, the Reynolds stress preserves similar profiles, if effects of dP_o/dx to the vortex chaos motions are uniform along the wall. However, by assuming only the Reynolds stress similarity, the independencies of λ and c' in (52.4) of the x-ordinate cannot be proved. Namely, similarities of both the Reynolds stress and the mean velocity do not generally hold together. The inconsistency always brings about complicated situations, unlike the case of a decaying turbulence. From the standpoint of the transfer theory, however, the analyses in an idealized case of the two kinds of similarities should be established first, before proceeding to discussions of general characters of nonsimilar velocity profiles. Expression (52.3), together with the condition (52.4), can be taken as the Reynolds equation for the turbulent boundary layer of the similarities preservation.

53. SINGULARITY CHARACTER NEAR THE WALL

In this section, characteristics of flow in the vicinity of wall shall be surveyed. When the expression (51.6) of ℓ near the wall is substituted into the formula (51.3) of momentum transfer, the Reynolds equation (52.3) for the boundary layer of the similarities preservation becomes

$$(f'\int_0^\eta f'\eta d\eta - ff'\eta) + (f^2 - f'\int_0^\eta f d\eta - 1)\lambda = c(\eta^2 f'^2)',$$

$$c = \frac{c'^2}{\frac{\delta}{L}}. \tag{53.1}$$

When the nondimensional stream function F is given by

$$F = \int_0^\eta f d\eta, \tag{53.2}$$

(53.1) is further transformed into

$$2\eta(F'' + \eta F''') + \frac{\lambda+1}{c}F - \frac{\lambda}{c}\frac{F'^2-1}{F''} = 0. \tag{53.3}$$

At the limit of $\eta \to 0$, F tends to zero in (53.2). If one neglects, near $\eta = 0$, the second and third terms in (53.3) by assuming $(F'^2-1)/F'' \longrightarrow 0$ at $\eta \to 0$, F is integrated into

$$F = \eta \ln \eta, \tag{53.4}$$

with the condition $F'=1$ at $\eta = 1$. If F of the function (53.4) is taken, the second and third terms in (53.3) are proved conversely to vanish at $\eta = 0$. Namely, the expression (53.4) is seen to be the essential character of flow near the wall.

When the quantity

$$U_\tau = \sqrt{\frac{\tau_w}{\rho}} \tag{53.5}$$

is introduced as a frictional velocity, (53.4) gives the following formula of the velocity profile:

$$\frac{\bar{U}-U_e}{U_\tau} = \frac{1}{c_1} \ln \eta, \tag{53.6}$$

where c_1 is the same as in (51.6). Expression (53.6) is the logarithmic formula of the velocity-defect law proposed by Kármán (reference 12). It is significant that the logarithmic expression holds independently of the parameters λ and c of the pressure gradient and the x-Reynolds number. Expression (53.6) is further transformed into

$$\frac{\bar{U}}{U_\tau} = A + \frac{1}{c_1} \ln \frac{U_\tau y}{\nu}, \tag{53.7}$$

with a constant A, that is known as the wall law proposed by Prandtl (reference 20).

Thus, the logarithmic law (53.6) or (53.7) has been taken to be the fundamental character of all kinds of the nondecaying turbulence near the wall. Attention shall be given to the singularity of the solution at η =0. By the character of logarithmic function, the mean velocity decreases rapidly as η approaches zero. But, it is not natural that the velocity diverges to the negative infinity at the wall. It must be connected to a finite value of the mean velocity at the boundary of the viscous sublayer. The logarithmic formula $\ln \eta$ comes from the formula (51.6) of ℓ . If (51.8) is used instead of (51.6), the above analyses lead to the formula

$$\frac{\bar{U}-U_e}{U_\tau} = \frac{2}{c_2} (\sqrt{\eta}-1). \tag{53.8}$$

Although the velocity of (53.8) does not diverge at η =0, $\partial \bar{U}/\partial y$ has still a singularity there. As seen in the analyses of the logarithmic law, the singularity is caused by the fact that the highest order term F''' in the ordinary differential equation (53.3) is multiplied by zero at η =0. This is the same for the case of (53.4). Namely, it is the wall condition (51.4) that derives the singularity. In a word, the idealized formula (51.4) of the physical interpretation of the production of new small vortices along the wall brings about the singularity character to the mean-velocity profile at the wall.

In the general case of a laminar flow along a wall, the velocity increases linearly from zero at the wall and tends to a constant value of the free-stream. In the case of turbulent flow, however, the mean velocity is always observed to increase rapidly and to tend gradually to the constant value. The above-mentioned singularity at η =0 may be supported by these well-known experimental facts. Figure 86 shows experimental data in various cases of nondecaying turbulent flows, which may clarify the singularity character near the wall.

54. CHANNEL OR PIPE FLOW

A channel flow between parallel walls is taken. δ and L are taken as the radius and a standard length, respectively, to the x-direction, and suffix o is made to denote the value at the center line, as shown in Figure 87. In a channel flow, δ is generally smaller than L, and the Reynolds equations are simplified into Prandtl's equation (52.1) with a constant pressure P_o to the y-direction.

In a fully developed channel flow where effects of the inlet region are neglected, no free stream exists and the similarity condition of the flow can be adapted. The continuity condition proves U_o to be constant to the x-direction. Thus, since δ is constant, the inertia terms in (52.1) become zero, and the equation for the similarities flow, as in (52.3) in the case of a turbulent boundary layer, is reduced to

$$\frac{d\left(\frac{P_o}{\frac{1}{2}\rho U_o^2}\right)}{d\xi} = \left[\frac{2\left(\frac{v_*}{U_o}\right)^2}{\frac{\delta}{L}}\right] g'. \tag{54.1}$$

As both sides are functions respectively of ξ and η only, they must take a constant value. By integrating with a condition $\tau = 0$ at $\eta = 1$, we get the expression

$$\tau = \tau_w (1-\eta). \tag{54.2}$$

Figure 88 shows observed results of the shearing stress of channel flow, where the relation (54.2) is supported except in the vicinity of the viscous sublayer.

When the assumptions (51.3) and (51.6) of the transfer theory are substituted into (54.2), it becomes

$$\frac{df}{d\eta} = \frac{1}{C_1}\left(\frac{U_\tau}{U_o}\right)\frac{(1-\eta)^{\frac{1}{2}}}{\eta}. \tag{54.3}$$

In order to find the fundamental expression of f, expression (54.3) is integrated by taking only the first term of the series,

$$(1-\eta)^{\frac{1}{2}} = 1 - \frac{1}{2}\eta - \frac{1}{8}\eta^2 - \frac{1}{16}\eta^3 - \cdots,$$

to get the same formula of (53.6),

$$\frac{\bar{U}-\bar{U}_0}{U_\tau} = \frac{1}{c_1}\ln\eta. \tag{54.4}$$

In the case of turbulent flow in a circular pipe with a constant radius δ, the inertia terms vanish in the Reynolds equation and the logarithmic formula (54.4) is obtained as the fundamental expression of the velocity profile. Figure 89 shows observed results in the case of a circular pipe, in which the linear relation of $\bar{U}/U_\tau \sim \log(U_\tau y/\nu)$ can be found more clearly than in the case of a boundary layer flow without a pressure gradient shown in Figure 86.

55. TURBULENT BOUNDARY LAYER ALONG A FLAT PLATE

In the case of a boundary layer flow, accuracy of the logarithmic law is inadequate as seen in Figure 86. Namely, the inertia force of flow and the pressure gradient of free stream remote from the wall cannot be neglected. In this section, the effect of inertia force shall be surveyed by taking a simple case of the turbulent boundary layer along a flat plate. As an idealized formulation, two similarities of the shearing stress and the mean velocity in (52.2) are assumed. As the transfer hypotheses, the approximative expression (51.8) of ℓ near the center in a section shall be introduced to the momentum-transfer formula (51.3). Then, the Reynolds equation (52.3) becomes

$$F + cF'' - 2c(1-\zeta)F''' = 0,$$

$$\zeta = 1-\eta, \tag{55.1}$$

with the nondimensional stream function (53.2) used, where the Reynolds-number parameter c is the same as in (53.1) and the prime on F denotes the differentiation by ζ. As the boundary conditions f=1 and $df/d\eta$ =0 at η =1 and F =0 at η =0 are taken, namely,

$$F' = -1, \quad F'' = 0 \quad \text{at} \quad \zeta = 0,$$

$$F = 0, \quad \text{at} \quad \zeta = 1, \tag{55.2}$$

is obtained.

When F is expressed in the series,

$$F = \sum_{i=0}^{\infty} a_i \zeta^i, \tag{55.3}$$

with constant coefficient a_i and substituted into the equation (55.1), such a recurring formula,

$$a_{i+3} = \{2c(i+3)(i+2)(i+1)\}^{-1} a_i + \{(2i+1)(2i+6)^{-1}\} a_{i+2}, \tag{55.4}$$

is derived. At large values of i, the first term which contains the parameter c can be neglected in (55.4). Thus, when F' and F'' of (55.3) are expressed respectively in $\sum_{i=0}^{\infty} a'_i \zeta^i$ and $\sum_{i=0}^{\infty} a''_i \zeta^i$ with constant coefficients a'_i and a''_i, the following conditions are obtained at the limit of $i \to \infty$:

$$\begin{aligned} \frac{a_{i+2}}{a_{i+3}} &= \frac{i+3}{i+0.5}, \\ \frac{a'_{i+1}}{a'_{i+2}} &= \frac{i+2}{i+0.5}, \\ \frac{a''_i}{a''_{i+1}} &= \frac{i+1}{i+0.5}, \qquad (i \gg 1). \end{aligned} \tag{55.5}$$

By Gauss' criterion of a power series, it is proved that $\sum_{i=0}^{\infty} a_i \zeta^i$ and $\sum_{i=0}^{\infty} a'_i \zeta^i$ are convergent in $1 \geqq \zeta \geqq 0$ and that $\sum_{i=0}^{\infty} a''_i \zeta^i$ is convergent in $1 > \zeta \geqq 0$ but divergent at $\zeta = 1$, because the difference between the denominator and the numerator is larger than unity except in the last expression in (55.5). Namely, the mean velocity f takes a finite value of the viscous sublayer at $\eta = 0$, but $df/d\eta$ always diverges, and the singularity character at the wall mentioned in Section 53 is mathematically proved for the case of a flat-plate boundary layer.

By the boundary conditions (55.2) and the recurring formula (55.4), the coefficient a_i of the series (55.3) can be calculated according to a parametric value of c. Figure 90 shows the calculated results. In the representation of $U/U_o \sim \eta$, the value of $U(0)/U_o$ at the boundary of the viscous sublayer depends explicitly upon the parameter c. This is supported by the experimental fact that even in the case of a flat-plate boundary layer, the value U/U_o near the wall varies with the Reynolds number of the flow, and the form parameter of the ratio of the momentum- and displacement-thickness is not constant. However, when the velocity profiles are expressed in the relative form $(\bar{U}-U_o)/(U_o-\bar{U}(0)) \sim \eta$, the parameter c affects only implicitly. The effect of c in four evaluated cases can be

covered within a single curve as shown in Figure 90.

At the limit of $\eta \to 0$, the value of $U_o - \bar{U}(0)$ is seen by (53.6) or (53.8) to be proportional to U_τ independently of c. Thus, if

$$\frac{\bar{U}-U_o}{U_\tau} = f_o \tag{55.5}$$

is written in this case, f_o can be considered to vary only with η, independently of the Reynolds number or of the roughness of wall. In Sections 53 and 54, the universal character of (53.6) or (53.8) is interpreted near the wall of a boundary layer or in a pipe flow. The function f_o can be taken as an extended formula of the velocity-defect law which holds in the whole section of a turbulent boundary layer along a flat plate.

Figure 91 shows a comparison of the calculated results of f with experimental data. Although the values on the two axes must be taken suitably in the theoretical curve, the functional form of f_o is preferable in the whole section of the layer, at least when compared with the logarithmic expression of (53.6). As mentioned in Section 51, the expression (51.8) of ℓ can be represented by the two formulas of (51.6) near the wall and (51.7) near the free-stream. In order to improve the logarithmic law, the velocity profiles can be represented by two kinds of the inner and outer solutions of them as has been widely attempted (references 72 and 76). As a simple expression, however, the above analysis based upon (51.8) may be preferable.

56. SOLUTIONS OF SIMILARITIES FLOW OF TURBULENT BOUNDARY LAYER

The analysis of the similarities flow along a flat plate mentioned in the last section shall be extended into general cases of a pressure gradient. When the transfer hypotheses (51.3) and (51.8) are introduced, the Reynolds equation (52.3) becomes

$$(\lambda+1)F + cF'' - \frac{\lambda(F'^2-1)}{F''} - 2c(1-\zeta)F''' = 0,$$

$$\zeta = 1-\eta, \tag{56.1}$$

which is the extended formula of (55.1) of no pressure gradient. The boundary conditions are given by (55.2). By solving (56.1), the effects of the two parameters of the pressure gradient λ of (52.4) and of the Reynolds number c of (53.1) shall be surveyed.

On account of the nonlinear term $\lambda\,(F'^2 - 1)/F''$, it is very difficult to solve mathematically the differential equation (56.1). A digital computer was necessary to get numerical solutions. Namely, expression (56.1) was first integrated step by step with a suitably selected value of F(0). The conditions F*(0)=1, F''(0)=0 in (55.2) and an appropriate initial value of F(0) was searched for, which ensured that F(1)=0. The integration was made by 16,000 steps in $\zeta = 0 \sim 1$, and the computed error was less than 0.0001 in the stream function F. Figure 92 shows an example of the solution. As shown in Figures 93 and 94, the Reynolds-number parameter has little effect on the relative profile of $(\bar{U}-U_\infty)/(U_0-\bar{U}(0)) \sim \eta$ for each value of λ, as in the case of $\lambda = 0$, although it appears explicitly in the conventional plot of $\bar{U}/U_0 \sim \eta$. As interpreted in the case of $\lambda = 0$, $U_0 - \bar{U}(0)$ is proportional to U_τ independently of λ and c near the wall. Thus, when

$$\frac{\bar{U}-U_0}{U_\tau} = f_\lambda \tag{56.2}$$

is written, velocity profile f_λ is seen to hold in the whole section independently of the parameter c for each value of λ. Figure 95 shows relative forms of f_λ expressed in $(\bar{U}-U_0)/(U_0-\bar{U}(0)) \sim \eta$, where the curves are obtained from the computed results for several values of c, with $\bar{U}(0)/U_0$ in about $0.3 \sim 0.7$ in each case of λ. Namely, in the expression $f_\lambda \sim \eta$ of a generalized velocity-defect law, the effect of the pressure gradient can be surveyed without being affected by the Reynolds number.

57. TURBULENT BOUNDARY LAYER WITH A SEPARATION

By computing the equation of motion (56.1) of the similarities flow, it has been found that as the value of $-\lambda$ increases, variations due to the parametric value of c become large even in the relative profile of $(U-U_0)/(U_0-\bar{U}(0)) \sim \eta$. At a value of $-\lambda$ greater than 0.25, the relative profiles cannot be covered with a single curve. Further, for some values of λ and c, an important feature of alternation of the sign of $\partial \bar{U}/\partial y$ at y=0 from positive to negative large values were found. Probably this means the reverse of a sign of the infinity in the mathematical solution, and it can naturally be assumed that the reversing point of

$$\frac{\partial \bar{U}}{\partial y} = 0 \qquad at \qquad y = 0 \tag{57.1}$$

is the point of separation of turbulent boundary layer, because $\partial \bar{U}(0)/\partial y = -\infty$ implies the existence of a back flow near the wall. Figure 96 shows computed examples of velocity profiles near the reversal point. As in the theory of a laminar boundary layer, the separation condition (57.1) cannot be characterized strictly by the principal parameter λ. However,

when the displacement- and momentum-thickness of the boundary layer are evaluated on the relative profiles of $(\bar{U}-U_o)/(U_o-\bar{U}(0)) \sim \eta$, their variations versus λ are as shown in Figure 97. By Figures 96 and 97, it is assumed that a turbulent boundary layer with $\bar{U}(0)/U_o \fallingdotseq 0.5 \sim 0.7$, which implies standard values of the Reynolds number, separates from the wall at the critical value near

$$\lambda \fallingdotseq -0.3. \tag{57.2}$$

As experimental examinations for the computed results of the equation (56.1), in Figures 98 and 99, observed results of the mean velocity in the cases of similar flows in Figures 77 and 78 are plotted. Although the Reynolds stress has somewhat similar profiles as shown in Figures 77 and 78, the value of λ is not strictly constant, as shown in Figure 98 and 99. The corresponding computed curves in Figure 95 are also drawn in the experimental data.

By the solution in Figure 95 and the above-mentioned comparisons, the variation in the relative velocity profile due to λ is not large. This character anticipates that the velocity profile of the turbulent boundary layer with an arbitrary pressure distribution may be assimilated with the computed profile derived from the similarities condition, provided that the local value of λ of the former coincides with the pre-fixed λ-value of the latter. From this point of view, velocity profiles near $\lambda = -0.15$ were selected from some published experimental results. Since observed data are given in terms of the displacement thickness δ_* instead of δ in many cases, the value of λ is evaluated experimentally by assuming $\delta/\delta' = \delta_*/\delta_*'$. Figure 100 shows the comparison of experimental and theoretical results.

The point at which a real boundary-layer flow separates instantaneously is difficult to determine even by experimental works. Statistically for time, however, the layer usually separates behind an inflexion point of the pressure curve drawn along the wall from the point of minimum pressure towards the turbulent wake. When the experimental value of λ is plotted along the wall, it generally decreases gradually from zero at the minimum-pressure-point until it attains the minimum just behind the inflexion point. It can be found that these experimentally evaluated minimum values of λ are near the critical value of (57.2). Figure 101 shows some experimental data of velocity profiles near the minimum values of λ, together with the values of λ. For comparison with the theoretical results of the critical condition (57.1), a computed curve of velocity profile was inserted at $\lambda = -0.30$ and $c=0.35$. Although exact value of λ is difficult to determine both theoretically and experimentally, the discrepancy between the theoretical and experimental results does not seem to be large.

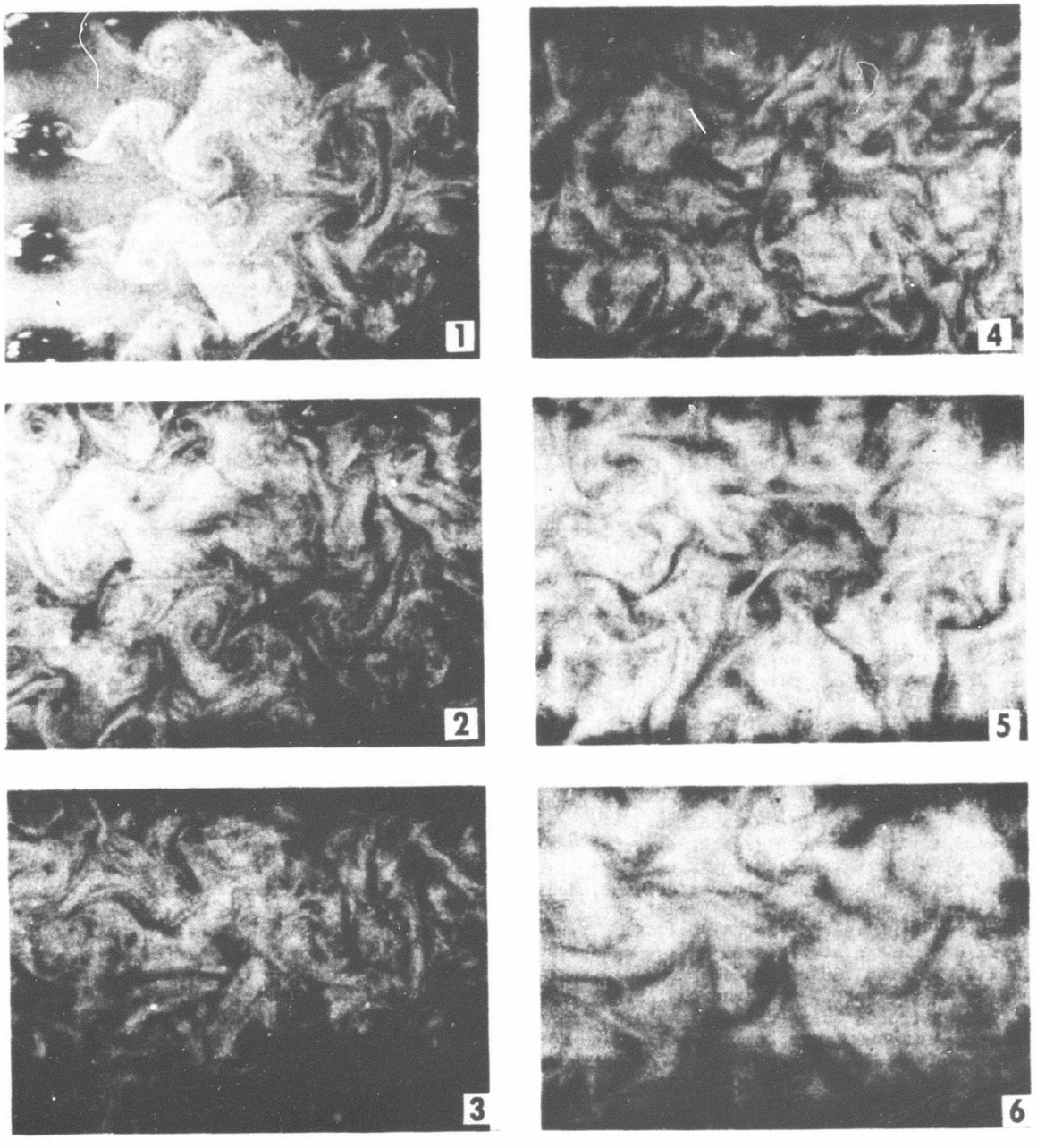

Figure 1. Observation of the Turbulent Flow of Water Behind a Two-Dimensional Lattice Moving With a Constant Velocity (reference 1). Diameter of rods of the lattice is 1.5 cm.; the speed is 6.65 cm/sec; and the time interval of each figure is 1.35 sec.

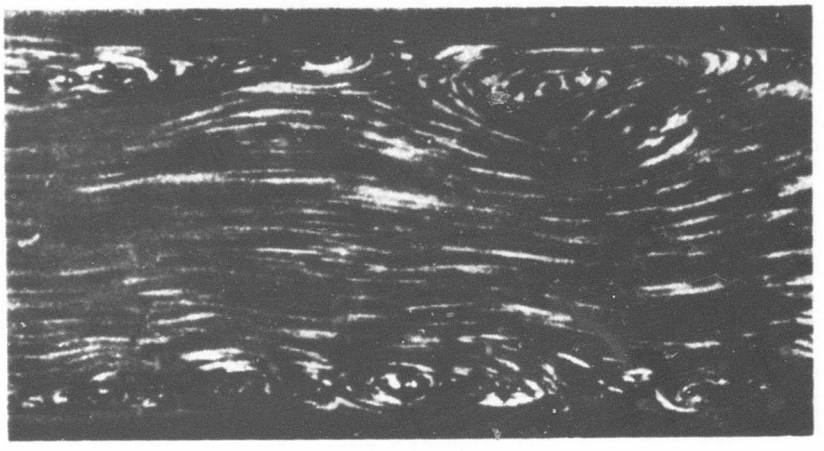

A. Taken by a Moving Camera With the Speed of Flow Near the Wall.

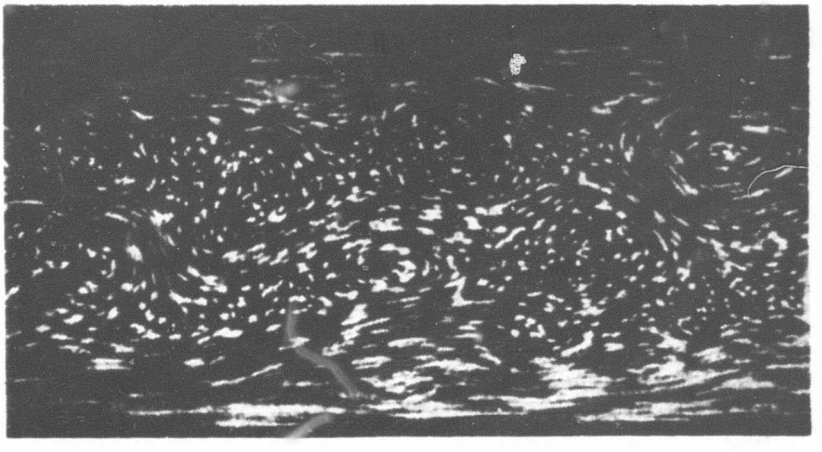

B. Taken by a Moving Camera With the Speed of Flow Near the Center.

Figure 2. Observation of the Turbulent Flow of Water in an Open Channel (reference 2).

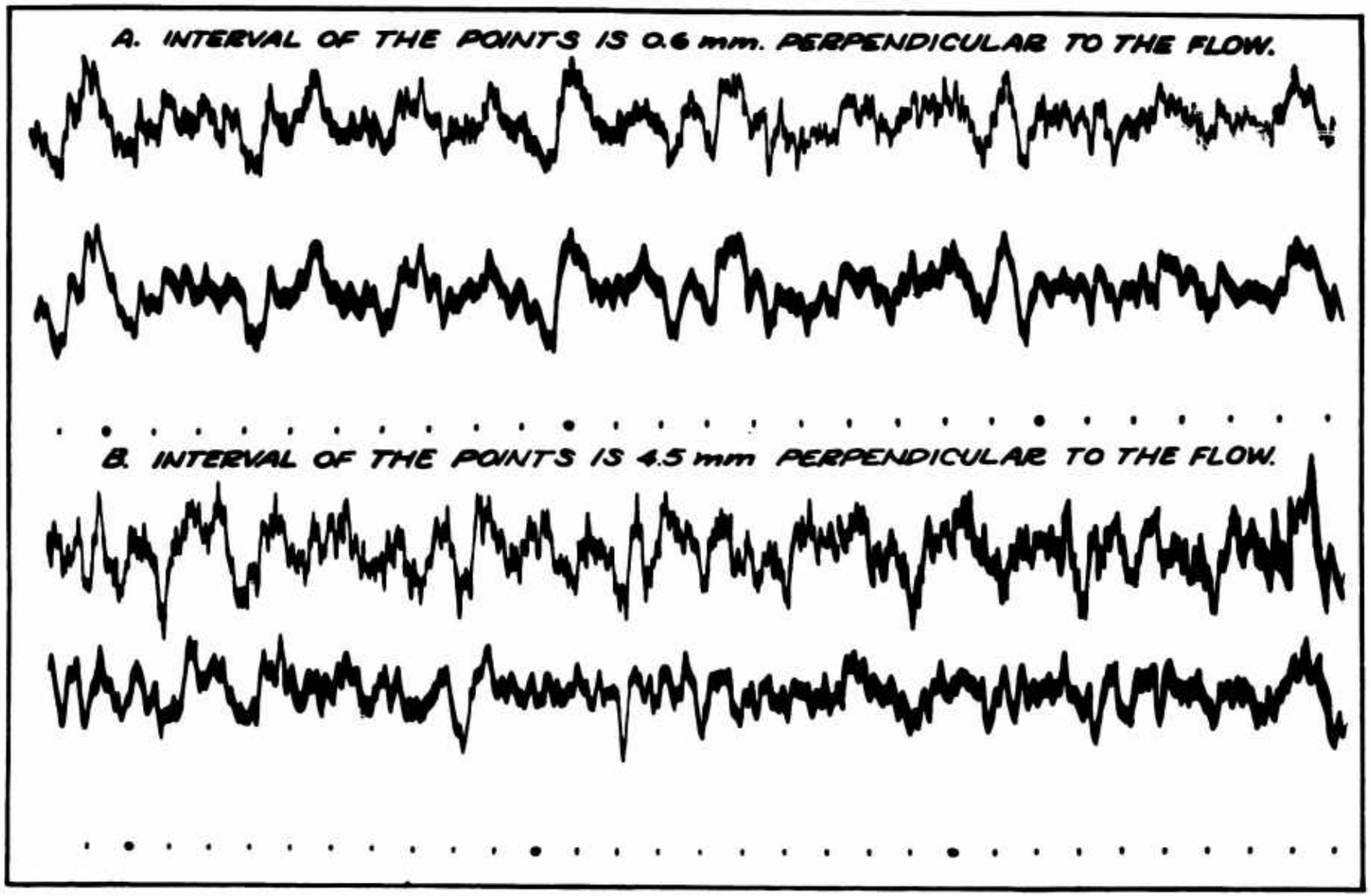

Figure 3. Simultaneous Records of Velocity Fluctuations at Two Points in a Wind Tunnel Stream. Oscillograms show the u-component parallel to the flow. The timing mark is 0.01 sec and the mean speed is 14.3 m/sec.

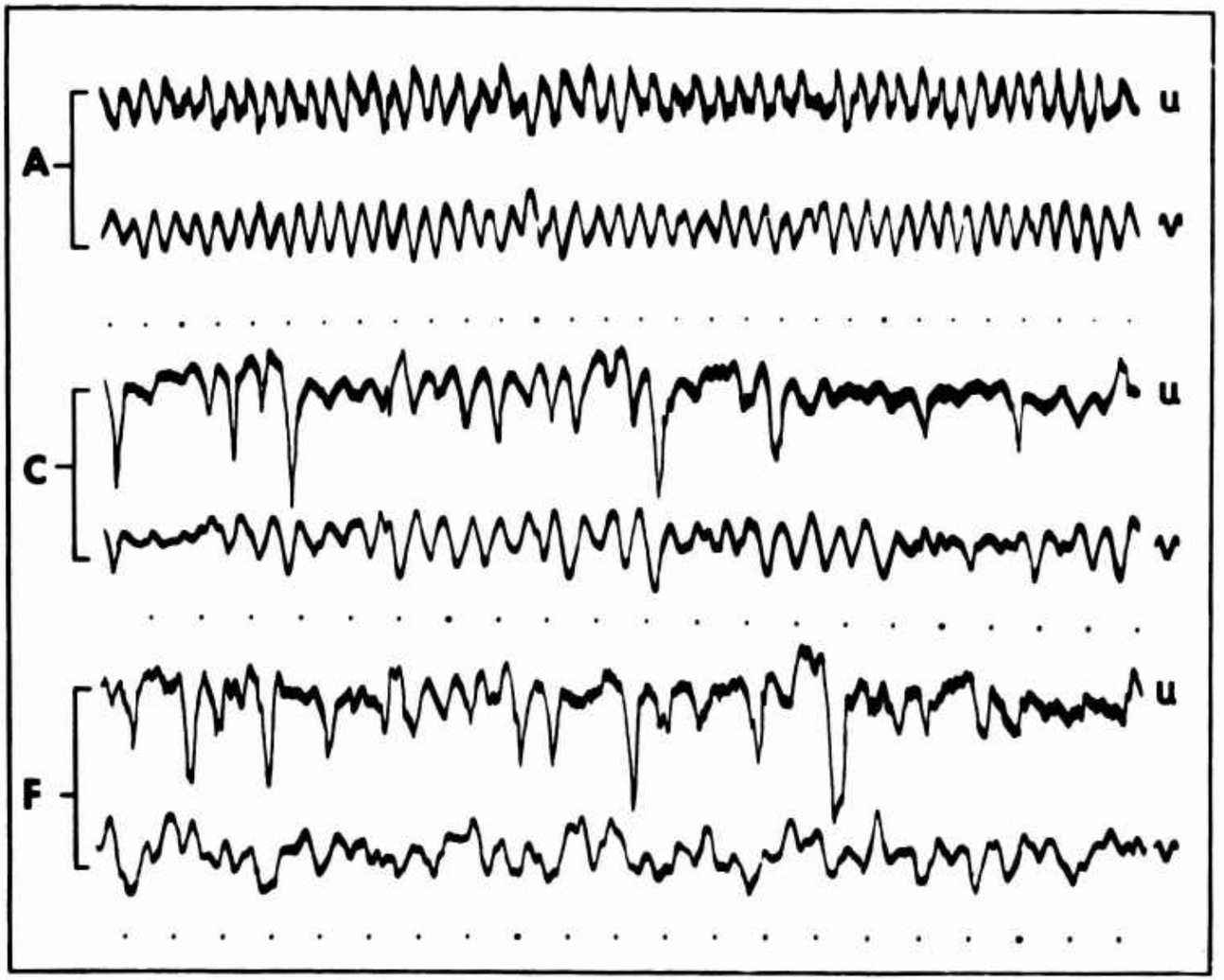

Figure 4. Simultaneous Records of the u- and v-Components (perpendicular to the flow) of Velocity Fluctuation at a Point on the Center Line Behind a Circular Cylinder (reference 17). The distance from the cylinder is (A) 9.0 cm., (C) 14.0 cm., and (F) 37.7 cm. The timing mark is 0.01 sec. The velocity of the main flow is 14.3 m/sec, and the diameter of the cylinder is 2.0 cm.

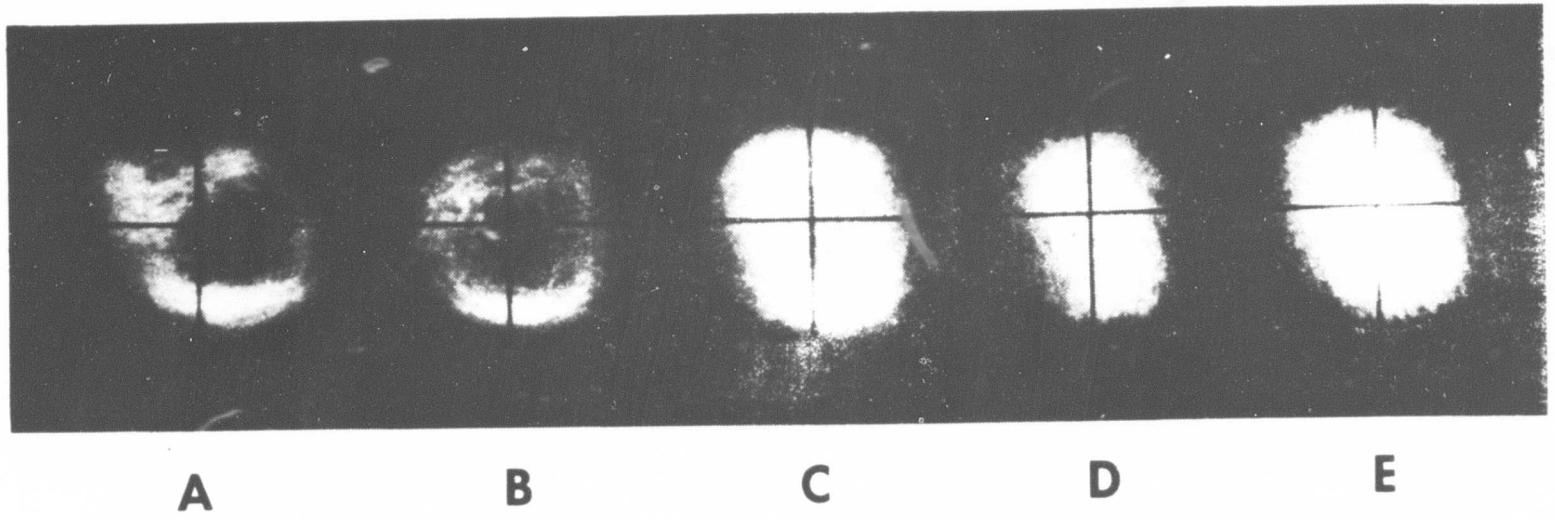

Figure 5. Photographs Showing the Change of the Probability Distribution of the u- and v-Fluctuation Behind a Circular Cylinder (reference 17). The state of flow and the locations of observation are the same as in Figure 4. The distance from the cylinder is (A) 9.0 cm., (B) 11.0 cm., (C) 14.0 cm., (D) 18.0 cm., and (E) 25.0 cm. The photos were taken on the surface of an oscilloscope, with an exposure time of 15 sec. The origin of the coordinates is the position of the mean velocity with the ordinates as v-fluctuation and abscissae as u-fluctuation.

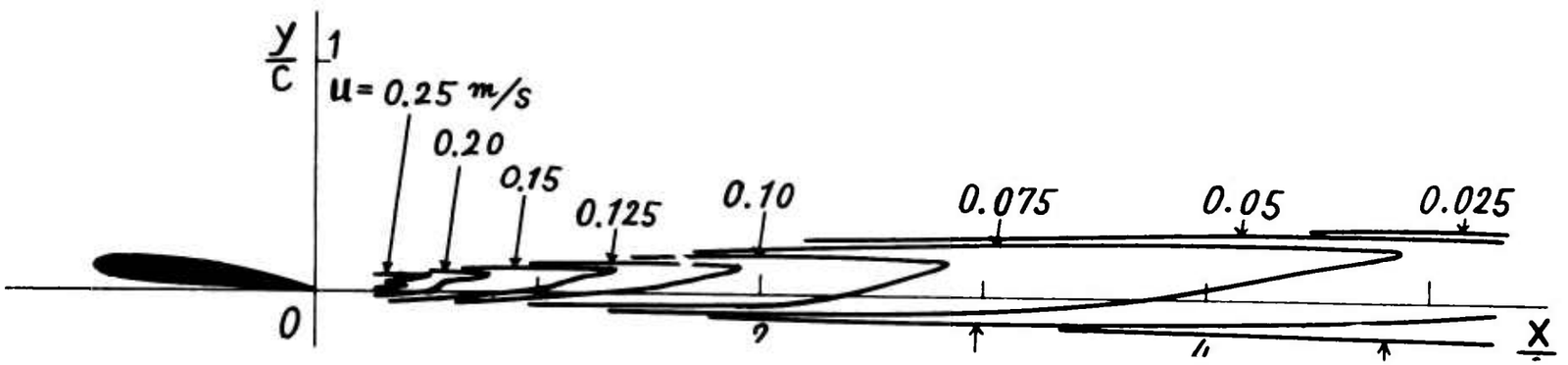

Figure 6. The Distribution of the Intensity of the u-Fluctuation in the Turbulent Wake Behind an Airfoil. The airfoil is NACA-2412 of a cord length of 17.0 cm., and the attack angle is 5 degrees in a uniform flow of velocity 7.28 m/sec.

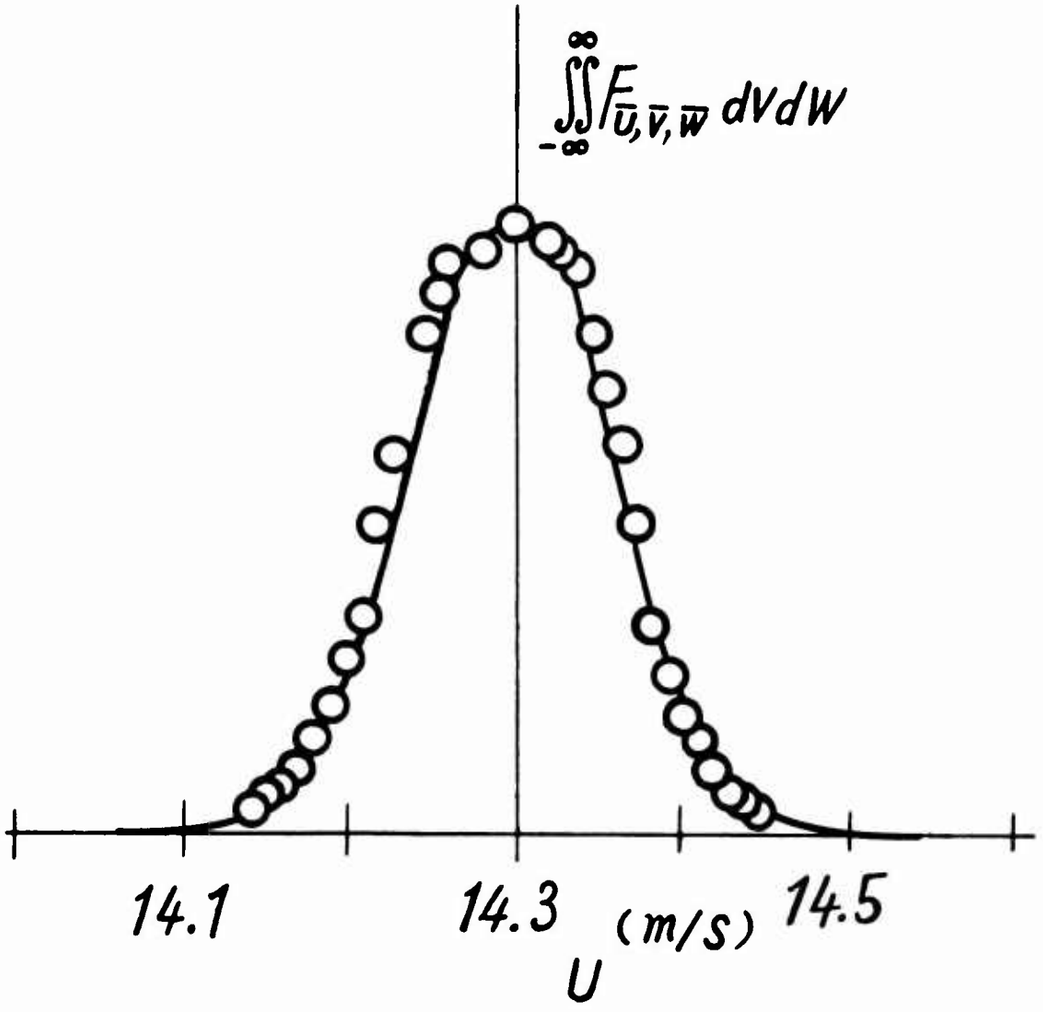

Figure 7. Probability Distribution of u-Fluctuation Around a Mean Velocity in a Wind Tunnel Stream. O is the observed result and the curve is the Gaussian distribution function.

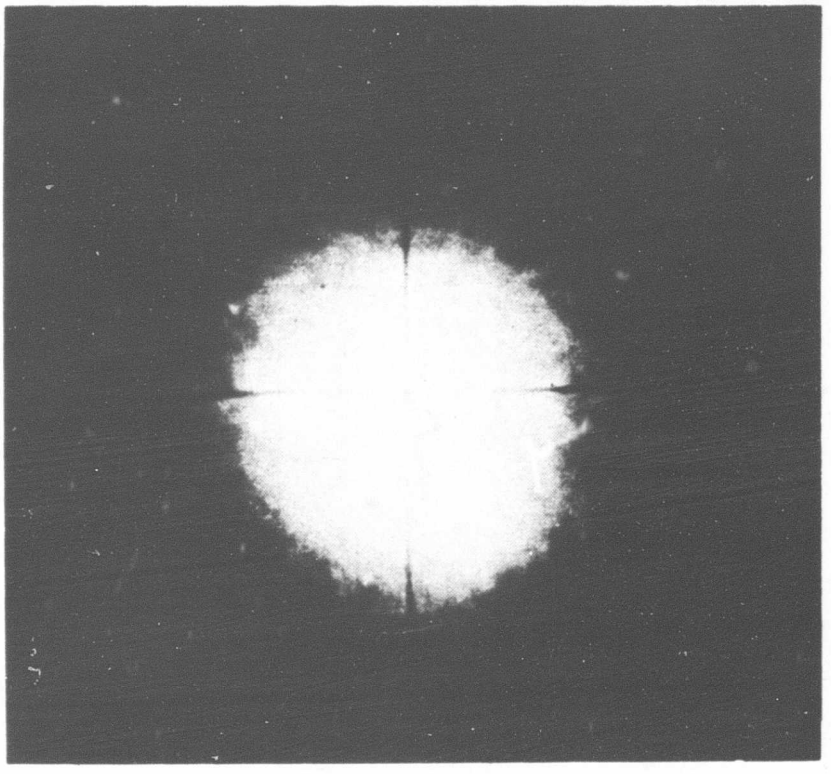

Figure 8. Photograph Showing the Probability Distribution of the u- and v-Fluctuation in a Wind Tunnel Stream (reference 18). The photo was taken on the surface of an oscilloscope with an exposure of 20 sec. The coordinate axes on the picture are the same as in Figure 5. The state of flow is the same as in Figure 7.

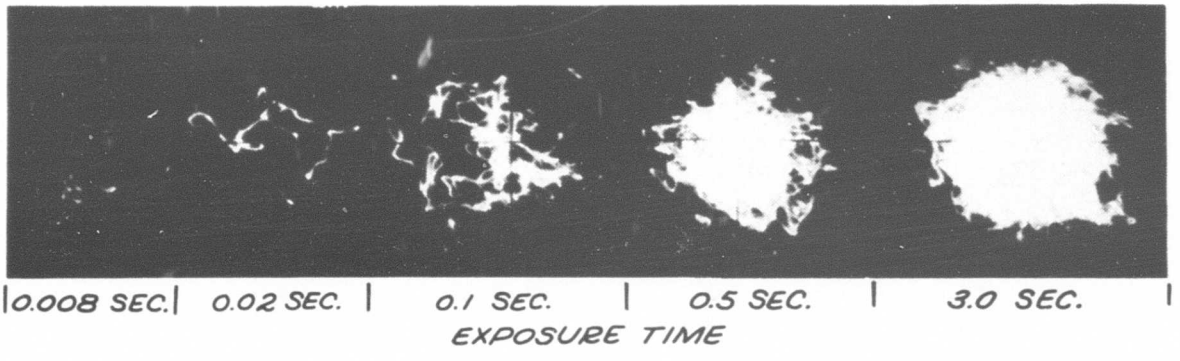

Figure 9. Photographs Showing the Formation of the Probability Distribution of the u- and v-Fluctuation in the Turbulent Wake Behind a Two-Dimensional Lattice (reference 18). The pictures have the same meaning as Figure 8.

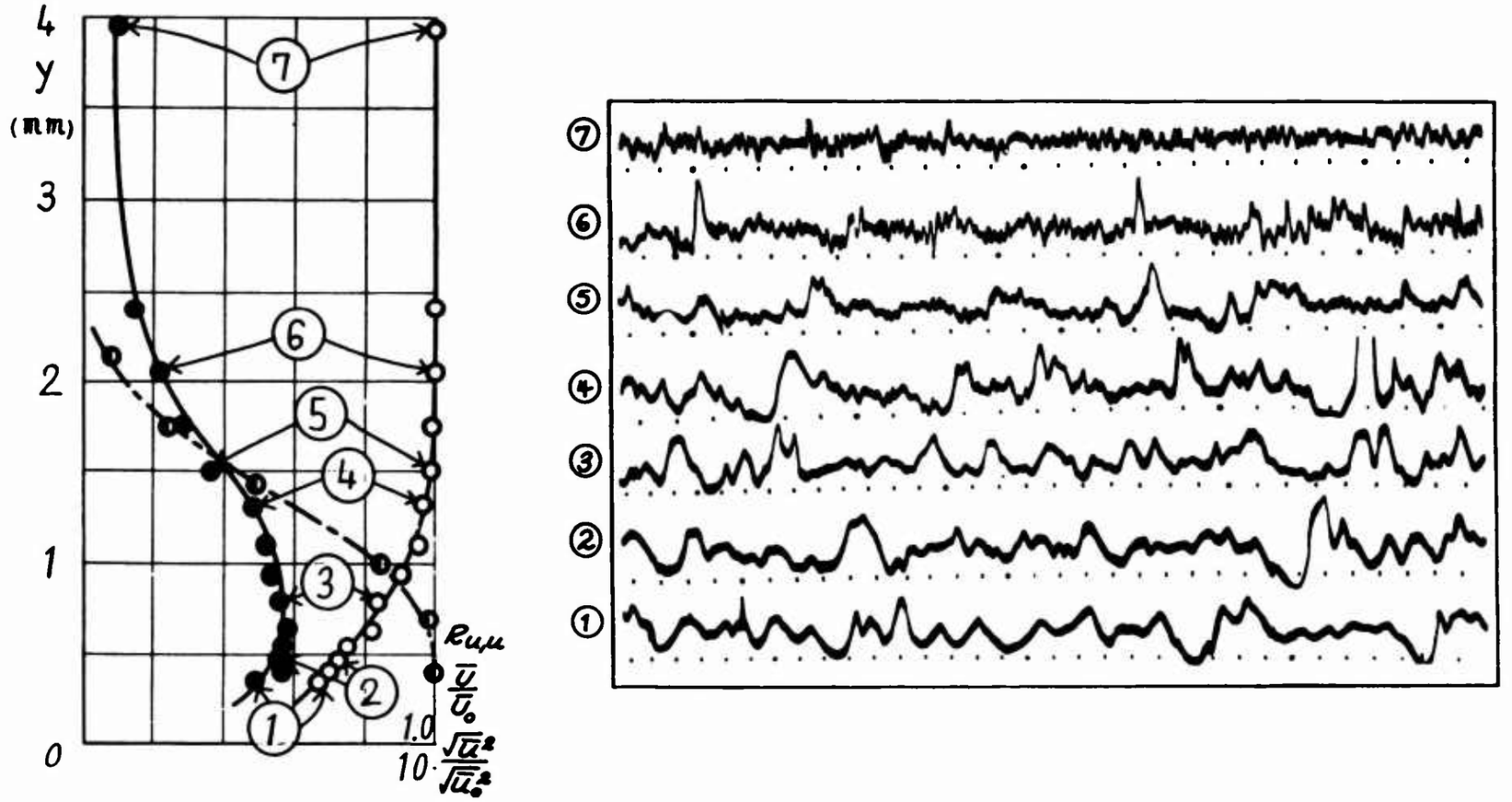

Figure 10. Laminar Boundary Layer Oscillation Along a Flat Plate (reference 19). The position of observation is 35 cm. from the leading edge. O, ● and ◐, are, respectively, the observed values of the mean velocity, intensity of u-fluctuation and the correlation coefficient $R_{u_1u} = u_1u/(\sqrt{\overline{u_1^2}}\ \sqrt{\overline{u^2}})$, with u_1 the value at y = 0.4 mm. from the plate. The mean velocity U_o and the turbulent intensity $\sqrt{\overline{u_o^2}}/U_o$ outside the layer are 14.3 m/sec and 0.45 per cent, respectively. The numbers are the corresponding locations of the observations. The timing mark is 0.01 sec.

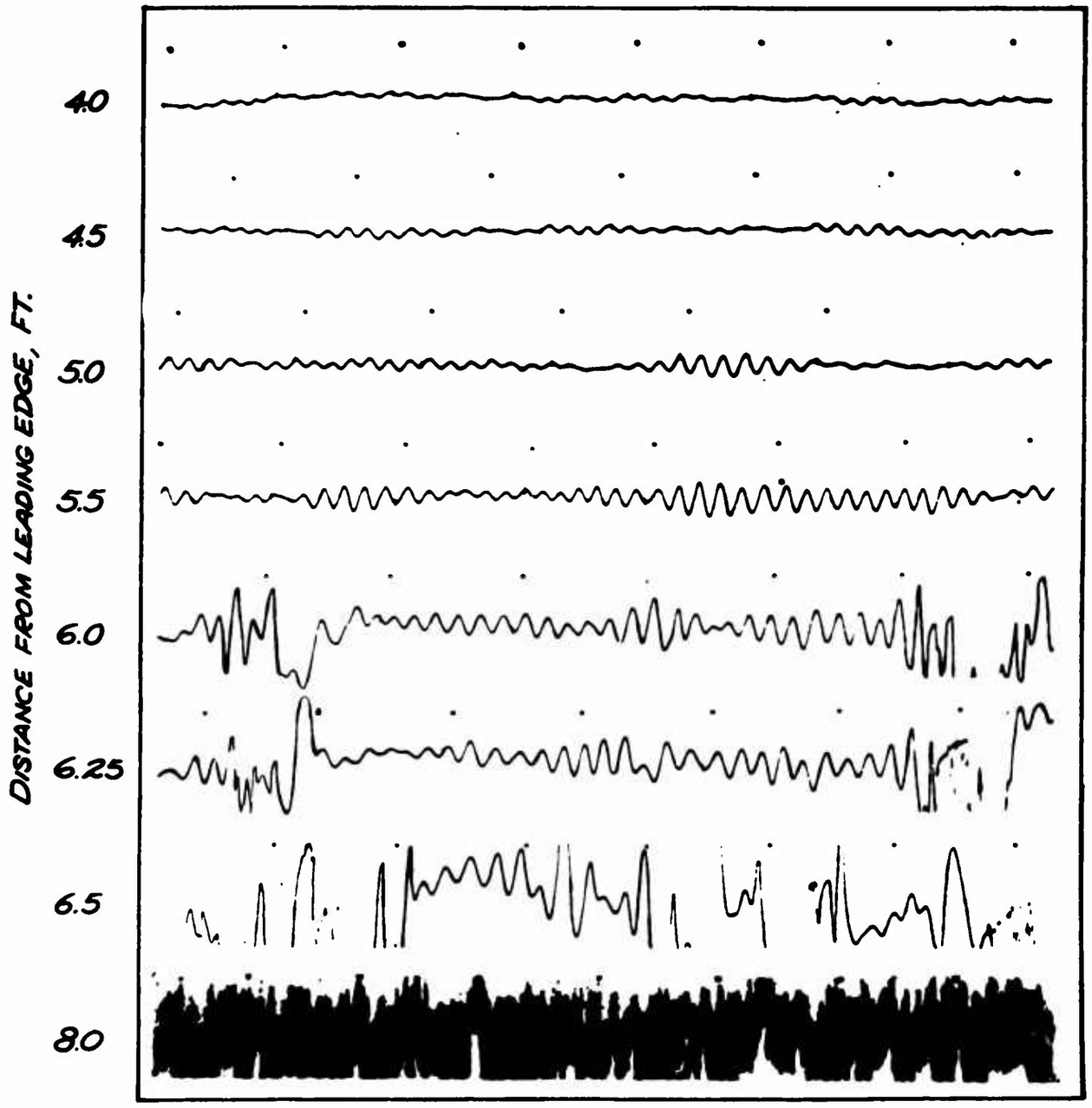

Figure 11. Development of Natural Laminar Oscillation in the Laminar Boundary Layer Along a Flat Plate in a Low-Turbulence Wind Tunnel (reference 6). The distance from the wall is 0.57 mm. and the timing mark is 1/30 sec.

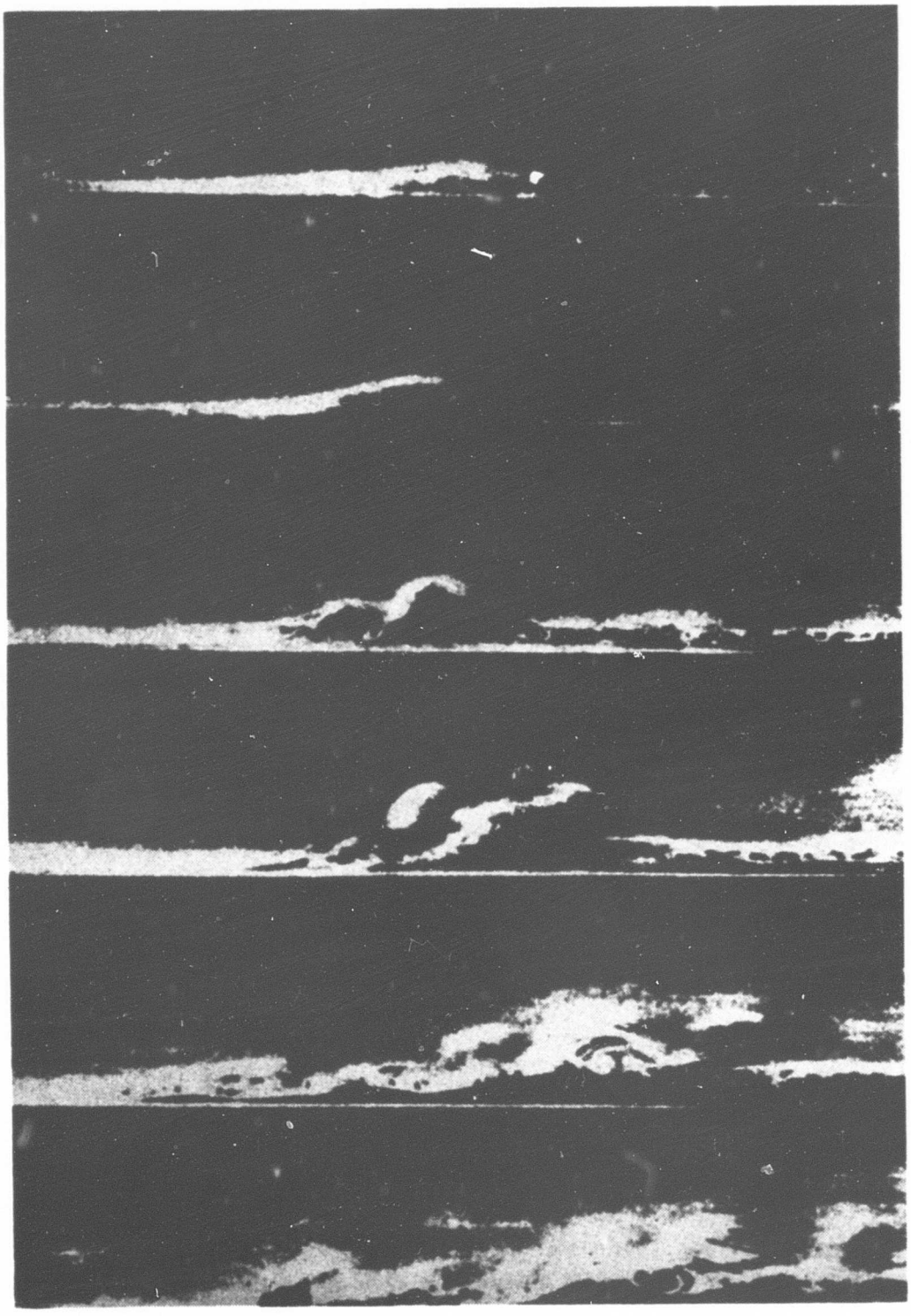

Figure 12. Observation of Natural Transition of Laminar Boundary Layer of Water Along a Flat Plate (reference 20).

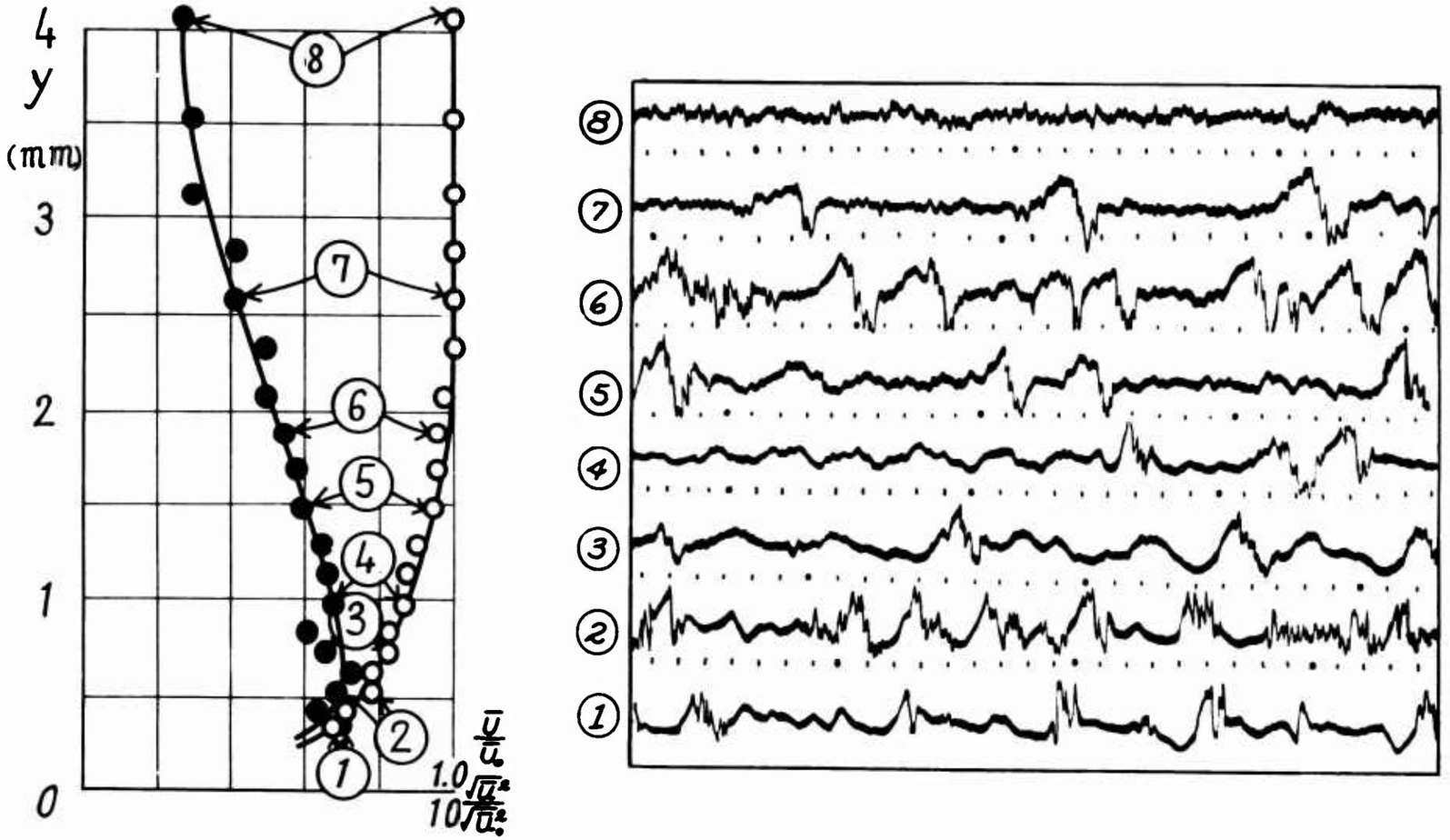

Figure 13. Measurement of the Mean and the Fluctuational Velocity at the Transition Region in the Laminar Boundary Layer Along a Flat Plate in a Wind Tunnel Stream (reference 19). O is the observed result of the mean velocity and ● is the intensity of the u-fluctuation. Numbers on the figures are the corresponding locations of the observations. The timing mark is 0.01 sec.

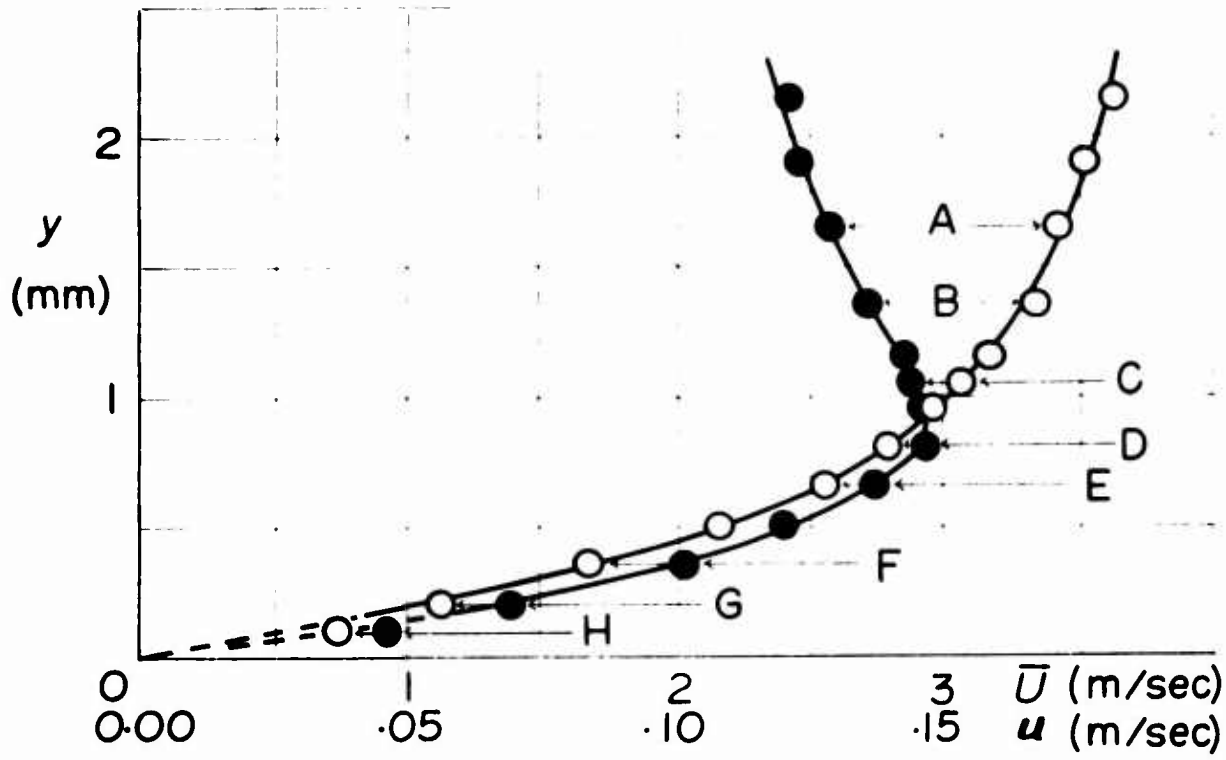

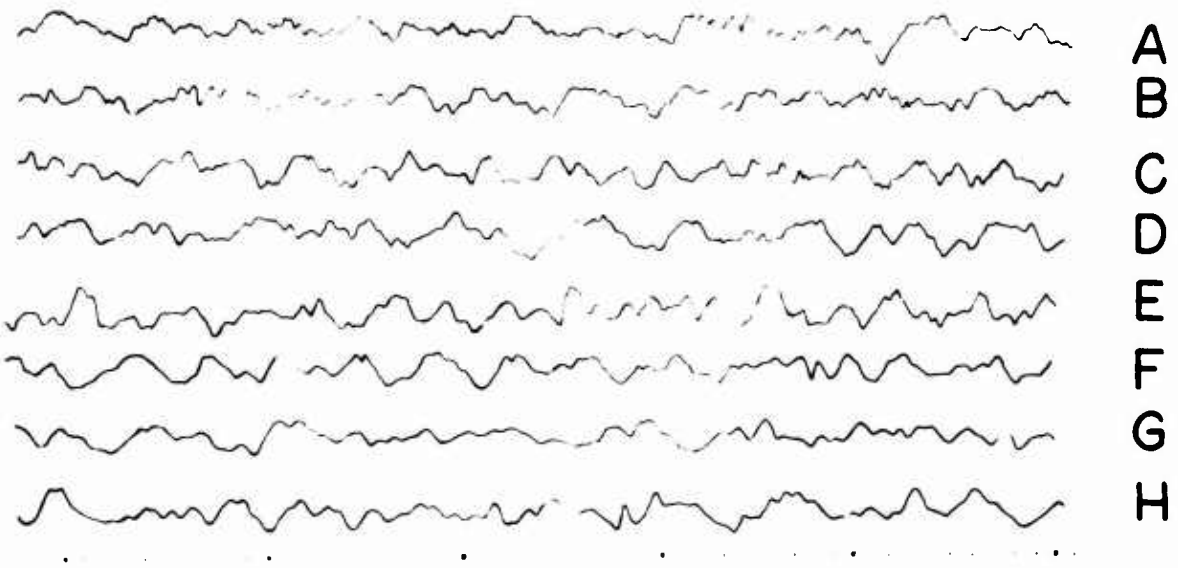

Figure 14. Distributions of Mean Velocity (○) and the Intensity of the u-Fluctuation (●) in the Immediate Vicinity of a Flat Plate in a Turbulent Boundary Layer (reference 22). The velocity outside the boundary layer is 5.30 m/sec. Oscillograms show the u-fluctuations where marks A, B, ... indicate the corresponding positions in the diagram. The timing mark is 0.01 sec.

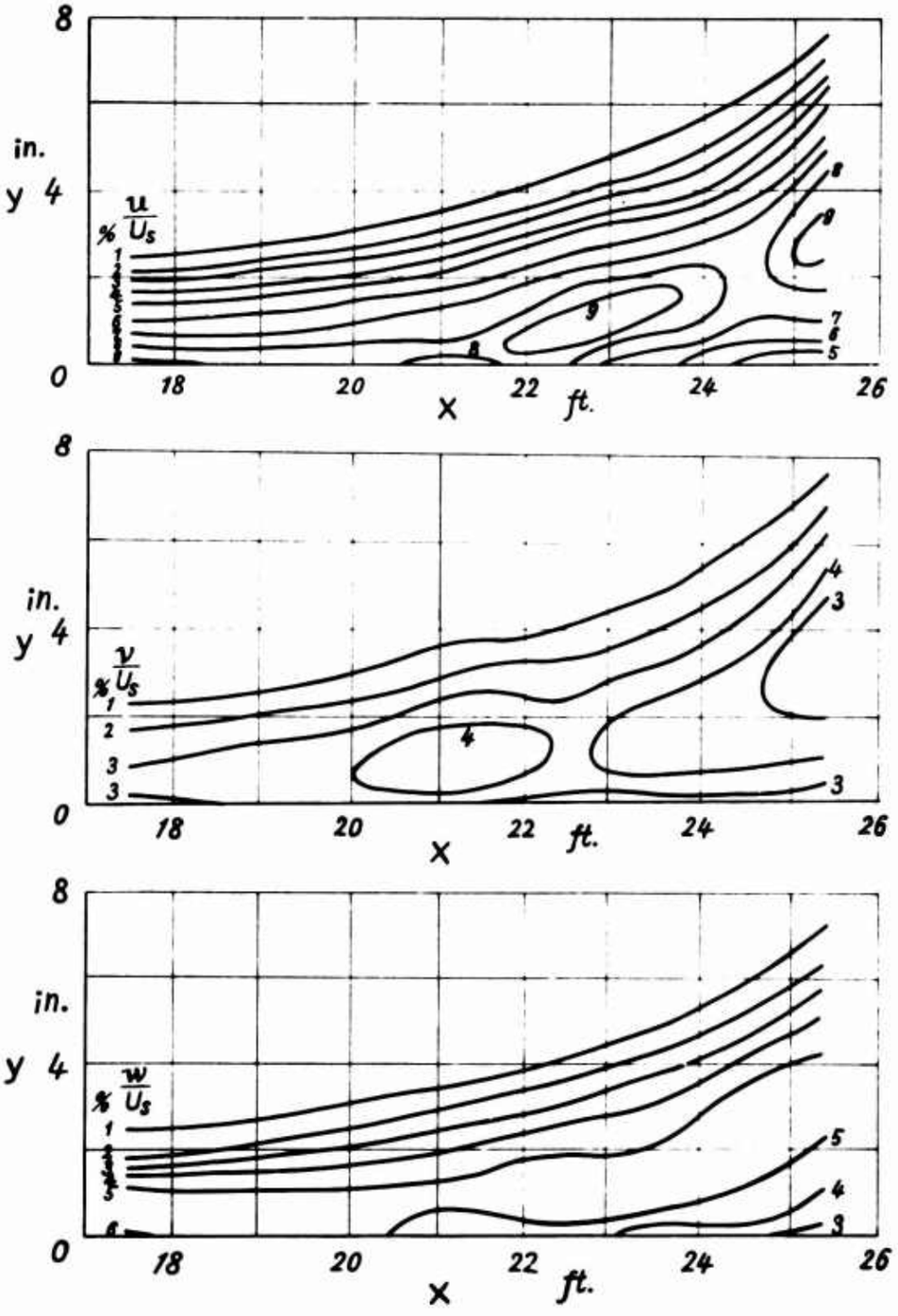

Figure 15. Distributions of the Intensities of the u-, v- and w-Fluctuation in Turbulant Boundary Layer Along a Curved Wall (reference 24). Undisturbed velocity U_s is 160 ft/sec at the position x = 17.5 ft., and the separation occurs near x = 25.7 ft.

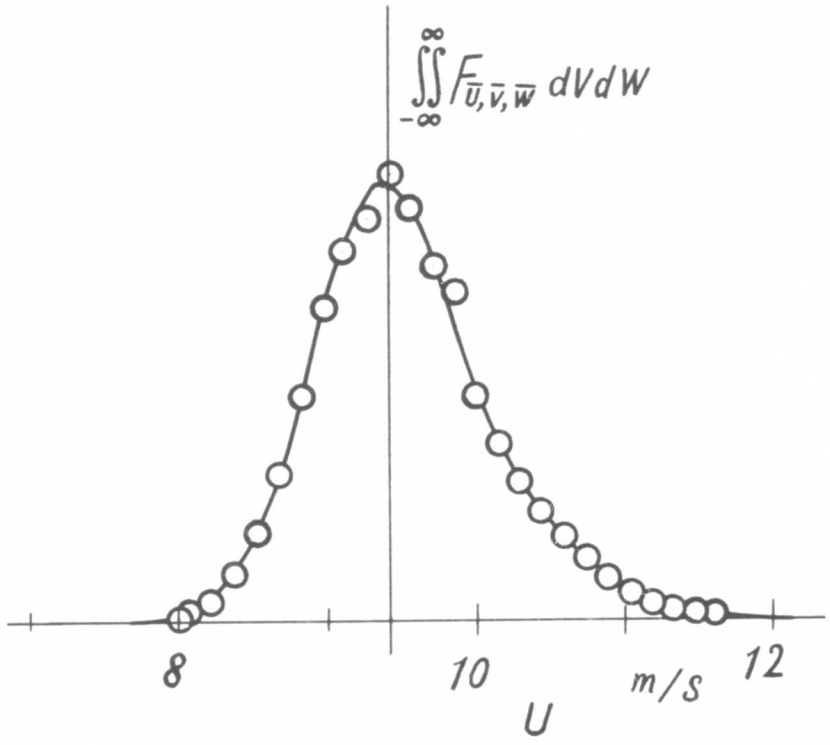

Figure 16. Observed Result of the Probability Distribution of the u-Fluctuation Around the Mean Velocity in a Turbulent Boundary Layer Along a Flat Plate.

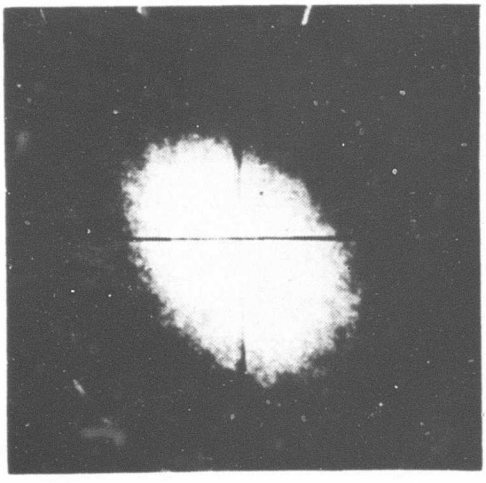

Figure 17. Photograph Showing the Probability Distribution of the u- and v-Fluctuation in a Turbulent Boundary Layer (reference 18). The state of flow is the same as in Figure 16. The coordinate axes on the picture have the same meaning as Figure 5.

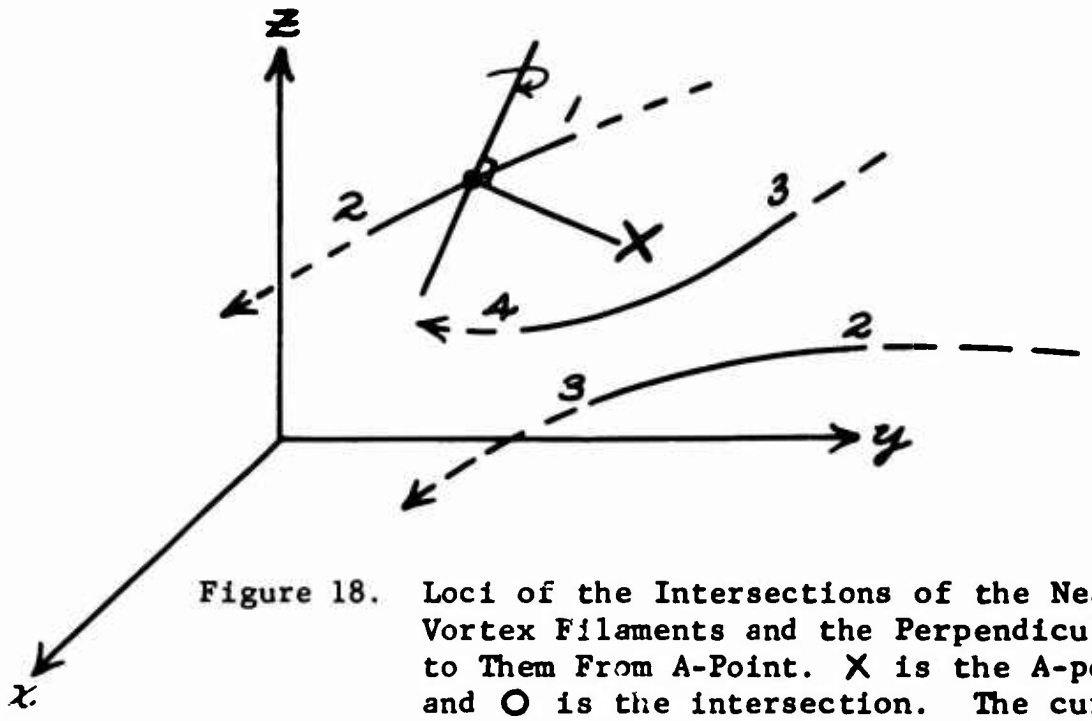

Figure 18. Loci of the Intersections of the Nearest Vortex Filaments and the Perpendiculars to Them From A-Point. X is the A-point and O is the intersection. The curves are the loci of the intersections whose parts of the full line are those in the nearest relation. Numbers 1, 2, 3, ... indicate the connections of a continuous time progress.

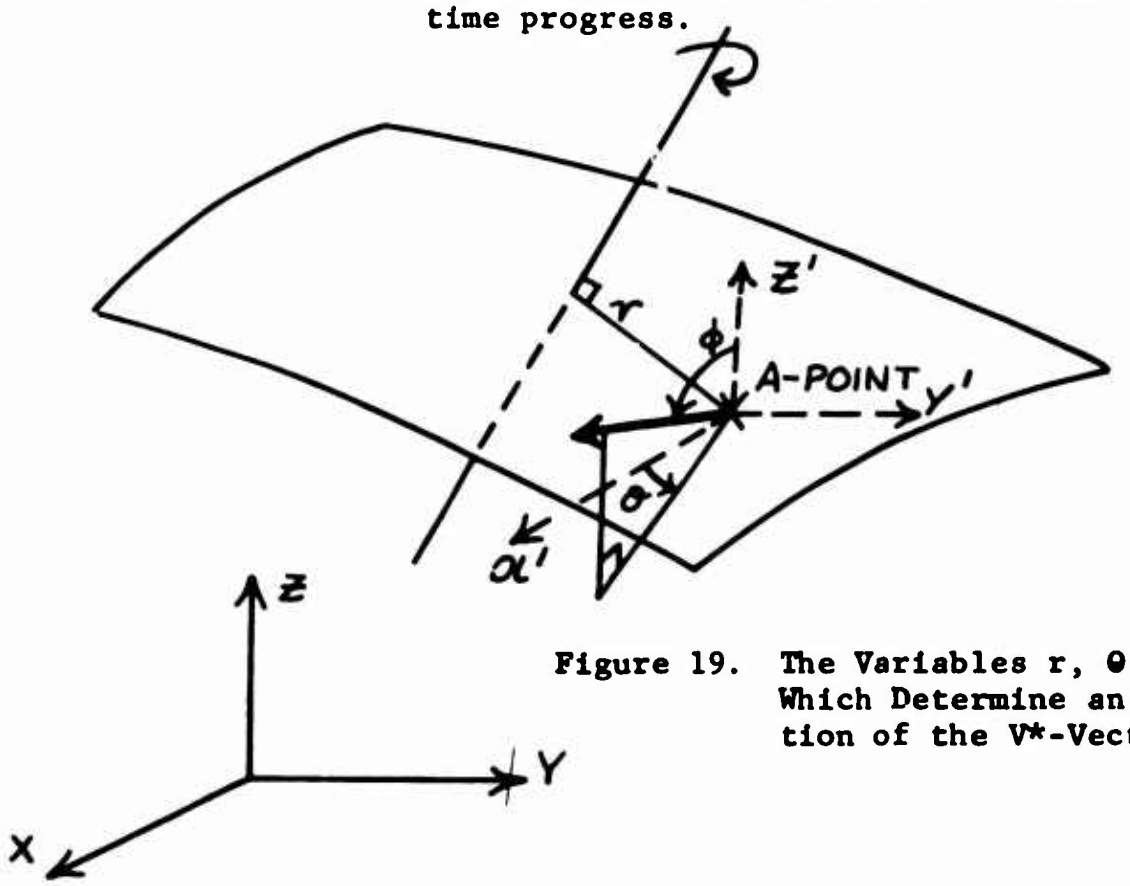

Figure 19. The Variables r, θ and φ Which Determine an Orientation of the V*-Vector.

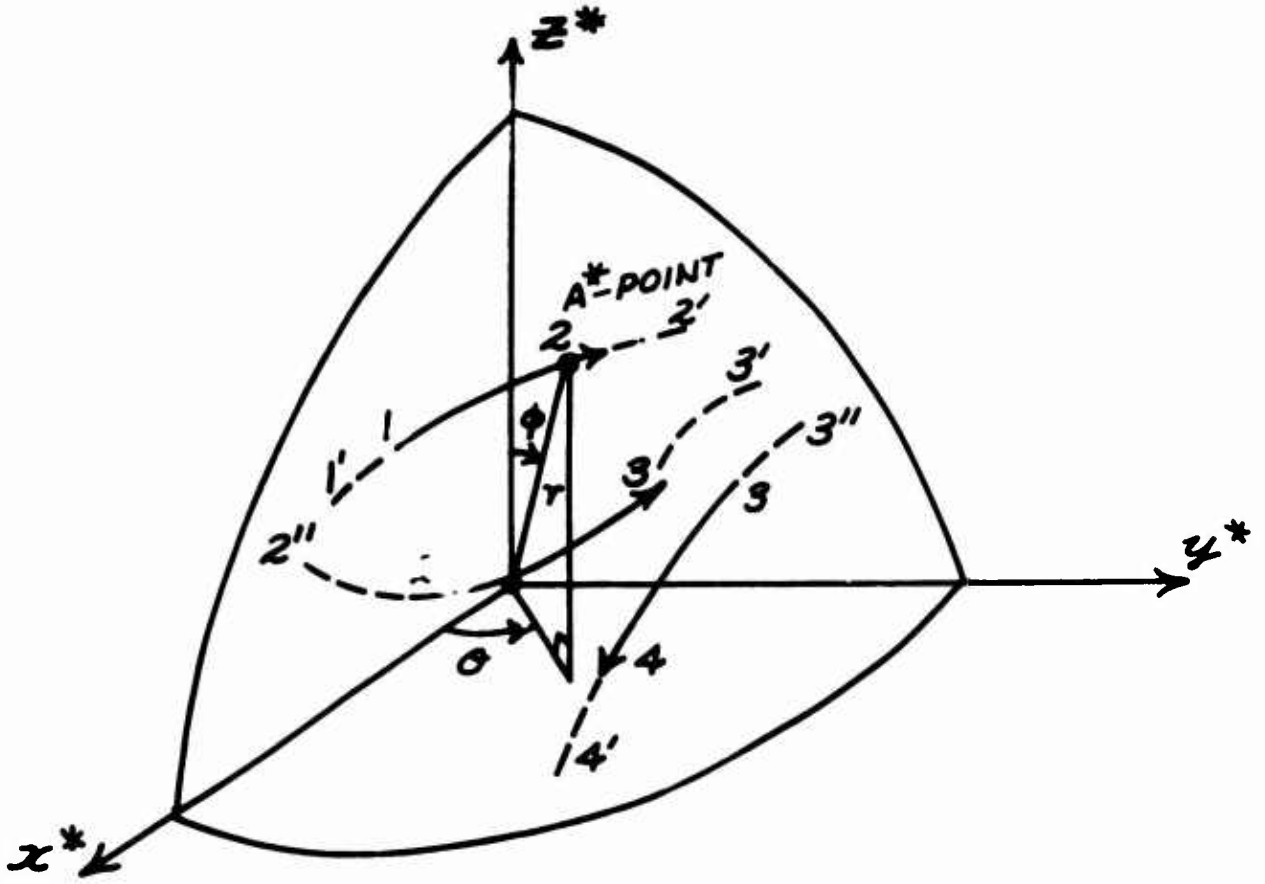

Figure 20. D*-Domain in the x*y*z*-Space. The full lines 12, 23, 34, ... correspond to the loci of the intersections shown in Figure 18. The dotted lines 1'1, 22', ... are the excessive parts included in Δt of (11.3), where the points 1', 2', ... are all on the boundary of D*-domain.

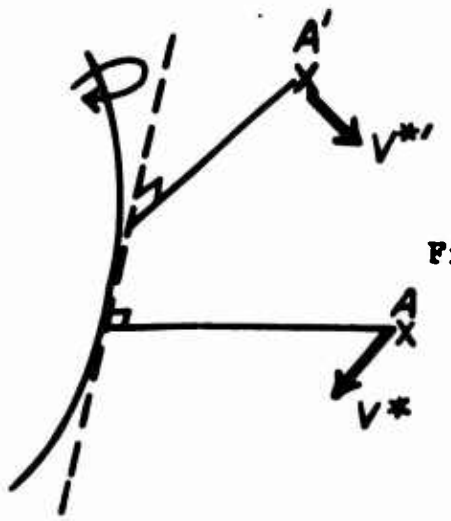

Figure 21. The V*- and V*'-Vectors, Respectively, at the A- and A'-Points Which Are due to the Nearest Vortex Motion to the A-Point.

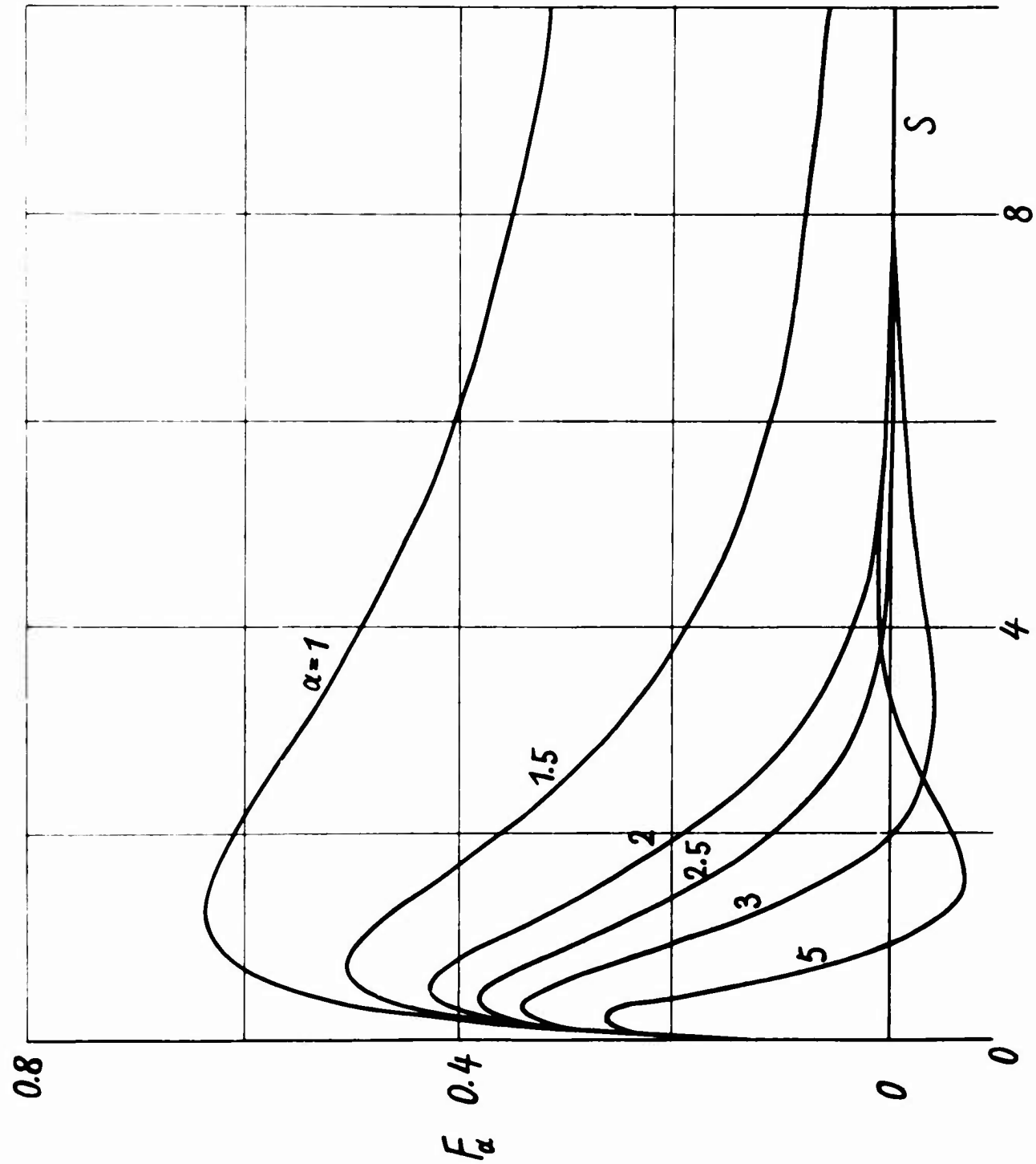

Figure 22. Functional Forms of Turning Velocity $F_\alpha(s)$ in (14.6).

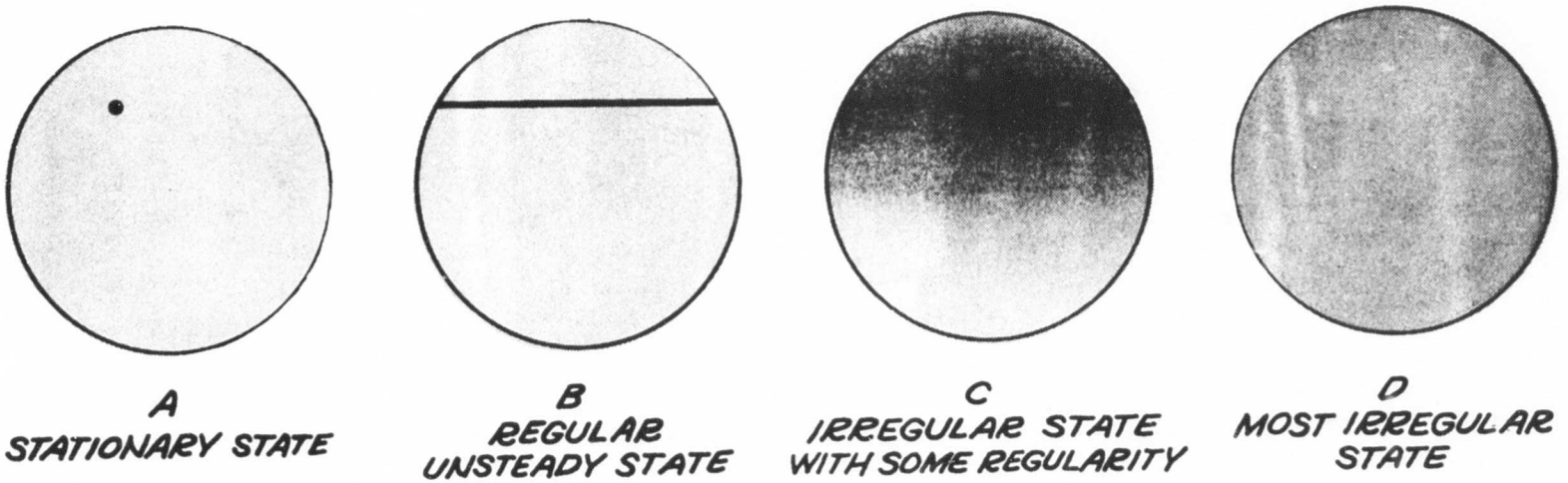

Figure 23. Conceptional Diagram Illustrating the Following Transition Character of the P*-Function in a Vortex Chaos Motion:

Vortex chaos motion : regular ⟶ irregular,
P*-function : singular ⟶ uniform.

Figures 4 and 5 show velocity fluctuations in the transition regions from (B) to (C) or (D). To study the state of flow in (A) or (B), hydrodynamical equations of motion must be taken as the foundation, but in cases (C) or (D), a statistical treatment becomes essentially important.

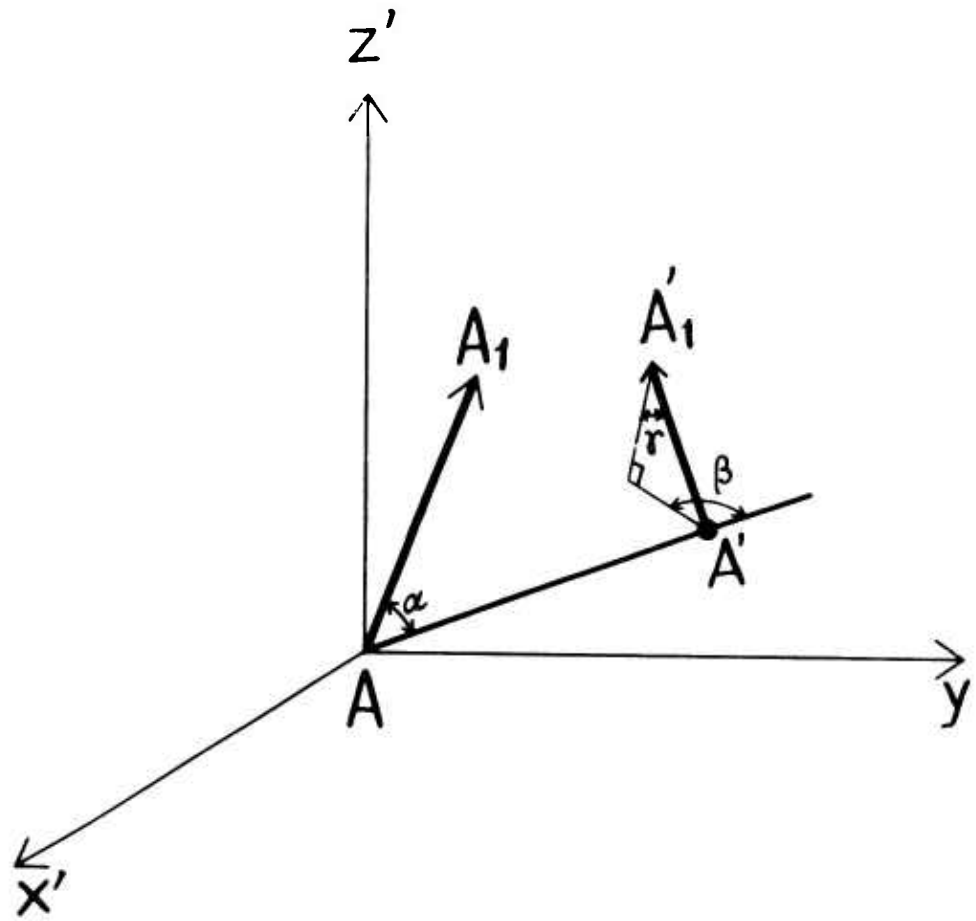

Figure 24. **Representation of Two Vectors $\overrightarrow{AA_1}$ and $\overrightarrow{A'A_1}$, Respectively, at the A- and A'-Points in the Field of Flow.**

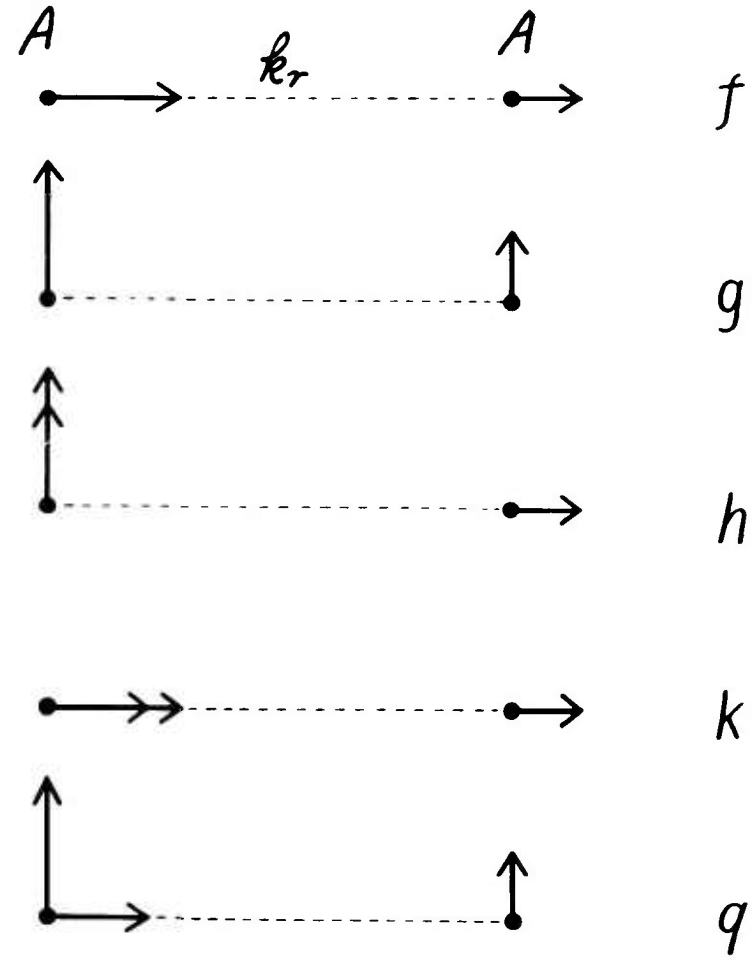

Figure 25. Fundamental Double and Triple Correlations.

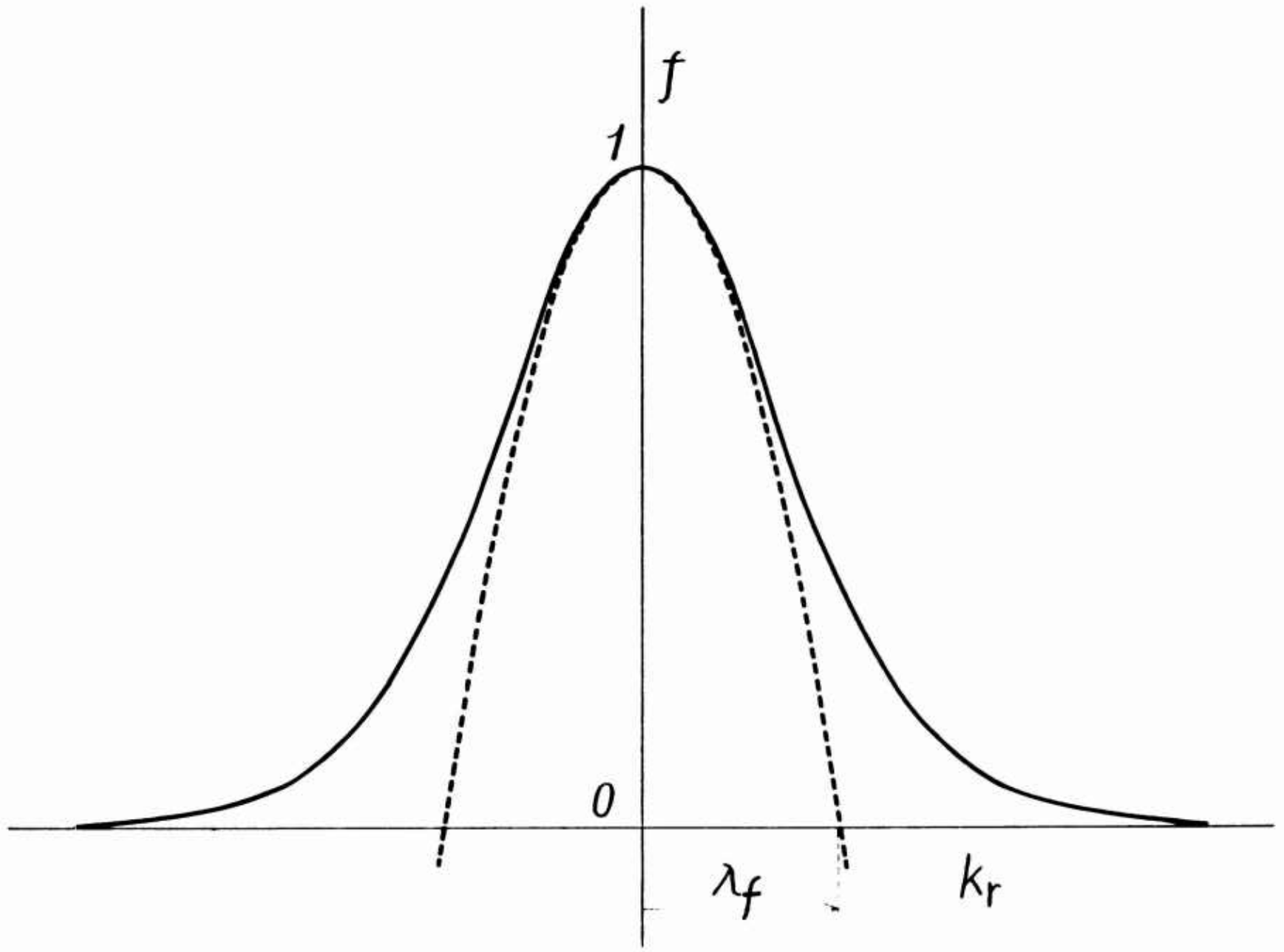

Figure 26. Definition of Microscale.

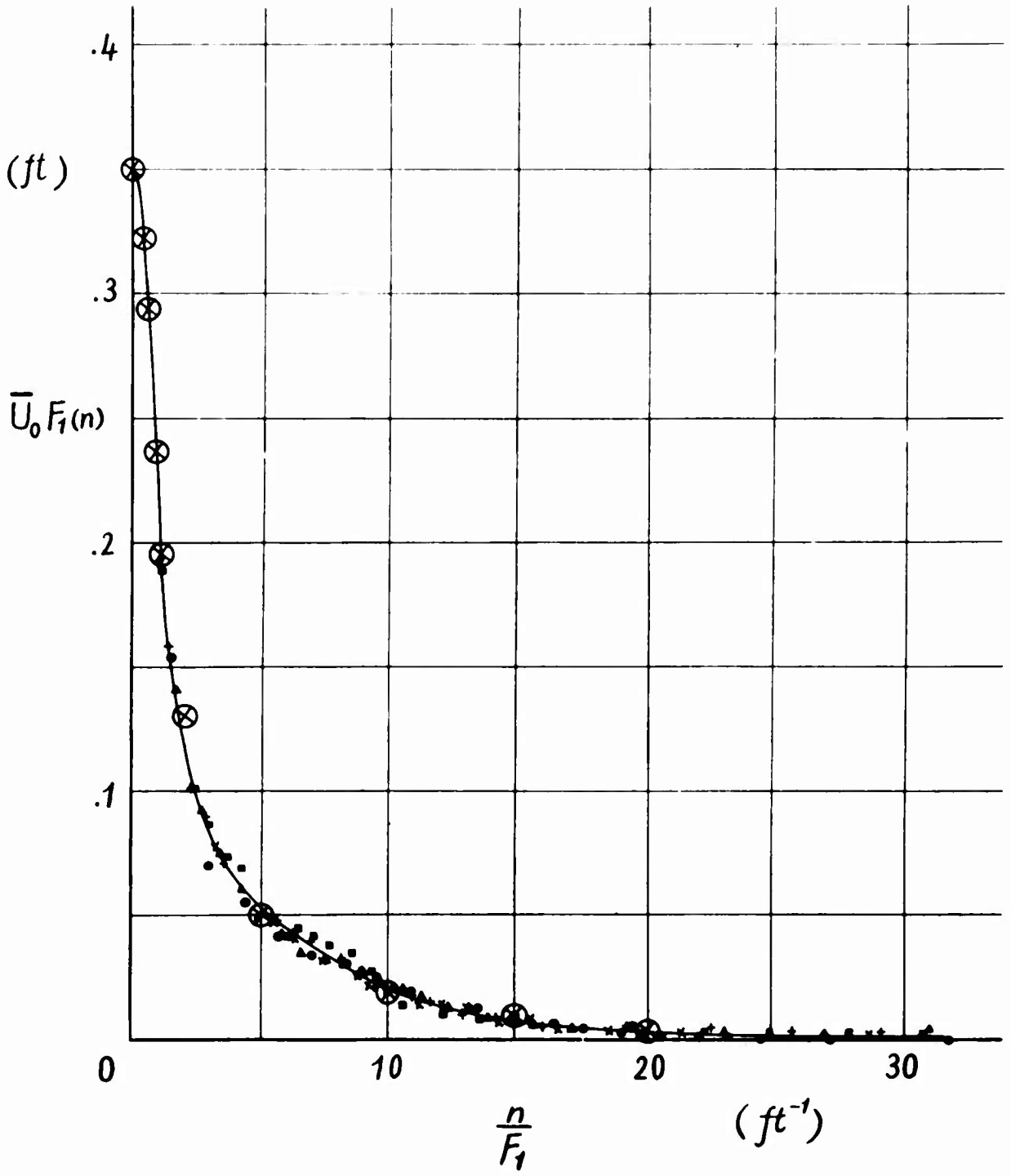

Figure 27. Spectrum Distributions in a Uniform Turbulent Wake Behind a Grid (reference 29). Mesh length M of the grid is 3 in., and measurements are made at the position x = 27M with various mean velocities of $\bar{U}_o$ = 15 (O), 20 (X), 25 (△), 30 (+), and 35 (□) ft. per sec. ● indicates the value evaluated by the second formula of (19.5) from observed values of $f(k_r)$ in Figure 28 for this case of the flow.

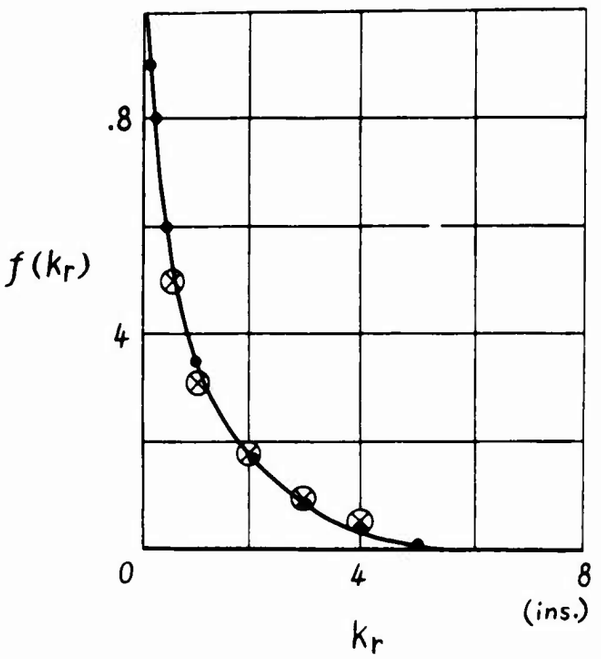

Figure 28. Correlation Distribution in a Uniform Turbulent Wake Behind a Grid (reference 29). ● is an observed value and ⊗ indicates the value evaluated by the first formula of (19.5) from the observed curve of $F_1(k_i)$ in Figure 27.

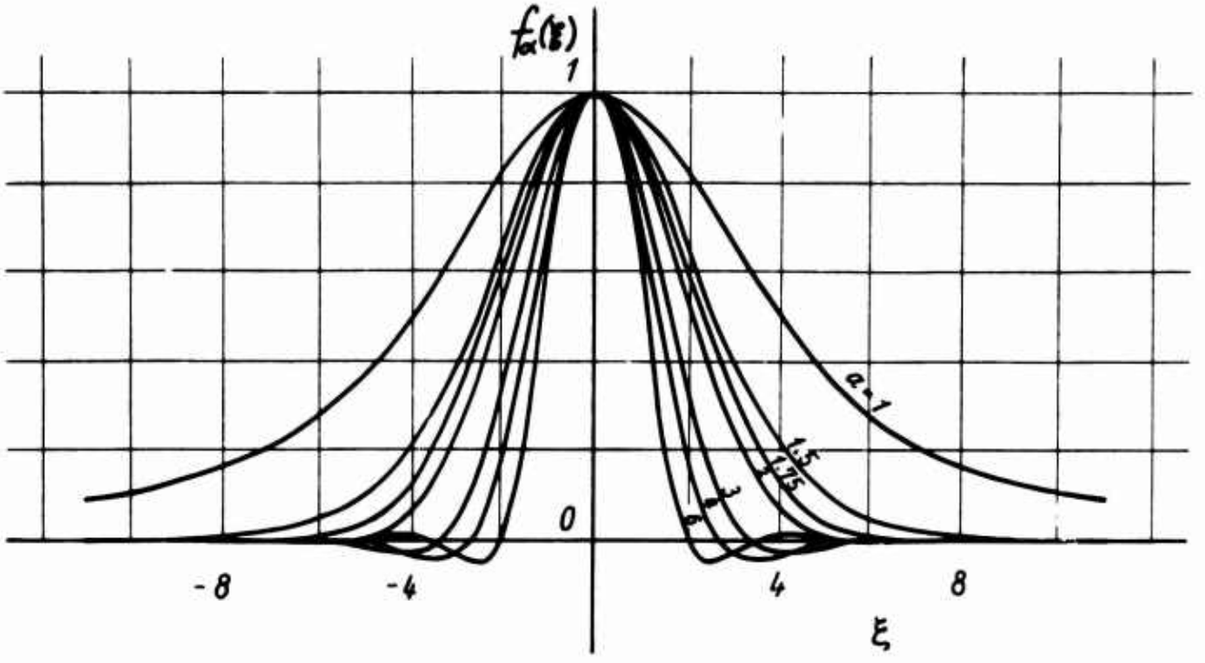

Figure 29. Functional Forms of the Similarity Correlation $f_\alpha(\xi)$ in (20.14).

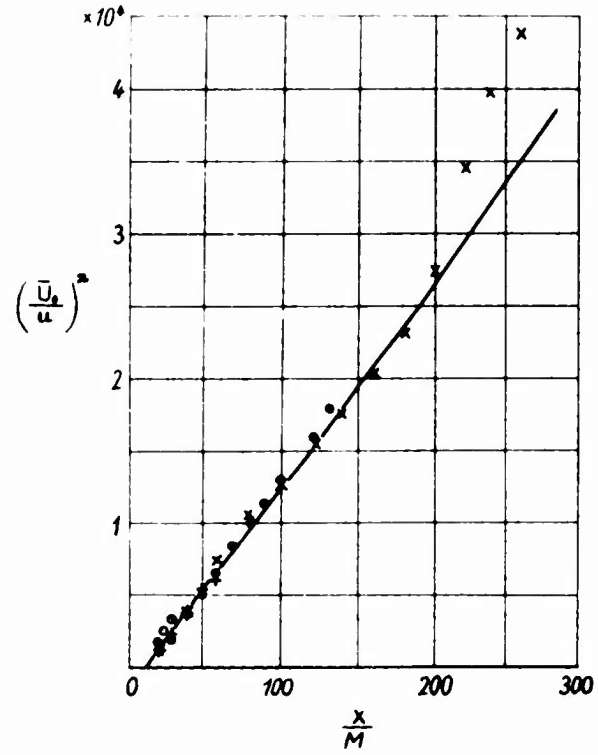

Figure 30. Decay of u-Intensity in a Uniform Turbulent Wake Behind a Grid (reference 32). Various grids of mesh length M of 0.635 cm. (X), 1.27 cm. (●), 2.54 cm. (+), and 5.08 cm. (⊙) are used in a mean velocity U_o of 12.86 m/sec.

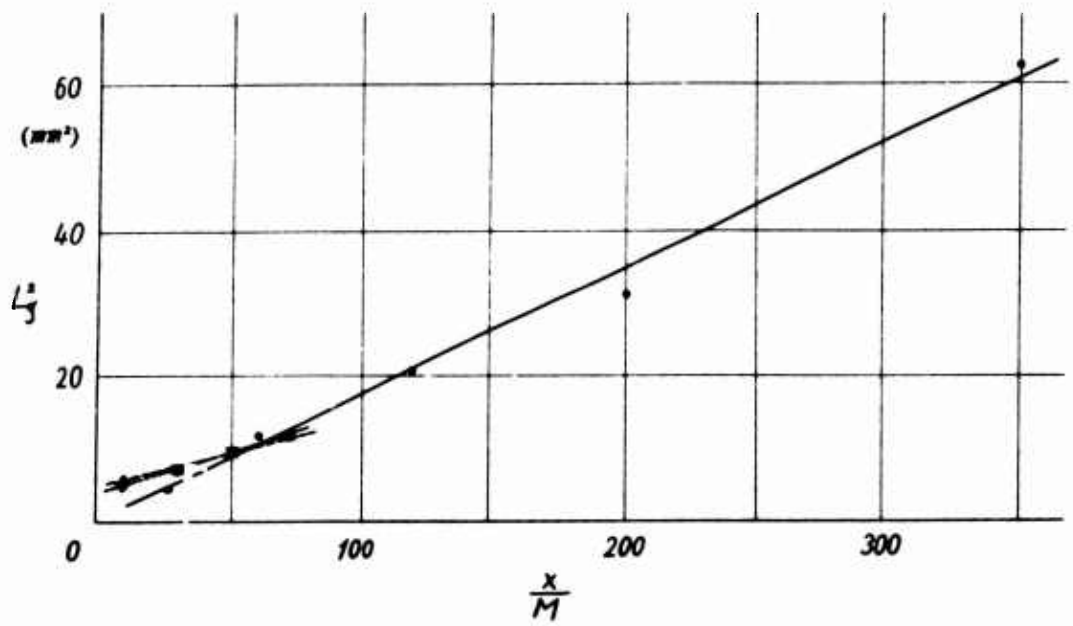

Figure 31. Distributions of an Integral Scale in a Uniform Turbulent Wake Behind a Grid (references 33 and 34). L is defined from the correlation g in the same manner as (20.15).

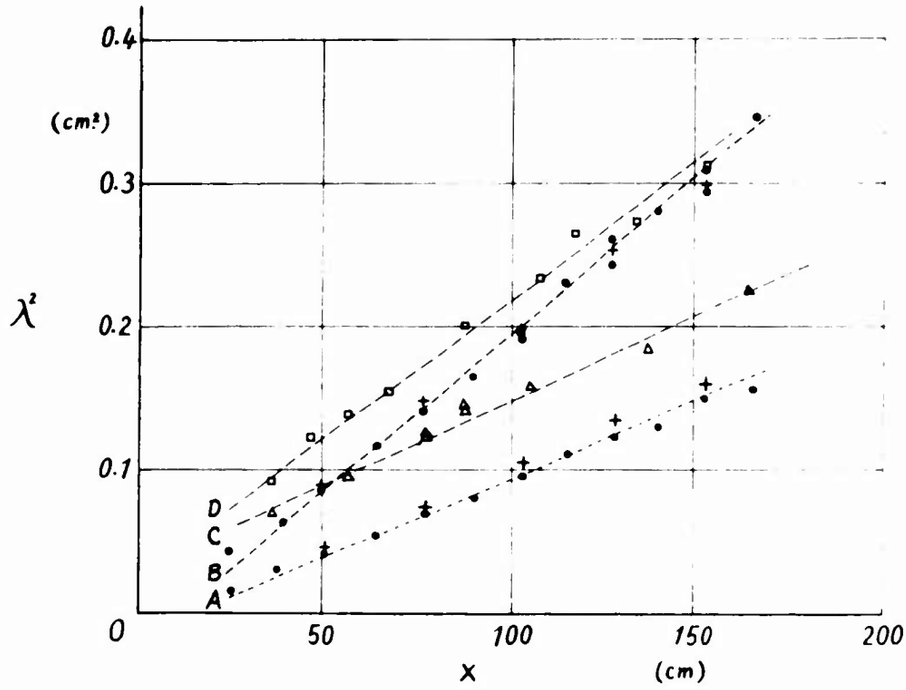

Figure 32. Distribution of the Microscale λ in a Uniform Turbulent Wake Behind a Grid. In one series of experiments (reference 35), three kinds of grids of mesh length M = 1.27 cm. (●), 2.5 cm. (+), and 5.08 cm. (⊙) are used with different mean velocity U_o = 12.86 m/sec (A-line) and 6.43 m/sec (B-line). In the other series (reference 36), a grid of M = 1.68 cm. is used with mean velocity U_o = 11.30 m/sec (Δ) (C-line) and 6.30 m/sec (□) (D-line).

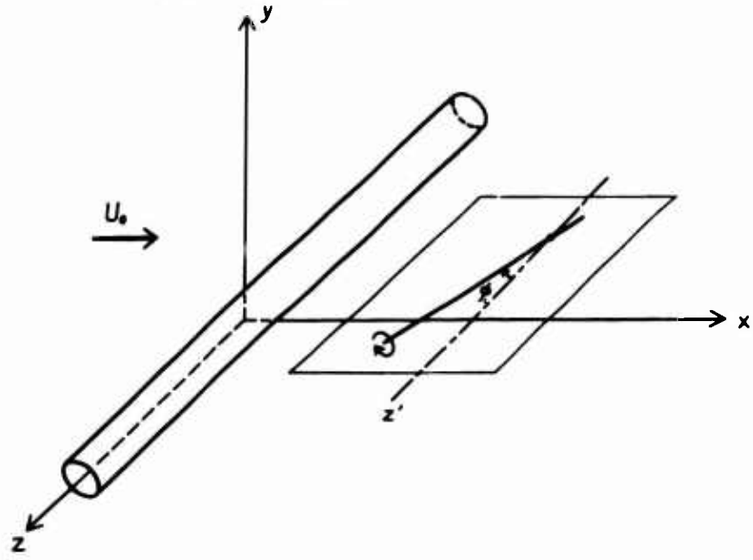

Figure 33. Orientation of Vortex Filament Behind a Circular Cylinder.

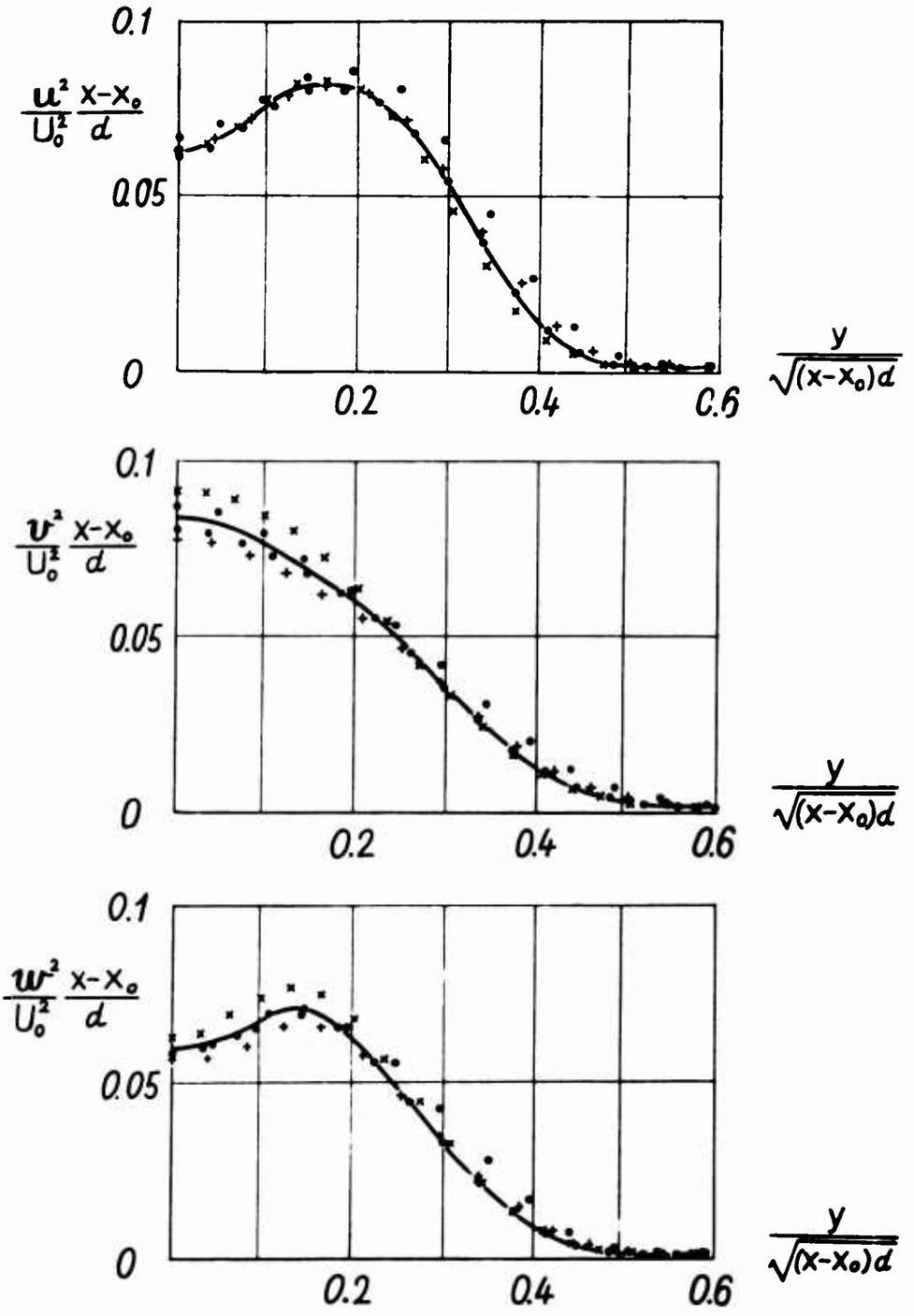

Figure 34. Distributions of u-, V- and W-Intensities Across the Turbulent Wake Behind a Circular Cylinder (reference 38). Measurements are made with the Reynolds number of $U_0 d/\nu$ = 1360 at different positions of x/d = 500 (●), 650 (+), 800 (○), and 950 (X), where d is the diameter of the cylinder.

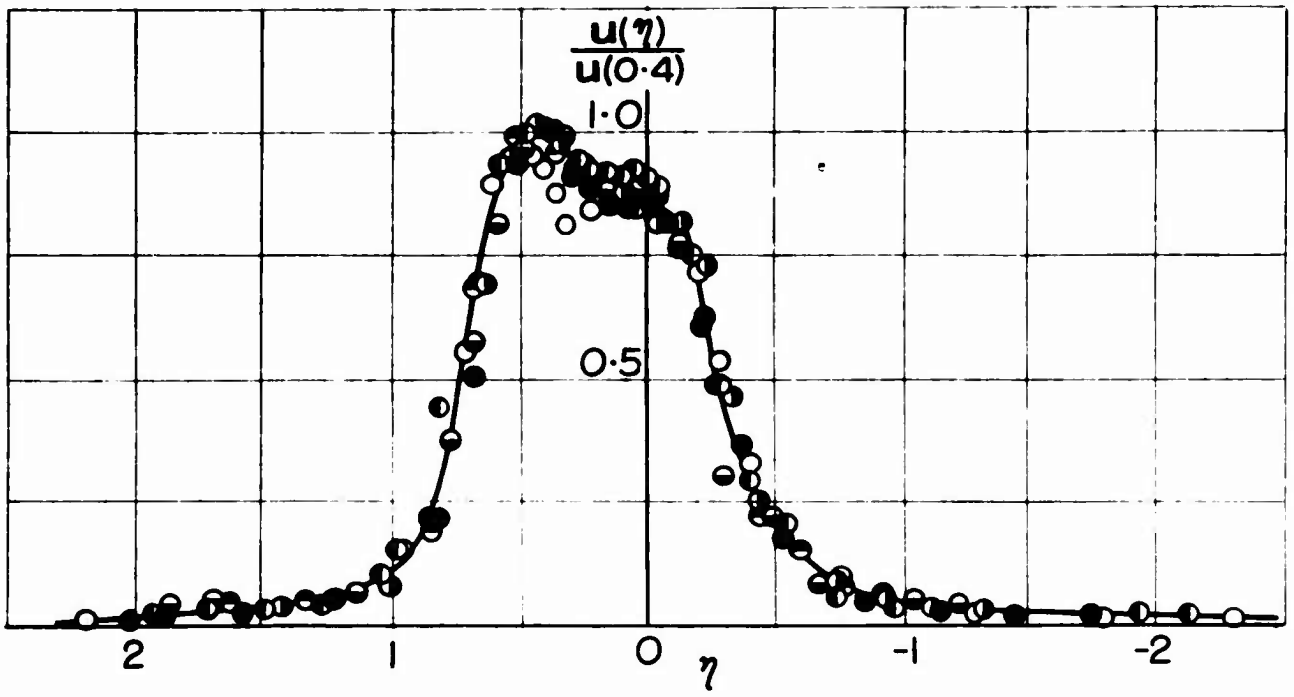

Figure 35. Distribution of u-Intensity Across a Turbulent Wake Behind an Airfoil (reference 18). The state of flow is the same as in Figure 6. Measurements are made at x/c = 0.37 (○), 1.38 (●), 2.32 (◐), 3.23 (◑), 4.41 (◒), and 5.13 (◓). η is defined by the half-width in the u - distribution, and the center line $\eta = 0$ is taken parallel to the mean flow from the trailing edge.

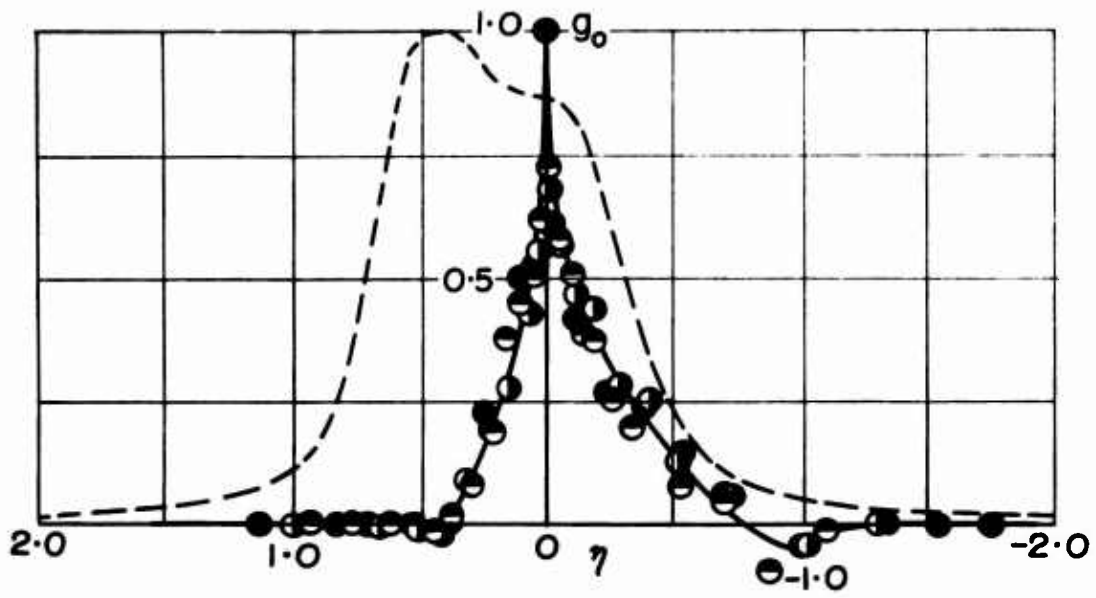

Figure 36. Distribution of the g-Correlation in the Turbulent Wake Shown in Figure 35 (reference 18). ●, ◑ and ◒ are in the same positions as in Figure 35, and the broken line shows the u-distribution.

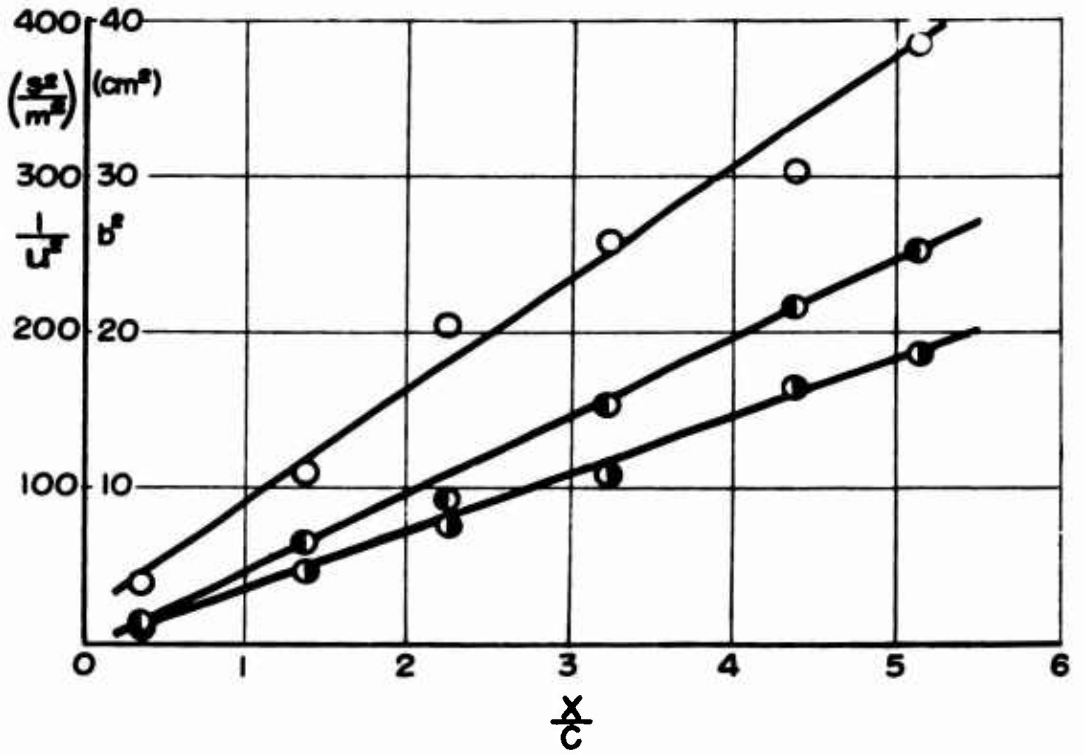

Figure 37. Distribution of Turbulent Intensity and Scale Along the Turbulent Wake Shown in Figure 35 (reference 18). ◐ and ◑ are observed values of u-intensity at η = 0 and 0.4. b is that of the half-width in the u-distribution.

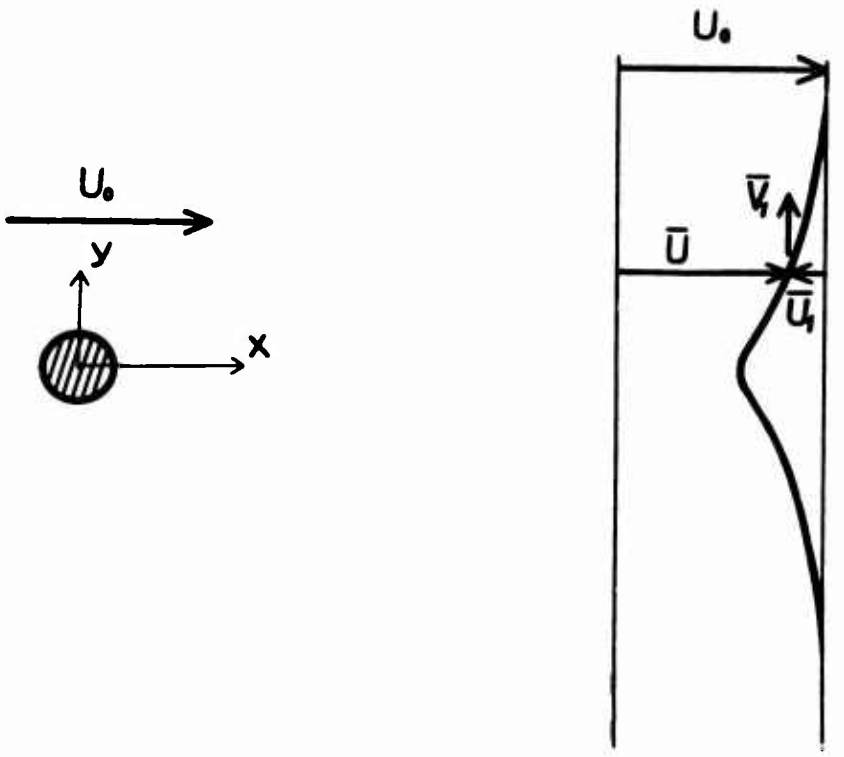

Figure 38. Representation of Velocity Profile Behind a Circular Cylinder.

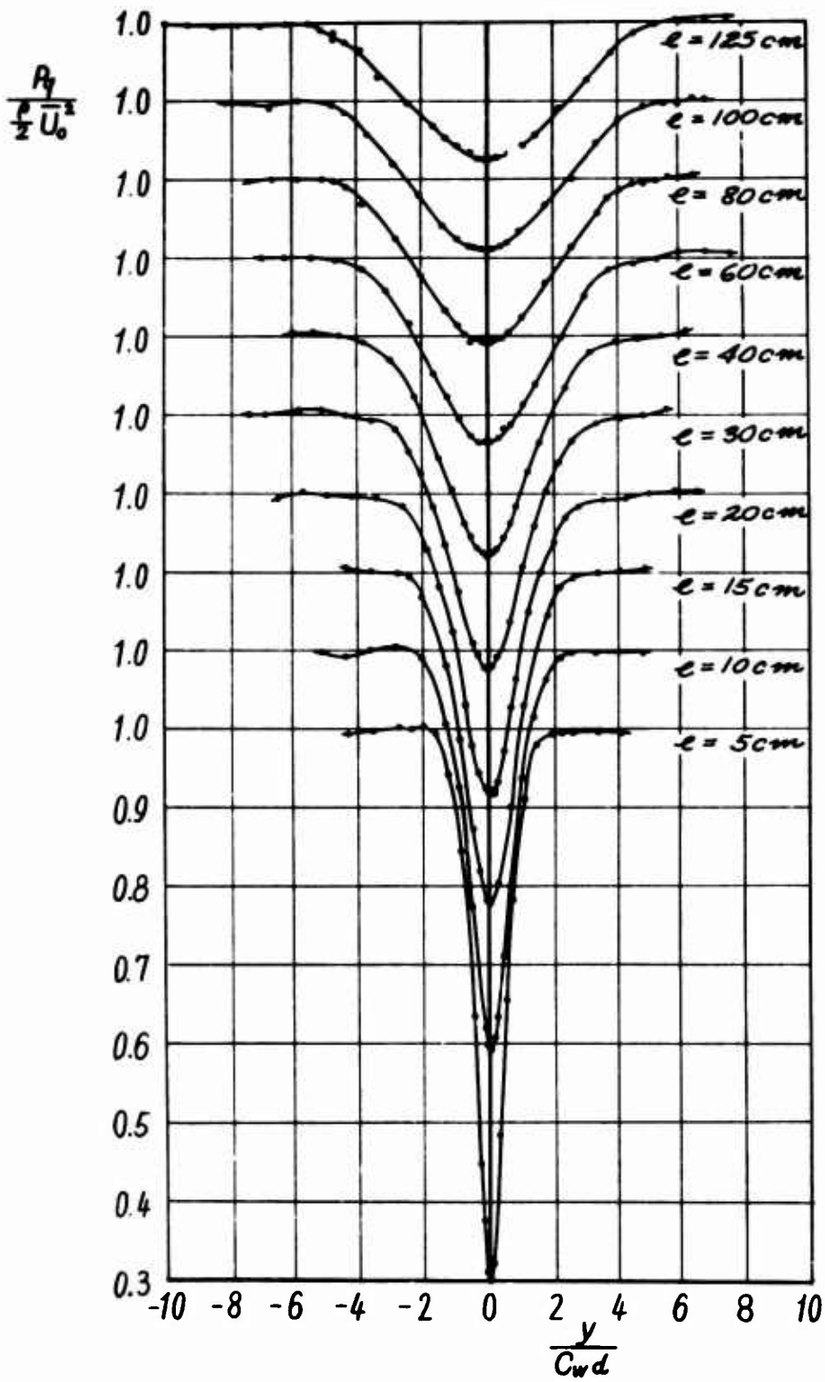

Figure 39. Distributions of Total Pressure Behind A Circular Cylinder. The diameter, d, is 1 cm.; the resistance coefficient C_w is 1.32; and the Reynolds number $\bar{U}_o d/\nu$ is 2.38×10^4. The distance from the cylinder is denoted by e.

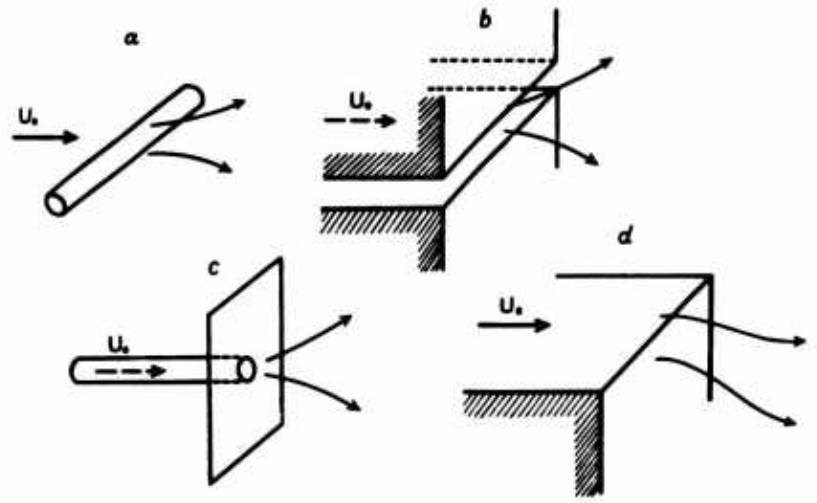

Figure 40. Illustration of Typical Decaying Shear Turbulence.

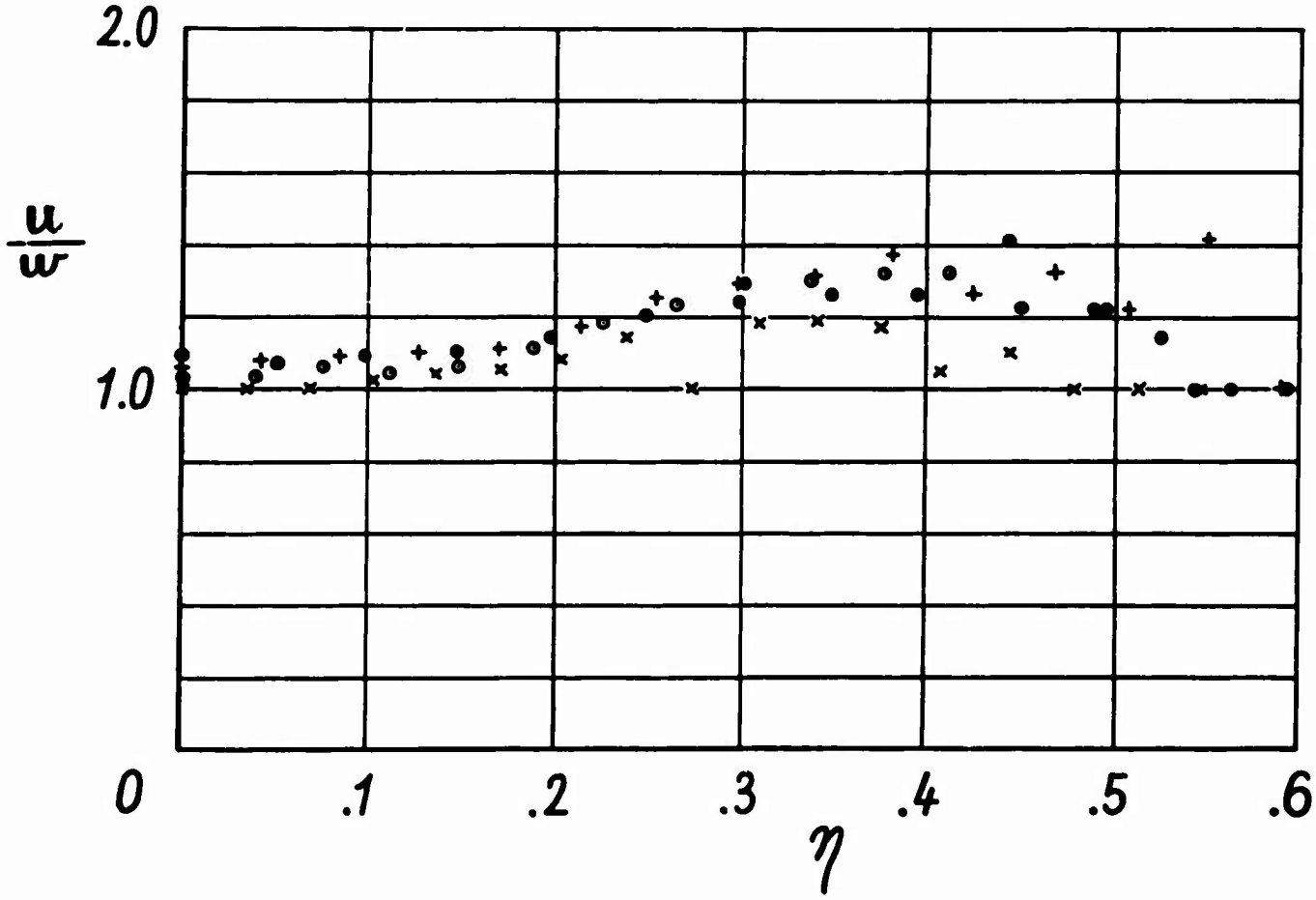

Figure 41. Distribution of u/w Across the Turbulent Wake Shown in Figure 34 (reference 38). ●, +, ⊙, and X are the evaluated values from the data in Figure 34 at the locations of x/d = 500, 650, 800, and 950, respectively.

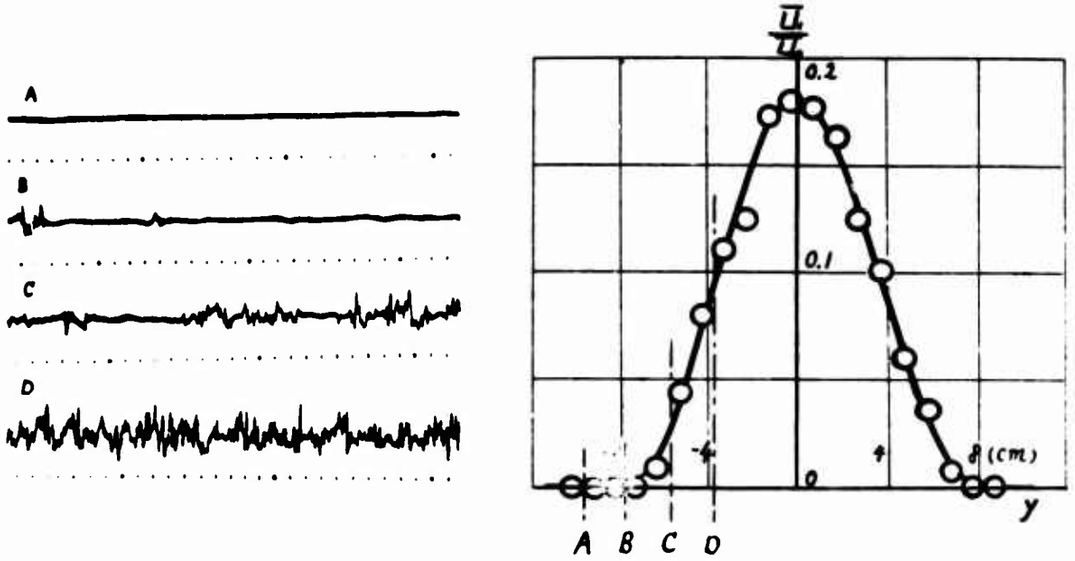

Figure 42. Measurement of the Mean and the Fluctuational Velocity in the Turbulent Wake Behind a Circular Cylinder. A, B, C, D on the mean-velocity curve indicate the respective positions of the oscillogram. The diameter is 1.5 cm., the distance is 48.7 cm., and the undisturbed velocity $\overline{U}_0$ is 3.54 m/sec.

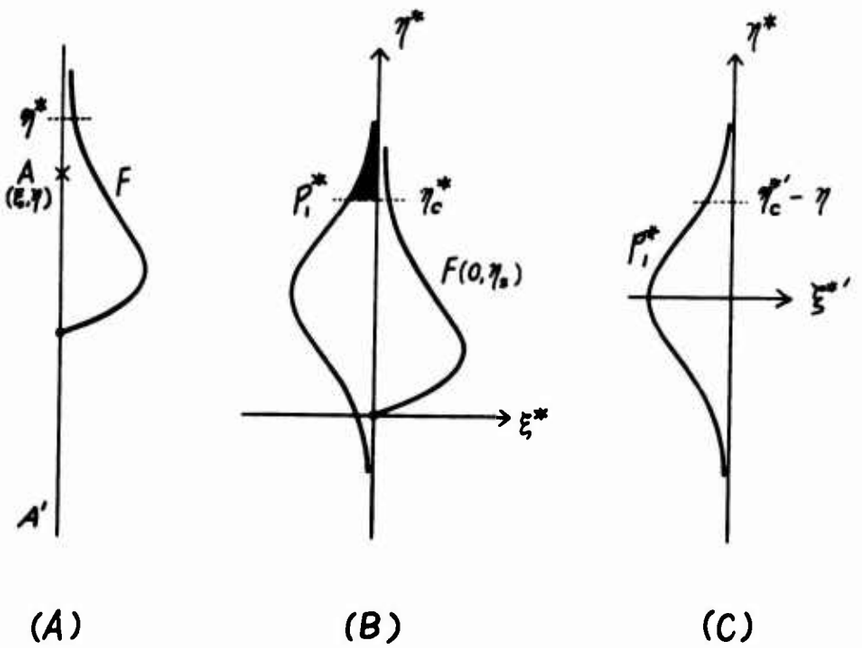

Figure 43. Illustration of the P*- and F-functions at a Point in the Initial Period.

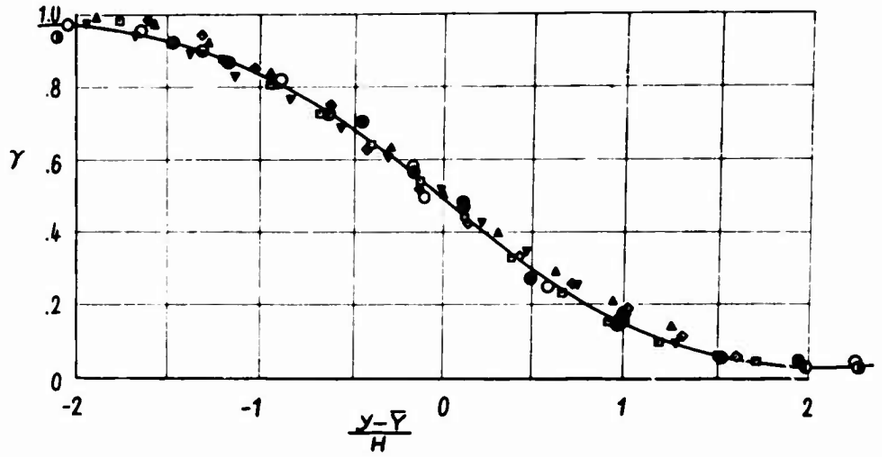

Figure 44. Distribution of the Intermittency Factor γ Across the Turbulent Wake Behind a Circular Cylinder. Measurements are made at positions of x/d = 500 (△), 650 (◇), 800 (□), and 950 (▽) in one series (reference 42); and in another series with various mean velocities of U_o = 3.07 (○), 7.26 (●), 10.85 (◑), 14.92 (◐), and 19.96 (◒) m/sec. at a position of x/d = 33.7 behind a cylinder of the diameter d = 1.5 cm. (reference 37). The curve shows the Gaussian-integral formula (26.7) with Y and H, the position of the center and the dispersion of the formula, respectively.

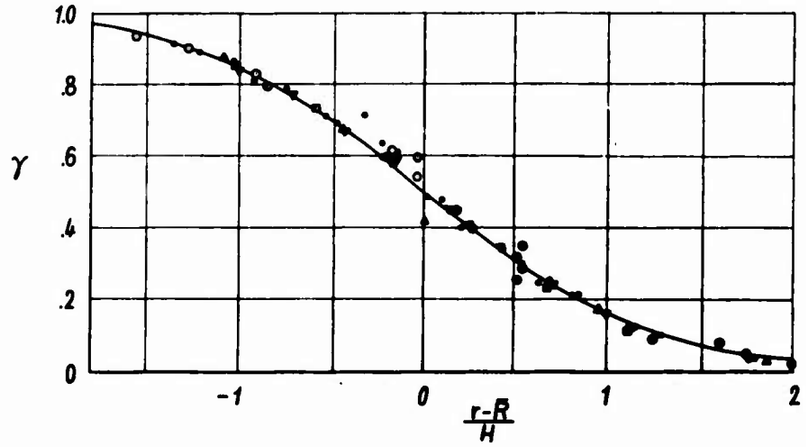

Figure 45. Distribution of the Intermittency Factor γ Across a Turbulent Round Jet (reference 41). Measurements are made at $x/(2r_o)$ = 20 (△), 37 (●), 37 (⊙), 46 (□), 64.5 (▽), and 76 (○). The curve shows the Gaussian-integral formula (26.7) with R the position of the center and r_o the radius of the nozzle.

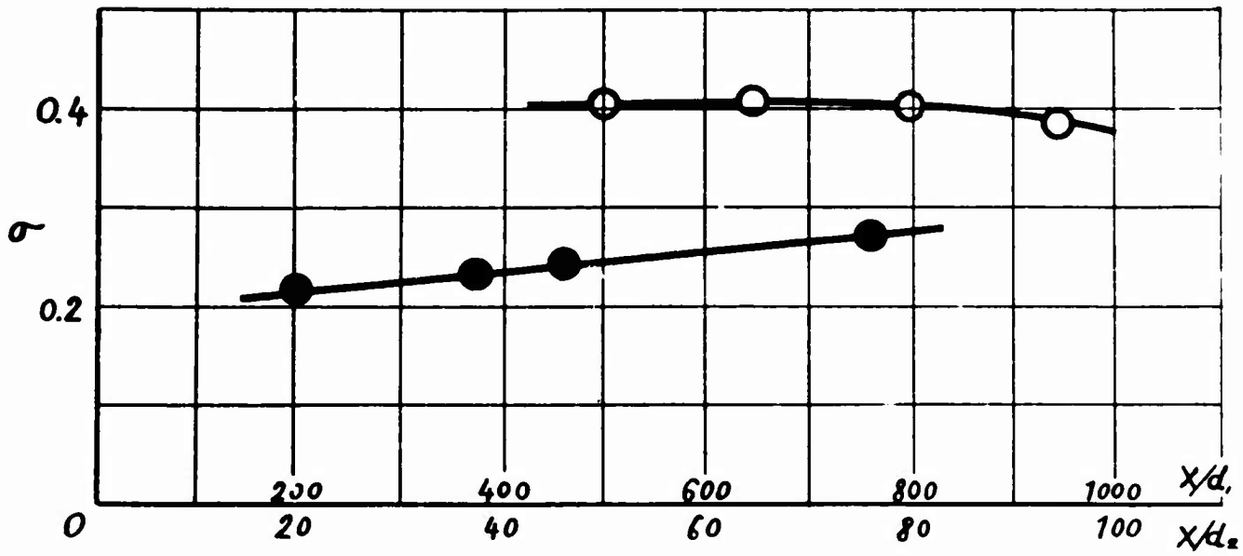

Figure 46. Distribution of the Nondimensional Dispersion σ Along the Flow. O is the evaluated value from the data in the turbulent wake behind a circular cylinder referred to in Figure 44 (reference 42), and ● is from the data of the turbulent round jet in Figure 45 (reference 39). d_1 and d_2 are diameters of the cylinder and nozzle, respectively.

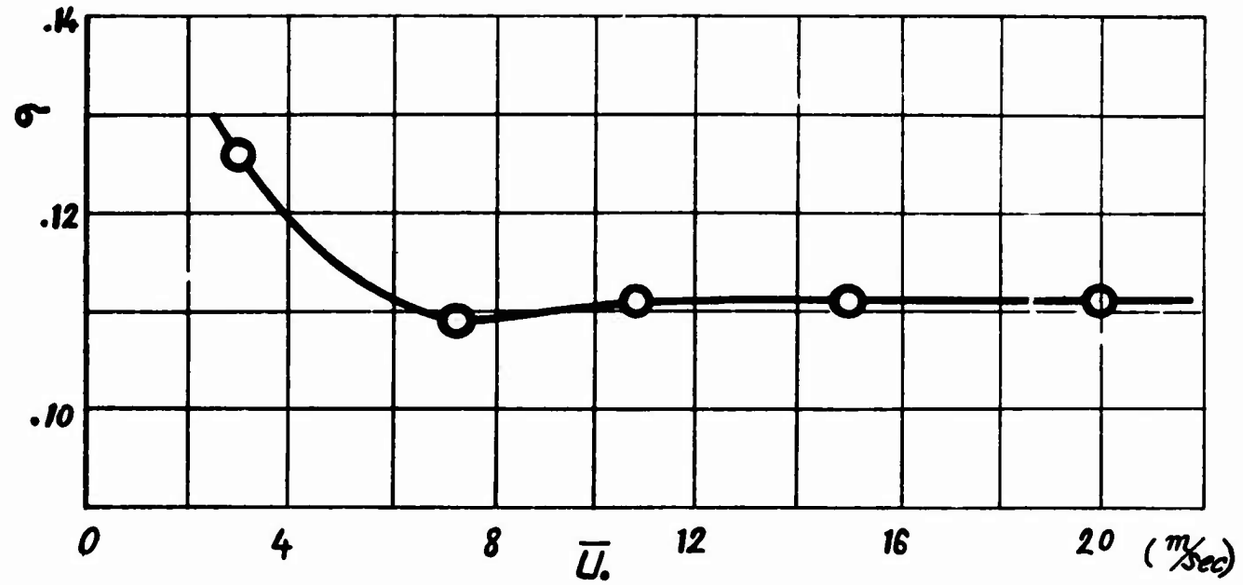

Figure 47. Variation of the Nondimensional Dispersion σ Versus the Mean Velocity $\bar{U}_o$ in the Turbulent Wake Behind a Circular Cylinder (reference 37). Data are taken from the same experiment as in the second series of the experiment in Figure 44.

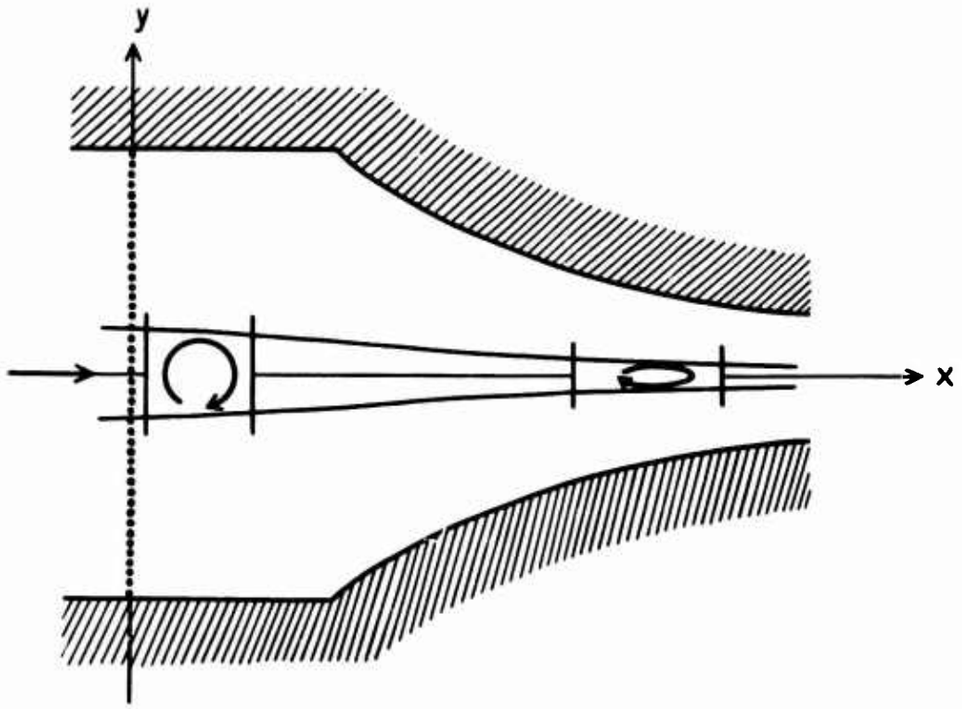

Figure 48. Diagonal Sketch of a Nonuniform Shearless Turbulence.

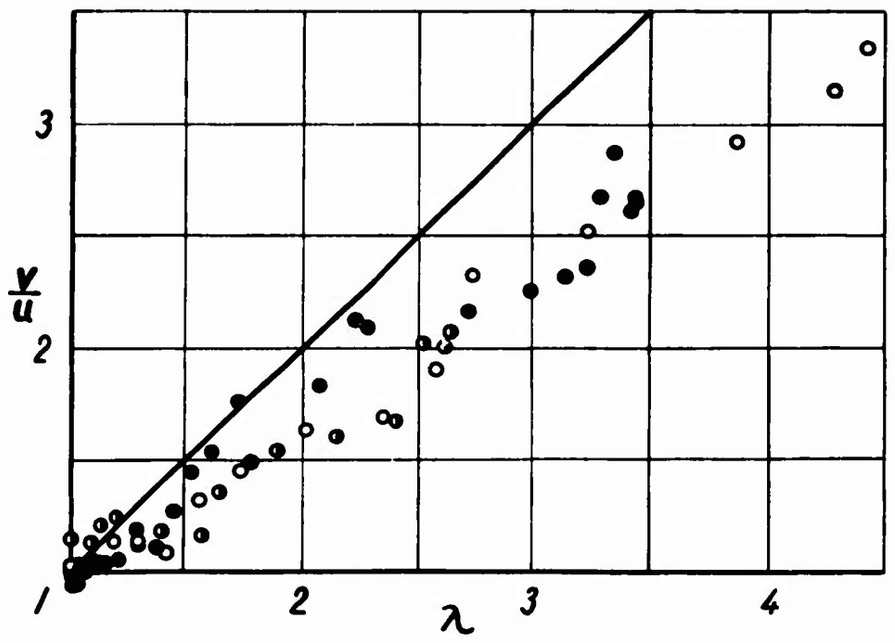

Figure 49. Variation of v/u Versus the Contraction Ratio λ of (27.1) (reference 37). Different marks imply experimental set-ups with different contraction ratios. The straight line is deduced from (27.3).

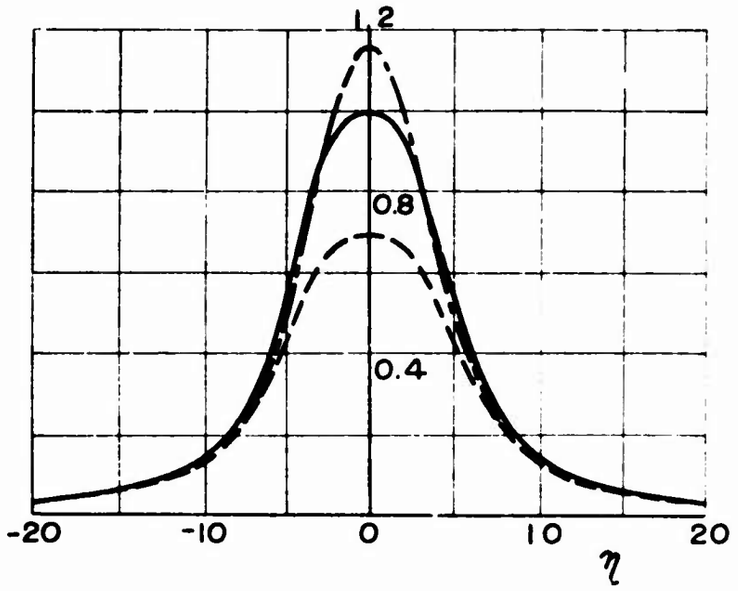

Figure 50. Calculated Curves of Relative Profiles of $C_u^2(\eta)$ (solid line), C_v^2 (chain line), and $C_{\overline{uv}}(\eta)$ (broken line) of (25.2) Across an Idealized Symmetrical Shear Turbulence.

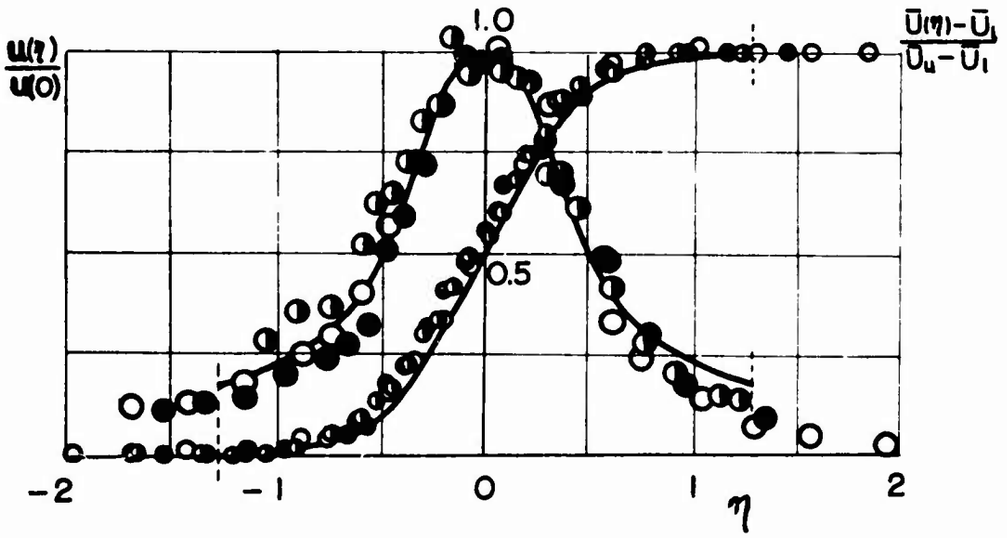

Figure 51. Distribution of Mean Velocity (small marks) and u-Intensity Across a Half-Jet as Shown in Figure 40 (d). $\bar{U}_u$ and $\bar{U}_l$ are mean velocities at upper and lower parts of the free stream. ○, ● and ◑ are observed values at x = 25.0, 40.9, and 56.7 cm. from the step along the x-axis, and the undisturbed velocity $\bar{U}_o$ is 18.7 m/sec. The two curves are calculated curves in Figure 50 and from equation (24.16).

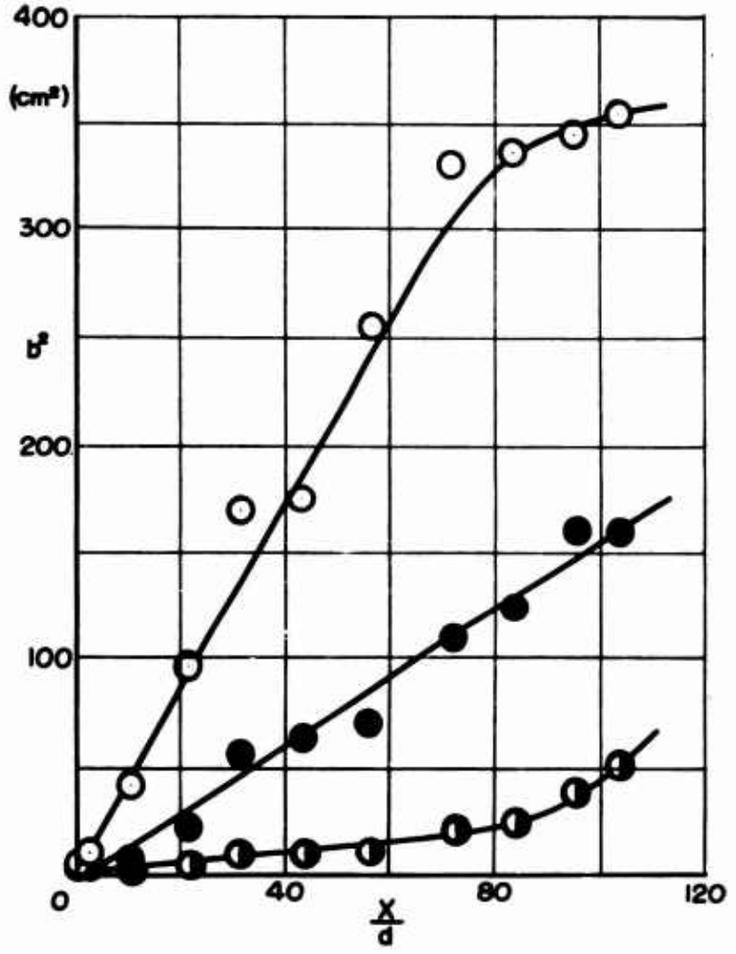

Figure 52. Distribution of the Width of a Turbulent Wake Behind a Circular Cylinder. The diameter d = 1.5 cm. and the undisturbed velocity U_o = 3.74 m/sec. ◑, ●, and ○ are observed values at the sections where $\overline{U}_1(\eta)/U_o(o)$ = 0.95, 0.50, and 0.10.

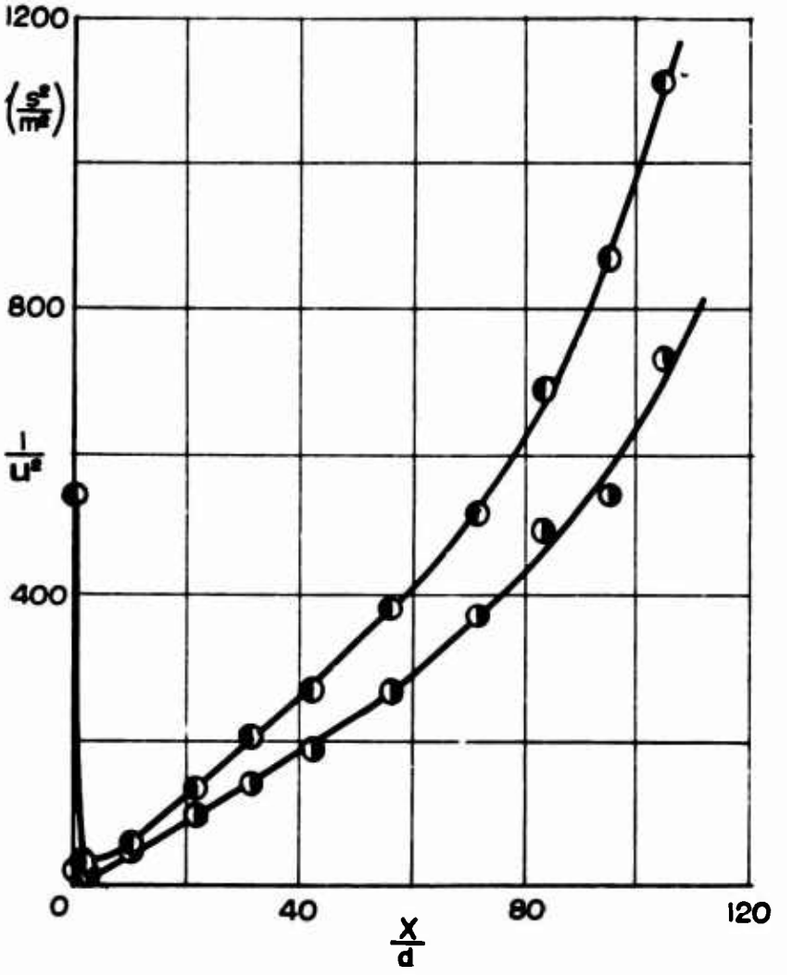

Figure 53. Distribution of u-Intensity Along the Turbulent Wake in Figure 52. ◐ and ◑ are observed values at η = 0 and 0.4 (maximum across the wake) (cf. Figure 34).

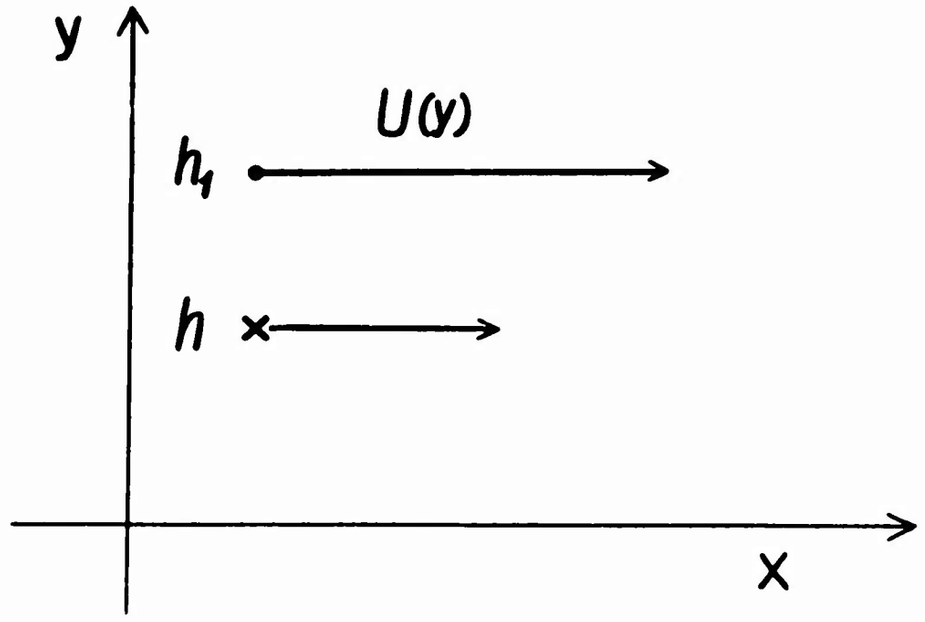

Figure 54. Representation of Velocities at Two Points Across a Shear Flow.

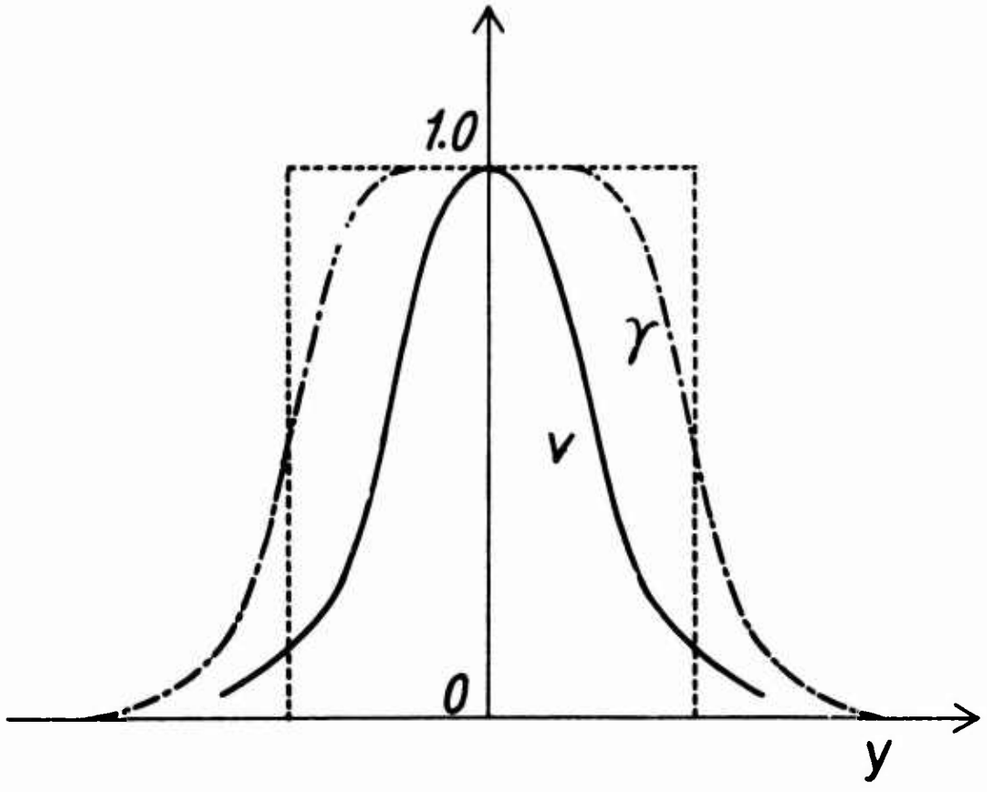

Figure 55. Profiles of an Intermittency Factor γ and Velocity v Across a Decaying Turbulence.

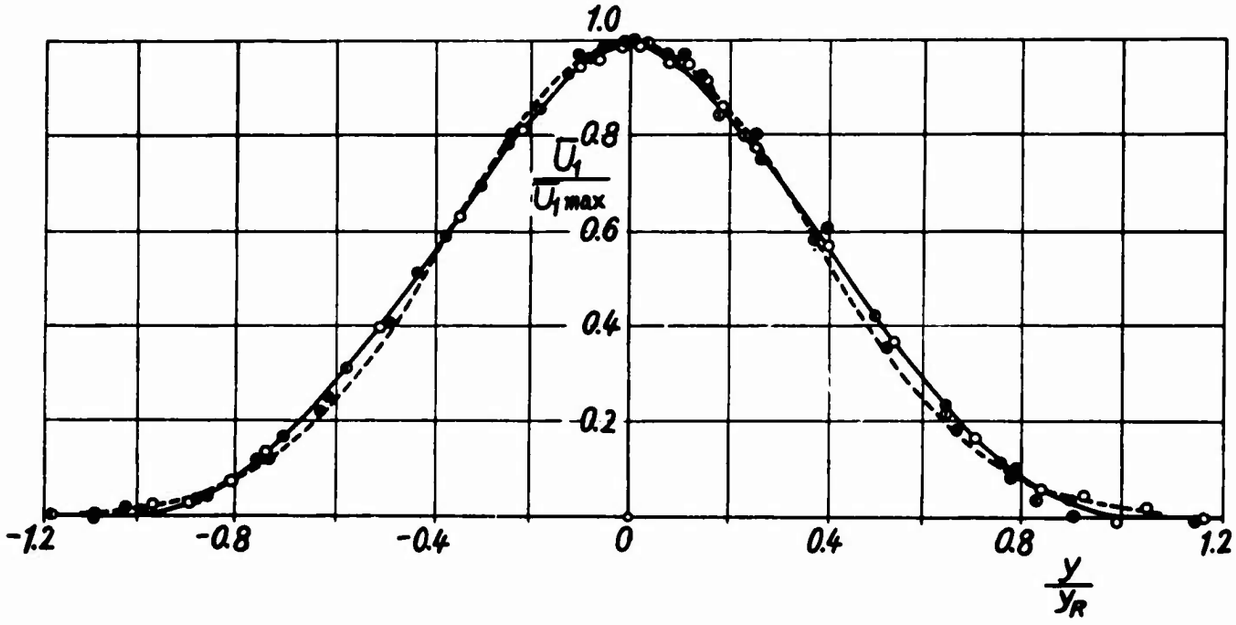

Figure 56. Distribution of Mean Velocity Across the Turbulent Wake Behind a Circular Cylinder. The full and broken lines show the solutions respectively of (34.13) and (34.9). ○, ⊙, ⊗, and ● are observed values, respectively, at x/d = 80, 100, 166.5, and 208 (reference 39). Y_R is the width of the wake.

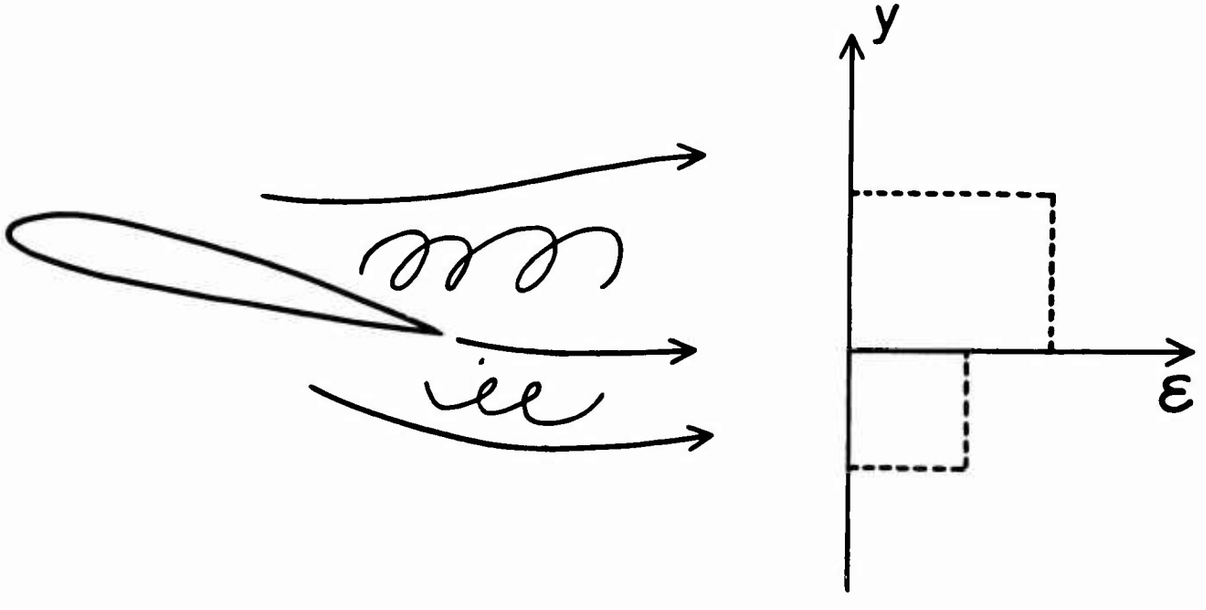

Figure 57. Diagonal Sketch of the Profiles of Different Values of ε Across the Wake Behind an Asymmetric Airfoil.

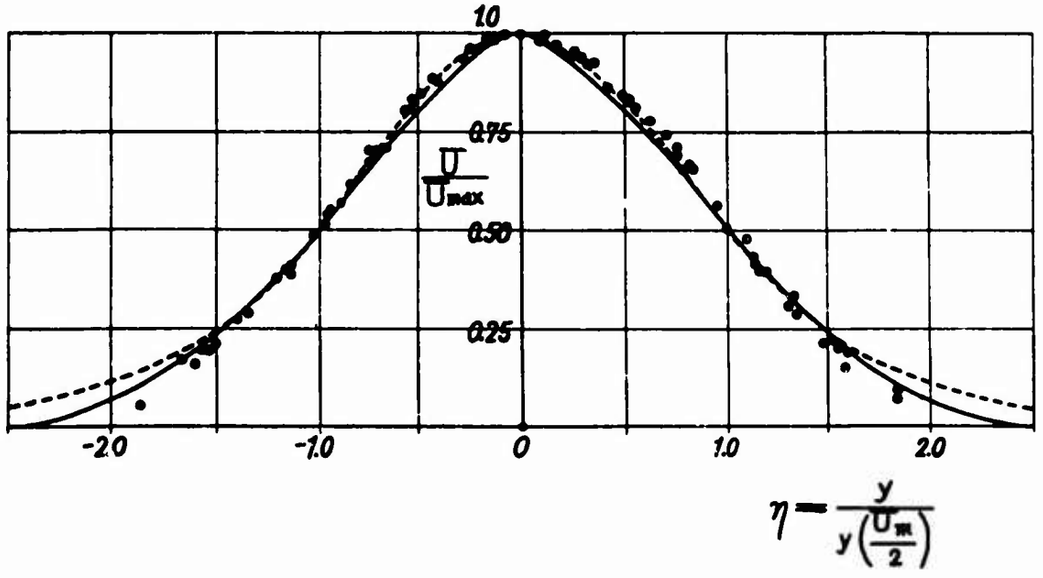

Figure 58. Distribution of Mean Velocity Across a Turbulent Jet from a Two-Dimensional Slit. The full and broken lines show the respective solutions of (35.4) and (35.3). ○, ◑, ◐, ⊖ and ● are observed values at x = 20, 35, 50, 60, and 75 cm. from the slit (reference 52).

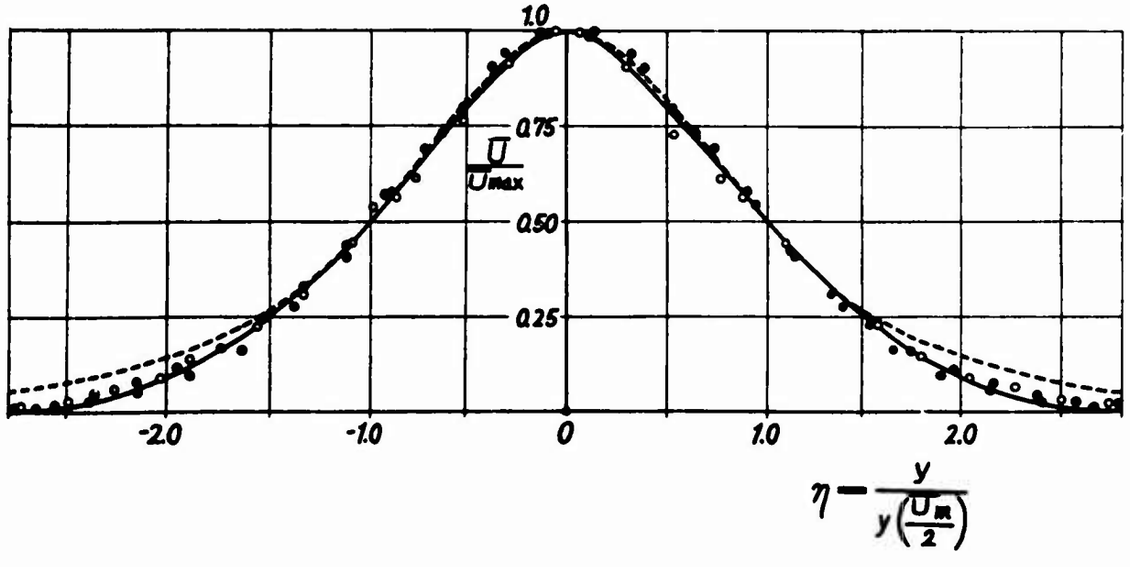

Figure 59. Distribution of Mean Velocity Across a Turbulent Jet From a Round Nozzle. The full and broken lines show the respective solutions of (35.7) and (35.6). ●, ◑, and ○ are observed values at x = 20, 26, and 45 cm. from the nozzle (reference 47).

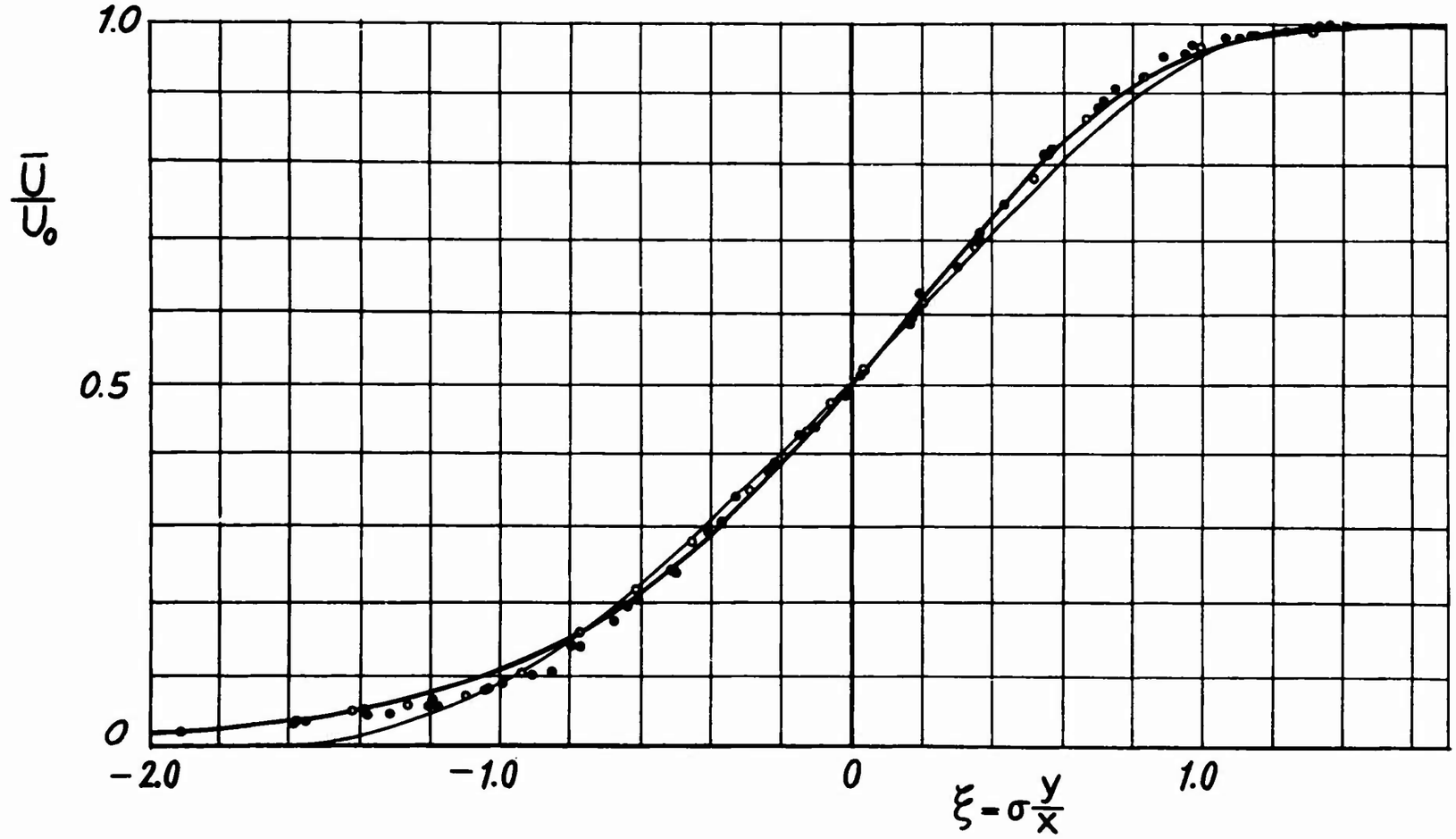

Figure 60. Distribution of Mean Velocity Across a Half-Jet. The thick and thin lines show the solutions of (35.11) and (35.12), respectively. ○, ●, ◒, and ◐ are observed values at x = 54.3, 65, 75, and 90 cm. from the step (reference 53).

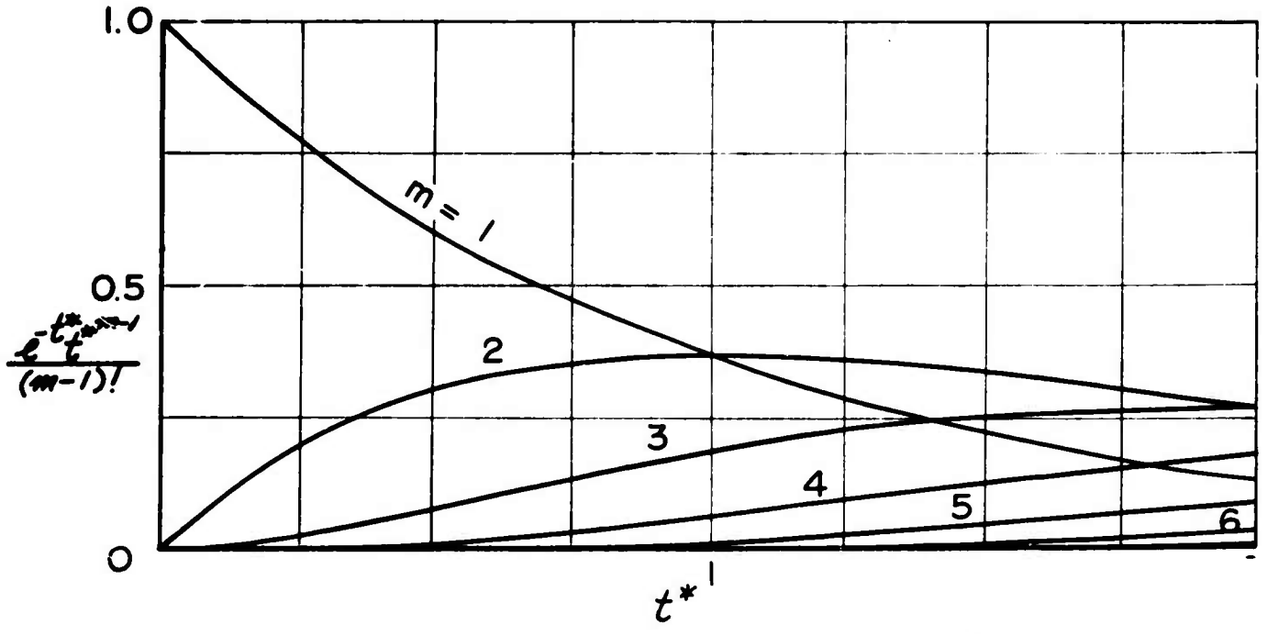

Figure 61. General View of the Poisson Process of $\ddot{\bar{P}}^*$ of (37.3).

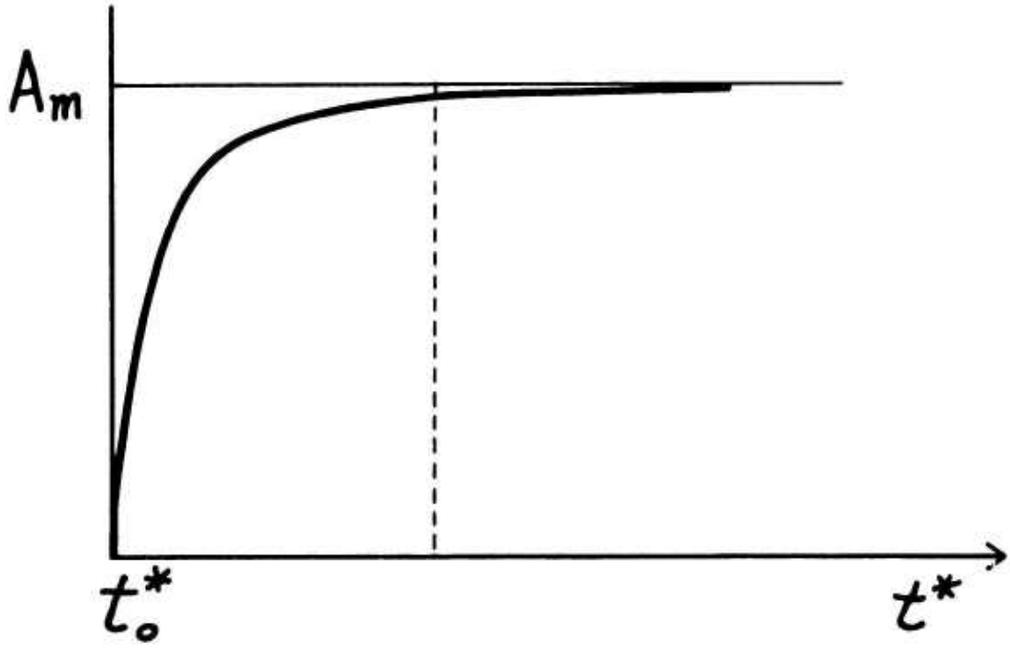

Figure 62. Variation of the Value of A_m Very Near the Production Instant of a Vortex Motion.

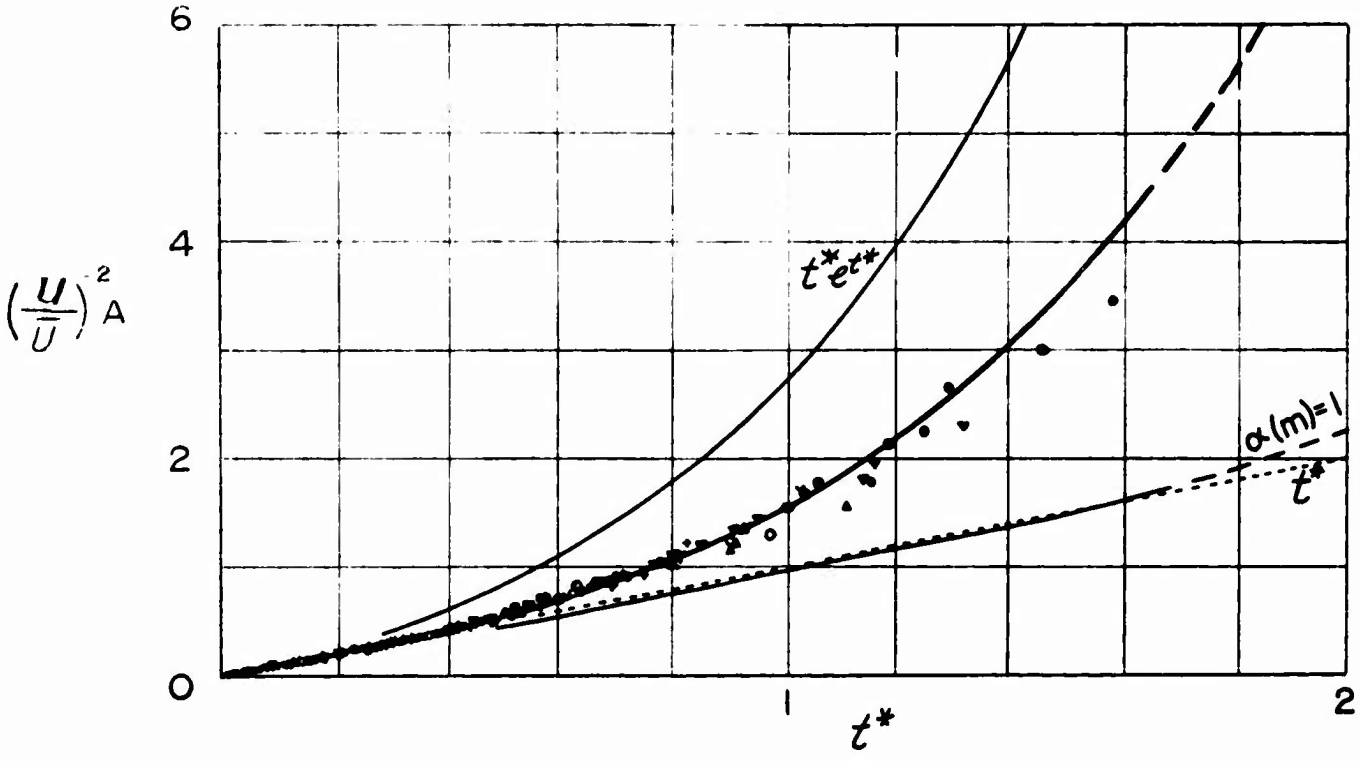

Figure 63. Decay of u-Intensity Along Uniform Decaying Turbulence (reference 54). The thick line is the evaluated curve from (38.7). +, Y are the observed values behind a circular cylinder referred to in Figure 53 as ◑ and ◐ respectively. Others are the observed values along the turbulent wake behind a grid with the following conditions:

	$\bar{U}_o$ (m/sec)	M (cm)	d (cm)	
○	9.06	0.16	0.03	(reference 55)
⊖	12.96	0.16	0.03	
◐	6.20	0.16	0.03	
⊙	12.86	0.64	--	(reference 32)
▽	11.30	1.68	--	(reference 36)
▼	--	--	--	(reference 56)
▼	19.68	0.14	0.02	(reference 33)
▼	15.00	0.14	0.02	
▽	9.61	0.14	0.02	
△	10.00	1.00	0.20	(reference 34)
△	10.00	5.00	1.00	

$\bar{U}_o$, M, and d are the undisturbed velocity, mesh length and rod diameter of the grid or cylinder, respectively.

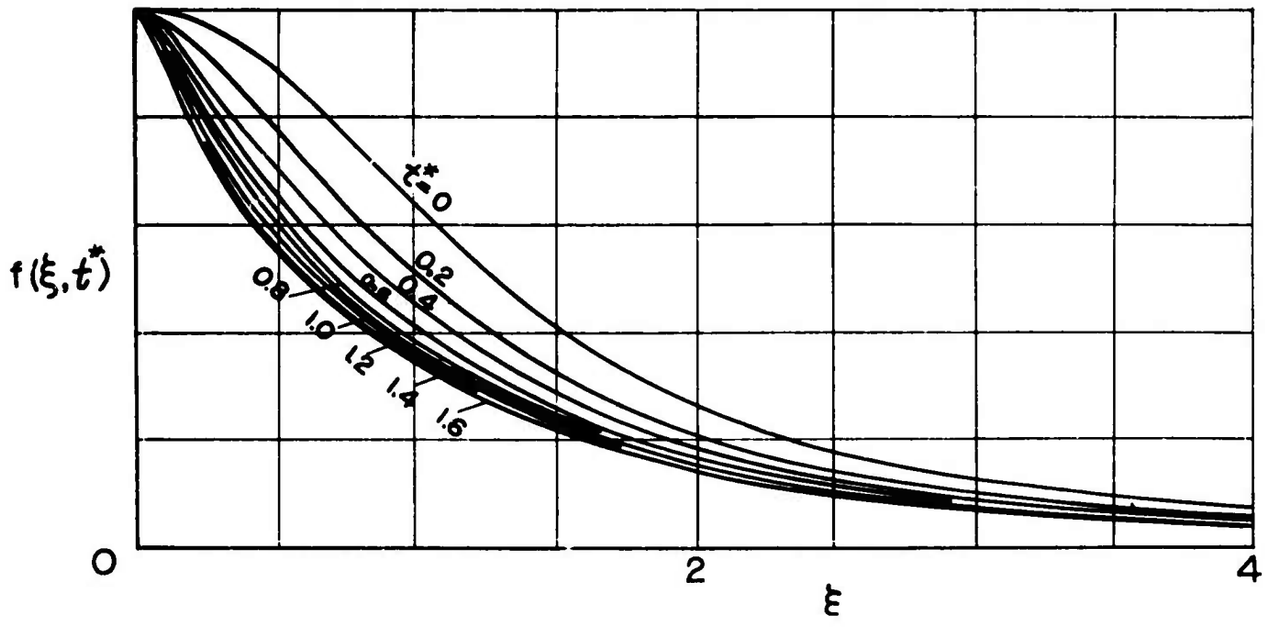

Figure 64. Variation of the f-Correlation in Isotropic Turbulence.

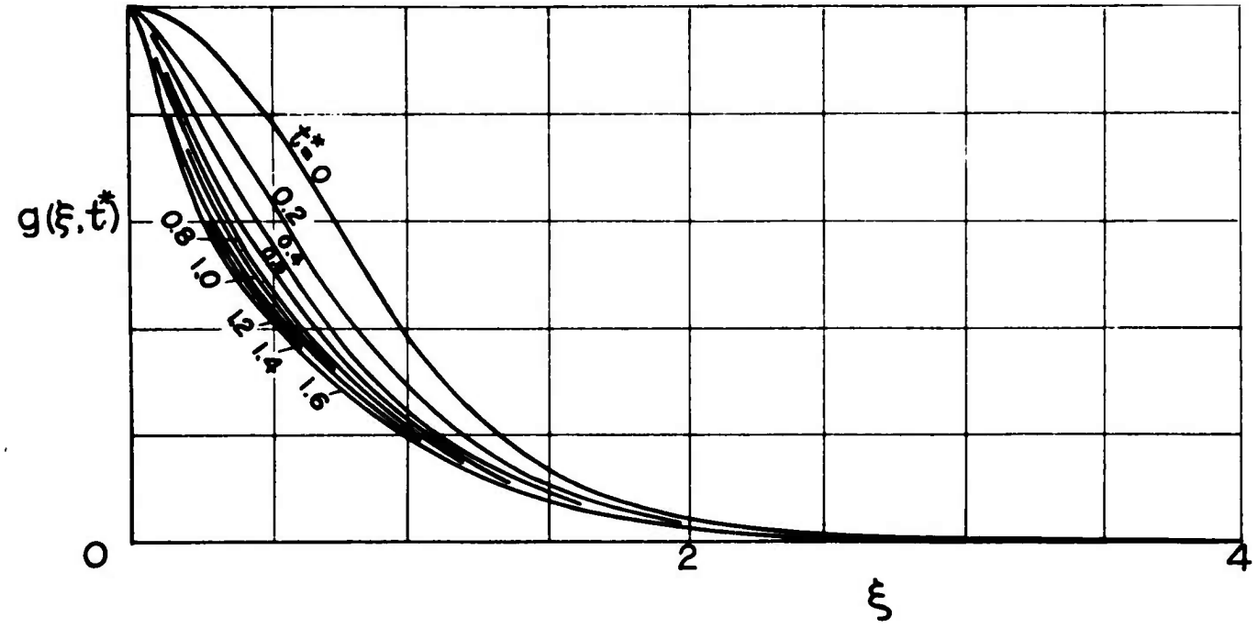

Figure 65. Variation of the g-Correlation in Isotropic Turbulence.

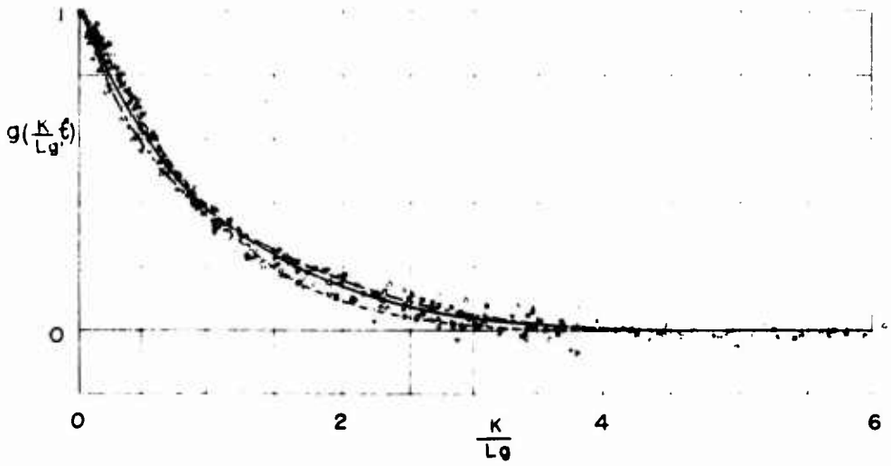

Figure 66. Distribution of the g-Correlation in Isotropic Turbulence (reference 54). The dotted, full and chain lines indicate the curves of $t^* = 0.4$, 1.0, 1.6, respectively, in Figure 65. The following symbols correspond to the observed values in the turbulent wake behind a grid as proposed by different authors under the following conditions:

	$\bar{U}_o$ (m/sec)	M(cm)	d (cm)	x/M	$R_M \times 10^{-5}$	
○	10.00	1.00	0.2	20		
⊙	10.00	1.00	0.2	60		
⊖	10.00	1.00	0.2	120		(reference 34)
⊖	10.00	1.00	0.2	200		
⊘	10.00	1.00	0.2	350		
⊘	10.00	1.00	0.2	550		
△	-----	10.16	---	---	3.0	
◁	-----	10.16	---	---	1.0	(reference 36)
◁	-----	10.16	---	---	0.4	
▽	20.00	14.00	0.2	10		
▷	20.00	14.00	0.2	30		
▷	20.00	14.00	0.2	50		(reference 33)
◁	20.00	14.00	0.2	70		
□	-----	-----	---	37		
⊡	-----	-----	---	231		(reference 57)
⊠	-----	15.24	---	---	1.3	
⊠	-----	-----	---	50	3.2	(reference 58)
⊞	parallel	2.54	---	60		
⊟	cylinder	2.54	---	60		
⊞	square	5.08	---	30		
●	mesh	2.54		35		(reference 59)
■	slot	1.90	---	47		
●	----	1.90	---	47		

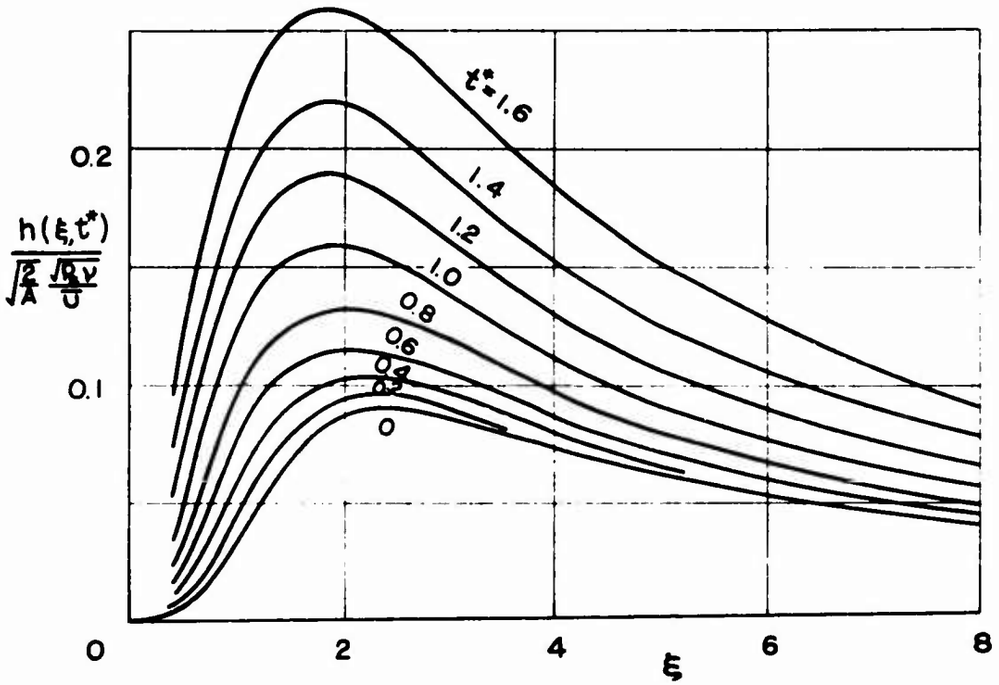

Figure 67. Variation of the Triple Correlation h in Isotropic Turbulence.

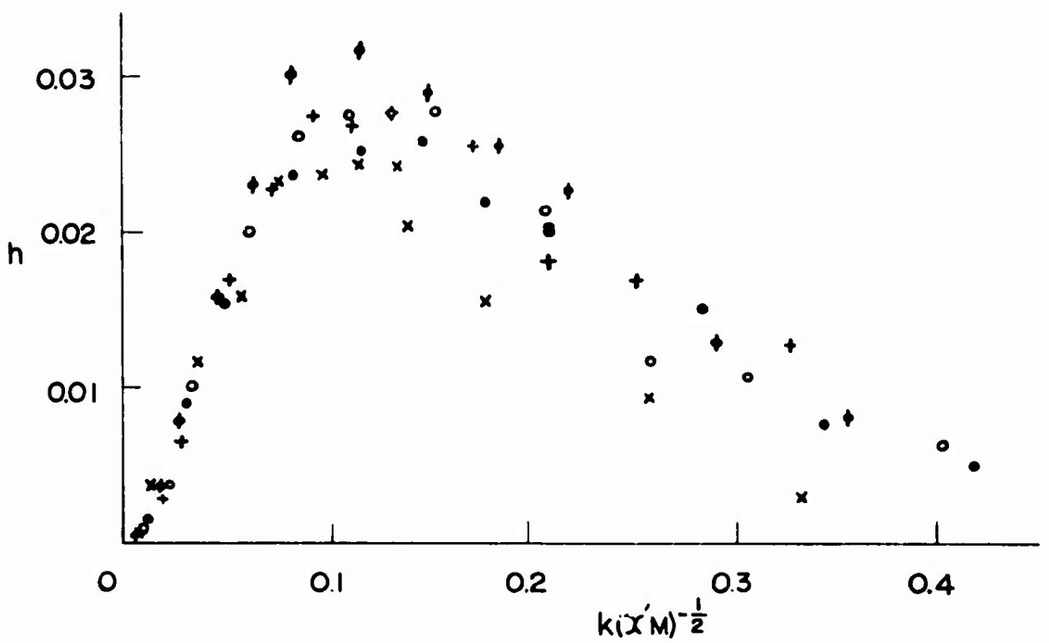

Figure 68. Growing of the h-Correlation Observed Along the Turbulent Wake Behind a Grid (reference 60). X, ●, O, +, and ◆ are observed values, respectively, at x/M = 20, 30, 60, 90, and 120, where R_M = 5300.

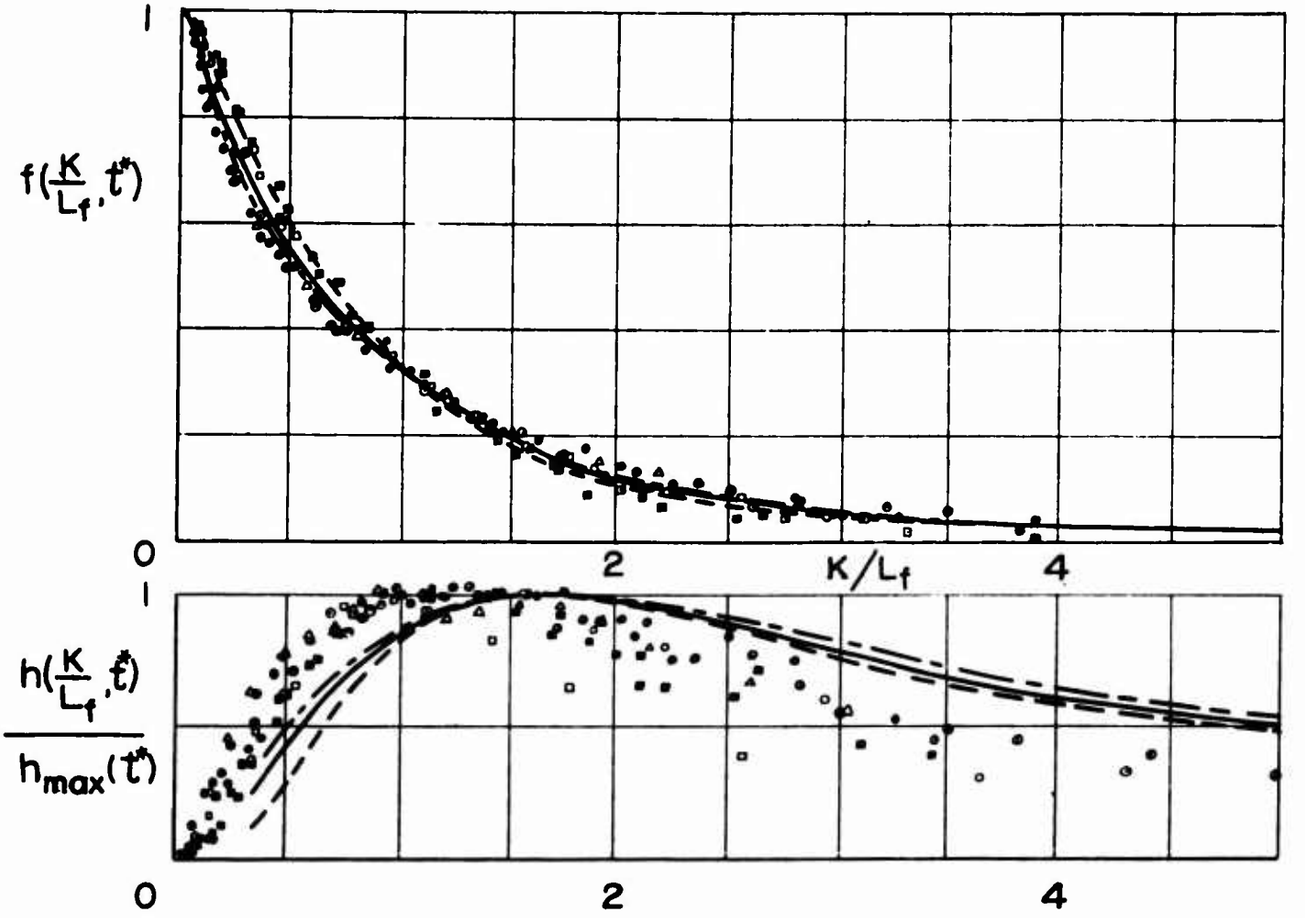

Figure 69. Distribution of the f- and h-Correlations in Isotropic Turbulence Plotted Versus the Same Abscissa k/L_f (reference 54). The dotted, full, and chain lines indicate the respective curves of $t^* = 0.4$, 1.0, and 1.6 in Figures 64 and 67. The following symbols correspond to the observed values of f and h at the same time in the turbulent wake behind a grid under the following conditions:

	x/M	$R_M\ 10^{-5}$	
○	30	0.53	(reference 59)
⊙	30	2.12	
⊕	30	4.24	
⊖	30	11.50	
□	20	0.53	(reference 60)
⊡	30	0.53	
▣	60	0.53	
⊟	90	0.53	
△	120	0.53	
	---	R = 56.2	(reference 61)

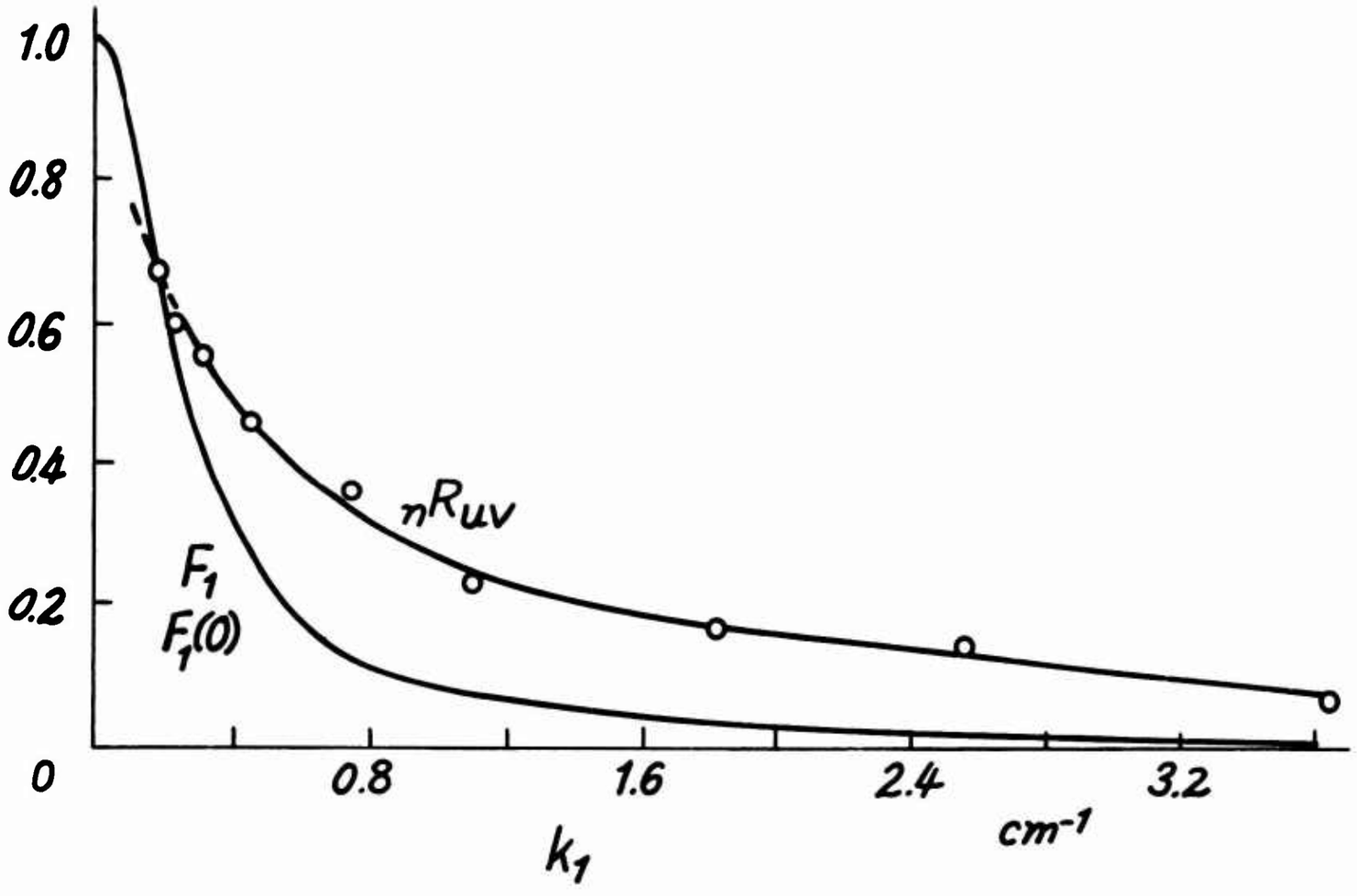

Figure 70. Observed Results of the One-Dimensional Spectrum F_1 of u-Fluctuation and the Shear-Correlation Spectrum ${}_nR_{uv} = (\overline{uv})_n/(u_n v_n)$. Measurements are made in the region of maximum shear at x/d = 20 in a turbulent round jet from an orifice of the diameter d = 1". Existence of the local isotropy can be seen by a rapid decreasing of ${}_nR_{uv}$ with k_1.

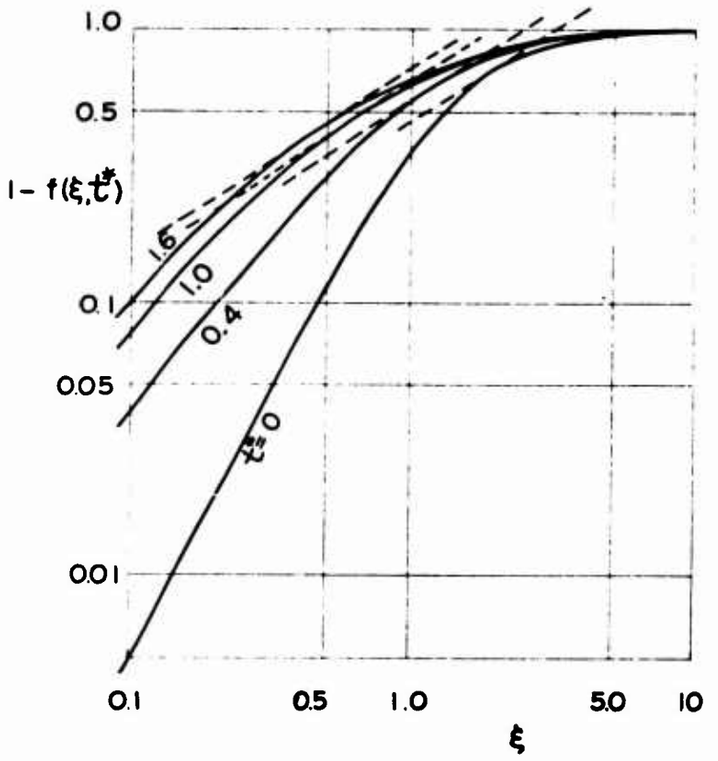

Figure 71. Comparison of the 2/3-Power Law (dotted lines) of (44.9) With the Curves of 1-f Shown in Figure 64.

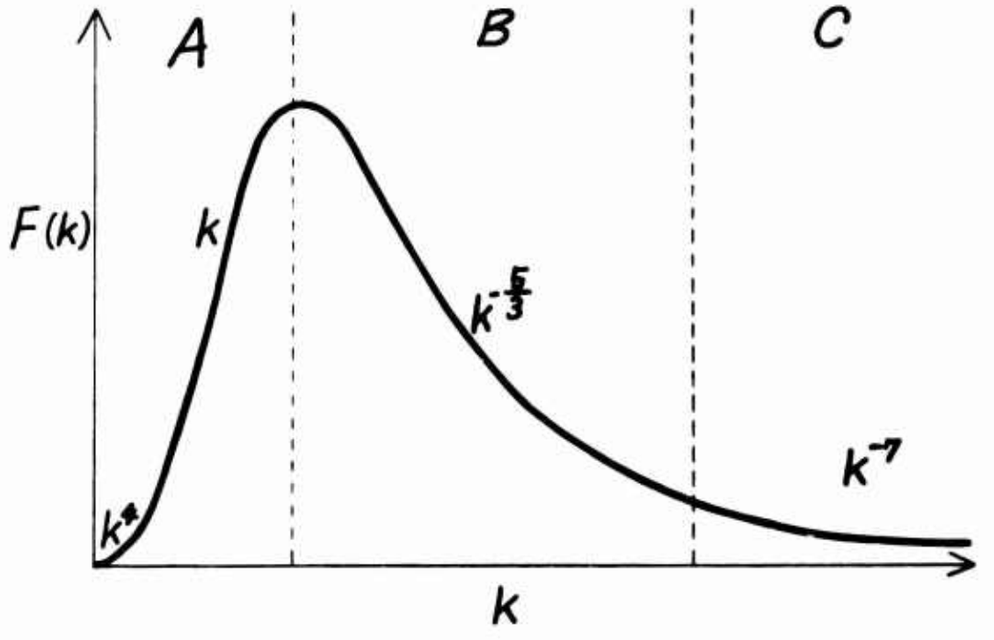

Figure 72. Local Characteristics of the Spectrum Function F(k).

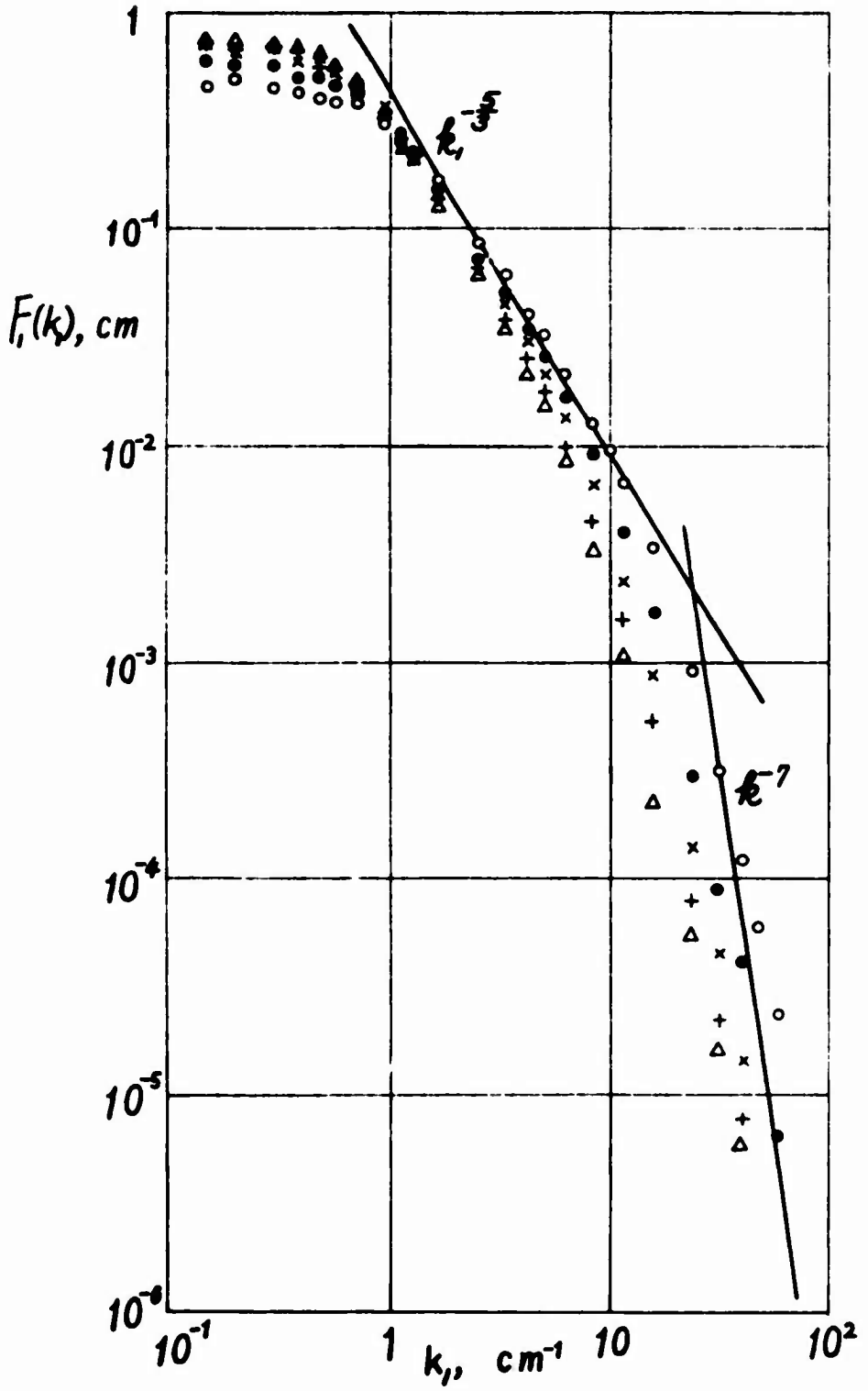

Figure 73. Observed Results of the One-Dimensional Spectrum in the Turbulent Wake Behind a Grid (reference 66) and the Curves of (45.4) and (45.5). Measurements are made at x/M = 20 (○), 40 (●), 60 (X), 80 (+) and 100 (△).

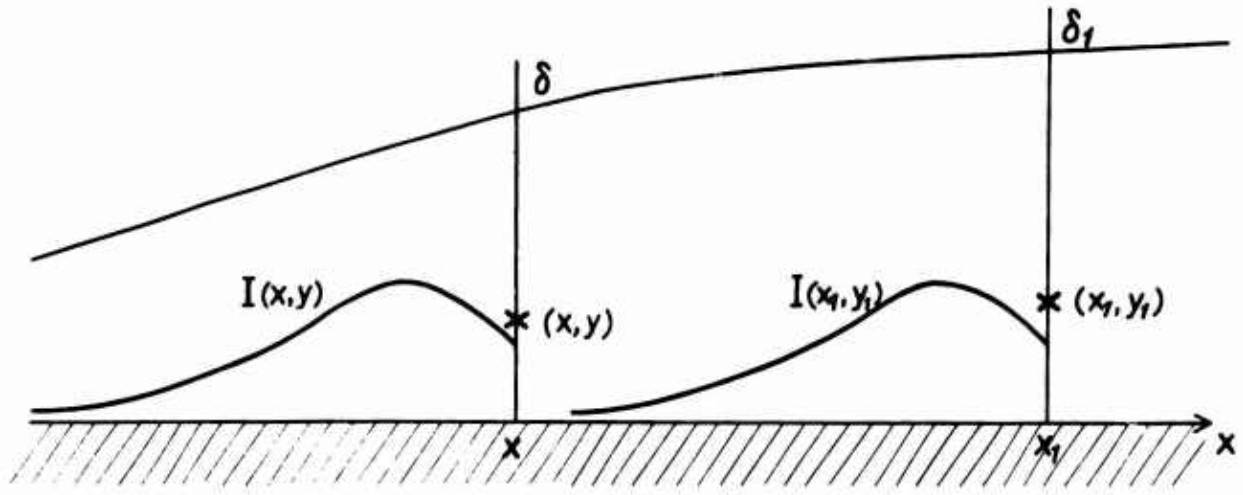

Figure 74. Distribution of Function I for Two Points in Turbulent Boundary Layer Along a Flat Plate.

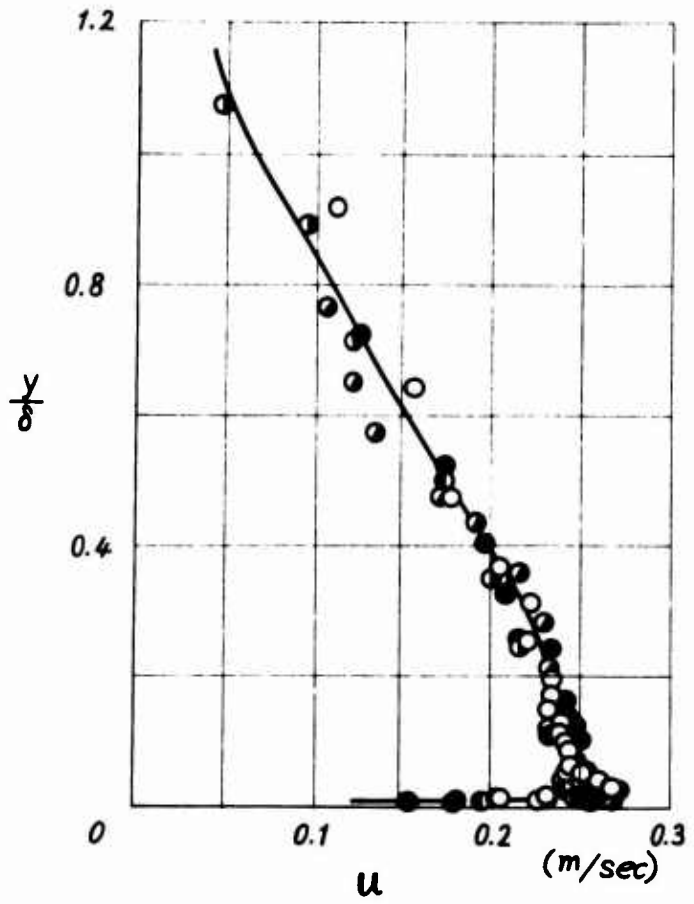

Figure 75. Distribution of u-Intensity Across Turbulent Boundary Layer Along a Flat Plate (reference 18). Transition is accomplished by spreading a wire on the plate across the flow of a mean velocity U_o = 10.13 m/s. Measurements were made at x = 49.3 cm. (○), 76.5 cm. (●), 102.5 cm. (◑), 121.2 cm. (◐), and 141.5 cm. (◕) from the wire.

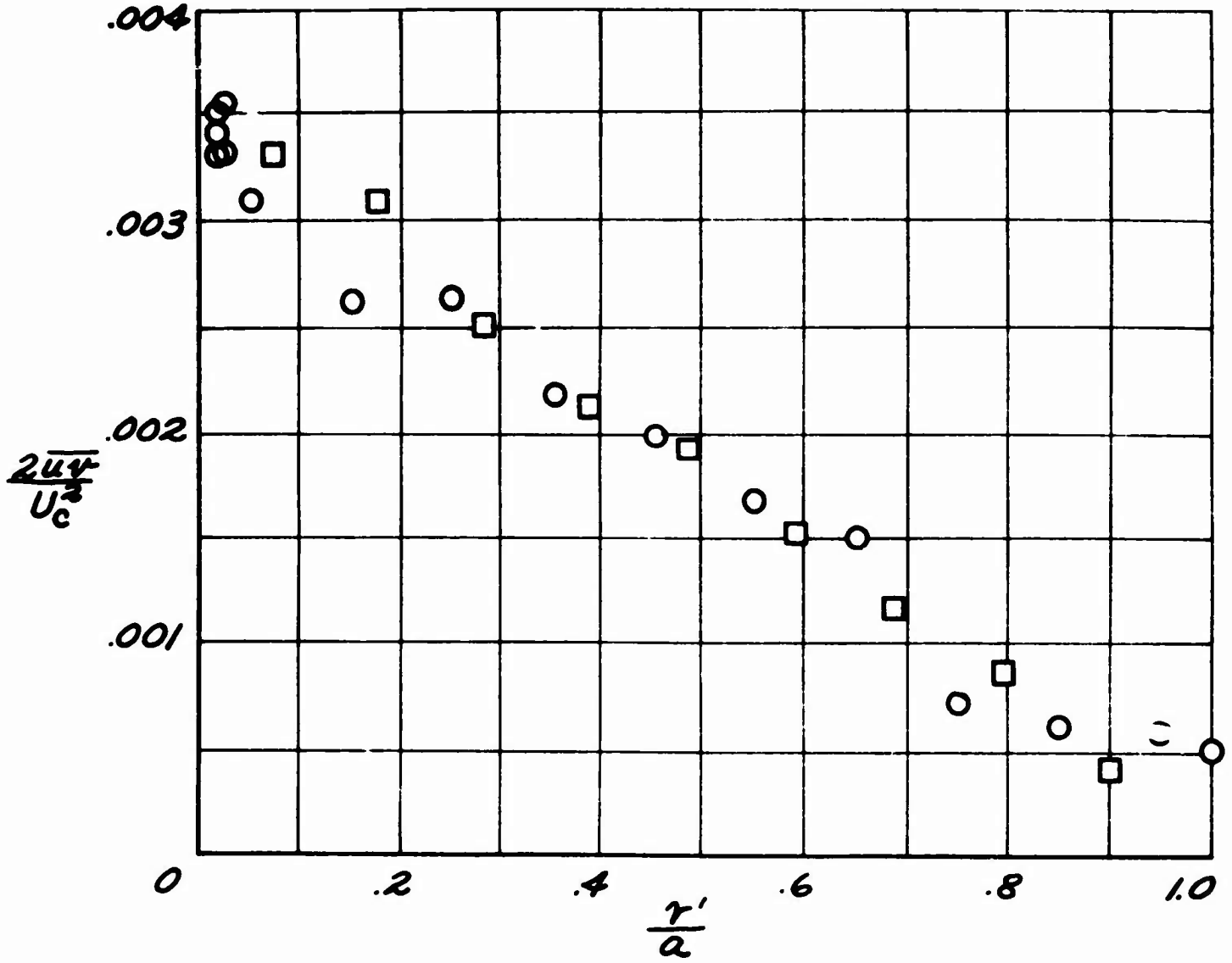

Figure 76. Distributions of Turbulent Shearing Stress Across a Circular Pipe (reference 67). Diameter of the pipe a is 4 in. (○) and 10 in. (□), and the Reynolds number of $(\bar{U}_o a)/\gamma$ is the same value of 25,000 where $\bar{U}_o$ is the mean velocity at the center of r'/a = 1.

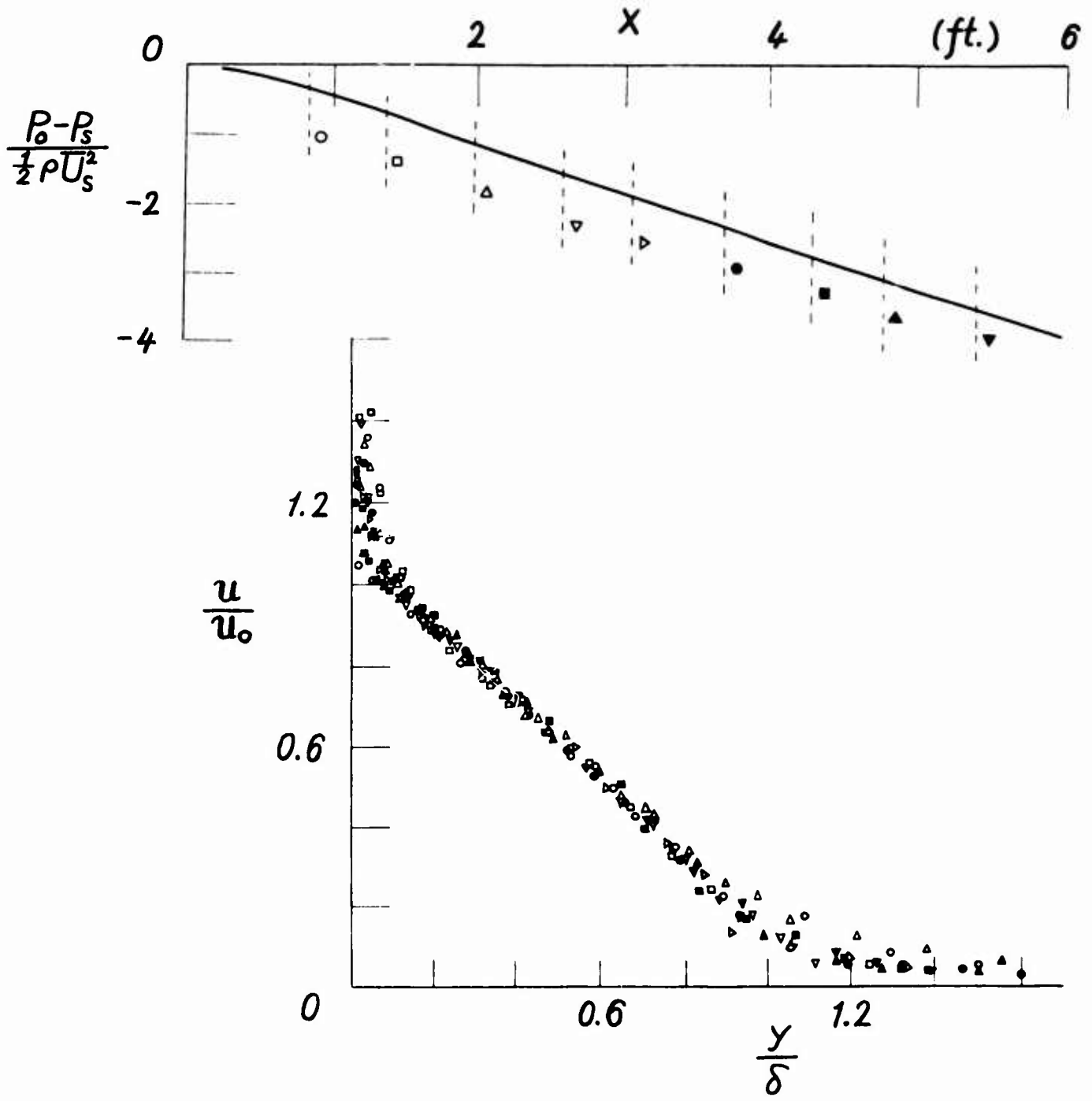

Figure 77. Distributions of u-Intensity (below) Across a Turbulent Boundary Layer With a Negative Constant Pressure Gradient (above) Along the Flow (reference 68). Several marks indicate the position of measurements, and suffix s means the value of the free-stream at the origin of the x-axis. $\overline{U}_s$ = 9.6 m/sec.

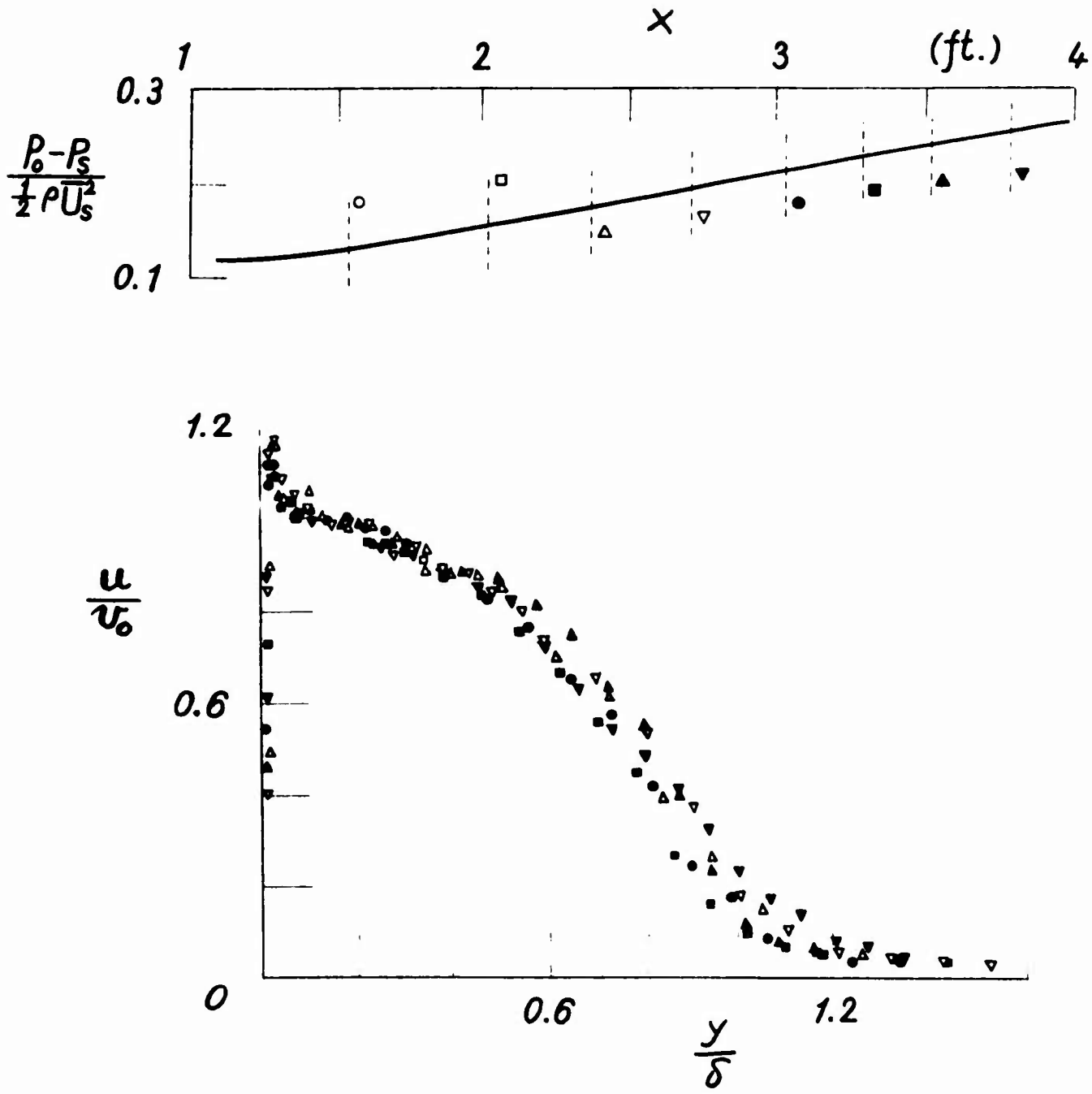

Figure 78. Distribution of u-Intensity (below) Across a Turbulent Boundary Layer With a Positive Constant Pressure Gradient (above) Along the Flow (reference 68). Several marks indicate the position of measurements, and suffix s means the value of the free-stream at the origin of the x-axis. U_s = 21.8 m/sec.

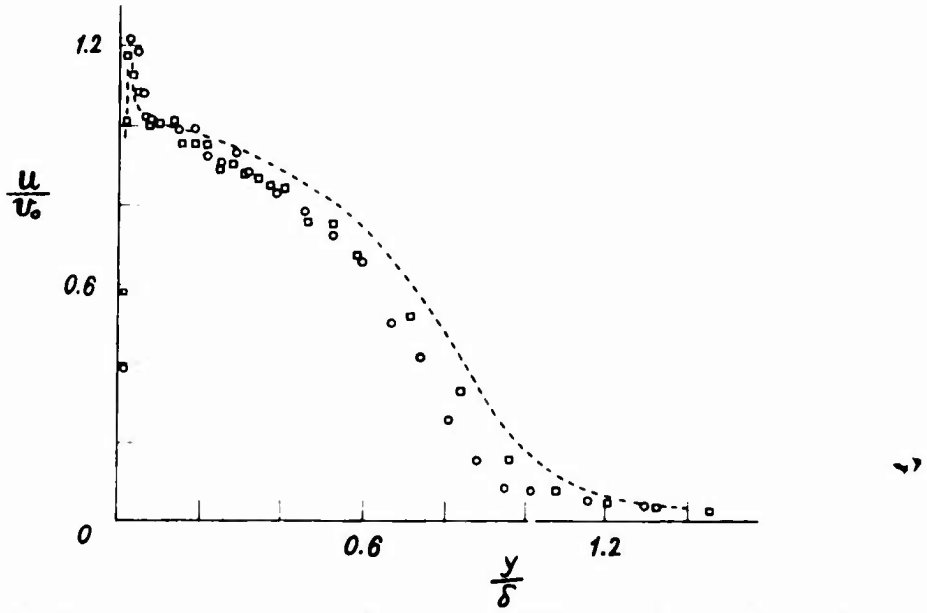

Figure 79. Deviation From the Similar Profiles of u-Intensity in the Case of Turbulent Boundary Layer in Figure 78. Dotted line shows the mean curve of the profile (below) in Figure 78; and ○ , □ correspond to the position in the pressure curve (above).

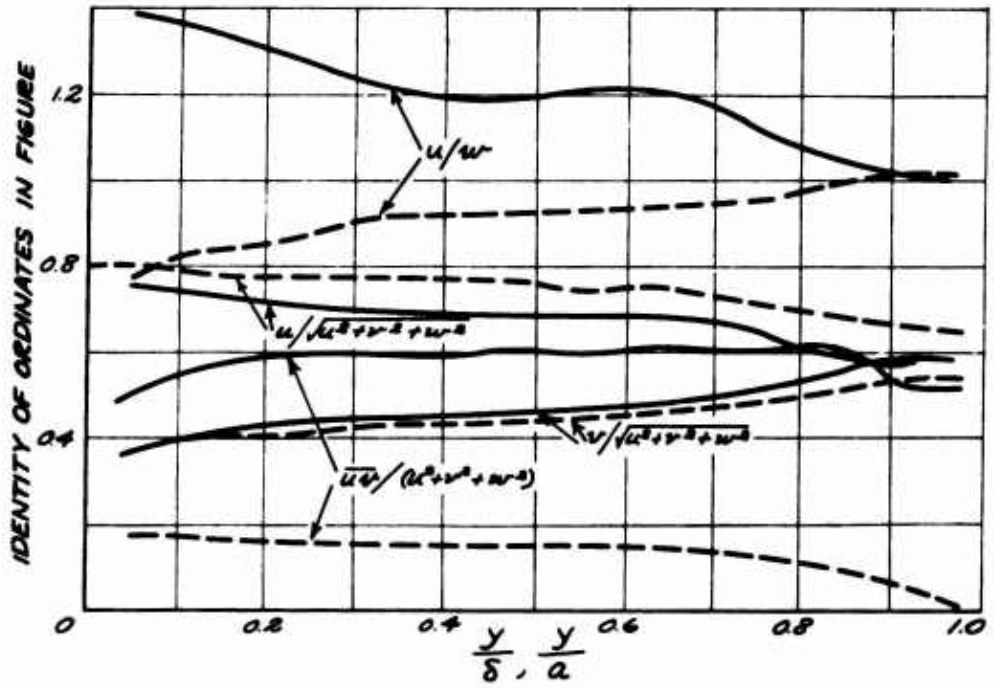

Figure 80. Distributions of $u/\sqrt{u^2 + v^2 + w^2}$, $v/\sqrt{u^2 + v^2 + w^2}$, $\overline{uv}/(u^2 + v^2 + w^2)$ and u/w Across Nondecaying Turbulent Flows. Full and broken lines are evaluated from experimental results respectively in turbulent boundary layer along a flat plate (reference 69) and in turbulent flow in a circular pipe of the radius a (reference 67).

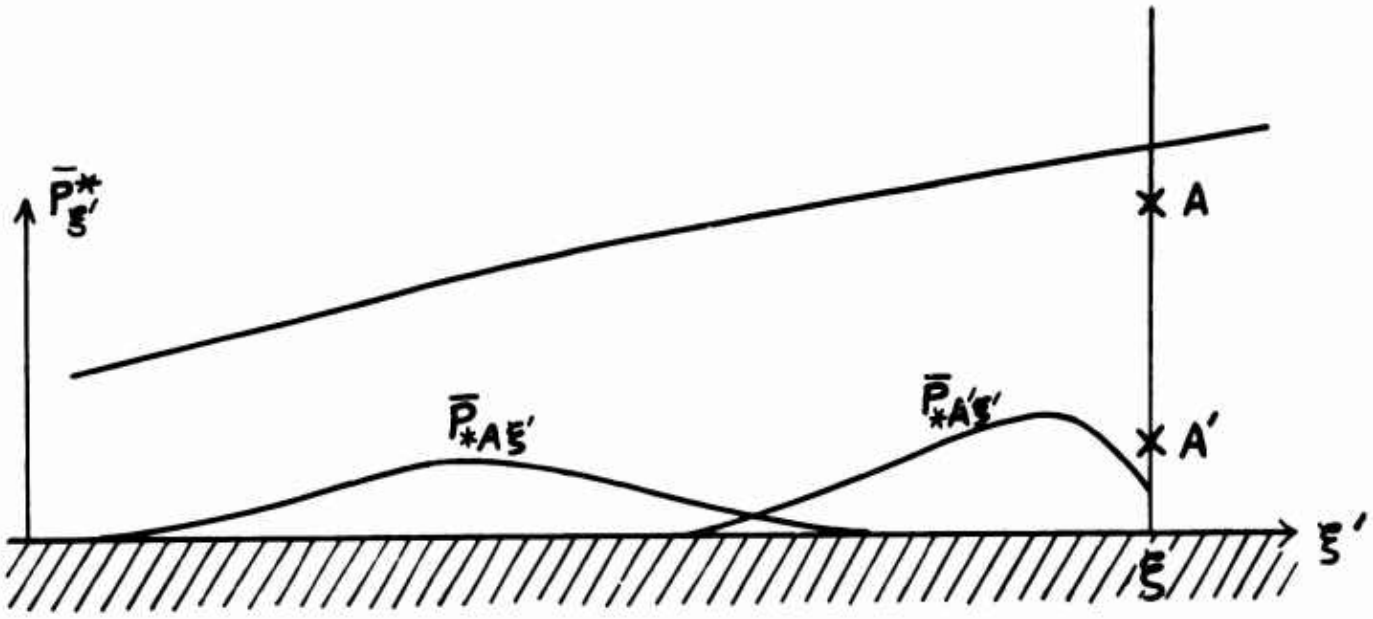

Figure 81. Distribution of the Function P* at the Two Points A and A' Near η = 1 and 0, Respectively, in Turbulent Boundary Layer.

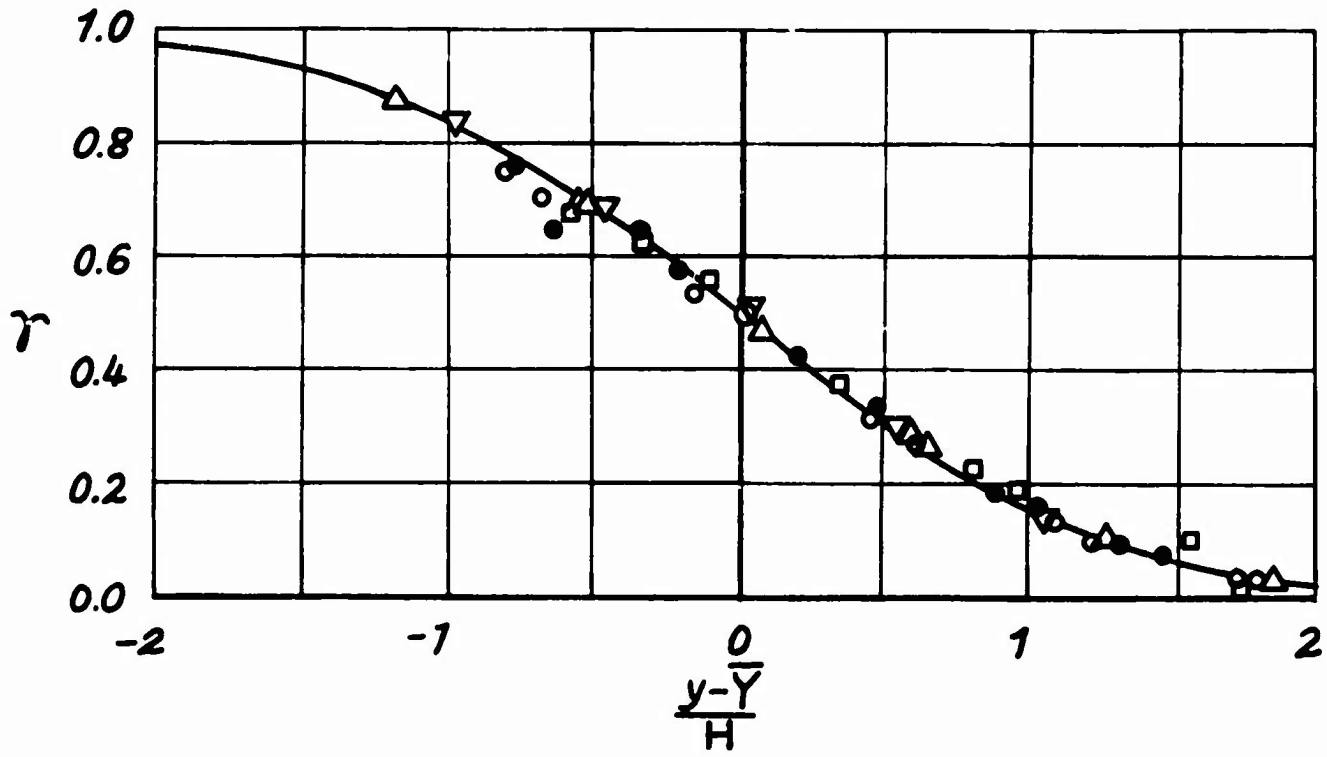

Figure 82. Distribution of the Intermittency Factor γ Across Turbulent Boundary Layer Along a Flat Plate (reference 41). Measurements are made at positions of x = 0 in. (○), 24.75 in. (△), 64 in. (□), 86.25 in. (▽) and 102 in. (●). The curve shows the Gaussian-integral formula with $\bar{Y}$ and H respectively of the position of the center and the dispersion of the formula.

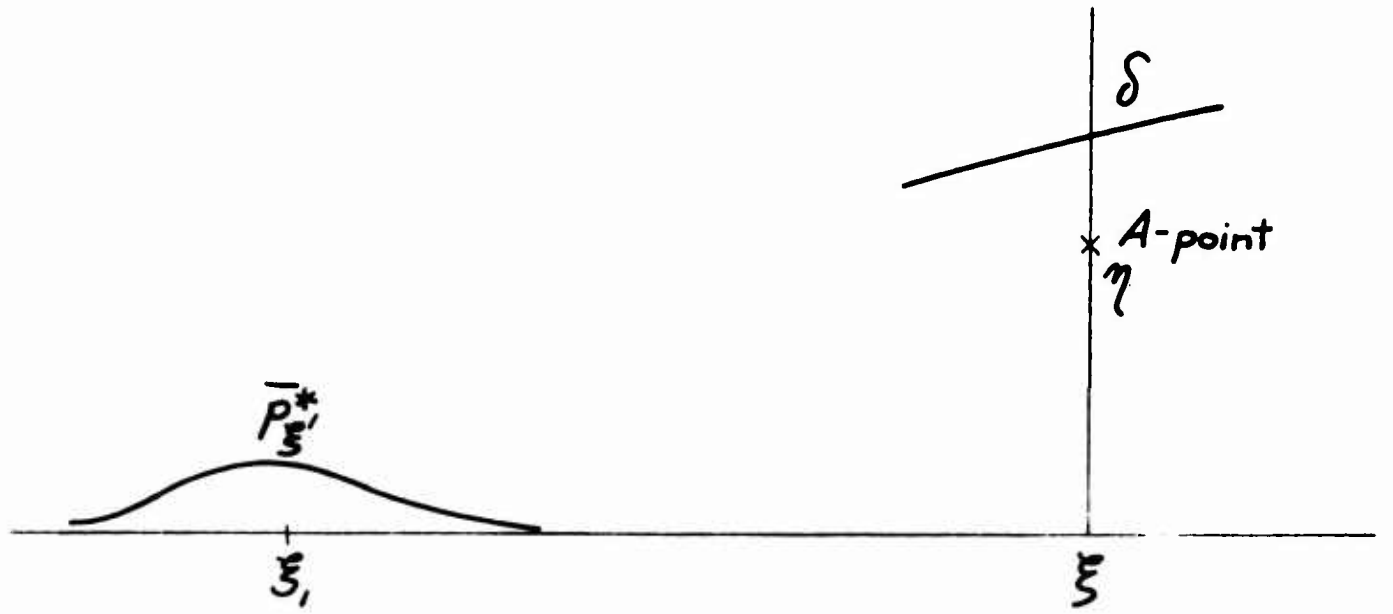

Figure 83. Distribution of $\widetilde{P}^*_{\xi}$, and the Location of ξ, for an A-point.

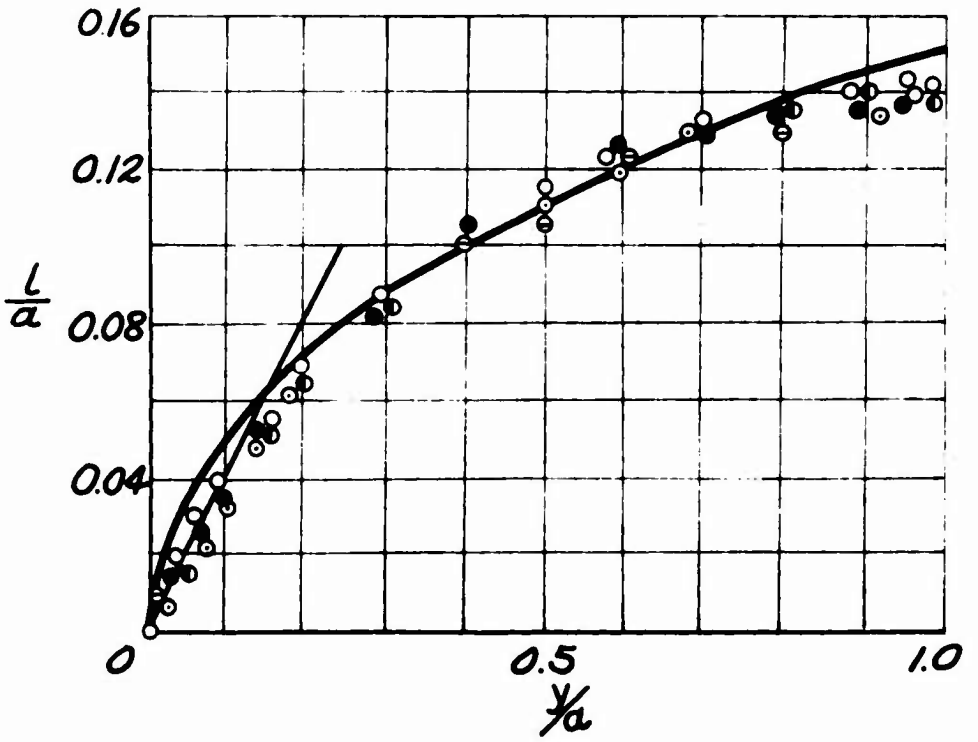

Figure 84. Distribution of the Mixing Length in a Pipe Flow (reference 71). Measurements are made with various Reynolds numbers Ua/ν of 105×10^3 (○), 396×10^3 (●), 1110×10^3 (◐), 1959×10^3 (⊙), and 3240×10^3 (⊖). a is the radius of the pipe. Thick and thin lines represent, respectively, the formulas (51.8) and (51.6).

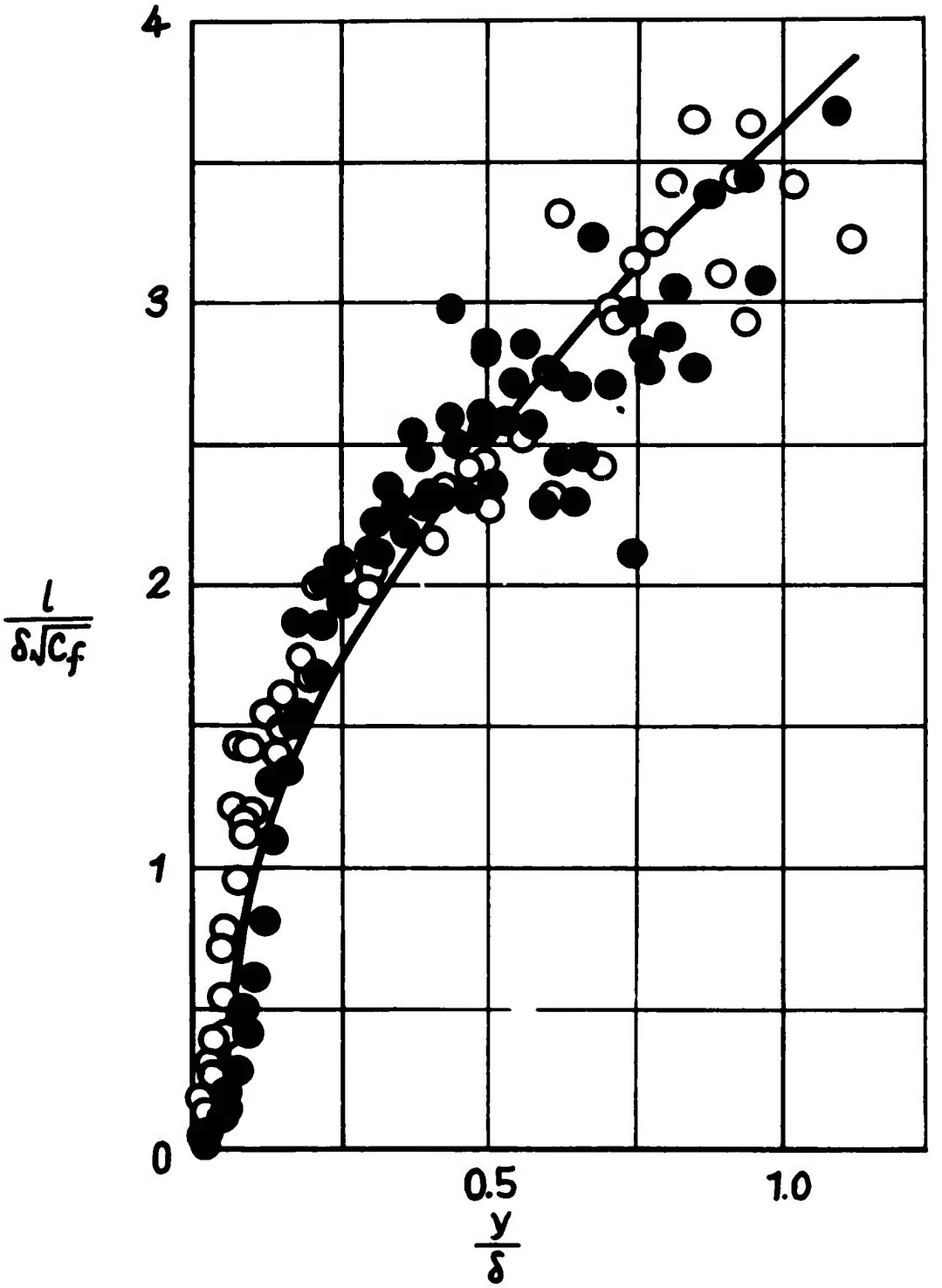

Figure 85. Distribution of the Mixing Length in Turbulent Boundary Layer Along a Flat Plate (reference 72). Measurements are made with two kinds of the Reynolds number. The curve represents the formula (51.8), where the origin is taken at $\eta = 0.04$ which is considered to be boundary of the viscous sublayer.

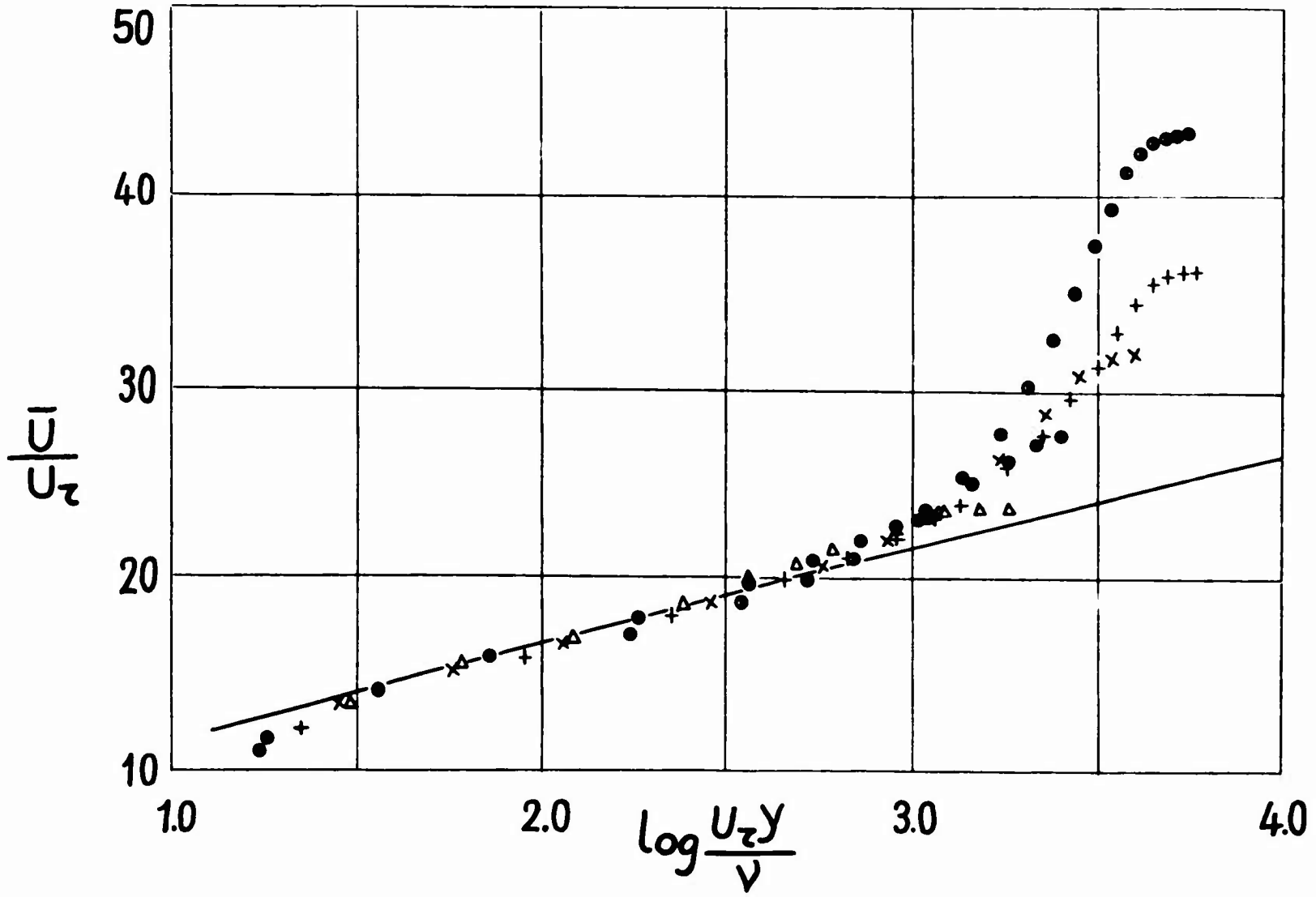

Figure 86. Distributions of Mean Velocity Across Turbulent Boundary Layer Expressed in $\bar{U}/U_\tau \sim \log(U_\tau y/\nu)$ (reference 73). Measurements are made in cases of a constant pressure of the Reynolds number of 7.98×10^3 (●), a moderate pressure rise of 2.65×10^4 (+), a great pressure rise of 1.48×10^4 (×), 3.25×10^4 (⊗), and a pressure drop of 2.86×10^4 (△). Reynolds numbers are evaluated based on the mean velocity outside the layer and on the momentum thickness.

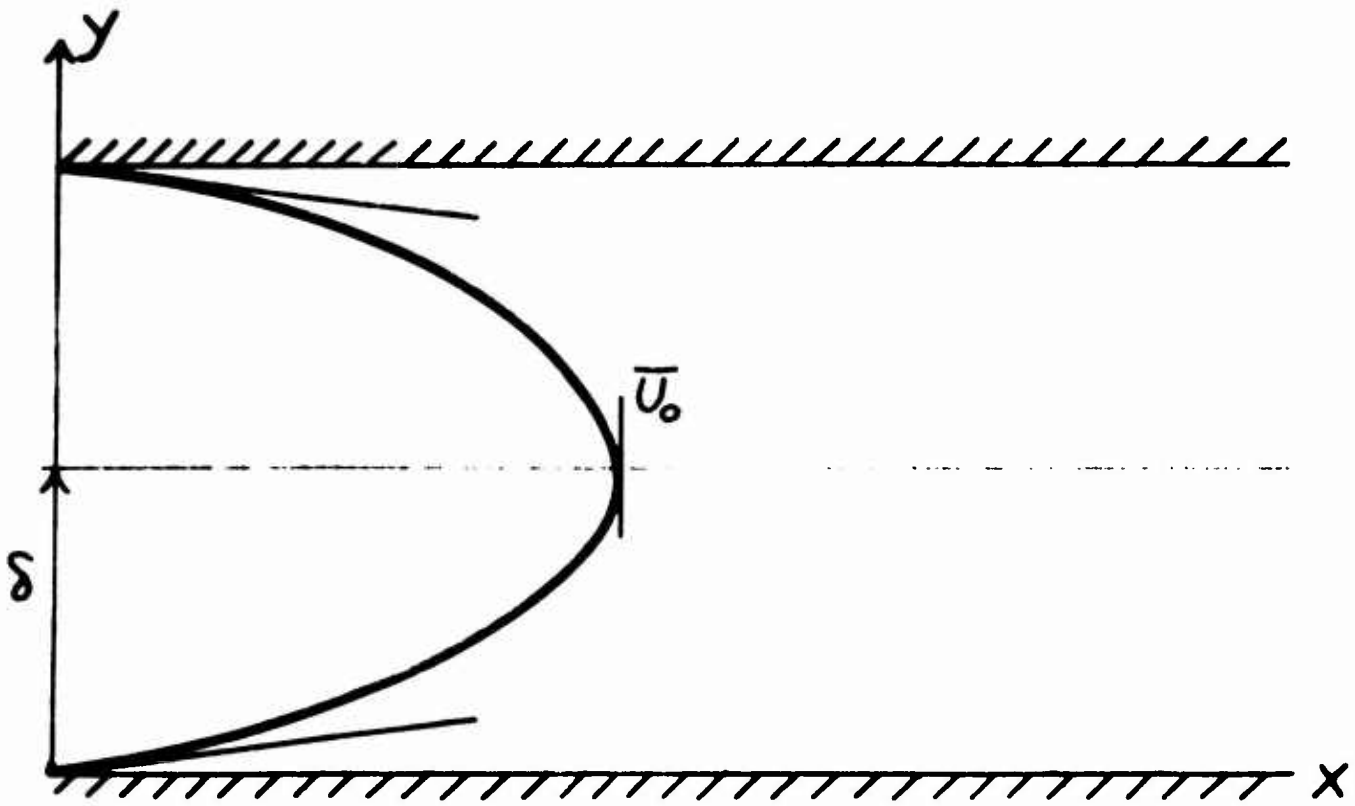

Figure 87. Profile of Mean Velocity Across a Channel.

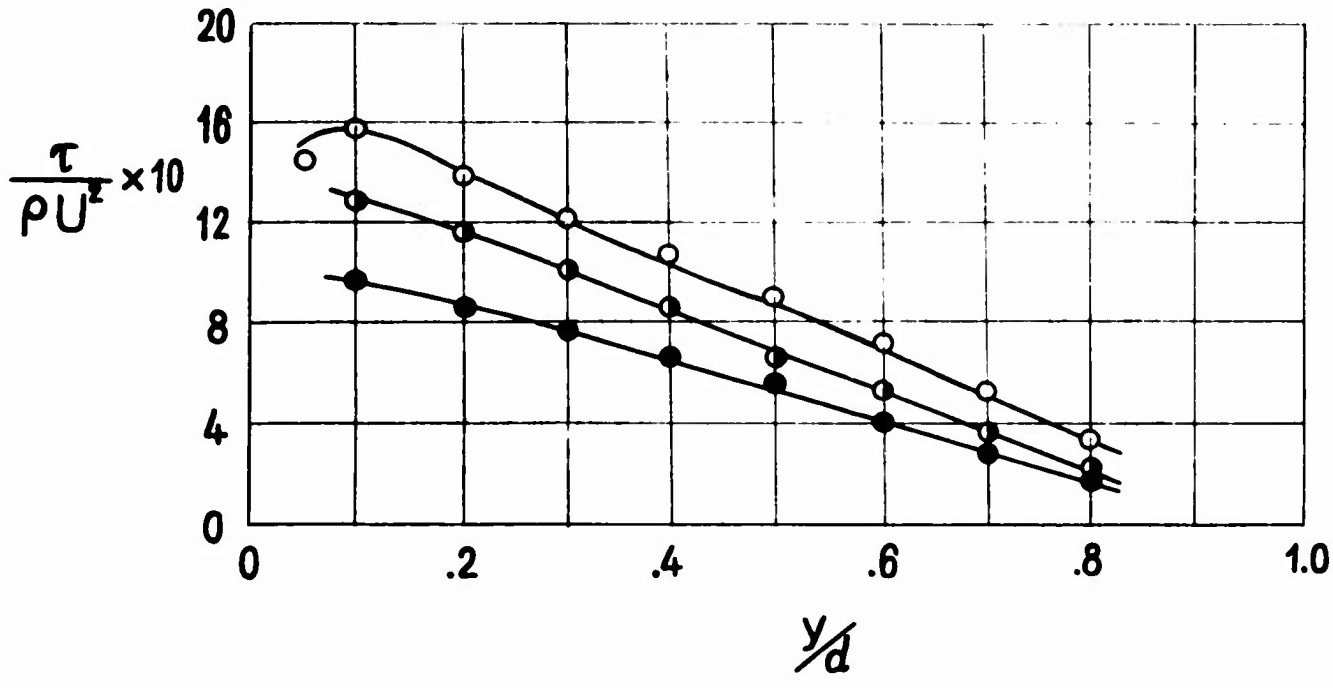

Figure 88. Distributions of Turbulent Shearing Stress Across a Circular Pipe (reference 76). Measurements are made of the Reynolds number of 12,300 (○), 30,800 (◑), and 61,600 (●).

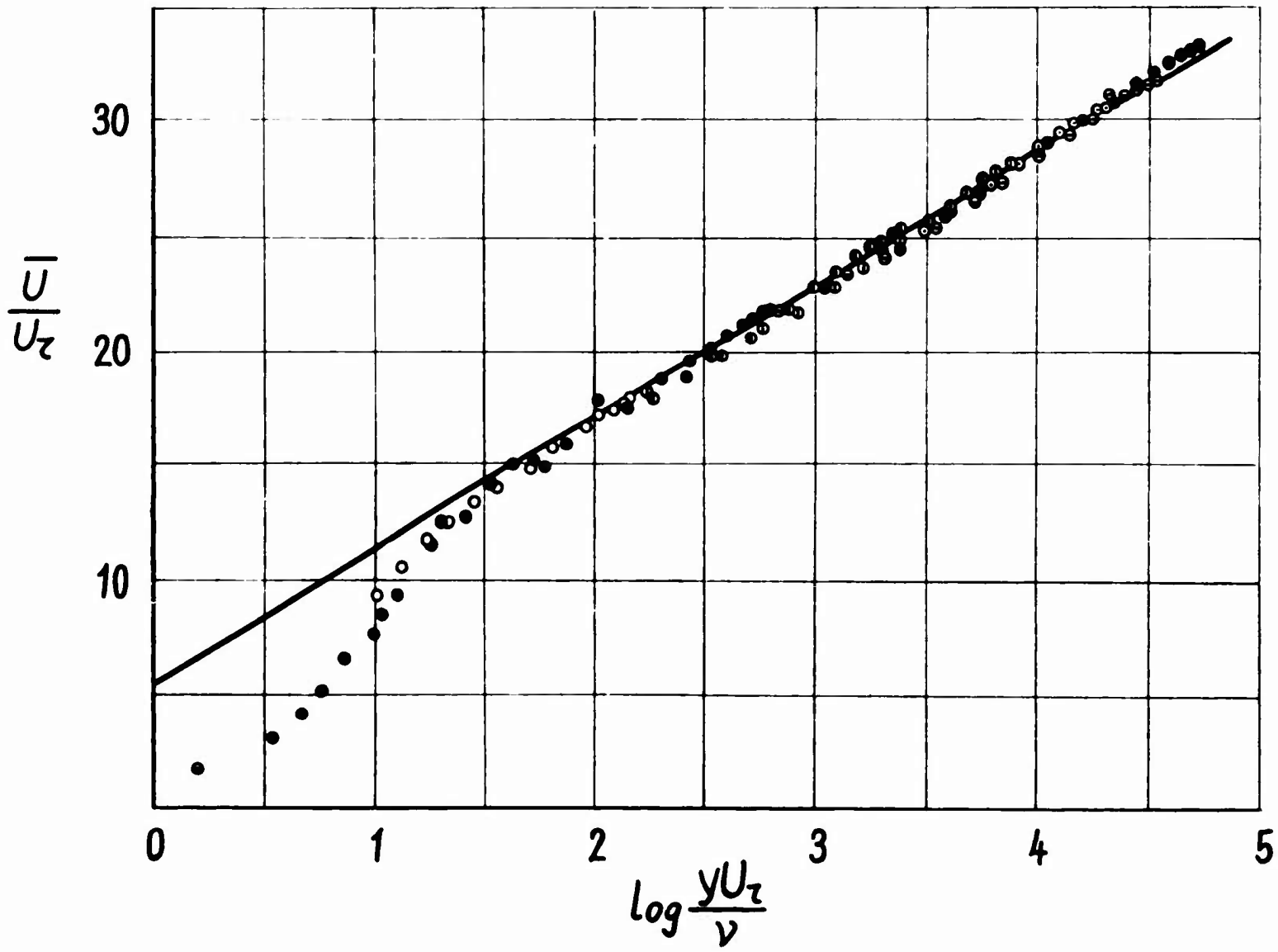

Figure 89. Distributions of Mean Velocity of Turbulent Flow Across a Circular Pipe Expressed in $\overline{U}/U_\tau \sim \log(U_\tau y/\gamma)$. Measurements are made by Nikuradse of the Reynolds number of 4.0×10^3 (○), 2.3×10^4 (●), 1.1×10^5 (◐), 4.0×10^5 (◑), 1.1×10^6 (◎), 2.0×10^6 (⊖), 3.2×10^6 (⊗) (reference 71) and by Reichardt (⊕) (reference 75).

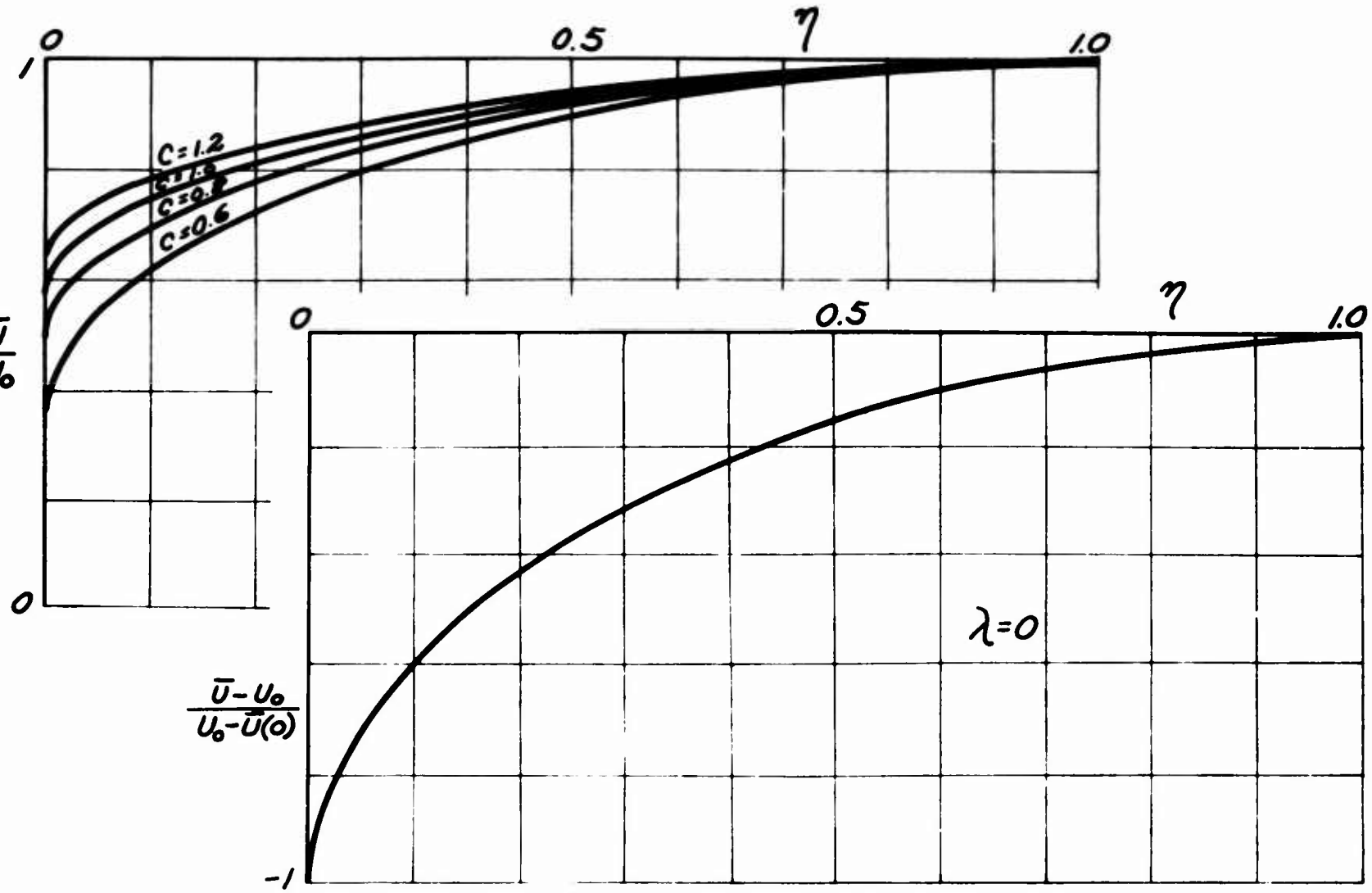

Figure 90. Calculated Velocity Profiles Across the Turbulent Boundary Layer Without a Pressure Gradient.

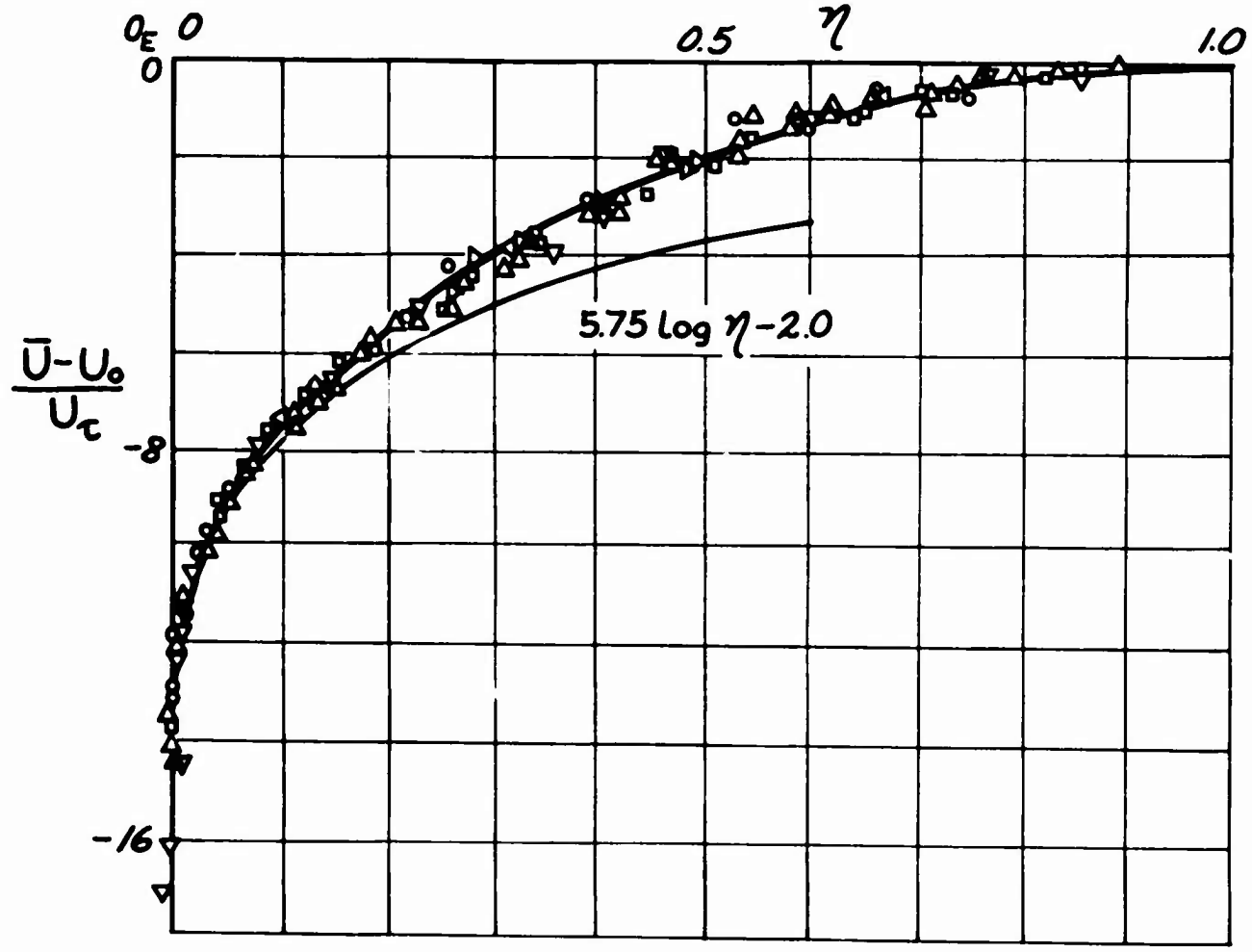

Figure 91. Distributions of Mean Velocity in the Expression of $(\bar{U}-U_0)/U_\tau \sim \eta$ in the Case of Turbulent Boundary Layer Along a Flat Plate. The thick line in $\eta = 0 \sim 1$ indicates the solution of (55.1) shown in Figure 90. The plotted marks show the experimental data (reference 77) measured by Freeman (○), Klevanoff-Diehl (□), Schultz-Grunow (△), Hama (▽), Clauser of rough wall (◁) and Moor of very rough wall (▷). O_E is the position of wall, and the thin line indicates the logarithmic law drawn from O_E.

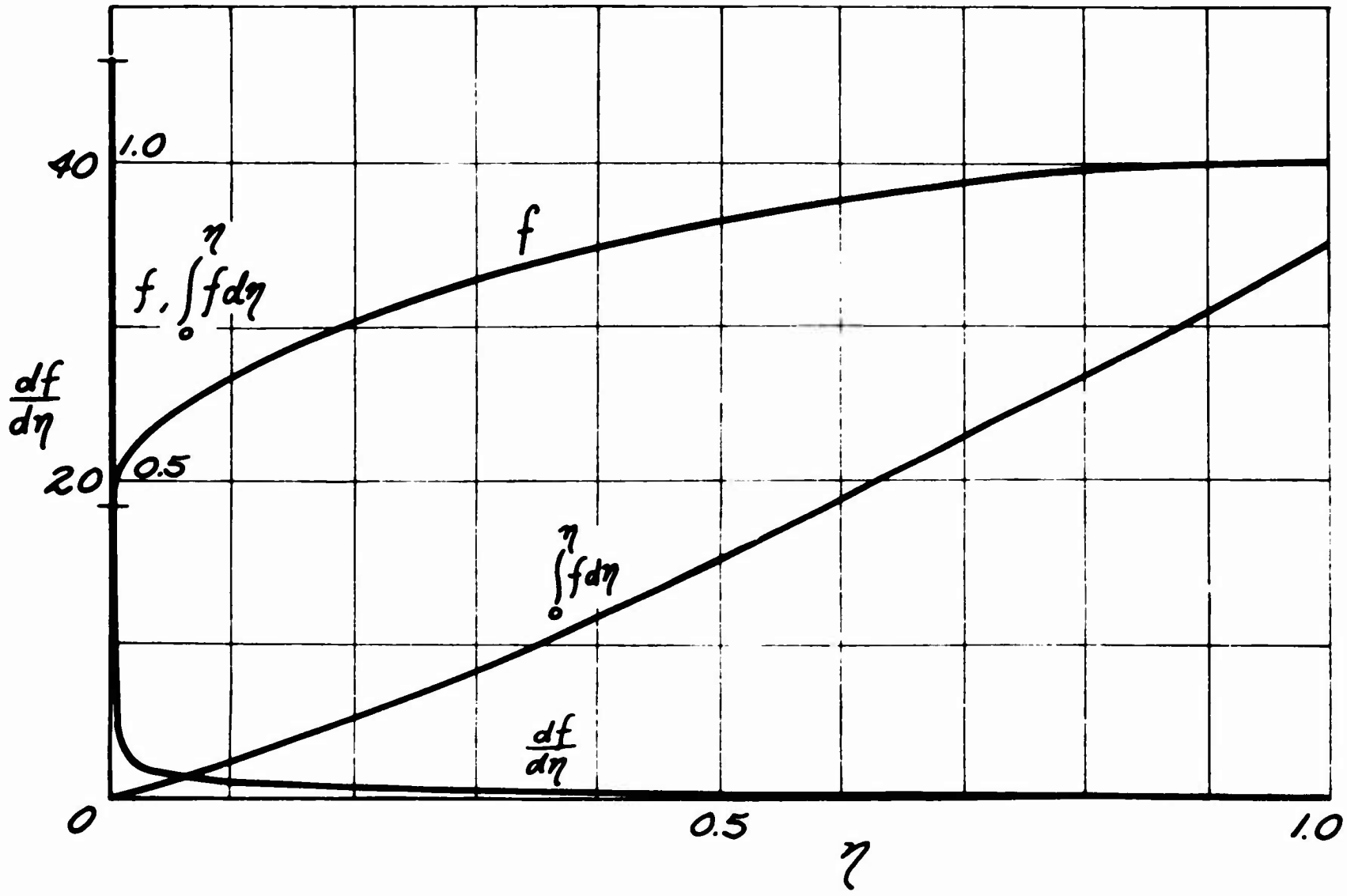

Figure 92. An Example of Computed Curves of f, $df/d\eta$ and $\int_0^\eta f\,d\eta$ Across a Similarities Boundary Layer of $\lambda = -0.1$ and $c = 0.6$.

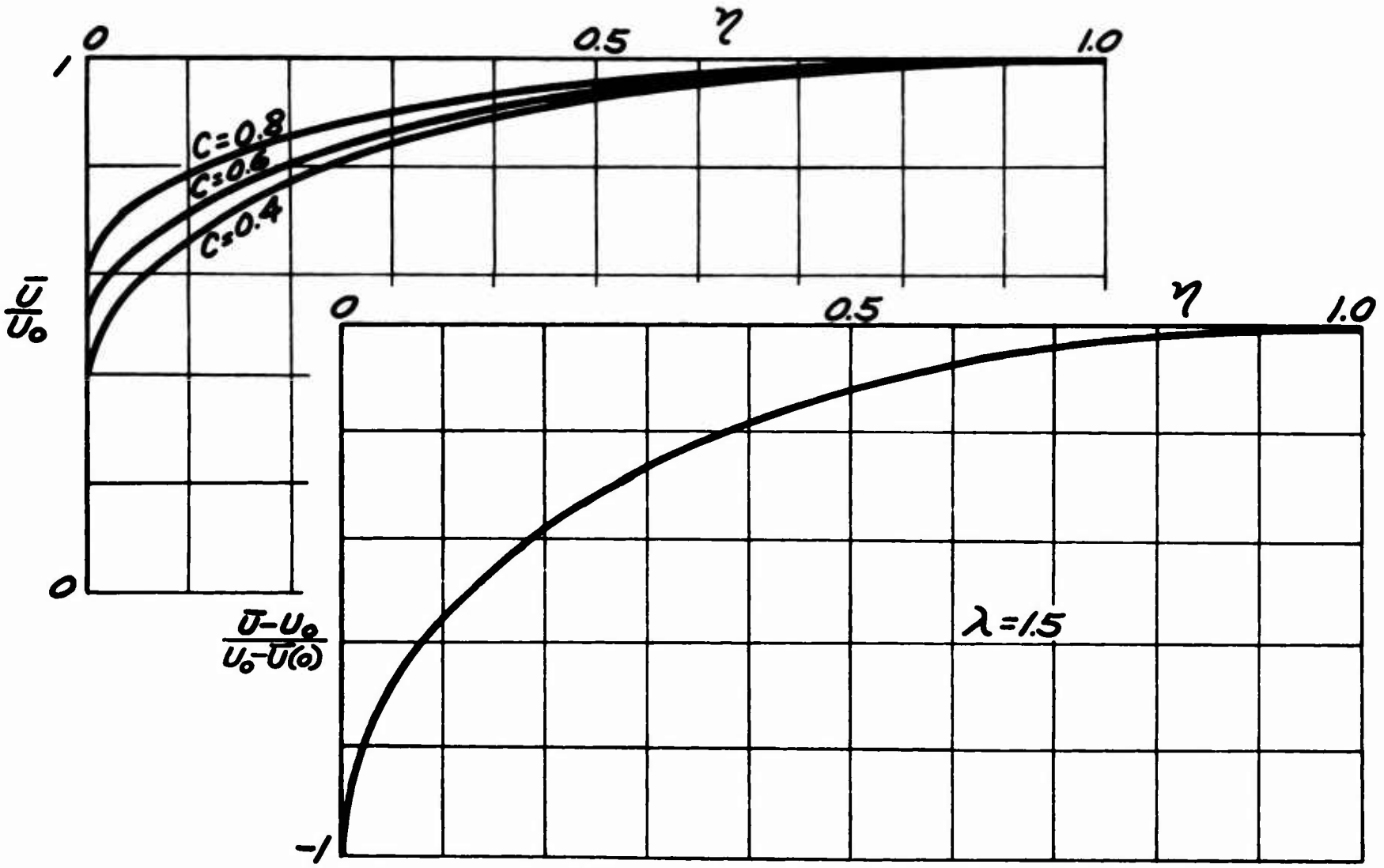

Figure 93. Computed Velocity Profiles of a Similarities Boundary Layer of $\lambda = 1.5$.

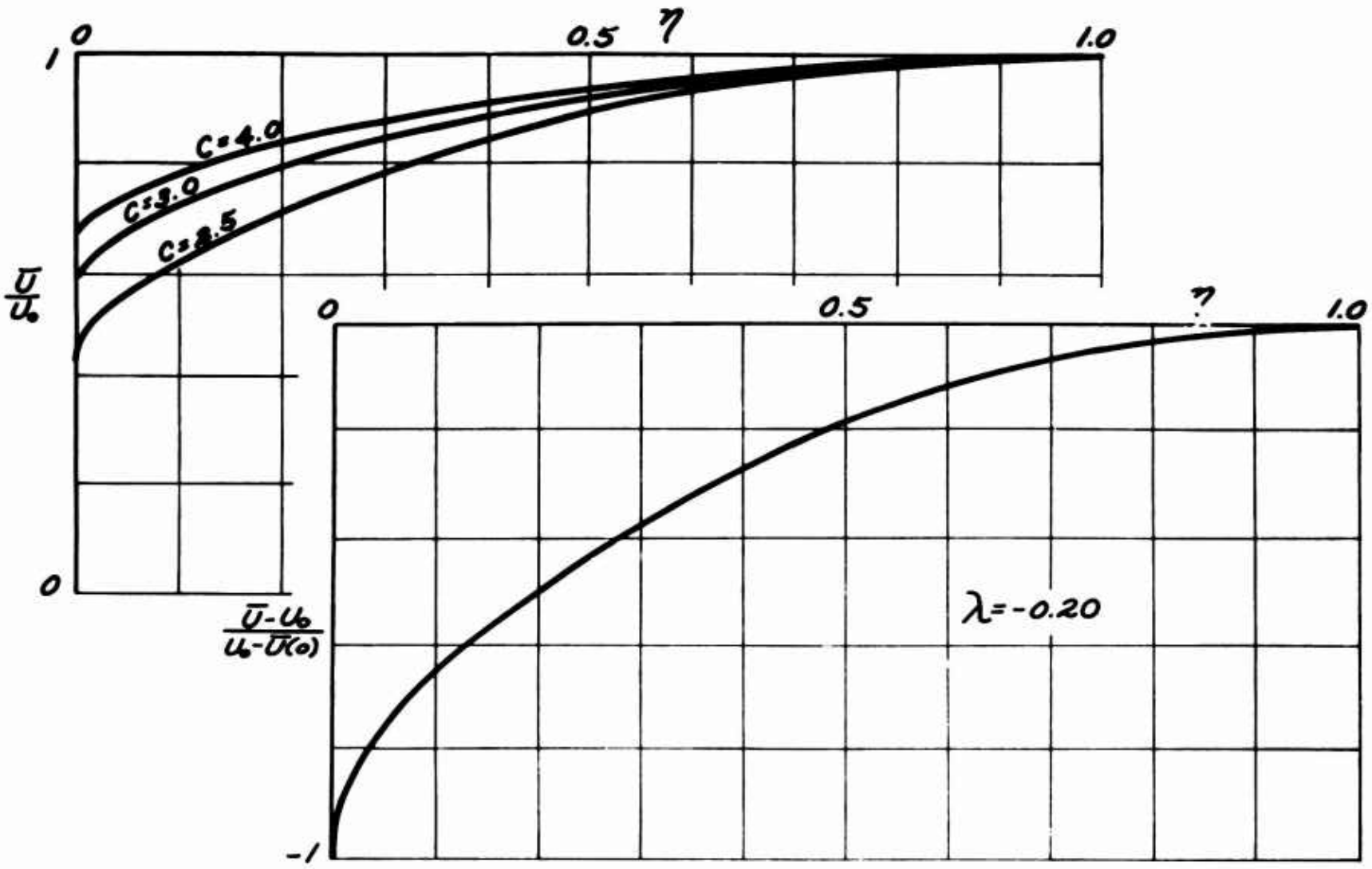

Figure 94. Computed Velocity Profiles of a Similarities Boundary Layer of $\lambda = -0.2$.

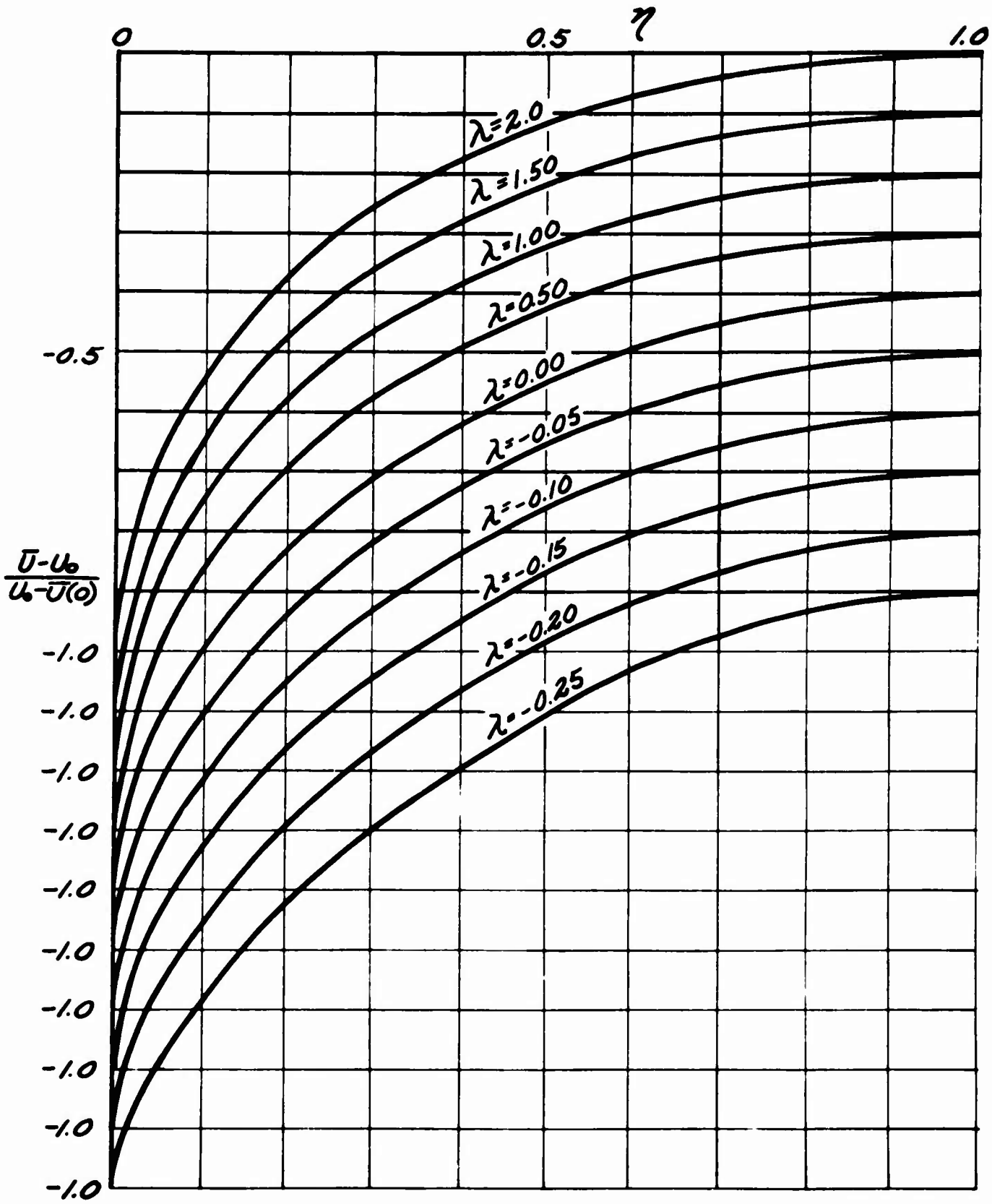

Figure 95. Computed Velocity Profiles of Similarities Boundary Layers Expressed in the Relative Form of $(\bar{U}-U_o)/(U_o-\bar{U}(0))\sim \eta$.

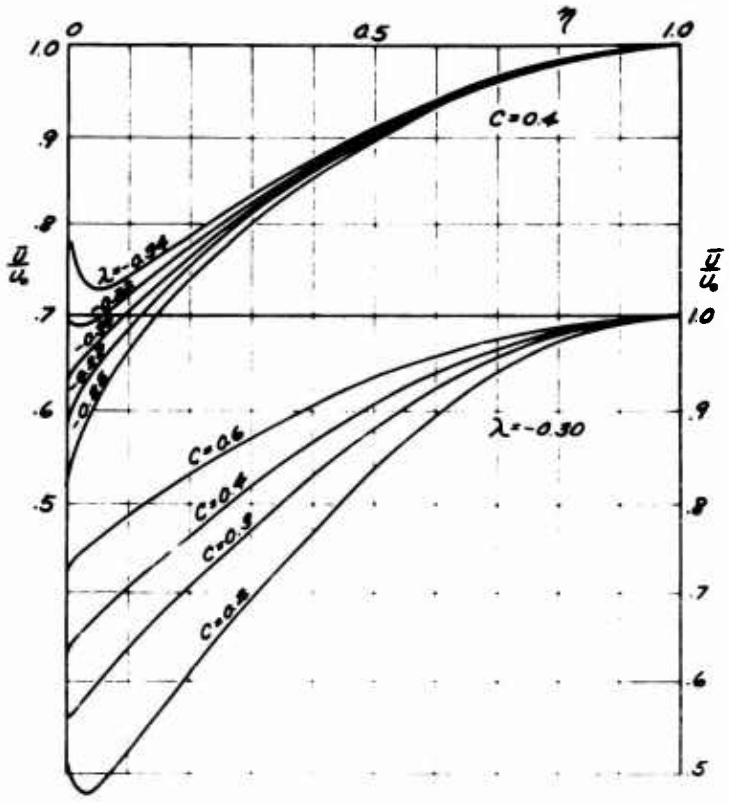

Figure 96. Computed Velocity Profiles Near the Critical Point of $\partial U(0)/\partial y = 0$.

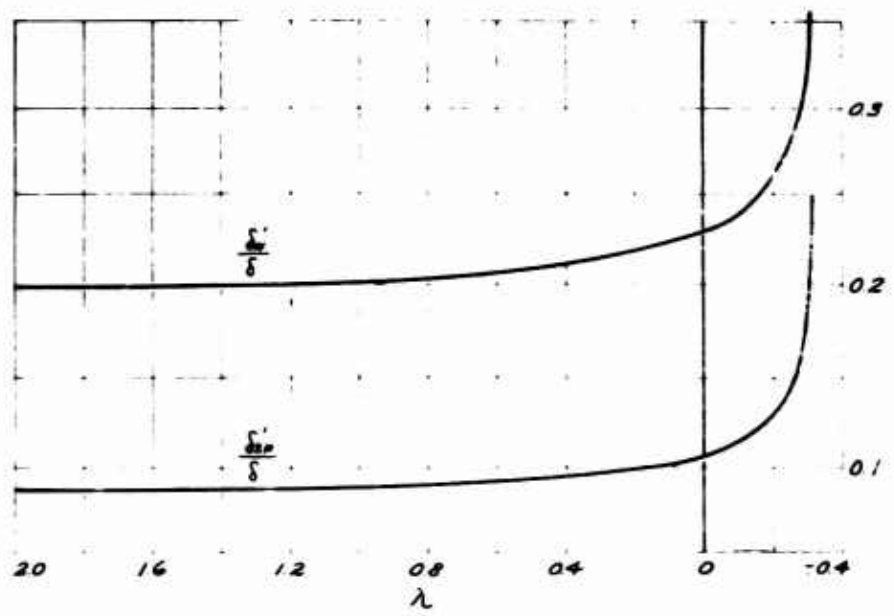

Figure 97. Variations of the Momentum-(δ'_{**}) and Displacement-Thickness (δ'_{*}) Versus λ Evaluated From the Relative Profiles Shown in Figure 95.

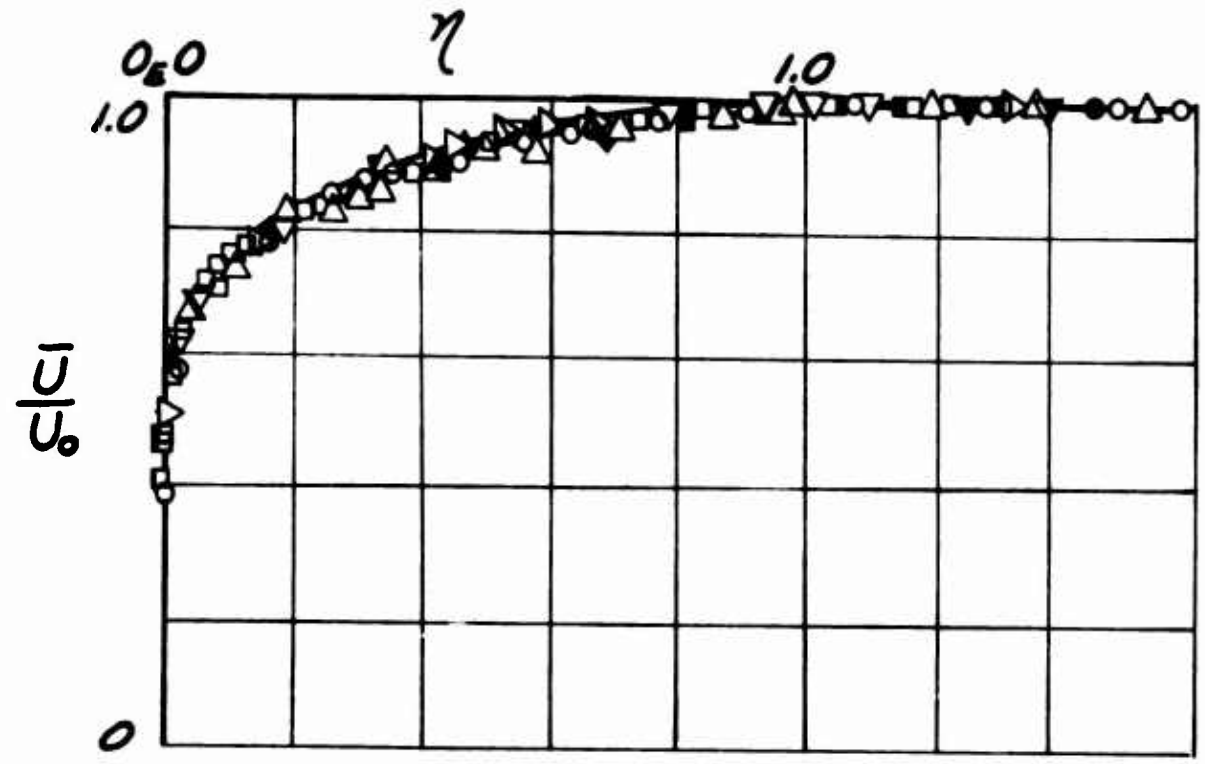

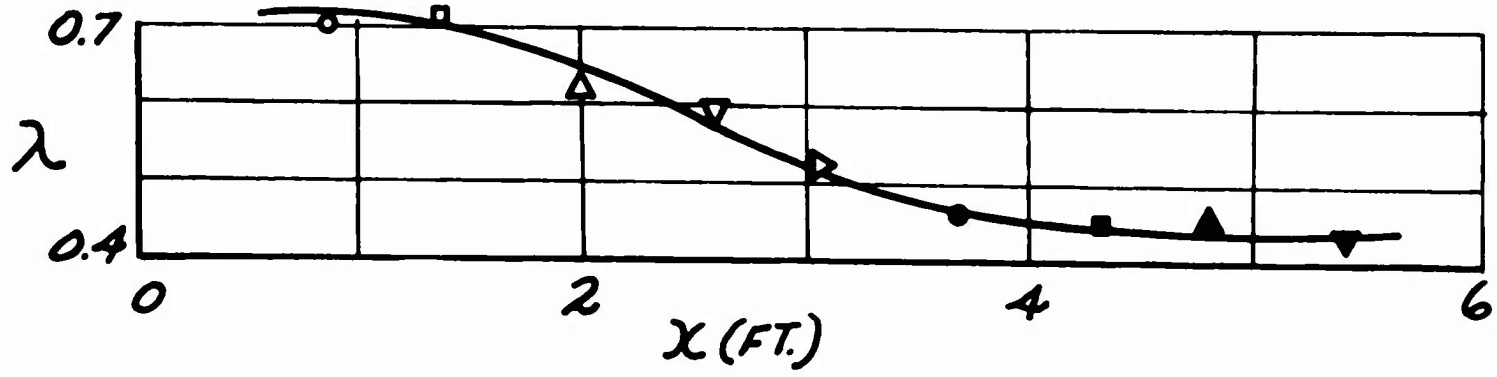

Figure 98. Comparison of the Computed Profiles of $\lambda = 0.5$ (full line) and $\lambda = 1.0$ (broken line) in Figure 95 With Experimental Data of the Mean Velocity of the Similarity Boundary Layer Shown in Figure 77. Observed values are shown in the lower figure. O_E and 0 on the abscissa have the same meanings as in Figure 91.

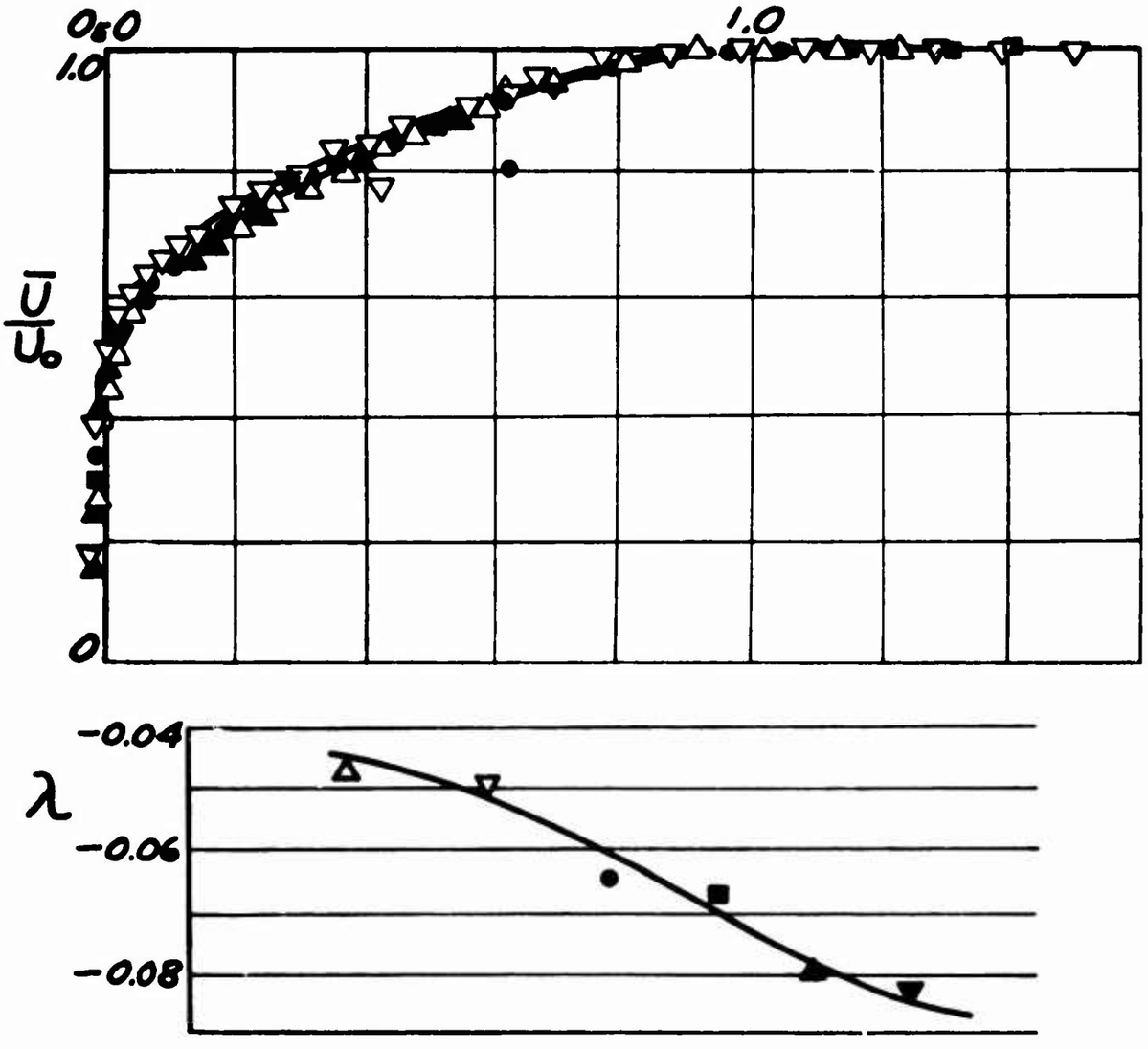

Figure 99. Comparison of the Computed Profiles of $\lambda = -0.10$ (full line) and $\lambda = -0.05$ (broken line) in Figure 95 With Experimental Data of the Mean Velocity of the Similarity Boundary Layer Shown in Figure 78 (reference 68). Observed values of λ are shown in the lower figure. O_E and 0 on the abscissa have the same meaning as in Figure 91.

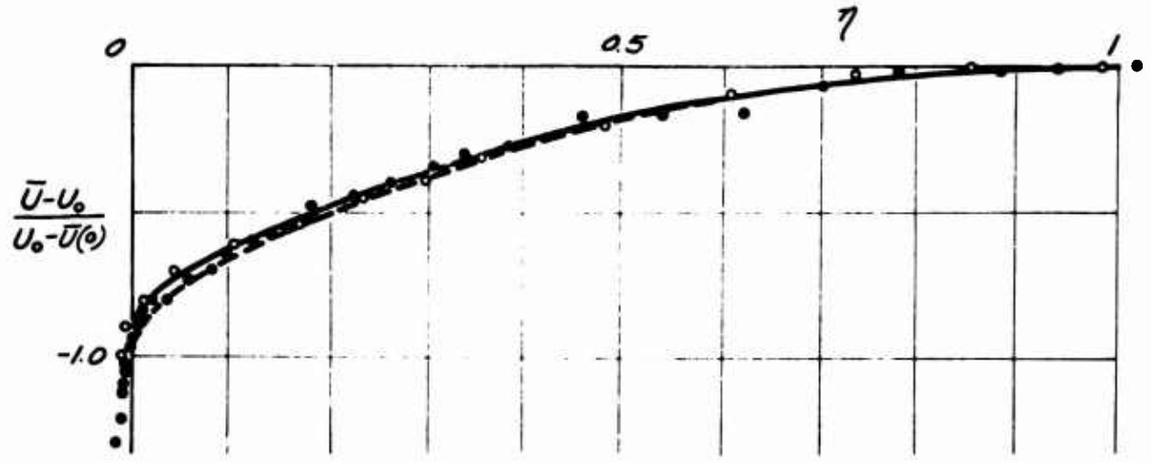

Figure 100. Comparison of the Computed Relative Profiles of λ = -0.15 (full line) and λ = -0.20 (broken line) in Figure 95 With Observed Mean Velocity of the Turbulent Boundary Layer With Positive Pressure Gradients. Measurements are made by Wieghardt-Tillman (○) with experimental value of λ = -0.16 (reference 73) and by Sandborn-Slogar (●) with λ = -0.17 (reference 78).

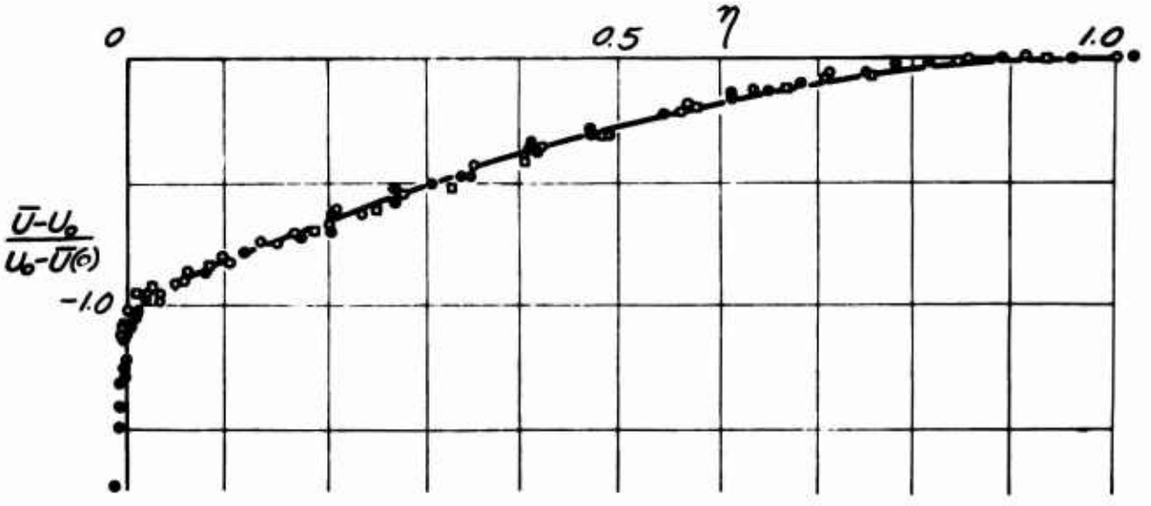

Figure 101. Comparison of a Computed Profile of $\underline{\lambda}$ = -0.30 and c = 0.35 Near the Critical Condition $\partial \bar{U}/\partial y = 0$ (cf. Figure 96) With Observed Mean Velocity Near the Point of Turbulent Separation. Measurements are made by Wieghardt-Tillmann (○, ◑) with experimental values of λ = -0.27 and -0.26 respectively (reference 79), by Sandborn-Slogar (●) with λ = -0.28 (reference 78), and by Schubauer-Klevanoff (□) with λ = -0.28 (reference 24).

REFERENCES

1. Prandtl, L., "Beitrag zum Turbulenz Symposium", Proceedings of the Fifth International Congress of Applied Mechanics, 1938.

2. Prandtl, L., and O. Tietjens, Hydro- und Aeromechanik, Volume 2, Springer, Berlin, Germany, 1931.

3. Reynolds, O., "An Experimental Investigation of the Circumstances which Determine Whether the Motion of Water Shall be Directed or Sinuous and of the Law of Resistance in Parallel Channels", Transactions of the Royal Society of London, Series A, Volume 174, 1883, pp. 935-982.

4. Taylor, G. I., "Stability of a Viscous Liquid Contained Between Two Rotating Cylinders", Philosophical Transaction, Series A, Volume 223, 1923, pp. 289-343.

5. Tollmien, W., "Über die Entstehung der Turbulenz, I", Mitteilung, Nachrichten Gesselschaft von Wissenschaft Gottingen, Mathatische und Physihalishe Klasse 21, 1929.

6. Schubauer, G. B., and H. K. Skramstad, Laminar Boundary Layer Oscillations and Transition on a Flat Plate, NACA Technical Report, No. 909, 1948.

7. Taylor, G. I., "Statistical Theory of Turbulence, Part V", Proceedings of the Royal Society, Series A, Volume 156, 1936, pp. 307-317.

8. Reynolds, O., "On the Dynamical Theory of Incompressible Viscous Fluids and the Determination of the Criterion", Philosophical Transactions of the Royal Society, Series A, Volume 186, 1895, pp. 123-165.

9. Taylor, G. I., "Diffusion by Continuous Movements", Proceedings of the London Mathematical Society, Volume 20, 1920, pp. 196-211.

10. Prandtl, L., "Über die Ausgebildete Turbulenz", Zeitschrift für angewandte Mathematik und Mechanik, Volume 5, 1925, pp. 136-139.

11. Taylor, G. I., "The Transport of Vorticity and Heat Through Fluids in Turbulent Motion", Proceedings of the Royal Society, Series A, Volume 135, 1932, pp. 685-702.

12. Kármán, T. V., "Mechanische Ahnlichkeit und Turbulenz", Nachrichten der Gesselschaft von Wissenschaft, Gottingen, Mathatische und Physihalishe Klasse, 1930, pp. 58-76.

13. Taylor, G. I., "Statistical Theory of Turbulence, Part I, II, III, IV", Proceedings of the Royal Society, Series A, Volume 151, 1935, pp. 421-478.

14. Kármán, T. V., and L. Howarth, "On the Statistical Theory of Isotropic Turbulence", Proceedings of the Royal Society, Series A, Volume 164, 1938, pp. 192-215.

15. Dryden, H. L., and A. M. Kuethe, The Measurements of Fluctuations of Air Speed by the Hot-Wire Anemometer, NACA Technical Report, No. 320, 1929.

16. Kolmogoroff, A. N., "The Local Structure of Turbulence in Incompressible Viscous Fluid for Very Large Reynolds Numbers", Comptes Rendus of the Academy of Science, U. R. S. S., Volume 30, 1941, pp. 301-305.

17. Shigemitsu, Y., "Statistical Theory of Turbulence, I. Hypothesis of Vortex Chaos Motion", Journal of the Physical Society of Japan, Volume 10, 1955, pp. 472-482.

18. Shigemitsu, Y., "Statistical Theory of Turbulence, II. Foundation of Similarity Theory of Turbulence", Journal of the Physical Society of Japan, Volume 10, 1955, pp. 890-902.

19. Shigemitsu, Y., "On the Velocity Fluctuations in the Laminar Boundary Layer, I", Journal of Physical Society of Japan, Volume 5, 1950, pp. 298-304.

20. Prandtl, L., "Neuere Ergebnisse der Turbulenzforschung", Zeitschrift für Verhandlung der Deutsche Ingenieur, Volume 77, 1933, pp. 105-114.

21. Suyehiro, K., "A Note on Resistance of Flow of Viscous Fluid", Journal of the Society of Naval Architects of Japan, Volume 36, 1925, pp. 87-92.

22. Shigemitsu, Y., "Experimental Studies on Laminar Sub-Layer in Turbulent Boundary Layer Involving Separation", Journal of the Physical Society of Japan, Volume 12, 1957, pp. 183-190.

23. Kline, S. J., and P. W. Runstalder, "Some Preliminary Results of Visual Studies of the Flow Model of the Wall Layers of the Turbulent Boundary Layer", Journal of Applied Mechanics, Volume 26, Series E, 1959, pp. 166-170.

24. Schubauer, G. B., and P. S. Klevanoff, Investigation of Separation of the Turbulent Boundary Layer, NACA Technical Note, No. 2133, 1950.

25. Lamb, H., Hydrodynamics, Sixth Edition, Section 328, Cambridge University Press, Cambridge, England, 1932, p. 577.

26. Reynolds, O., "On the Dynamical Theory of Incompressible Viscous Fluid and the Determination of the Criterion", Philosophical Transaction, Series A, Volume 186, 1895, pp. 123-164.

27. Ringleb, F. O., Vortex Motion, Research Report of the Aerophysics Department, Mississippi State University, State College, Mississippi, No. 47, Chapter 6, 1963, p. 33.

28. Batchelor, G. K., The Theory of Homogeneous Turbulence, Cambridge University Press, Cambridge, England, 1953.

29. Taylor, G. I., "The Spectrum of Turbulence", Proceedings of the Royal Society, Series A, Volume 164, 1938, pp. 476-490.

30. Darrieus, G., "Contribution a l'analyse de la Turbulence en Tourbillons Cellulaires", Proceedings of the Fifth International Congress of Applied Mechanics, 1938, pp. 422-427.

31. Stewart, R. W., "Triple Velocity Correlations in Isotropic Turbulence", Proceedings of Cambridge Philosophical Society, Volume 47, 1951, pp. 146-157.

32. Batchelor, G. K., and A. A. Townsend, "Decay of Isotropic Turbulence in the Initial Period", Proceedings of the Royal Society, Series A, Volume 193, 1948, pp. 539-558.

33. Hama, R., "Experimental Studies on Isotropic Turbulence", Report of the Institute of Science and Technology, University of Tokyo, Volume 7, 1953, pp. 145-174.

34. Tsuji, H., "Experimental Studies on the Characteristics of Isotropic Turbulence Behind Two Grids", Journal of the Physical Society of Japan, Volume 10, 1955, pp. 578-586.

35. Batchelor, G. K., and A. A. Townsend, "Decay of Vorticity in Isotropic Turbulence", Proceedings of the Royal Society, Series A, Volume 190, 1947, pp. 534-550.

36. Liepmann, H. W., J. Laufer, and K. Liepmann, On the Spectrum of Isotropic Turbulence, NACA Technical Note, No. 2473, 1951.

37. Shigemitsu, Y., "Statistical Theory of Turbulence, III, Extension of Similarity Theory of Turbulence", Journal of the Physical Society of Japan, Volume 10, 1955, pp. 1077-1087.

38. Townsend, A. A., The Structure of Turbulent Shear Flow, Cambridge University Press, Cambridge, England, 1956.

39. Schlichting, H., "Uber das ebene Windschattenproblem", Ingenieur Archiv, 1930, pp 537-571.

40. Townsend, A. A., "Momentum and Energy Diffusion in the Turbulent Wake of a Cylinder", Proceedings of the Royal Society, Series A, Volume 197, pp. 124-140.

41. Corrsin, S., and A. L. Kistler, The Free-Stream Boundaries of Turbulent Flows, NACA Technical Note, No. 3133, 1954.

42. Townsend, A. A. "The Fully Developed Turbulent Wake of a Circular Cylinder", Australian Journal of Scientific Research, Volume 2, 1949, pp. 451-468.

43. Taylor, G. I., "Turbulence in a Contracting Stream", Zeitschrift für angewandte Mathematik und Mechanik, Volume 15, 1935, pp. 91-96.

44. Jeans, J. H., The Dynamical Theory of Gases, Fourth Edition, Cambridge University Press, Cambridge, England, 1925, Chapter Nine.

45. Prandtl, L., "Bemerkungen zur Theorie der Freien Turbulenz'", Zeitschrift für angewandte Mathematik und Mechanik, Volume 22, 1942, pp. 241-243.

46. Gortler, H., "Berechnung von Aufgaben der Freien Turbulenz auf Grund eines neuen Naherungsansatzes", Zeitschrift für angewandte Mathematik und Mechanik, Volume 22, 1942, pp. 244-254.

47. Reichardt, H., "Gesetzmäszigkeiten der freien Turbulenz'", VDI Forschungsheft, Volume 414, 1942.

48. Goldstein, S., Modern Developments in Fluid Dynamics, Clarendon Press, Oxford, England, 1938, Chapter XIII.

49. Schlichting, H., Grenzschicht - Theorie, G. Braunschweig Karlsruhe, Germany, 1958. Kapitel XXIII.

50. Swain, L. M., "On the Turbulent Wake Behind a Body of Revolution", Proceedings of the Royal Society, Series A, Volume 125, 1929, pp. 647-659

51. Tollmien, W., "Berechnung Turbulenter Ausbreitungsvorgange", Zeitschrift fur angewandte Mathematik und Mechanik, Volume 6, 1926, pp. 468-478.

52. Forthmann, E., "Über Turbulente Strahlausbreitung", Ingenieur Archiv, Volume 5, 1935, pp. 42-54.

53. Liepmann, H W., and J. Laufer, Investigations of Free Turbulent Mixing, NACA Technical Note, No 1257, 1947.

54. Shigemitsu, Y., "Nonsimilarity Theory of Decaying Turbulence", Journal of the Physical Society of Japan, Volume 14, 1959, pp. 91-103.

55. Batchelor, G. K., and A. A. Townsend, "Decay of Turbulence in the Final Period", Proceedings of the Royal Society, Series A, Volume 194, 1948, pp 527-543

56. Dryden, H. L., "A Review of the Statistical Theory of Turbulence", Quarterly of Applied Mathematics, Volume 1, 1943, pp. 7-42.

57. Frenkiel, F. N., "The Decay of Isotropic Turbulence", Journal of Applied Mechanics, Volume 15, 1948, pp. 311-321.

58. Townsend, A. A., "Experimental Evidence for the Theory of Local Isotropy", Proceedings of the Cambridge Philosophical Society, Volume 44, 1948, pp 560-565.

59. Stewart, R. W., and A A. Townsend, "Similarity and Self-Preservation in Isotropic Turbulence", Philosophical Transaction, Series A, Volume 243, 1951, pp. 359-386.

60. Stewart, R. W., "Triple Velocity Correlations in Isotropic Turbulence", Proceedings of the Cambridge Philosophical Society, Volume 47, 1951, pp. 146-157.

61. Proudman, I., "A Comparison of Heisenberg's Spectrum of Turbulence with Experiment". Proceedings of the Cambridge Philosophical Society, Volume 47, 1951, pp. 158-176.

62. Kolmogoroff, A. N., "On Degeneration of Isotropic Turbulence in an Incompressible Viscous Liquid", Comptes Rendus of the Academy of Science, U. R. S. S., Volume 31, 1941, p. 538.

63. Kolmogoroff, A. N., "Dissipation of Energy in Locally Isotropic Turbulence", Comptes Rendus of the Academy of Science, U. R. S. S., Volume 32, 1941, pp. 16-19.

64. Heisenberg, W., "Zur statistischen Theorie der Turbulenz", Zeitschrift für Physik, Volume 124, 1948, pp. 628-657.

65. Heisenberg, W., "On the Theory of Statistical and Isotropic Turbulence", Proceedings of the Royal Society, Series A, Volume 195, 1948, pp. 402-406.

66. Tsuji, H., "Experimental Studies on the Spectrum of Isotropic Turbulence Behind Two Grids", Journal of the Physical Society of Japan, Volume 11, 1956, pp. 1096-1104.

67. Sandborn, V. A., Experimental Evaluation of Momentum Terms in Turbulent Pipe Flow, NACA Technical Note, No. 3178, 1954.

68. Shigemitsu, Y., "Velocity-Defect Law of Turbulent Boundary Layer", Report of Transportation Technical Research Institute of Japan, No. 51, 1962.

69. Klevanoff, P. S., Characteristics of Turbulence in a Boundary Layer with Zero Pressure Gradient, NACA Technical Note, No. 3178, 1954.

70. Coles, D., "The Law of the Wake in the Turbulent Boundary Layer", Journal of Mechanics, Volume 1, 1956, pp. 191-226.

71. Nikuradse, J., "Gesetzmaszigkeiten der Turbulenten Stromung in Flatten Rohren", Forschungs-Arbeiten der Ingenieur-Wesentlichkeiten, Volume 356, 1932.

72. Tani, I., and R. Hama, "Turbulent Boundary Layer Along a Flat Plate", Boundary Layer War-Time Report of Japan, Volumes 1-4, 1945.

73. Ludwieg, H., and W. Tillmann, Investigations of the Wall-Shearing Stress in Turbulent Boundary Layers, NACA Technical Memorandum, No. 1285, 1950.

74. Laufer, J., Investigation of Turbulent Flow in a Two-Dimensional Channel, NACA Technical Note, No. 2123, 1950.

75. Reichardt, H., "Vollstandige Darstellung der Turblenten Geschwindigkeitsverteilung in glatten Leitungen", Zeitschrift für angewandte Mathematik und Mechanik, Volume 31, 1951, pp. 208-219.

76. Clauser, F. H., "The Turbulent Boundary Layer", Advances in Applied Mechanics, New York, Volume 4, 1956, pp. 1-51.

77. Clauser, F. H., "Turbulent Boundary Layer in Adverse Pressure Gradient", Journal of Aeronautical Science, Volume 21, 1954, pp. 91-108.

78. Sandbern, V. A., and R. J. Slogar, Study of the Momentum Distribution of Turbulent Boundary Layers in Adverse Pressure Gradients, NACA Technical Note, No. 3264, 1955.

79. Wieghardt, K., and W. Tillman, On the Turbulent Friction Layer for Rising Pressure, NACA Technical Memorandum, No. 1314, 1951.

Unclassified

Security Classification

DOCUMENT CONTROL DATA - R&D

(Security classification of title, body of abstract and indexing annotation must be entered when the overall report is classified)

1 ORIGINATING ACTIVITY (Corporate author) Mississippi State University Aerophysics Department State College, Mississippi	2a REPORT SECURITY CLASSIFICATION Unclassified 2b GROUP

3 REPORT TITLE

Statistical Theory of Turbulence

4 DESCRIPTIVE NOTES (Type of report and inclusive dates)

5 AUTHOR(S) (Last name, first name, initial)

Shigemitsu, Yutaka

6 REPORT DATE	7a TOTAL NO OF PAGES	7b NO OF REFS
June 1966	251	79

8a CONTRACT OR GRANT NO DA 44-177-AMC-892(T) b PROJECT NO Task 1P125901A14203 c d	9a ORIGINATOR'S REPORT NUMBER(S) USAAVLABS Technical Report 66-25 9b OTHER REPORT NO(S) (Any other numbers that may be assigned this report) Aerophysics Research Report No. 64

10 AVAILABILITY/LIMITATION NOTICES

Distribution of this document is unlimited

11 SUPPLEMENTARY NOTES	12 SPONSORING MILITARY ACTIVITY
	U. S. Army Aviation Materiel Laboratories Fort Eustis, Virginia

13 ABSTRACT

The purpose of this report is to discuss the system of a statistical theory of turbulence in general cases from isotropic turbulence to turbulent boundary layer. In the first three chapters, mathematical formulations are given to the Euler correlation or the Reynolds stress, according to a basic physical picture of vortex chaos motion in which many kinds of vortices are carried along the flow in agitating situations. When the formula is combined with the Reynolds equations, quantitative discussions are developed by dividing the cases into two fundamental groups of wake or jet flow in Chapters Four through Seven and of boundary layer or pipe flow in Chapters Eight and Nine.

DD FORM 1 JAN 64 1473

Unclassified

Security Classification

14. KEY WORDS	LINK A		LINK B		LINK C	
	ROLE	WT	ROLE	WT	ROLE	WT

INSTRUCTIONS

1. ORIGINATING ACTIVITY: Enter the name and address of the contractor, subcontractor, grantee, Department of Defense activity or other organization *(corporate author)* issuing the report.

2a. REPORT SECURITY CLASSIFICATION: Enter the overall security classification of the report. Indicate whether "Restricted Data" is included. Marking is to be in accordance with appropriate security regulations.

2b. GROUP: Automatic downgrading is specified in DoD Directive 5200.10 and Armed Forces Industrial Manual. Enter the group number. Also, when applicable, show that optional markings have been used for Group 3 and Group 4 as authorized.

3. REPORT TITLE: Enter the complete report title in all capital letters. Titles in all cases should be unclassified. If a meaningful title cannot be selected without classification, show title classification in all capitals in parenthesis immediately following the title.

4. DESCRIPTIVE NOTES: If appropriate, enter the type of report, e.g., interim, progress, summary, annual, or final. Give the inclusive dates when a specific reporting period is covered.

5. AUTHOR(S): Enter the name(s) of author(s) as shown on or in the report. Enter last name, first name, middle initial. If military, show rank and branch of service. The name of the principal author is an absolute minimum requirement.

6. REPORT DATE: Enter the date of the report as day, month, year; or month, year. If more than one date appears on the report, use date of publication.

7a. TOTAL NUMBER OF PAGES: The total page count should follow normal pagination procedures, i.e., enter the number of pages containing information.

7b. NUMBER OF REFERENCES: Enter the total number of references cited in the report.

8a. CONTRACT OR GRANT NUMBER: If appropriate, enter the applicable number of the contract or grant under which the report was written.

8b, 8c, & 8d. PROJECT NUMBER: Enter the appropriate military department identification, such as project number, subproject number, system numbers, task number, etc.

9a. ORIGINATOR'S REPORT NUMBER(S): Enter the official report number by which the document will be identified and controlled by the originating activity. This number must be unique to this report.

9b. OTHER REPORT NUMBER(S): If the report has been assigned any other report numbers *(either by the originator or by the sponsor)*, also enter this number(s).

10. AVAILABILITY/LIMITATION NOTICES: Enter any limitations on further dissemination of the report, other than those imposed by security classification, using standard statements such as:

(1) "Qualified requesters may obtain copies of this report from DDC."

(2) "Foreign announcement and dissemination of this report by DDC is not authorized."

(3) "U. S. Government agencies may obtain copies of this report directly from DDC. Other qualified DDC users shall request through _____."

(4) "U. S. military agencies may obtain copies of this report directly from DDC. Other qualified users shall request through _____."

(5) "All distribution of this report is controlled. Qualified DDC users shall request through _____."

If the report has been furnished to the Office of Technical Services, Department of Commerce, for sale to the public, indicate this fact and enter the price, if known.

11. SUPPLEMENTARY NOTES: Use for additional explanatory notes.

12. SPONSORING MILITARY ACTIVITY: Enter the name of the departmental project office or laboratory sponsoring *(paying for)* the research and development. Include address.

13. ABSTRACT: Enter an abstract giving a brief and factual summary of the document indicative of the report, even though it may also appear elsewhere in the body of the technical report. If additional space is required, a continuation sheet shall be attached.

It is highly desirable that the abstract of classified reports be unclassified. Each paragraph of the abstract shall end with an indication of the military security classification of the information in the paragraph, represented as *(TS), (S), (C), or (U)*.

There is no limitation on the length of the abstract. However, the suggested length is from 150 to 225 words.

14. KEY WORDS: Key words are technically meaningful terms or short phrases that characterize a report and may be used as index entries for cataloging the report. Key words must be selected so that no security classification is required. Identifiers, such as equipment model designation, trade name, military project code name, geographic location, may be used as key words but will be followed by an indication of technical context. The assignment of links, rules, and weights is optional.

3591-66